PROJECT GENESIS:

NASw-4435

MARS *IN SITU* PROPELLANT TECHNOLOGY DEMONSTRATOR MISSION

FINAL REPORT

NASA/USRA Advanced Design Program

University of Washington
Department of Aeronautics and Astronautics
Seattle, Washington 98195

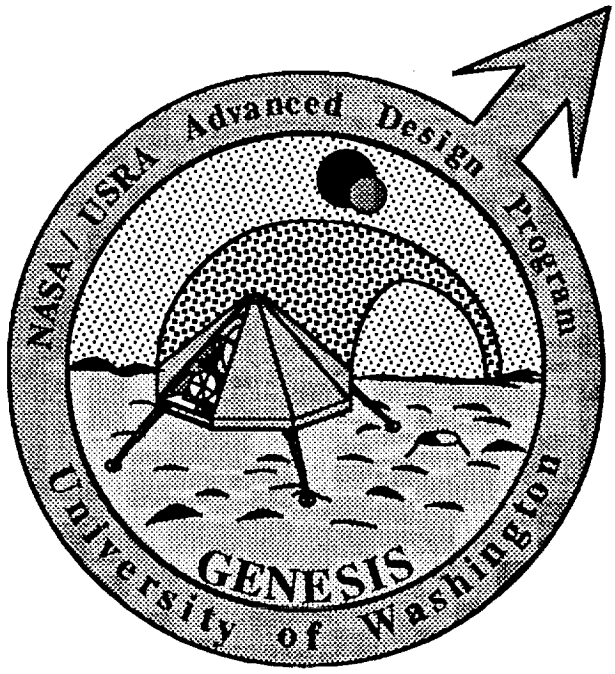

July 31, 1994

PROJECT GENESIS:
MARS *IN SITU* TECHNOLOGY DEMONSTRATOR MISSION

FINAL REPORT

Space Systems Design, AA 420/421
NASA/USRA Advanced Design Program

Prepared By

Francisco Garcia Acosta	Jared Kipp	Daniel Pasco
Scott Anderson	Takahisa Kobayashi	Norihito Tsuji
Jason Andrews	Mohrli Marcelo	Igor Turek
Matt Deger	Karen Mark	Chris Wilman
Matt Hedman	Mark Matheson	Keith Yang

Instructor: Prof. Adam P. Bruckner

Teaching Assistant: Brian Thill

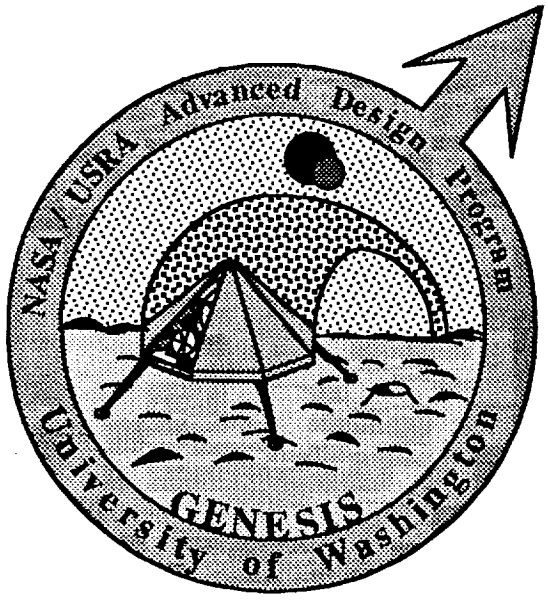

University of Washington
Department of Aeronautics and Astronautics
Seattle, Washington 98195

July 31, 1994

ABSTRACT

Project Genesis is a low cost, near-term, unmanned Mars mission, whose primary purpose is to demonstrate *in situ* resource utilization (ISRU) technology. The essence of the mission is to use indigenously produced fuel and oxidizer to propel a ballistic hopper. The Mars Landing Vehicle/Hopper (MLVH) has an Earth launch mass of 625 kg and is launched aboard a Delta II 7925 launch vehicle into a conjunction-class transfer orbit to Mars. Upon reaching its target, the vehicle performs an aerocapture maneuver and enters an elliptical orbit about Mars. Equipped with a ground penetrating radar, the MLVH searches for subsurface water ice deposits while in orbit for several weeks. A deorbit burn is then performed to bring the MLVH into the Martian atmosphere for landing. Following aerobraking and parachute deployment, the vehicle retrofires to a soft landing on Mars. Once on the surface, the MLVH begins to acquire scientific data and to manufacture methane and oxygen via the Sabatier process. This results in a fuel-rich O_2/CH_4 mass ratio of 2, which yields a sufficiently high specific impulse (335 sec) that no additional oxygen need be manufactured, thus greatly simplifying the design of the propellant production plant. During a period of 153 days the MLVH produces and stores enough fuel and oxidizer to make a 30 km ballistic hop to a different site of scientific interest. At this new location the MLVH resumes collecting surface and atmospheric data with the onboard instrumentation. Thus, the MLVH is able to provide a wealth of scientific data which would otherwise require two separate missions or separate vehicles, while proving a new and valuable technology that will facilitate future unmanned and manned exploration of Mars. Total mission cost, including the Delta launch vehicle, is estimated to be $200 million.

PREFACE

During the 10 years of the existence of the NASA/USRA Advanced Design Program, participating students in the Department of Aeronautics and Astronautics at the University of Washington have carried out innovative design studies related to the critical needs of space prime power, propulsion, and transportation, most based on ongoing research in our Department. Since the 1991-92 academic year we have directed our attention to the issue of *in situ* resource utilization on Mars. *In situ* resource utilization (ISRU) is a concept wherein indigenous materials at the site of an interplanetary mission are used to produce rocket propellants for the flight back to Earth or local travel, thus obviating the need to import all the mission propellants from Earth. The use of extraterrestrial resources on Mars was first proposed by Robert Ash, Giulio Varsi, and James French at JPL in 1978, and was subsequently also studied by Kumar Ramohalli and co-workers at the University of Arizona. More recently, ISRU has been strongly advocated and further developed by Robert Zubrin and his colleagues at Martin Marietta, by Diane Linne *et al* at NASA Lewis Research Center, and by a group headed by David Kaplan at the Johnson Space Center. On Mars, ISRU is accomplished by using the carbon dioxide in the Martian atmosphere as the basic feedstock of the propellant production process. ISRU can dramatically reduce the Earth launch mass of a Mars mission, greatly lowering the mission cost, and thus making manned exploration of Mars much more feasible.

At the University of Washington we initially focused on missions which produce methane and oxygen from the reaction of carbon dioxide from the Martian atmosphere with seed hydrogen brought from Earth, but later also examined the alternative of producing carbon monoxide and oxygen directly from the atmosphere, without recourse to any feedstock gases brought from Earth. We found that with either scenario *in situ* resource utilization offers striking benefits compared to conventional mission scenarios. For example, in our 1992-93 study we

were able to show that in a sample return mission the use of ISRU can greatly increase the quantity of Martian soil and rock samples brought back to Earth, or conversely, greatly reduce the Earth launch mass required to return a specified amount of Martian samples.

With interest in an ISRU-enhanced sample return mission rapidly increasing within NASA, there is a growing need to demonstrate *in situ* propellant production technology on a smaller and less expensive scale. The mission design presented in this report responds to this need: it is a low-cost, near-term Mars ISRU propellant technology demonstrator which is also capable of a significant science return. The essence of this mission is to use indigenously produced fuel and oxidizer to propel a ballistic rocket hopper capable of a range of approximately 30 km on Mars. The Mars landing vehicle and hopper are one and the same vehicle. This integrated approach is simple to implement and offers the possibility of being modified for multiple hops or, ultimately, for a sample return mission.

Although much work remains to be done to develop and implement the technology of ISRU, our studies indicate that it can be accomplished at modest cost and on a relatively short time scale. The mission presented here, for example, could be launched within five to seven years at a total cost, including the launch vehicle, of only $200 Million.

Adam P. Bruckner
Professor of Aeronautics and Astronautics
July 31, 1994

ACKNOWLEDGMENTS

The University of Washington Space systems Design Class of 1994 would first and foremost like to thank the NASA/USRA Advanced Design Program for the grant that made this project possible. Many thanks are due to Vicki Johnson, Director, and her staff for their skillful management of this program.

Without a significant amount of outside help, Project Genesis wouldn't have taken off the ground let alone make a ballistic hop. Only a Martian could provide better Mars information than Jim Tillman of the Department of Atmospheric Sciences at the University of Washington. For this, we are very grateful. Robert Zubrin's work on ISRU at Martin Marietta has provided much inspiration. In particular, his recent experimental research on a small-scale Sabatier propellant plant was an invaluable source of data. Steve Hamlin, a UW graduate student, was very helpful with the finite element code ANSYS, which was used for the MLVH structural analysis. Dan Marin at McDonnell Douglas, was a key source of information on the Delta Launch Vehicle. We are also indebted to the following people for the wealth of information provided on the propellant production plant: R. Frisbee, C. Weisbin, B. Wilcox, D. Johnson, J. Jones, and W. Zimmerman at JPL, D. Kaplan and D. Weaver at Johnson Space Center, D. Rethhe at Hamilton Standard, R. Ramos at NASA Ames, S. Neville and E. Ryba at Hughes, P. Thomas at the USAF Phillips Lab, and C. Kuckolls at Motorola.

Dana Andrews and Eric Wetzel of the Boeing Defense and Space Group took time off their busy schedules to take part in our preliminary design review. Their feedback was invaluable. The authors are also indebted to Carl Pilcher and his colleagues at NASA Headquarters for their interest and valuable suggestions regarding the scope of the project.

Last but definitely not least, we would like to especially thank Professor Adam Bruckner and our Teaching Assistant, Brian Thill. Without them, this whole mission wouldn't have existed. They have guided us steadfastly throughout the duration of this project, making sure that everything fell into place.

TABLE OF CONTENTS

1.0 INTRODUCTION

Francisco Garcia Acosta

Scott Anderson

Jared Kipp

Takahisa Kobayashi

Norihito Tsuji

Igor Turek

Karen Mark

Keith Yang

TABLE OF CONTENTS

1.1 BACKGROUND
(Norihito Tsuji)

Ever since mankind first stepped on the surface of the Moon, the dream of many has been to expand the field of manned space exploration to Mars. Although the astronomically high cost of a manned mission to Mars has kept this dream from reality, for the past 30 years Mars has been explored by unmanned space probes, beginning with the Mariner series in the 1960's and followed in the mid 1970's by Viking I and Viking II. These missions have provided a wealth of data, have answered many mysteries about Mars, and have given rise to numerous new questions. With the MESUR Pathfinder program establishing the return to exploration of the red planet beginning in 1996, Mars is again receiving attention as a possible target for manned exploration in the early 21st century.

The future of Mars exploration is primarily constrained by high cost. The key to reducing mission cost is to use a simplified and streamlined mission architecture. However, the main issue in reducing cost is decreasing Earth launch mass. One method of accomplishing this is to incorporate low mass components into mission architecture, while another is to use *in situ* propellant production, i.e., using resources available on Mars to manufacture propellant for the return trip to Earth [1]. While lowering the mass of components has always been important in reducing launch mass, *in situ* propellant production could drastically reduce mission costs, thus bringing a manned mission to Mars closer to reality.

The concept behind using planetary resources to manufacture propellant is relatively simple. A plant for propellant production is brought from Earth, and upon arrival begins producing propellant from local resources. As propellant is manufactured, the return vehicle tanks are filled. The plant can also be used as a refueling station for other mission operations such as surface rovers. *In situ* resource utilization (ISRU) on Mars, was first proposed by Ash *et al.* at JPL in 1978 [1] and more recently studied by Ramohalli *et al.* [2] and by Zubrin [3,4]. On

Mars, ISRU is accomplished by using the carbon dioxide in the Martian atmosphere as the basic feedstock of the propellant production process.

In 1992, the University of Washington's NASA/USRA Advanced Design Program developed Project Minerva, a preliminary design of a manned mission utilizing *in situ* propellant production [5,6]. Its estimated cost of $55 billion represented a 90% reduction in the cost of the conventional NASA concepts of the time. Because of the large investment such a mission would nevertheless entail, unmanned precursor missions will need to be attempted first. Accordingly, in 1993 we proposed Project Hyreus, a mission which utilizes *in situ* propellant manufactured on Mars to return 25 kg of Martian samples, a quantity nearly two orders of magnitude greater than current sample returns scenarios [7,8].

Prior to embarking on ISRU-augmented missions of the type described above, it will be necessary to demonstrate *in situ* propellant production technology and its benefits on a smaller and less expensive scale. Project Genesis, this year's mission study, is a low-cost Mars ISRU propellant technology demonstrator mission which could be launched as early as 2001. The essence of this mission is to use indigenously produced fuel and oxidizer to propel a ballistic rocket hopper capable of a range of approximately 30 km on Mars. The Mars landing vehicle and hopper are one and the same vehicle, henceforth referred to as the MLVH. The entire MLVH makes the ballistic hop, leaving nothing behind. This integrated approach is simple to implement, contains the possibility of being modified for multiple hops or for a sample return mission, and is capable of a significant science return.

1.2 MISSION SCENARIO
(Takahisa Kobayashi, Keith Yang)

As shown in Fig. 1, the mission scenario begins with the launch of a Delta II 7925 rocket into a low Earth orbit (LEO) in the year 2001. The vehicle's payload consists of the MLVH with

its aerobrake attached. Once in LEO, the upper stage of the launch vehicle injects the payload into a fast conjunction-class transfer orbit to Mars. At Mars the MLVH performs an aerocapture maneuver to enter an elliptical orbit around the planet. Using a ground penetrating radar (GPR) system, the vehicle acts as a remote sensing satellite to detect water ice deposits. After about a month in orbit, and following confirmation by an imaging camera that there are no dust storms over the selected landing site, the MLVH begins its descent to the surface with a small rocket burn and aerobraking maneuvers. When a specific descent velocity is reached, a parachute is deployed to further decrease the velocity of the MLVH. Maximum reduction in terminal velocity is required in order to minimize the propellant requirements for the landing engines. The parachute is jettisoned shortly before touchdown and the retro-rockets are ignited to provide a soft landing on the Martian surface.

As soon as the MLVH lands on Mars, the propellant production plant starts producing the fuel and oxidizer for the ballistic hop, and the science package begins to collect data. When the production of the propellants is completed approximately five months later, the MLVH executes a ballistic hop to a new location 30 km away and repeats the scientific data gathering process. Although the main objective of Project Genesis is to demonstrate *in situ* propellant utilization and ballistic hopping technology, a significant science return is also accomplished.

1.3 IN SITU PROPELLANT PRODUCTION

(Scott Anderson, Karen Mark)

Two scenarios exist that could be used to produce *in situ* propellants on Mars. One would produce methane and oxygen by combining seed hydrogen brought from Earth with carbon dioxide found in the Martian atmosphere. The other scenario would produce carbon monoxide and oxygen directly from the carbon dioxide.

The methane system uses the well known Sabatier reaction to produce methane and water [3,4]. Compressed carbon dioxide enters the Sabatier reactor and reacts with hydrogen brought from Earth. The water from the Sabatier reaction is sent to an electrolyzer to be separated into oxygen and hydrogen. This hydrogen is recycled through the system until there is no hydrogen left in the tanks.

The carbon monoxide system uses a zirconia electrolyzer to produce carbon monoxide and oxygen by dissociating carbon dioxide [1,2]. Its advantage is that it does not depend on seed hydrogen brought from Earth; thus, a CO/O_2 production plant could, in principle, produce unlimited quantities of propellants, so long as its power source remains operational. However, zirconia electrolyzers require relatively large quantities of power, are fragile, and are prone to single point failure. Accordingly, zirconia electrolyzers are not suitable for a small, low-cost, near-term demonstrator mission. Alternatively, a reverse water-gas-shift reactor and water electrolyzer could be used to produce carbon monoxide and oxygen [1]. This approach uses carbon dioxide and a small amount of seed hydrogen (which is fully recyclable) to form carbon monoxide and oxygen. Unfortunately, very little research has been done on this alternative to date, making it undesirable for a near-term demonstrator mission. A more detailed discussion of the carbon monoxide production concepts can be found in Appendix A.

The methane scenario was selected for Project Genesis, for several reasons: 1) a methane MLVH has a lower Earth launch mass than a carbon monoxide MLVH for a ballistic hop of the same distance; 2) the configuration for the methane scenario is much simpler than for the carbon monoxide scenario; 3) the Sabatier reaction has been used in industry for many years and its technology is well developed and robust [3,4]. In addition, components developed for a methane ISRU system (such as the rocket engines) could be used in other space applications, such as reaction control systems.

1.4 MARS SCIENCE
(Francisco G. Acosta, Jared Kipp)

Following the initial exploration of Mars by Mariner spacecraft, the Soviet Mars-series, and the Viking landers, it is necessary to expand our knowledge of Mars in all areas of scientific interest involving a single type of probe. Project Genesis will provide unique science data not obtainable with any other proposed mission, and will greatly expand our knowledge of Mars. *In situ* measurements from two different locations would begin a new phase in the exploration of Mars, providing information which cannot be obtained from an orbiter and/or a single stationary lander. This mission has three major science goals, which complement other proposed scientific objectives for the continued exploration of Mars [9]:

- Surface composition
- Meteorology
- Location of ice/water deposits

The first two goals will be accomplished by the MLVH while on the Martian surface. The versatility created by the ability of the MLVH to perform a hop allows the second landing site to be selected after the initial landing. The third scientific goal will be accomplished by means of ground penetrating radar from the spacecraft's initial parking orbit, prior to landing at the first site. The possibility of finding deposits of water ice on Mars opens up vast opportunities for future missions, such as *in situ* H_2/O_2 propellant production and life support systems.

1.5 REPORT ORGANIZATION
(Igor Turek)

The mission architecture of Project Genesis is presented in the following format: Chapter 2 is devoted to the discussion of the propellant production plant and Chapter 3 presents the MLVH configuration and conceptual design. The avionics and communication systems are

described in Chapter 4, while the science aspects of the mission are discussed in Chapter 5. The astrodynamics, atmospheric entry and landing sequences, and the choice of launch vehicle are detailed in Chapter 6. A mission cost analysis follows in Chapter 7 and concluding remarks are presented in Chapter 8. Two appendices are also included; the first contains details of an alternative propellant production plant that produces carbon monoxide and oxygen, and the second appendix describes experiments performed by one of the authors with a small, laboratory-scale methane-oxygen rocket engine.

NOMENCLATURE

ISRU	*In Situ* Resource Utilization
GPR	Ground Penetrating Radar
MLVH	Mars Landing Vehicle and Hopper

REFERENCES

1. Ash, R.L., Dowler, W.L., and Varsi, G., "Feasibility of rocket propellant production on Mars," *Acta Astronautica*, Vol. 5, 1978, pp. 705-724.

2. Ramohalli, K., Dowler, W., French, J., and Ash, R., "Novel Extraterrestrial Processing for Space Propulsion," *Acta Astronautica*, Vol. 8, 1987, pp. 511-526.

3. Zubrin, R., Baker, D., and Gwynne, O., "Mars Direct: A Simple, Robust, and Cost Effective Architecture for the Space Exploration Initiative," Paper No. AIAA 91-0326, AIAA 29th Aerospace Sciences Meeting and Exhibit, Reno, NV, January 7-10, 1991.

4. Zubrin, R. M., "In-Situ Propellant Production: The Key Technology Required for the Realization of a Coherent and Cost-Effective Space Exploration Initiative," Paper No. IAA 91-668, 42nd Congress of the International Astronautical Federation, Montreal, Canada, October 5-11, 1991.

5. "Project Minerva: A low-Cost Manned Mars Mission Based on Indigenous Propellant Production," Final Report, AA420/421 Space Systems Design, NASA/USRA Advanced Design Program, Department of Aeronautics and Astronautics, University of Washington, June 1992.

6. Bruckner, A.P., Cinnamon, M., Hamling, S., Mahn, K., Phillips, J., and Westmark, V., "Low Cost Manned Mars Mission Based on Indigenous Propellant Production," Paper No. AIAA 93-1010, AIAA/AHS/ASEE Aerospace Design Conference, Irvine, CA, February 16-19, 1993.

7. "Project Hyreus: Mars Sample Return Mission Utilizing In Situ Propellant Production", Final Report, AA420/421 Space Systems Design, NASA/USRA Advanced Design Program, Department of Aeronautics and Astronautics, University of Washington, July 1993.

8. Bruckner, A.P., Nill, L., Schubert, H., Thill, B., and Warwick, R., "Mars Rover Sample Return Mission Utilizing In Situ Production of the Return Propellants," Paper No. AIAA 93-2242, AIAA/SAE/ASME/ASEE 29th Joint Propulsion Conference and Exhibit, Monterey, CA, June 28-30, 1993.

9. *COMPLEX, Strategy for Exploration of the Inner Planets: 1977-1987*, National Academy of Sciences, Washington, DC, 1978

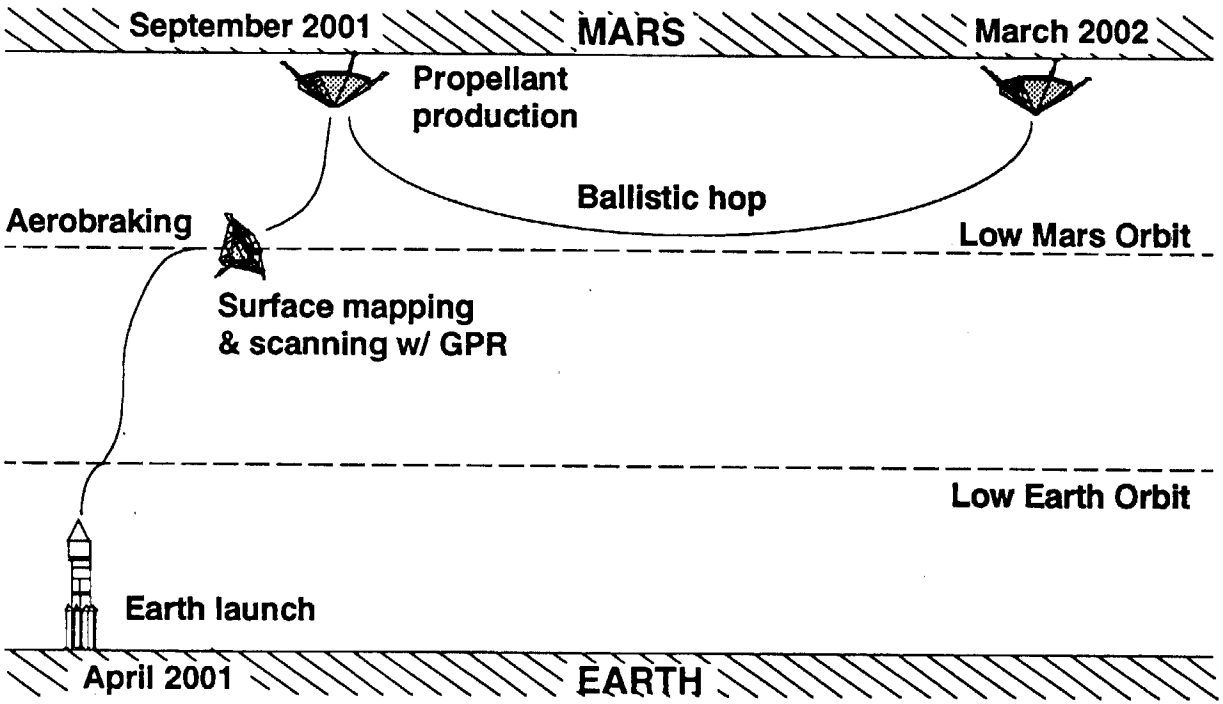

Fig. 1.1 Mission scenario.

2.0 PROPELLANT PRODUCTION AND POWER

Scott Anderson

Jason Andrews

Karen Mark

Daniel Pasco

Norihito Tsuji

TABLE OF CONTENTS

2.1 INTRODUCTION

(Karen Mark, Scott Anderson)

The purpose of Project Genesis is to demonstrate *in situ* propellant production. With *in situ* propellant production, the scientific return on future unmanned missions to Mars can be greatly improved. As an example, the scientific return on this mission is increased since data is taken in two locations, the initial landing site and the landing site after the hop. Thus, our knowledge of the Martian environment would definitely increase if a single vehicle could do numerous hops. However, the landing vehicle would be extremely massive if all the fuel for each jump must be brought from Earth. *In situ* propellant production decreases the overall mass of a spacecraft because the propellant needed for hopping or returning to Earth does not need to be brought to Mars.

Several options exist for *in situ* propellant production. Of these, methane-oxygen and carbon monoxide-oxygen are the options which have been examined in the greatest detail. For this mission, the methane-oxygen option was chosen for several reasons. The methane system uses the well understood Sabatier reaction of combining carbon dioxide and hydrogen to produce methane and water[1]. Sabatier reactors have been used in industry for many years and typical conversion rates are about 94%[2]. The carbon monoxide system requires either a zirconia electrolyzer, which dissociates carbon dioxide into carbon monoxide and oxygen, or a reverse water-gas shift reactor, which takes carbon dioxide and hydrogen to produce carbon monoxide and water. The zirconia electrolyzer requires a lot of power and is very fragile. Having such a fragile system in the mission increases the possibility of failure. The reverse water-gas shift reactor has typically low efficiencies, around 10%. Much more study needs to be done on increasing the efficiency of the reverse water-gas shift reactor before it can be used in a mission to Mars. A study of using the carbon monoxide option is presented in Appendix A. The methane system has the added advantages that the design is very simple and the methane engines developed could be used on Earth, as well as Mars. As a propellant, methane is a potentially effective rocket fuel. It is

capable of a specific impulse of 385 seconds when burned with oxygen at an optimal oxidizer to fuel (O/F) mass ratio of 3.5. The main disadvantages to the methane system are that some hydrogen needs to be brought from Earth and once it is used up, no more propellant can be produced.

A main concern with the propellant production plant is power. Although different components of the propellant plant may be started at different times, the peak power usage occurs at startup. Accordingly, the choice of an appropriate power source is influenced by this need. Several different power supplies are considered. Solar power and batteries were not considered since they would be unduly massive just to satisfy the power requirement of the production plant alone. Only a radioisotope power source is capable of providing the power necessary to run the plant continuously over a period of many months.

This chapter covers the methane propellant production plant components, mass, and power requirements. It also includes a trade study on various power sources.

2.2 METHANE PROPELLANT PLANT

(Karen Mark, Daniel Pasco, Scott Anderson)

Since the Martian atmosphere consists of 95.3% carbon dioxide, methane and oxygen can be easily produced by catalytically converting carbon dioxide and seed hydrogen, brought from Earth, with a Sabatier reactor and a water electrolyzer[1]. The Sabatier reaction is:

$$CO_2 + 4H_2 \rightarrow CH_4 + 2H_2O \qquad \Delta H = -174 \text{ J/kg}$$

The water electrolysis reaction is:

$$2\,H_2O \rightarrow 2H_2 + O_2 \qquad \Delta H = 13.4 \text{ kJ/g}$$

Sabatier reactors have been proven to be reliable through many years of testing and use in various applications throughout the industrial world in large production plants. This includes a Sabatier

unit developed by Hamilton Standard for the space station[1]. The system also has the added benefit that it can be made lightweight and compact.

By these two processes, oxygen and methane are produced at an O/F ratio of 2, which although far from the optimum ratio of 3.5, nevertheless offers a respectable I_{sp} of 344 seconds which is more than adequate for the mission goals. The ballistic jump of this mission requires 47 kg of methane and 94 kg of oxygen to be produced by the Propellant Production Plant (PPP). Methane is produced at a rate of 0.333 kg/day and oxygen is produced at a rate of 0.667 kg/day over a period of 141 days. This requires 11.75 kg of imported hydrogen to be used at a rate of 0.0833 kg/day, but 16.75 kg are brought to Mars to account for losses due to boiloff.

The total propellant production rate of this plant is 1 kg/day. This production rate was chosen, because it allows this mission to use a breadboard design by Robert Zubrin of Martin Marietta to fulfill the production rate[2]. This cuts down on the amount of development and thus the cost that will be needed for the propellant production plant. In order to attain a higher mass flow rate, a second water electrolyzer would be required. This would increase the power required by the PPP by 150 W. This makes the total power requirement for the spacecraft to be more than its radiators could handle and thus is unfeasible. Fortunately, a higher mass flow rate is not required to keep production within a limit that was set at 180 days. This limit was set to decrease the chance of failure from exposure on Mars for an extended period of time. The 141 days of production is well under the limit and thus keeps the chance of failure low.

The schematic and configuration of the PPP are presented in Figs. 2.1 and 2.2. After the Martian air is passed through a filter, it is compressed and sent to a storage tank. Then, the compressed carbon dioxide from this tank is pumped to the Sabatier reactor to produce water and methane. An electrolyzer is used to dissociate the water into oxygen and hydrogen. The oxygen and methane are liquefied and stored. The hydrogen from the electrolyzer is recycled back into the Sabatier reactor. Trace gases are vented after the methane is liquefied.

First, the filter must remove the majority of the dust and sand particles or any other debris from the Martian air entering the plant. Sand and dust could damage the plant and their presence could lead to impurities in the propellant. The filter must be lightweight and not have moving parts.

The output of the Sabatier reactor is gaseous; thus a condenser is needed to liquefy the water vapor. The condensate is then sent to an electrolyzer to separate the water into hydrogen and oxygen.

Other components needed to run the plant are: compressors, pumps, heat pipes, valves, tubing, and pressure and temperature sensors. The PPP also needs a controls package as well as a refrigeration system to maintain the oxygen and methane at cryogenic temperatures for the duration of the lander's stay on the Martian surface. The power system to run the propellant production plant, as well as the other systems of the vehicle are discussed later in this chapter.

2.2.1 Sabatier Reactor
(Scott Anderson, Karen Mark, Dan Pasco)

Once the carbon dioxide from the Martian atmosphere is compressed, it is reacted with imported seed hydrogen to produce water and methane by the methanation reaction, also known as the Sabatier reaction:

$$CO_2 + 4H_2 \rightarrow CH_4 + 2H_2O \qquad \Delta H = -174 \text{ J/kg}$$

The Sabatier reaction is exothermic, which means that no energy is required to drive it. It also means that at lower temperatures, the reaction produces greater yields. Heaters are still needed to raise temperatures to a level at which the reaction will run spontaneously in the presence of a catalyst. Thus, the temperature at which the reaction is run must be a comprise between an increase in yield and decrease in the effectiveness of the catalyst in aiding the reaction. Since

5 moles of gas are reacted to form 3 moles, higher pressures drives the reaction to the right. Thus, with higher pressures, the reaction will produce greater yields. The pressure at which the reaction is run must be a compromise between an increase in yield and the compression required to raise the pressure from Mars ambient of 8 mbar.

This reaction occurs spontaneously in the presence of a nickel-nickel oxide catalyst at 450 K and 1 bar[3]. Some heating will be required to get the chamber up to that temperature. However, there are many problems associated with using a nickel catalyst. Some of these are that the equilibrium constant, K, shifts if operating pressures and temperatures are not maintained within a very narrow range and that toxic carbonyl products can be formed[2]. Ruthenium-on-alumina catalysts are recommended because the reaction rates are much higher, operation can continue at temperatures as low as 150° C, and no toxic gases are produced. This catalyst has the advantage of being able to produce higher yields, because it can run with lower temperatures, as described above. Ruthenium-on-alumina catalysts have also a demonstrated shelf life of greater than 12 years[1]. Although ruthenium-on-alumina is more expensive than a nickel catalyst, only a small amount (1 kg) is needed to drive the reaction and the total estimated cost of ruthenium is about $300[3].

The Sabatier reaction chamber is a 5 cm diameter cylinder with two main sections along its axis. A diagram of the Sabatier reactor can be seen in Fig. 2.3. The first section is a mixing chamber. It has been determined that a 5 cm length would assure complete input gas mixing using gas diffusion alone[2]. The second section contains the ruthenium-on-alumina catalyst. Based on analytical model using published data for ruthenium-on-alumina catalyst, a 7 cm reaction length is required to get complete reaction of the carbon dioxide and hydrogen[2]. For a safety factor, a mixing length of 7 cm and reaction length of 10 cm was chosen for a total reactor length of 17 cm.

The Sabatier reaction chamber has heaters wrapped around it along its length. These heaters are used to raise the temperature of the reaction chamber to 150° C, which is needed for the

reaction to take place in the presence of the catalyst. These heaters initially require 200 W_e to heat the chamber. This power requirement is the startup power for the Sabatier reactor. While the reaction gives off energy, energy is also lost to the environment around the reactor. Thus, a small power requirement (0-10 W_e) may need to be given to the heaters to maintain a constant temperature.

The Sabatier reactor is oriented vertically, so that any water condensing in the reactor will drain out. The carbon dioxide and hydrogen enter reactor at the top and the water and methane leave at the bottom. Also, the heat exchanger is placed below the Sabatier reactor, with the condenser below it, so any more condensing water will end up in the condenser[2].

A Sabatier reactor produced by Packard Instruments will be suitable for the propellant production plant[3]. This reactor is available at a mass of 3 kg and is relatively small (2883 cm^3), using the Ruthenium catalyst, as suggested. Testing by Robert Zubrin of Martin Marietta shows that the Sabatier unit is capable of converting 94% of the carbon dioxide and hydrogen to methane and water[2].

2.2.2 Electrolyzer

(Daniel Pasco, Scott Anderson)

The water electrolyzer is used to dissociate water into diatomic hydrogen and oxygen in the following reaction:

$$2\,H_2O \rightarrow 2H_2 + O_2 \qquad \Delta H = 13.4\ kJ/g$$

Packard Instruments in Chicago, Illinois manufactures a solid polymer electrolyte (SPE) electrolyzers with a mass of 3 kg that can produce up to 0.0833 kg/day of hydrogen and 0.667 kg/day of oxygen[2]. SPE electrolyzers are in a very advanced state of development, with over 7 million cell-hours of operation[1]. The SPE electrolyzer has a rated power requirement of

160 W_e (tests indicate that the requirement is closer to 150 W_e)[2] and occupies a cylindrical volume of 514 cm^3. It is 25.4 cm long and has a diameter of 5 cm.

2.2.3 Filter

(Karen Mark, Scott Anderson, Jason Andrews)

The Martian atmosphere contains wind-blown dust and sand particles[4]. Thus, a filtration system is needed to remove the particles from the Martian air before it enters the plant. In order for a filter to be effective, it must be able to remove particles of size down to a micron. To fulfill this requirement, pleated filter cartridges and membrane filters are used. As the filter will eventually become clogged with dust, multiple filters are needed. Two pleated filter cartridges are placed in parallel ahead of the compressor and two membrane filters are placed in parallel after the compressor. In this configuration, only one of the filters in parallel is used at any one time. The filter cartridges are rated to remove particles down to 2 microns and the membrane filters are rated to remove particles down to 0.1 microns[5]. Differential pressure sensors are used to indicate how much dust has accumulated in the filter. When the mass flow rate is decreased significantly, a simple valve reroutes the flow to the unused filter.

To further reduce the dust intake, it is important to pay attention to atmospheric considerations. During high winds and dust storms the region directly above the surface up to 1 m is full of blowing dust. The ingestion of this dust should be reduced as much as possible to limit the work of the filtration system. As a result, we designed an intake device that consists of a periscope and a weathervane. Once the MLVH lands a small 2 inch diameter periscope is extended such that it rises just above the height of the lander. Attached to this periscope is a weathervane that is deflected in the direction of the prevailing wind. The weathervane ensures that in high winds, when dust ingestion is of great concern, that the atmospheric intake is sufficiently above the surface and shielded from the prevailing winds such that direct dust intake is minimized. A schematic diagram of the intake device can be seen in Fig. 2.4.

2.2.4 Compressor
(Karen Mark)

The atmospheric pressure on Mars, as measured at the two Viking sites, varied between 7 and 10 mbar[6]. A compressor is a necessary part of the PPP since the Sabatier reactor requires the inlet gases to be about 1 bar [7]. Assuming an average pressure and temperature of 8 mbar and 220 K on the Martian surface, a three-stage reciprocating compressor with interstage cooling and graphite lubrication can be used. The compressor is modeled as an isentropic process, assuming carbon dioxide is an ideal gas. Carbon dioxide can be assumed to be an ideal gas since the compressibility factor is almost 1 at very low pressures.

Figure 2.5 shows a schematic design of the compressor. Each stage has a compression ratio of 5 to 1, giving an overall compression ratio of 125 to 1. The system is cooled between each stage to reduce the power requirement and ensure that the cylinder temperatures do not exceed 450 K[8]. The atmospheric gases between each stage are cooled by heat pipes transferring heat to passive radiators. In designing the compressor, a trade-off must be made between reducing the radiator area and the exit temperature. The radiator area required is:

$$Area = \frac{q}{\varepsilon\sigma\left(T_r^4 - T_m^4\right)} \tag{2.1}$$

where: q = heat transfer rate (W)

ε = emissivity of radiator = 0.91

σ = Stefan-Boltzmann constant = 5.67×10^{-8} W/m^2·K

T_r = temperature exiting radiator, entering the next cylinder (K)

T_m = average Mars ambient temperature = 220 K

The heat transfer rate, q, can be found after applying the conservation of energy principle on each stage of the compressor:

$$q = w - m_{fr}\, Cp\, (T_r - T_i) \tag{2.2}$$

where: w = isentropic work done by compressor (W)

$$w = \frac{kRT_i}{k-1}\left[(CR)^{\frac{k-1}{k}} - 1\right] \tag{2.3}$$

m_{fr} = mass flow rate of gas (kg/s)

T_i = temperature entering the cylinder (K)

T_r = temperature entering the next cylinder, after exiting the radiator (K)

C_p = average specific heat of carbon dioxide between T_r and T_i

Figure 2.6 shows a plot of gas temperature entering the second and third cylinders and leaving the compressor versus intercooler radiator area. Note that the temperature leaving the compressor is fairly constant at 350 K as long as temperatures entering the second and third piston do not go above about 250 K. Thus, the total intercooler radiator area is only 0.162 m^2 if the temperature of the gas leaving the compressor is kept to about 350 K. The temperatures entering the second and third cylinder are 235 K and 245 K, respectively for a radiator area of 0.162 m^2. With these temperatures, the total isentropic work done by the compressor is calculated to be 2.86 W.

The size of the compressor is set by the volume of each cylinder, assuming a constant stroke length for each stage. A trade-off must be made between minimizing the volume and reducing the wear on the motor. Figure 2.7 shows the swept volume of each cylinder with the required stroke length and also compares how rotation rate (RPM) of the crankshaft varies with

stroke length. Note that the volume of each stage is at a minimum when the rotation rate is at a maximum. The volume of the first stage must be minimized since it is the largest due to the low density of the Martian atmosphere. Both the volume of the first stage and the rotation rate are extremely sensitive to the stroke length; changing the stroke length from 5 cm to 10 cm causes the volume and rotation rate to increase by almost a factor of two. An optimum occurs where the two curves on the graph intersect, at about a stroke length of 9 cm and 7 rpm. After this point, a relatively small decrease in the rotation rate would be accompanied by a large increase in the volume of the first stage. With such a small rotation rate, each stage compresses the gases very slowly, causing there to be times when there would be no gas flowing to the Sabatier reactor. The oscillations in the mass flow rate are evened out by pumping the output gases to a storage tank to be drawn out for use in the Sabatier reactor.

The estimated mass of the compressor and intercooler is 10 kg. The cylinders can be made from very lightweight metals like Aluminum while the intercooler radiator can be made with the same materials as the radiators used for the power supply. The electrical power needed is approximately 20 W_e, assuming an overall efficiency of 15%. The dimensions of the compressor are 25.2 x 12 x 27 cm (l x w x h) without the motor, assuming the radius of the first cylinder is 5 cm.

2.2.5 Condenser
(Karen Mark)

A condenser immediately follows the Sabatier reactor to liquefy the water vapor. The temperature and pressure of the gases coming out of the Sabatier reactor are about 350 K and 1 bar respectively[2]. The condenser liquefies the water vapor by rejecting heat to the radiator system through heat exchangers. The water vapor will condense out as the temperature in the condenser approaches 0°C. The condenser mass is estimated to be about 3 kg.

2.2.6 Propellant Liquefaction
(Karen Mark)

The methane and oxygen produced by the propellant production plant must be liquefied for storage in the propellant tanks. The propellants from the condenser and electrolyzer enter the liquefaction system at approximately the same pressure and temperature of 1 bar and 300 K. The minimum work to liquefy methane and oxygen from this initial condition is 1,110 kJ/kg and 638.4 kJ/kg respectively[8]. A total of 47 kg methane and 94 kg oxygen are produced over a period of 141 days, thus the liquefaction of methane requires 4.3 W_e and that of oxygen requires 4.93 W_e. Accordingly, the total power required for liquefaction is 9.23 W_e. Typical efficiencies of liquefaction cycles vary from 30% to 75%. Assuming a median efficiency of 50%, the total power required is 18.5 W_e. The total mass of the liquefaction system is about 15 kg.

The typical liquefaction cycle used in industry is the Joule-Thomson expansion cycle. The Joule-Thomson expansion cycle is modeled to be an isenthalpic, closed cycle system. (See Fig. 2.8.) Input gases are pumped through a heat exchanger and then throttled to bring the gases to a liquid-gas mixture. Trace gases from the Martian atmosphere are then vented after the methane is liquefied so that they do not reduce the performance of the rocket. The heat exchanger is assumed to be an all-metal assembly consisting of counter flowing annular passages. Neon gas, the working fluid of the refrigeration cycle, is run through the heat exchanger to satisfy the heat transfer requirement to liquefy both the oxygen and methane.

2.2.7 Propellant Refrigeration and Storage
(Karen Mark, Scott Anderson)

Since the lander will be on Mars for an extended period of time, refrigeration and storage is required for the propellants, because they must be stored at temperatures much lower than the average Martian temperature of 220 K in order to keep them in the liquid state.

One problem that occurs with storage of cryogens is boiloff in the tanks. Because of the temperature difference between the tank and the local environment, there is a net heat flux into the tanks which causes the propellants to boil. This results in a build up of pressure which must be relieved by venting to the atmosphere. Thermal protection is required to reduce the heat flux into the tanks to minimize this boiloff.

Multilayer Insulation (MLI) has been chosen to insulate the tanks because of its very low thermal conductivity (from 32 - 70 μW/m K). MLI is used in most cryogenic systems built for use in space. The two primary kinds of MLI that are commercially available are an insulation composed of alternating layers of metal foil and woven material and an insulation composed of layers of Mylar with metal coatings alternating with optional layers of padding[10].

Aluminized Mylar without padding is the lightest insulation, with a density of 38 kg/m^3[8]. It has an effective thermal conductivity of 32 μW/m K. However, the thermal conductivity could significantly increase since the launch loading would apply a large force to the thin sheets, effectively increasing the contact points. Some woven materials in between each layer would alleviate that concern. The insulation chosen for all the tanks is aluminized mylar with silk net. This additional padding raises the density of the MLI to 45 kg/m^3 and its thermal conductivity to 45 μW/m K[11], which are acceptable.

Methane and oxygen can both be stored at 90 K at 0.2 bar and 1 bar, respectively, so that one refrigeration system may be used. Assuming that the MLI can only partially reduce the heat flux, refrigeration is used to completely eliminate the boiloff of the propellants.

The two methane tanks and two oxygen tanks are each covered with a 1 cm layer of MLI around them. Each tank has a diameter of 46 cm without the MLI. To be conservative in the heat transfer analysis, each tank can be taken as a sphere alone in an environment with a background temperature of 321 K, which is the temperature of the power system's radiators. The metal tank walls provide essentially no heat transfer resistance compared to the MLI. Thus, the inner tank

radius, where the temperature will be 90 K, is 23 cm and the outer surface radius is 24 cm. The heat transfer equations are as follows[12]:

$$q = \frac{4}{3}\pi\sigma\varepsilon r_s^3 (T_s^4 - (321K)^4) = \frac{4\pi k((90K) - T_s)}{\frac{1}{r_i} - \frac{1}{r_s}} \tag{2.4}$$

where: q = heat transfer rate

σ = Stefan-Boltzmann constant (5.67×10^{-8} W/m^2·K^4)

ε = emissivity

r_s = outer surface radius

T_s = MLI surface temperature

k = thermal conductivity of MLI

r_i = inner tank radius

The rate of heat transfer into each tank is 0.65 W_{th}. Thus, the total heat transfer for the four tanks is approximately 2.6 W_{th}. The actual heat transfer rate will not be quite this high as the tanks will interact with each other and the Martian atmosphere and not solely with the radiators.

A single stage reverse turbo Brayton refrigerator, currently under development by Creare will be able to compensate for the heat transfer to prevent boiloff[13]. The system has a mass of 14 kg and consumes 50 W_e of power to cool at a rate of 3 W_{th} at 90 K[14]. The Creare system was chosen over a conventional Gifford-MacMahon refrigeration system because the Creare system is three times more efficient. The system has been tested and run continuously for nine years without mechanical failure[3].

In order to produce methane and oxygen on Mars, hydrogen must be imported from Earth. Unfortunately, hydrogen is difficult to store. A refrigeration system for hydrogen is prohibitive due to its high mass and large power requirements. This is because the liquid hydrogen must be

stored at very low temperatures, around 20 K. Thus, for this mission, the hydrogen will not be actively refrigerated and will be allowed to boiloff. The optimum storage conditions for the hydrogen for our mission is 23 K and 25 bar. These conditions define the optimum, because at 23 K and 25 bar the hydrogen has a high density of 71.88 kg/m^3. This keeps the volume and surface area of the tank down, which saves space and reduces the heat transfer. At higher and lower storage temperatures than 23 K, the heat transfer is higher than at 23 K. The overall size of the hydrogen tank is limited by the volume in the spacecraft which it can occupy. The tank is spherical, with a diameter of 76 cm. A 10 cm thickness of MLI is used to insulate the tank. This results in a heat transfer rate of 0.17 W. The tank can hold 16.65 kg of hydrogen initially. Approximately 4.9 kg of hydrogen boils off during the five and a half months of transit to Mars. This leaves 11.75 kg of hydrogen for propellant production upon arrival at Mars. The hydrogen which boils off while on Mars is tapped off for use in the Sabatier reaction, resulting in no additional losses after arrival on Mars.

2.2.8 Alternative Components
(Karen Mark, Scott Anderson)

Many components of the methane propellant plant raise concerns over reliability, effectiveness, and cost. The main concerns are with the CO_2 compressor and the refrigeration system. The compressor has received attention since it is a rotating machine which must run unattended for 141 days.

One way to increase the reliability of the mechanical compressors is to replace them with adsorption compressors. Adsorption pumps have been developed for nitrogen and hydrogen as part of Joule-Thomson refrigerators. These pumps operate on the principle that the gas can be adsorbed on materials to increase its density to that of a liquid. The gas then exits the pump at a higher pressure and temperature after being desorbed with waste heat from a power source. Since the rotating machinery of a conventional compressor is replaced by simple check valves and heat

switches, the adsorption compressors are highly reliable[15]. Through either chemical or physical adsorption, the compressor pressure ratio can be as high as 1000 in a single stage[16]. Thus, this kind of compressor would be able to replace a multistage mechanical compressor and be more reliable. The use of such a compressor should be investigated further.

Along the same lines as with the adsorption compressors, sorption refrigeration is a method of cooling wherein gas is compressed by adsorption techniques and then passed though an expansion valve to create cooling. The compressor portion of a sorption refrigerator runs on the same principles as discussed with the adsorption compressors. Sorption refrigeration systems have no moving parts, other than check valves, and thus could eventually have a potential lifetime of decades with virtually no vibration[17].

One way to improve the performance of the hopper is to produce the methane and oxygen at the I_{sp} optimum mass ratio of 3.5 to 1. With the 3.5:1 ratio, the specific impulse is raised to 365 s over the 344 s value at a 2:1 ratio. The additional oxygen needed for this scenario could be produced by a reverse water gas shift reactor, which combines carbon dioxide and hydrogen to form carbon monoxide and water. This water could be electrolyzed to form additional oxygen. A problem with the reverse water gas shift reactor is that an efficient reactor has yet to be built. Another possibility is to use a high temperature zirconia electrolyzer to separate the oxygen from the carbon dioxide directly without having to use seed hydrogen. There are concerns, however, that an oxygen-depleted zone can grow and lead to electrolyzer failure[15]. The simplest alternative is to bring more seed hydrogen and operate the Sabatier/electrolysis plant for a sufficiently long time to produce the required amount of oxygen and vent off the excess methane. However, this requires 75% more hydrogen and thus a larger tank, and also requires propellant production to occur over a period of 230 days, increasing the possibility of system failure. The added complexity and/or decreased system reliability which result from the generation of additional oxygen do not justify the slight improvement gained in specific impulse.

2.3 POWER SYSTEMS
(Norihito Tsuji)

Since Project Genesis requires a relatively large amount of power compared to previous missions to Mars, an efficient, reliable, and cost-effective power source is necessary to lead our mission to success. The following basic design criteria were considered to select the appropriate power system: reliability, availability, survivability, power-to-mass ratio, size, cost, and safety. To supply electric power for long-duration spacecraft, there are two types of power sources: solar and radioisotope systems. The trade study was done on the following power systems and are described sequentially in the next section.

- Solar arrays combined with rechargeable batteries
- Dynamic Isotope Power Systems (DIPS)
- Radioisotope Thermoelectric Generators (RTG)
- Radioisotope Thermophotovoltaic Generators (RTPV)

2.3.1 Solar Arrays and Batteries

The common efficiency for a photovoltaic solar array is at most about 20% with gallium arsenide (GaSb) cells [18], and the solar flux on Mars is at most, only 604 W/m^2 at the equator under dust-free conditions. Because solar arrays can be operated only during the daytime, the energy storage system is required to supply power at night. To estimate the size of this power system, assume that the propellant production takes place at the Viking-1 landing site (22.3^0 N) during Martian spring and summer. Under these conditions, the length of the day is 13.2 hours and the length of the night is 11.5 hours, and the average daytime irradiation is 305 W/m^2 [18]. The MLVH consumes up to 450 W_e, so the required area of a solar array, A_s, is estimated using the following equation:

$$A_s = \frac{P_e}{G\eta} + \frac{P_e t_n}{G\eta t_d} \tag{2.5}$$

Where: A_s = Area of a solar panel

P_e = power generated by a solar panel

G = solar flux on the Martian surface

η = efficiency of a solar panel

t_d = day length

t_n = night length

The first term in the left hand side of the equation represents the area of the solar arrays generating power for the MLVH equipment. The second term represents the area of the solar arrays recharging the energy storage system. According to this equation, the required area with GaAs cells for the solar array is 12.5 m^2. Since the solar array with GaAs cells has specific mass of 1.06 kg/m^2 [18], it would constitute a mass of 13.3 kg.

Among the many types of power storage systems, rechargeable batteries have been one of the most reliable and safe power storage systems in space. Among them, nickel cadmium (NiCd), nickel hydrogen (NiH_2) and nickel metal hydride (NiMH) have high performance. Of these three, NiMH has the highest specific density. Characteristics of NiMH are listed in Table 2.1.

Table 2.1 Characteristics of NiMH.

Specific energy (Wh/kg)	Energy density (Wh/liter)	Power density (W/kg)	Recharge time
80	215	470	15 min for 60% <1 hr for 100%

The mass of the batteries is estimated from the following equation:

$$m_b = \frac{P_e t_n}{\varepsilon D} \tag{2.6}$$

Where: m_b = mass of rechargeable batteries

ε = specific energy of batteries

D = depth of charge (40%)

According to the above equation, the batteries have a mass of 161 kg, and when the solar arrays and the rechargeable batteries are combined, total mass of the power system becomes 174 kg. Although rechargeable batteries are reliable, available, safe and cost-effective, they are a very "heavy" system for this mission compared to other power systems. In contrast, the RTPV has a mass of only 41 kg and provides 464 W_e 24 hours a day.

2.3.2 General-Purpose Heat Source (GPHS)

General-Purpose Heat Source (GPHS) modules are used as a heat supply for many radioisotope power systems. These modules have undergone stringent safety tests, and have flown on the Galileo and Ulysses missions [19]. As shown in Fig. 2.9 [19], Each GPHS module has four $^{238}PuO_2$ fuel pellets, providing a thermal power of 250 W. A pair of pellets is encapsulated in an iridium-alloy cladding, which is in turn covered by an impact shell. The impact shell is employed to help prevent fuel breakthrough in case of hard impact. Two impact shells are contained in an aeroshell which works as an ablator during emergency atmospheric re-entry. To withstand the high temperatures and impact of an accident, fine-weave pierced fabric, a three-dimensional carbon-carbon composite, is used for the impact shell and the aeroshell. Between the impact shell and the aeroshell, a low-density composite of carbon-bonded carbon fibers is used as a high-temperature thermal insulator. It protects the clads from overheating in re-entry and from overcooling during the subsequent supersonic decent [19].

To supply the total of 450 W_e for systems on the MLVH, 26 GPHS modules are required for the RTG, while the DIPS and the RTPV require 9 modules.

2.3.3 Radioisotope Thermoelectric Generators (RTG)

The RTG has been used for many previous missions, and has been a very reliable power supply for decades [8]. The RTG utilizes thermoelectric unicouples that convert heat directly into electricity by using a temperature gradient provided by Pu decay. Because this device is completely passive, it has no moving parts and no mechanical wear. Because the operational temperature of the radiator is high (575 K), it permits a smaller size radiator compared to other radioisotope systems, such as the RTPV (321 K) and the DIPS (295 K). However, the low efficiency of the RTG (6 to 8 %) would require more radioisotope fuel, which drives the cost and mass of the power system higher. For Project Genesis, the RTG would have a mass of 79 kg, and 26 heat source modules would be required.

2.3.4 Dynamic Isotope Power Systems (DIPS)

The dynamic isotope power systems (DIPS) employs a closed Brayton cycle system energized by GPHS. A cycle diagram of the DIPS is shown in Fig. 2.10. The working gas, He-Xe, is heated in the heat source assembly and flows to the turbine where the gas expands and performs work. Afterwards, the gas flows through a recuperator where thermal energy is transferred to gas entering the heat source. The gas then flows through the radiator where it transfers its heat directly to the radiator heat pipes. After being cooled by the radiator, the gas passes through the alternator, cooling it before flowing through the compressor. After compression, the gas is routed through the recuperator again, but this time it receives waste heat from the gas exiting the turbine. From the recuperator, the flow enters the heat source assembly, and the cycle repeats.

Table 2.2 shows the characteristics of the DIPS[20]. Although the DIPS has a high system efficiency, it is very massive compared to the RTPV and requires larger radiators compared to the

RTG. Because the mission requires a power system with high specific energy, the DIPS is not very feasible for this mission.

Table 2.2 Basic characteristics of the DIPS[20].

Compressor inlet temperature, (K)	250
Turbine Inlet Temperature, K	1144
Mission lifetime (yr)	10
Isotope thermal power, EOM (kW_t)	2.07
No. GPHS blocks	8
Gross electrical output, (W_e)	482
Net cycle efficiency, EOM (%)	24.1
Radiation area, (m^2)	12.9
Radiator temperature (K)	295
System mass, (kg)	121.7

2.3.5 Radioisotope Thermophotovoltaic Generators (RTPV)

In the RTPV systems developed by Boeing, thermophotovoltaic (TPV) cells convert infrared radiation emitted by a hot surface to electricity[20]. This technique can yield a conversion efficiency of more than 25%, which is considerably higher than that of the RTG. A schematic of the RTPV is shown in Fig. 2.11, and the layered composition of the RTPV, with two GPHS modules, is shown in Fig. 2.12 [19]. Until recently, Fairchild Space and Defense Corporation was adopting the RTPV for the Pluto Fast Flyby mission planned for launch around the year 2000. A comparison of the RTPV and RTG is given in Table 2.3.

Like the RTG and the DIPS, the RTPV uses GPHS modules. Since the MLVH requires a maximum of 450 W_e, 9 modules are required with the system efficiency of 20.6%. Because the RTPV has a higher efficiency than the RTG, it requires fewer GPHS modules. Therefore, there is

less mass and lower cost. The specific power of the RTPV is 11.0 W/kg, and the total power system including radiators has a mass of only 41 kg.

Table 2.3 Basic characteristics of the RTPV and RTG [19].

	RTG	RTPV
Generator mass (kg)	78.9	41
Number of Heat Source Modules	26	9
Thermal power (W_{th})	6500	2250
Operating Temperature (K)	1326	1210
Radiator Heat pipe (K)	none	321
Output Power (W_e)	455	464
System Efficiency (%)	7.0	20.6
Specific Power (W/kg)	5.7	11.0

TPV cells operate with higher efficiency at lower temperatures. Since its heat rejection temperature is low, the RTPV needs much larger radiator fins than typical RTGs. The RTPV, with a 20.6% system efficiency, requires a radiator temperature of 321 K. Although the efficiency of the RTPV can be as high as about 27% with lower radiator temperature, a larger radiator would be required, increasing total mass. The required area of the radiator is estimated using the following equations

$$Q = P_{th}(1-\eta) \tag{2.7}$$

$$A = \frac{Q + \alpha G A_{solar}}{\varepsilon\sigma\left\{F_{surf}(T_{rad}^4 - T_{surf}^4) + F_{sky}(T_{rad}^4 - T_{sky}^4)\right\}} \tag{2.8}$$

where:

Q = wasted heat from RTPV

P_{th} = thermal power of RTPV (2500 W_{th})

η = efficiency of RTPV = (20.6 %)

A = required area of the radiator

α = solar absorbtivity of radiator panels [21] (0.22)

G = solar flux = solar flux on the Martian surface

A_{solar} = maximum area of the radiator under direct sunlight (4.1 m^2)

ε = IR emissivity of radiator panels [21] (0.91)

σ = 5.67×10^{-8} $W/m^2 \cdot K$

F_{surf} = view factor of ground to radiator (0.28)

F_{sky} = view factor of sky to radiator (0.72)

T_{rad} = radiator operating temperature (321 K)

T_{surf} = surface temperature of Mars

T_{sky} = sky temperature of Mars

Two worst case situations are considered as listed in Table 2.4. At the worst case, the area of the radiator under direct sunlight is at the maximum, which occurs when the sun is directly above the MLVH. Therefore this area is approximately a plan area of the MLVH.

Table 2.4 Two worst situations of the radiator.

Case	Solar flux (W/m^2)	Sky Temperature (K)	Ground Temperature (K)	Required radiator area (m^2)
Clear day (most)	600	180	300	6.0
Global dust storm	160	235	235	5.0

According to the above equations, the RTPV will require a radiator area of 6.0 m^2 To provide an adequate margin of safety for heat rejection, actual total area of radiator is 6.5 m^2. The radiator has heat pipes inside of it and rejects heat through a face sheet. As shown in Fig. 2.13, the structure of the radiator is reinforced by aluminum honeycomb which is covered on both sides by aluminum face sheets. The face sheet on the emitting side is covered with a sheet of a graphitized carbon-carbon composite, which distributes the heat from the heat pipes over the width of the fins and also provides a high emissivity surface [19]. The exterior surface of the radiator is coated with titanium dioxide, which has a solar absorbtivity of 0.22 and an infrared emissivity of 0.91 [21]. The inside

face sheet is polished aluminum, covered with multilayer insulation (MLI) to minimize heating of MLVH components on board. MLI has a thermal conductivity of 4.5 x 10^{-5} W/m·K and a density of 45 kg/m^3 as discussed in Section 2.2.7. The rate of heat transferred through MLI is calculated from:

$$q = kA\frac{T_1 - T_2}{L} \tag{2.9}$$

where: q = the rate of heat transferred

k = thermal conductivity of MLI (4.5 x 10^{-5} W/m·K)

A = area of radiator (6.5 m$^{2)}$

T_1 = heat pipe temperature (321 K)

T_2 = inside temperature of MLVH (220 K)

L = thickness of MLI (0.01 m)

According to the above equation, 2.8 W of heat are transferred to the interior of the MLVH. This small amount of heat is expected to escape via radiation and convection from an opening provided on one side of the MLVH.

Dust accumulation could be a potential problem for the radiator. During global dust storms, several monolayers of dust are expected to accumulate, which could seriously reduce the performance of the radiator [22]. However, small vibrations from moving parts, such as the compressor and refrigerator of the PPP, may help shake the dust off the radiator. Having 80% of the radiator inclined at an angle of 46° and the rest inclined at an angle of 70° to the surface (see Section 3.2) also minimizes the accumulation of dust layers on the radiator.

Wind-blown dust is not likely to cause significant abrasion to the radiator, since the size of the dust particles does not typically exceed about 10 μm. However, saltation of sand-sized particles occurs close to the surface during dust storms. The particles are picked up as high as

20 cm above the surface and may cause abrasion to low lying components. This problem is circumvented by designing the landing gear height to be of the order of 1 m.

Although the RTPV requires a larger radiator area than an RTG system, the RTPV is the power system of choice because it has the advantage of having a lighter mass, higher specific energy, and lower cost compared to the other power systems presented above.

For this mission, four RTPV units are used and provide a total of 464 W_e. Three RTPV units have two GPHS modules and provide 103 W_e, and one RTPV unit has three GPHS modules and supply 103 W_e. Total mass of the RTPV including the radiator is 40.8 kg, and total power system including a bus controller, which regulates power distribution to the onboard equipment, is 54.4 kg. The mass inventory of the RTPV is shown in Table 2.5.

Table 2.5 Mass breakdown of RTPV.

Component	Mass(kg)
GPHS Modules	
Fuel (PuO_2)	5.35
Cladding (Ir)	2.12
Graphitics	5.50
Canister (Mo)	2.80
Multifoil Insulation (Mo)	0.40
Converter Elements, etc.	0.76
Housing for GPHS, etc.	2.40
Radiator	18.50
Multilayer Insulator (MLI)	2.92
TOTAL	40.75

2.4 SUMMARY

(Daniel Pasco, Karen Mark, Scott Anderson)

The current mass and power budgets required by the propellant production plant appear in Table 2.6. The total mass of the plant is 50 kg and the total steady state power requirement is 240 W_e. It should be noted that this estimate is conservative; an efficient compressor to handle low mass flow rates on the Mars surface has yet to be developed.

Table 2.6 Propellant plant mass and power budget.

Component	Mass (kg)	Steady state power (W)	Sabatier startup power (W)
Filter system	1	0	–
Pumps/Compressors	10	20	–
Sabatier reactor	4	0–10	200
Water electrolyzer (SPE)	3	150	–
Condenser	3	0	–
Liquefaction system	15	20	–
Refrigerator	14	50	50
TOTAL	50	240–250	250

NOMENCLATURE

A	Area (m^2)
A_s	Area of solar panel (m^2)
A_{solar}	Maximum area of the radiator under direct sunlight (m^2)
α	Solar absorbtivity
C_p	Specific heat at constant pressure (J/kg·K)
D	Depth of charge (%)
DIPS	Dynamic isotope power system
ε	Emissivity
ε	Specific energy of batteries (Wh/kg)
F_{sky}	View factor of sky to radiator
F_{surf}	View factor of ground to radiator
G	Solar flux (W/m^2)
GPHS	General purpose heat source
ΔH	Heat of reaction (J/kg)
I_{sp}	Specific impulse (s)
k	Thermal conductivity (W/m·K)
K	Equilibrium constant
L	Thickness (m)
m_b	Mass of rechargeable batteries (kg)
m_{fr}	Mass flow rate (kg/s)
MLI	Multilayer insulation
MLVH	Mars landing vehicle/hopper
η	Efficiency
O/F	Oxidizer to fuel

P_e	Power generated (W)
P_{th}	Thermal power of RTPV (W)
PPP	Propellant production plant
q	Heat transfer rate (W)
Q	Wasted heat from RTPV (W)
r_i	Inner tank radius (m)
r_s	Outer surface radius (m)
RTG	Radioisotope thermoelectric Generators
RTPV	Radioisotope thermophotovoltaic Generators
SPE	Solid polymer electrolyte
σ	Stefan-Boltzmann constant (5.67×10^{-8} W/m^2·K^4)
t_d	Day length (s)
t_n	Night length (s)
T_i	Temperature entering the cylinder (K)
T_m	Average Mars ambient temperature (K)
T_r	Temperature exiting radiator, entering the next cylinder (K)
T_{rad}	Radiator operating temperature (K)
T_s	MLI surface temperature (K)
T_{sky}	Sky temperature of Mars (K)
T_{surf}	Surface temperature of Mars (K)
T_1	Heat pipe temperature (K)
T_2	Inside temperature of MLVH (K)
TPV	Thermophotovoltaic
w	Isentropic work (J)

REFERENCES

1. Zubrin, R.M., "*In Situ* Propellant Production: The Key Technology Required for the Realization of a Coherent and Cost-Effective Space Exploration Initiative," AIAA Paper No. 91-668, 42nd Congress of the International Astronautical Federation, Montreal, Canada, October 5-11, 1991.

2. Zubrin, R., Price, S., Mason, L., and Clark, L., "Mars Sample Return With In Situ Resource Utilization," NASA Technical Manual, January 1994.

3. Zubrin, R., Martin Marietta, Denver, CO, Personal Communication, March 1994.

4. Gaier, J.R., and Perez-Davis, M.E., "Effects of Martian Dust on Power System Components," NASA Technical Report N91-2706, Sand and Dust on Mars, Feb. 4-5, 1991.

5. Washburn, M., Calhoun and DeJong, Inc., Seattle, WA, Fax transmittal, May 18, 1994.

6. Tillman, J., Department of Atmospheric Sciences, University of Washington, Seattle, WA, Personal Communication, Feb. 15, 1994.

7. Kleiner, G.N. and Cusick, R.J., "Development of an Advanced Sabatier CO_2 Reduction Subsystem," ASME Publication 81-ENAs-11, 1981, pp. 1-7.

8. "Project Hyreus: Mars Sample Return Mission Utilizing In Situ Propellant Production," AA420/421 Space Systems Design, NASA/USRA Advanced Design Program, Department of Aeronautics and Astronautics, University of Washington, Seattle, WA, June 1993.

9. Bruckner, A. P., Nill, L., Schubert, H., Thill, B., and Warwick, R., "Mars Rover Sample Return Mission Utilizing In Situ Production of the Return Propellants," AIAA Paper No. 93-2242, AIAA/SAE/ASME/ASEE 29th Joint Propulsion Conference, June 28-30, 1993, Monterey, CA.

10. Kaganer, M.G., Thermal Insulation in Cryogenic Engineering, 1966, pp. 116-120.

11. Zubrin, R.M., Martin Marietta, Denver, CO, Personal Communication, May 11, 1994.

12. Incropera, F.P and DeWitt, D.P., Fundamentals of Heat and Mass Transfer, 3rd ed., John Wiley and Sons, New York, NY, 1981, pp. 104, 815.

13. Swift, W., and Sixsmith, H., "Performance of a Long Life Reverse Brayton Cryocooler," Creare Incorporated, October 1, 1993.

14. Thomas, P., Philips Laboratory, Edwards AFB, CA, Personal Communication, May 19, 1994.

15. Frisbee, R.H., French Jr., J.R., and Lawton, E.A., "A New Look at Oxygen Production on Mars- In-Situ Propellant Production (ISPP)," AIAA Paper No. 87-0236, AIAA 25th Aerospace Sciences Meeting, Reno, NV, January 12-15, 1987.

16. Frisbee, R.H., "Mass and Power Estimates for Martian In-Situ Propellant Production Systems," Jet Propulsion Laboratory Report No. D-3648, October 1986.

17. Jones, J.A., "Sorption Cryogenic Refrigeration - Status and Future," International Cryogenic Materials Conference, Batavia, IL, June 14-18.

18. Research and Engineering Division of Boeing Defense & Space Group. "Thermophotovoltaic Thermal-to-Electric Conversion Systems Report," JPL Contract No. 959595, December 20, 1993.

19. Schock, A., Mukunda, M., Or, T., Kumar, V., and Summers, G., "Radioisotope Thermophotovoltaic (RTPV) Generator and Its Applicability to an Illustrative Space Mission," Fairchild Space and Defense Corporation, Germantown, MD, February 14, 1994.

20. Johnson, R.A. and Stadnik, A.G., "Compact, Long-lived Dynamic Isotope Power Systems for the Exploration of Space," Intersociety Energy Conversion Engineering Conference-90, August 12-17, 1990, Vol. 1, pp.216-221.

21. Wolfe, W.L., and Zissis, G.J., Eds., *The Infrared Handbook,* Donabedian, M., "Cooling Systems," Office of Naval Research, Department of the Navy, Washington, DC 1978.

22. Haberle, R. M., McKay, C. P., Gwynne, O. E., Atkinson, D. H., Appelbaum, J., Landis, G. A., Pollack, J. B., Zurek, R. W., and Flood, D. J., "Atmospheric Effects on the Utility of Solar Power on Mars," *Resources for Near-Earth Space*, University of Arizona Press Box, May 1992.

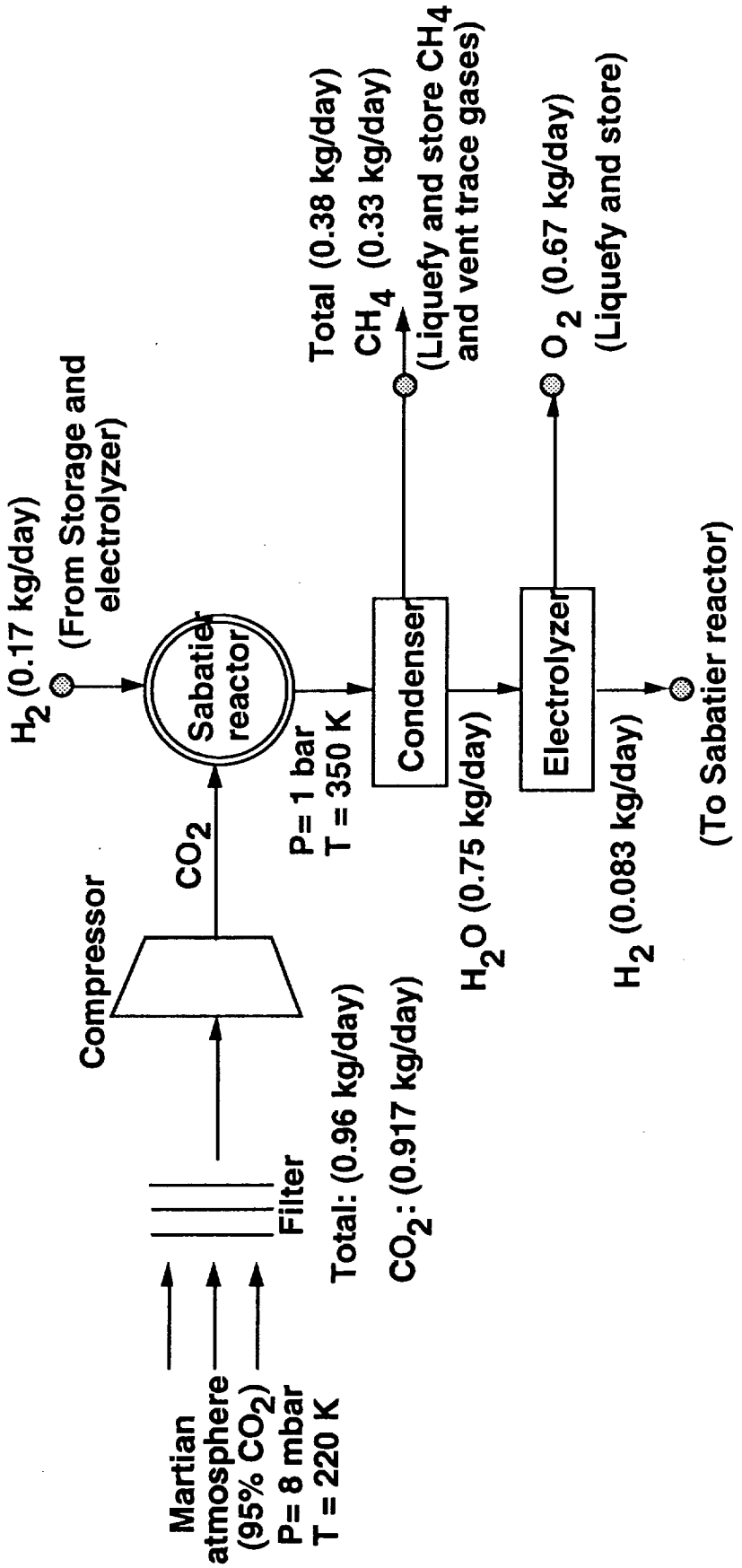

Fig. 2.1 Methane propellant production plant schematic.

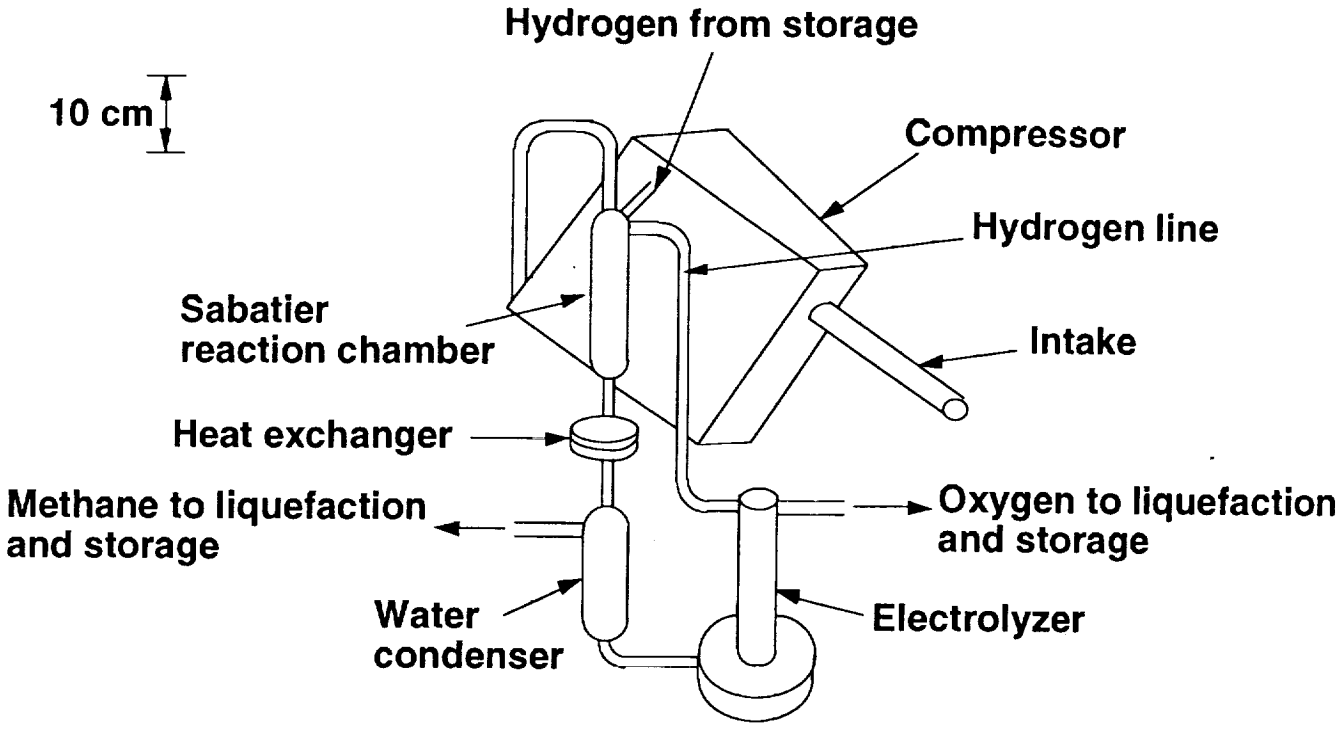

Fig. 2.2 Methane propellant plant configuration.

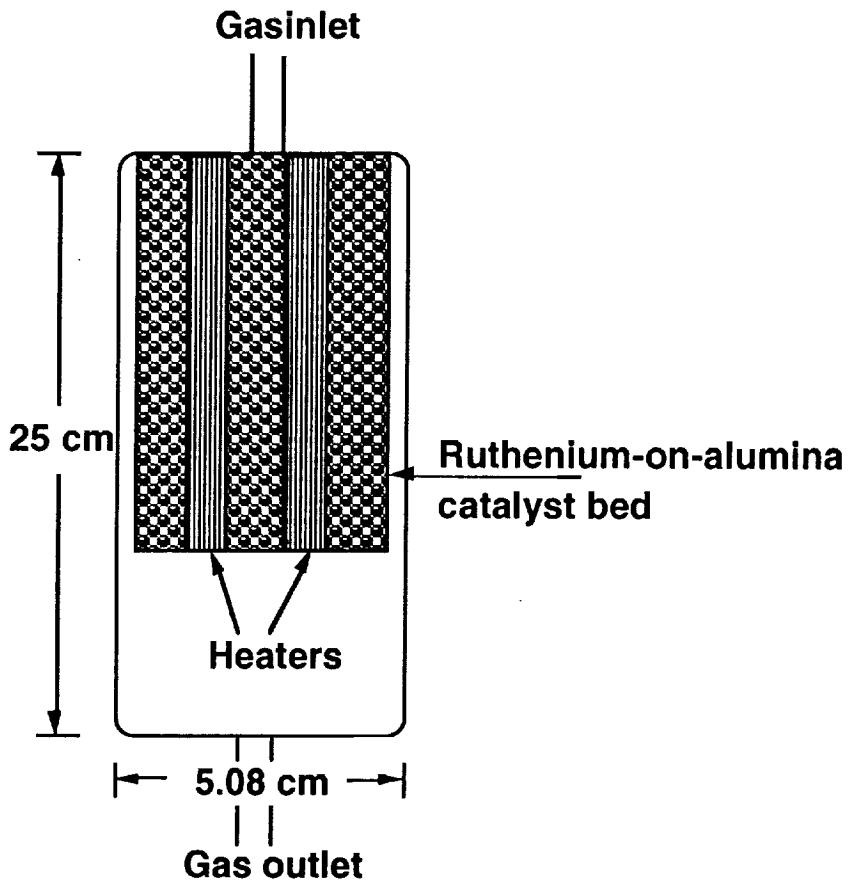

Fig 2.3 Schematic of Sabatier reaction chamber.

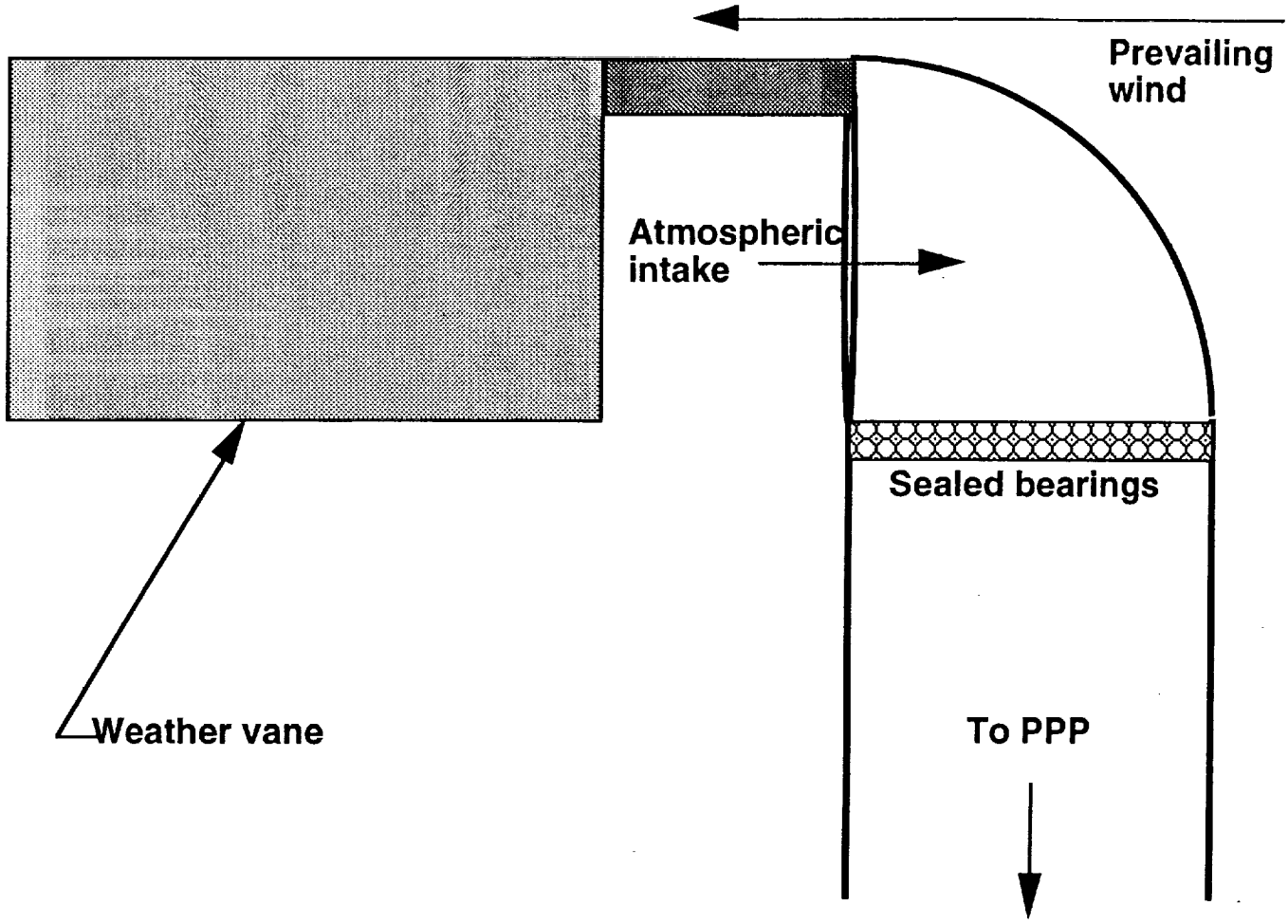

Fig. 2.4 Schematic of PPP filter intake device.

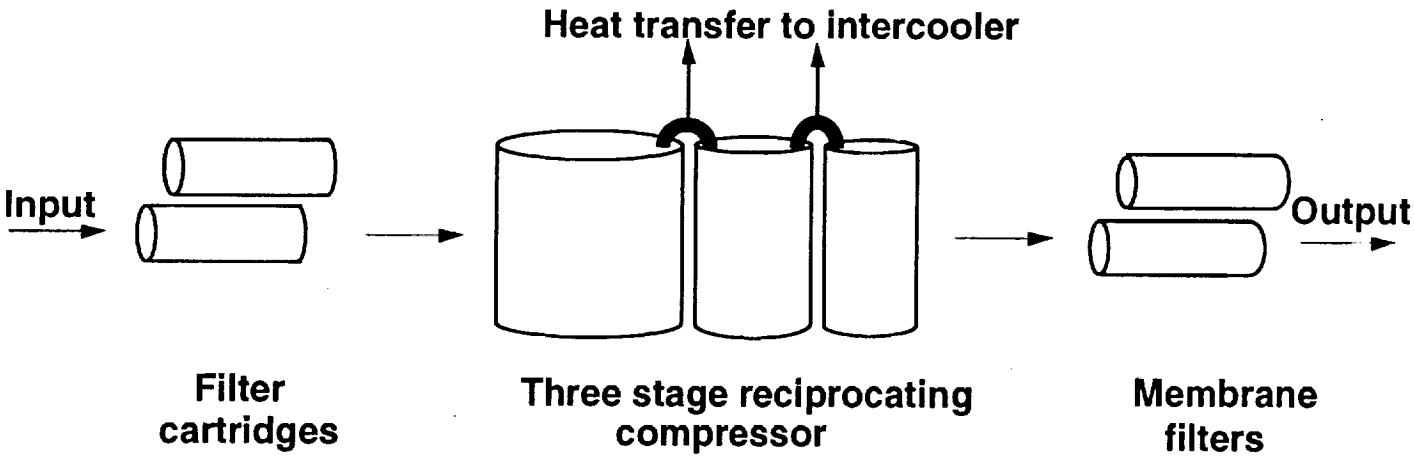

Fig. 2.5 Compressor schematic.

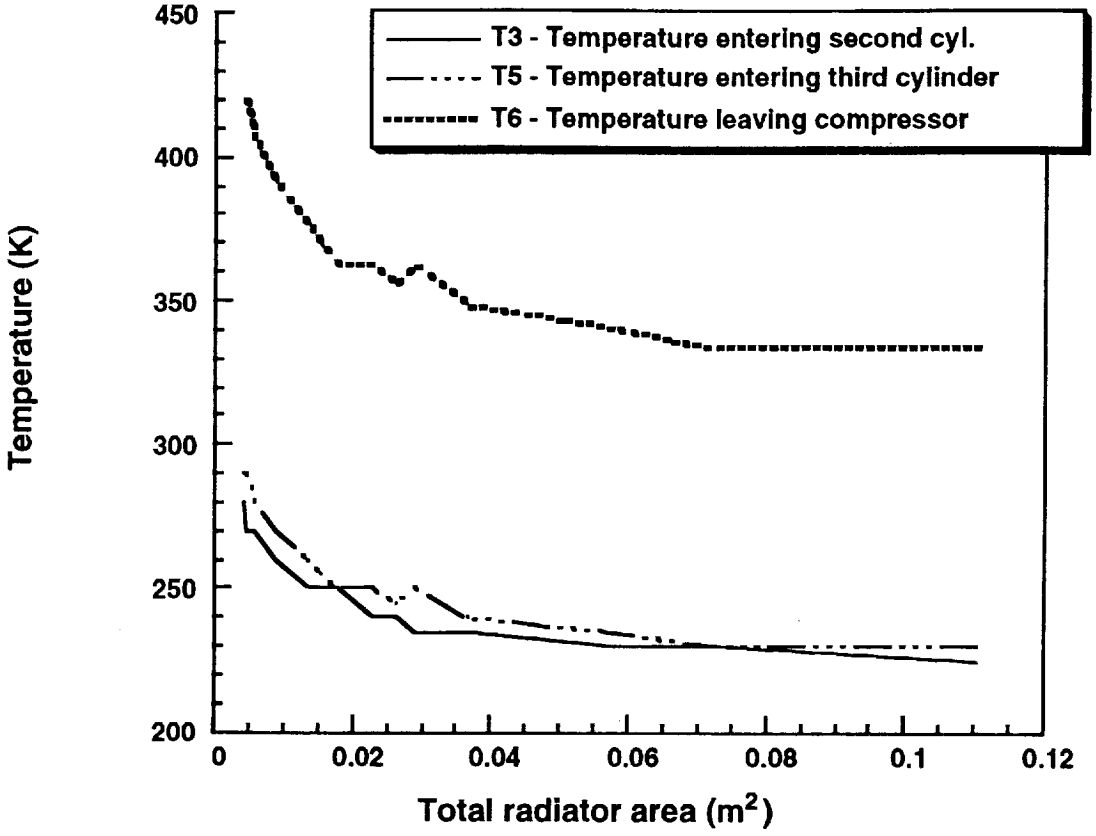

Fig. 2.6 Temperatures vs. total radiator area.

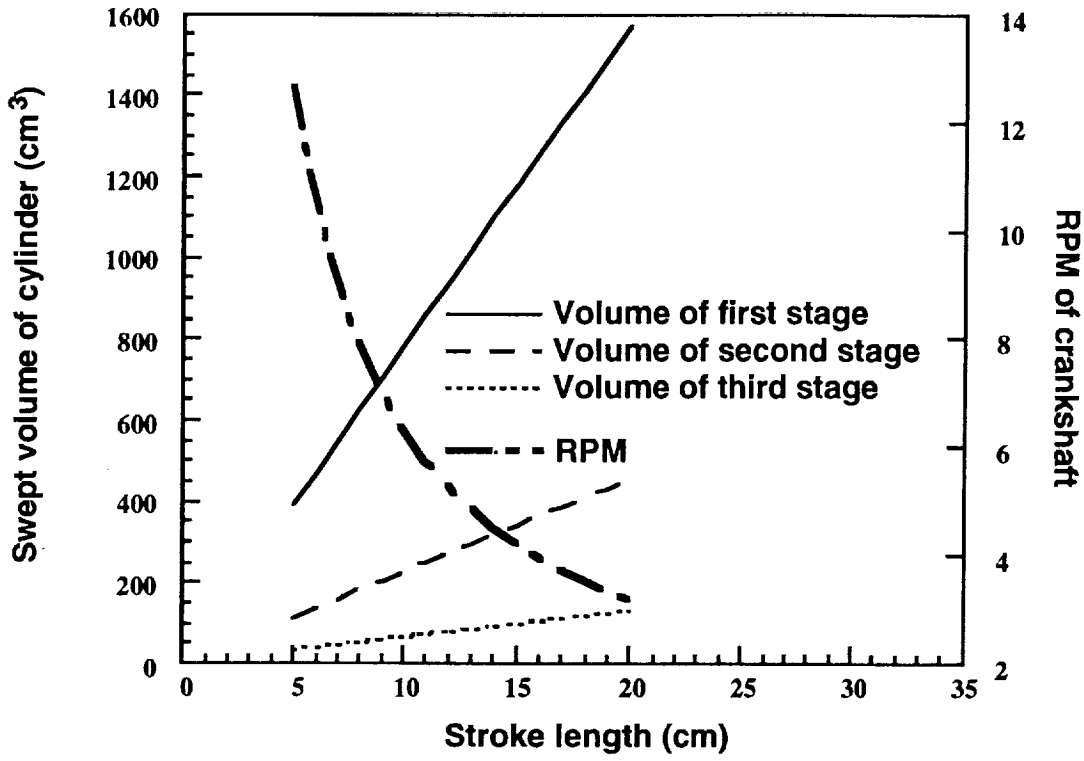

Fig. 2.7 Volume of compressor and RPM vs. stroke length.

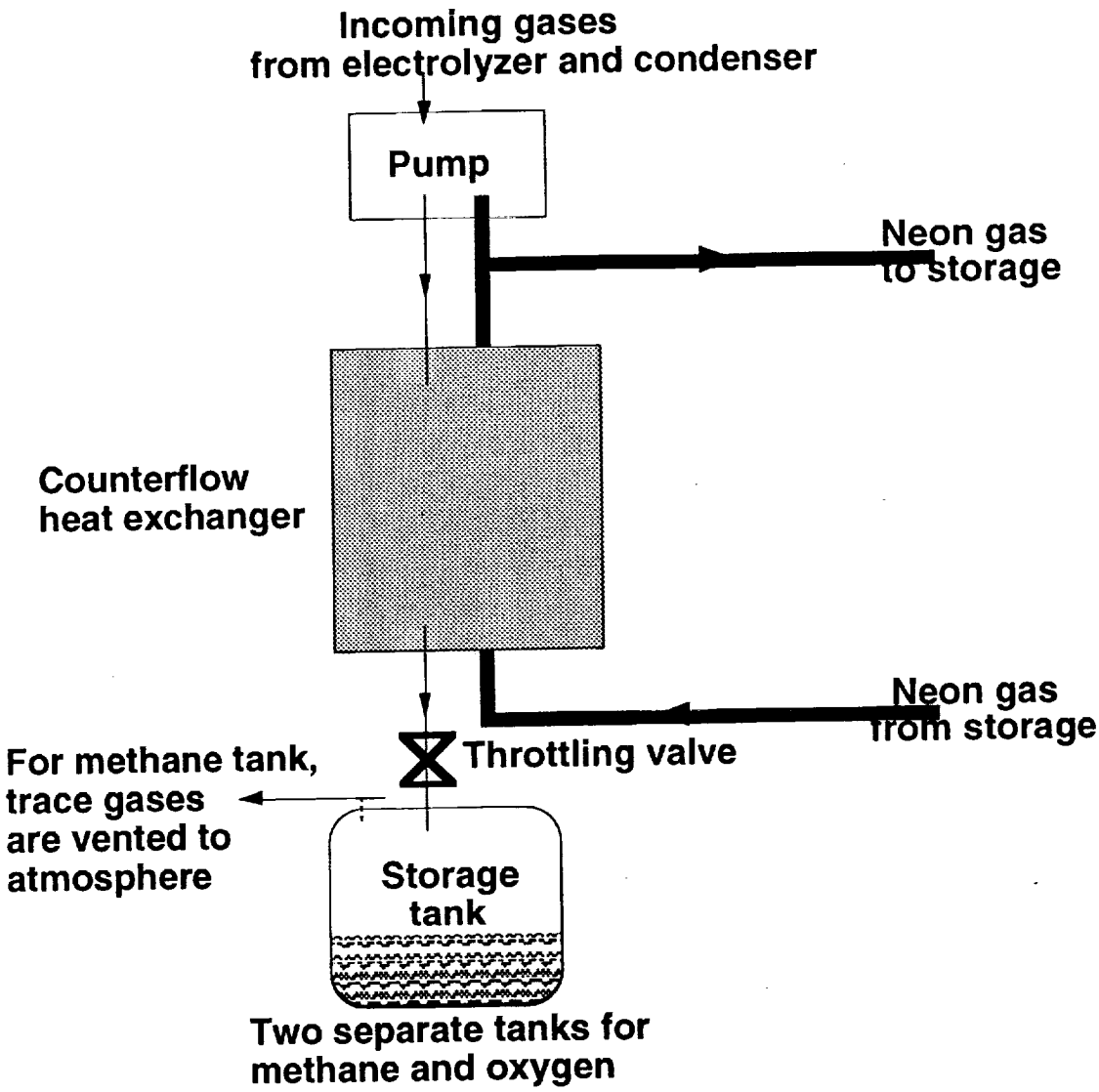

Fig. 2.8 Schematic of gas liquefaction system.

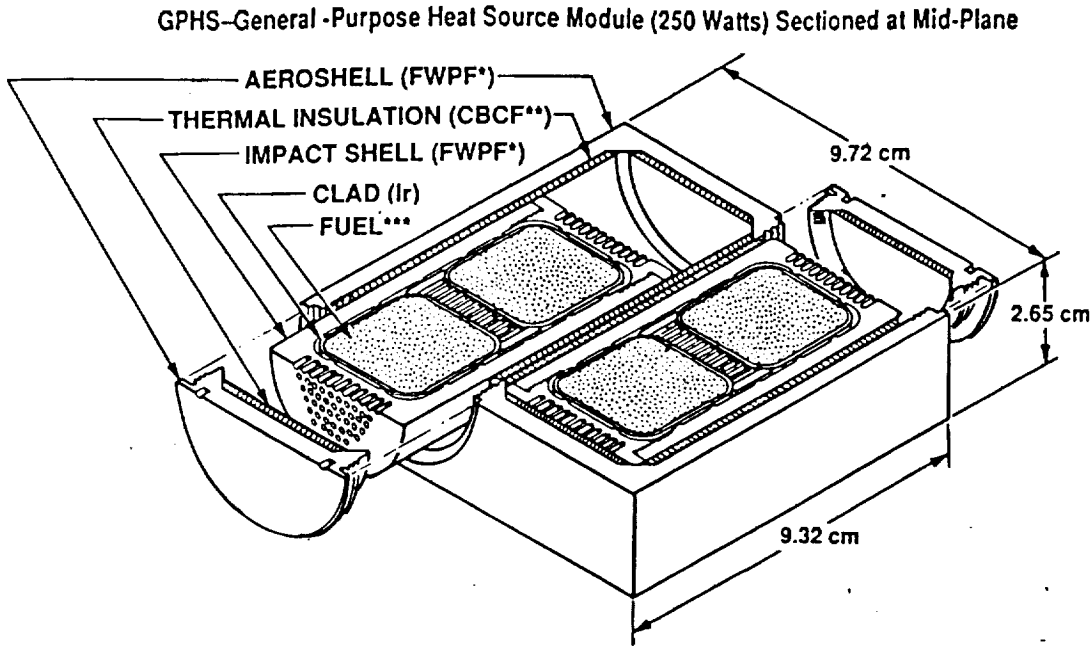

Fig. 2.9 General-Purpose Heat Source Module (250 W_{th}) sectioned at mid-plane[16].

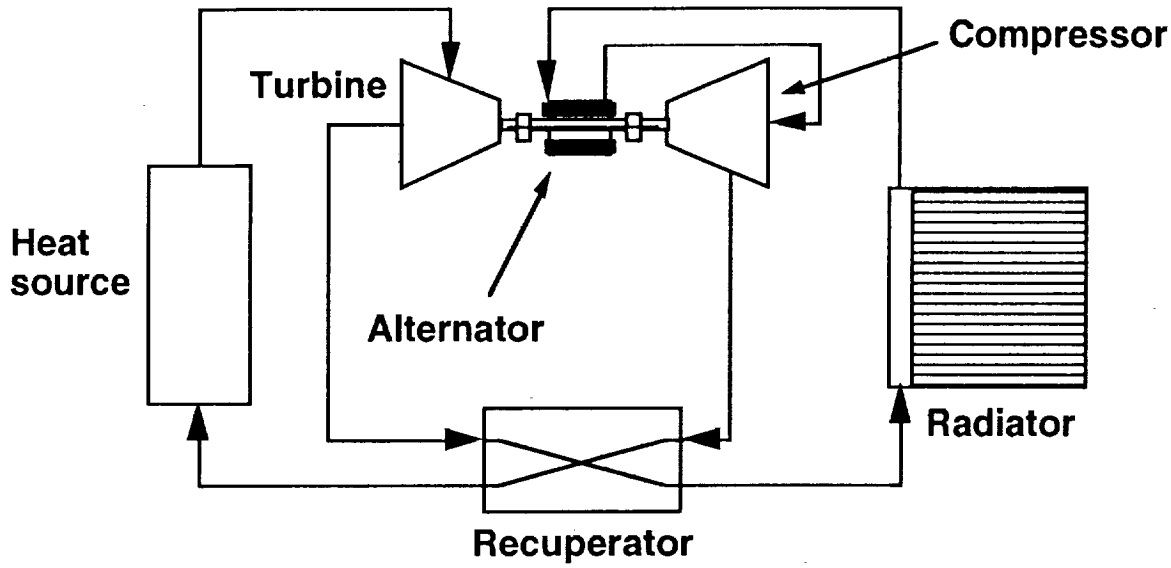

Fig. 2.10 Dynamic isotope power system cycle diagram [17].

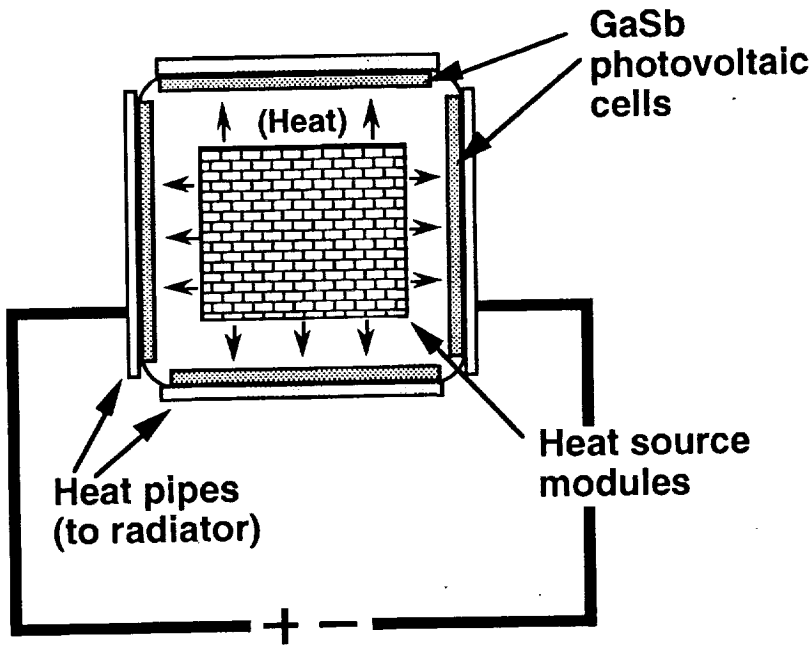

Fig. 2.11 Schematic of RTPV.

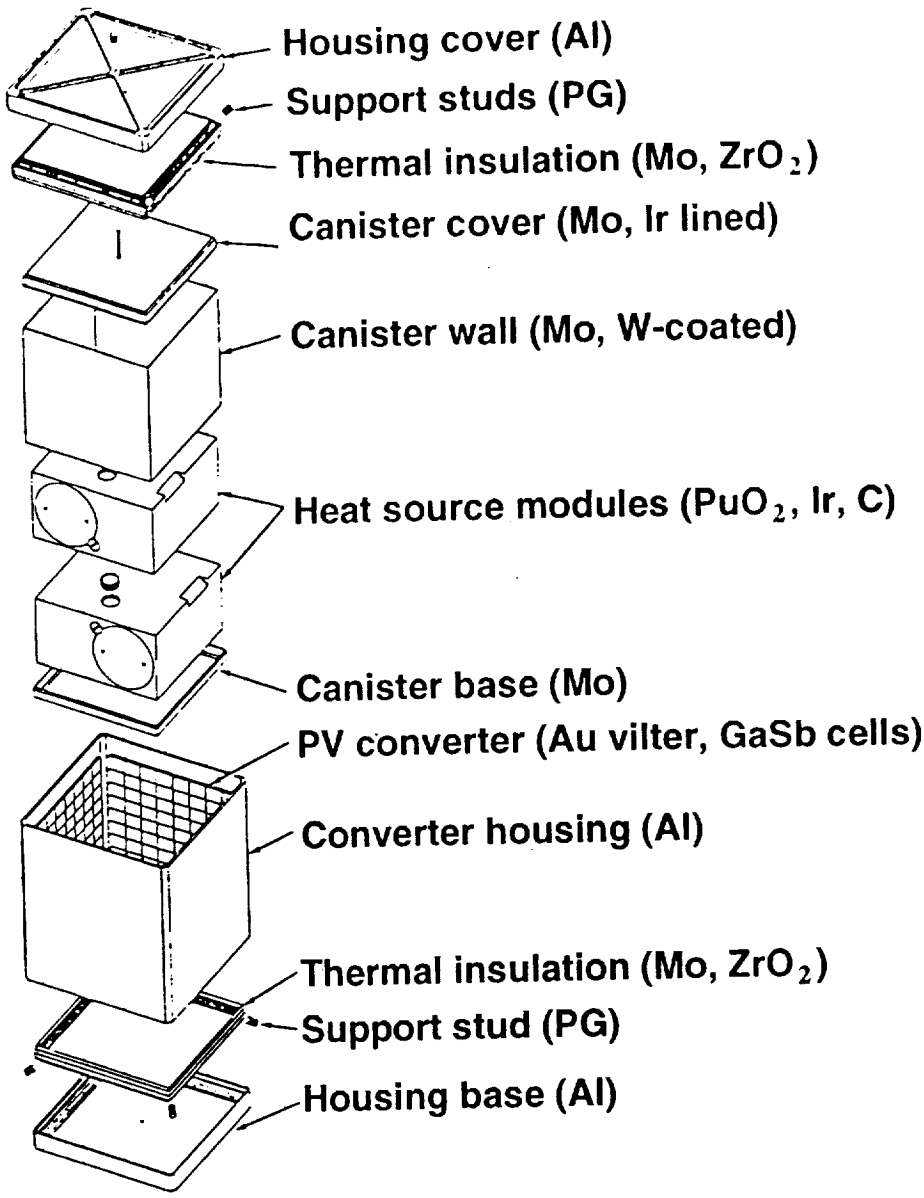

Fig. 2.12 Layered composition of RTPV with two GPHS modules [16].

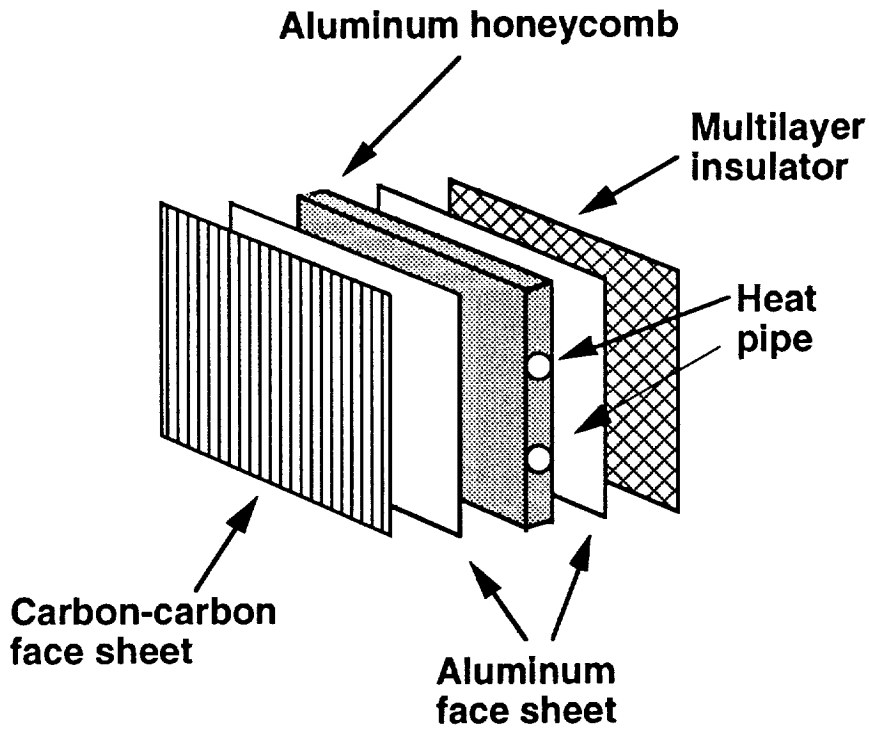

Fig. 2.13 Schematic of radiator.

3.0 MARS LANDING VEHICLE/HOPPER DESIGN

Francisco Javier Garcia Acosta

Matt Deger

Matt Hedman

Takahisa Kobayashi

Daniel Pasco

Igor Turek

Keith Yang

TABLE OF CONTENTS

3.1 INTRODUCTION
(Keith Yang)

The Mars Lander Vehicle/Hopper's (MLVH) main purpose on Mars is to demonstrate ballistic hopping abilities with the use of *in situ* propellant which is produced by the onboard propellant production plant. Fig. 3.1 shows the diagram of the MLVH. Besides the PPP, the MLVH also carries onboard the scientific instrumentation. Besides acting as a bus system for the instrumentation, the MLVH also carries out scientific data collecting. To do this, the MLVH enters a polar elliptical orbit at Mars where it remains for a period of a month, and maps the surface of Mars and scans for subsurface water ice deposits with a ground penetrating radar (GPR). Once the MLVH determines a suitable landing site from its orbit, the MLVH begins its descent phase. During this phase, the MLVH demonstrates aerobraking techniques used to reduce the landing velocity of the MLVH. To further decrease the landing velocity, the MLVH also utilizes a parachute and landing engines. Once terminal velocity is reached with the parachute, the parachute is jetisoned, and the landing engines activate for a soft surface landing. The MLVH propulsion system consists of four methane/LOX main engines. These engines are used as the landing engines and also as the main engines for the ballistic hop. Because Project Genesis was designed to be launched on a Delta, the MLVH was designed around the Delta's launching capabilities in terms of its payload mass limit and upper stage fairing dimensions. Based on these mass and size limits, the MLVH is designed for a ballistic hop of 30 km. The dimensions of the MLVH, base width is 2.4 m and frame height (excluding landing gear) is 1.7 m. The width of the aerobrake is 2.7 m.

The following sections discuss in detail, the MLVH configuration, structural design, and mass inventory. Also included into this section are the design of the main engines, the reaction control system, the parachutes, and the aerobrake.

3.2 MLVH CONFIGURATION
(Igor Turek)

The configuration of the MLVH is based on the following criteria:

- Ability to perform a ballistic sub-orbital hop
- Payload mass and size limitations of Earth launch vehicle
- Location of MLVH's components
- Flight stability and center of mass location

Each of the design criteria is discussed in the following sections.

3.2.1 Ballistic Hop
(Igor Turek)

As a starting point in the vehicle design, the MLVH was assumed to perform one ballistic hop of a 50 km range. Next, the configuration of the MLVH was designed with respect to the criteria given in section 3.2. Lastly, after the vehicle's parameters: mass, dimensions, etc., were calculated, the actual ballistic hop trajectory and range was computed. The details on the actual MLVH's ballistic hop characteristics are given in Chapter 6.

From the assumed ballistic hop range of 50 km, the MLVH's ballistic burnout velocity Δv_{bo} was calculated to be 0.43 km/s. Multiplying this velocity by 1.05 to account for the gravitational and drag losses, and adding a ballistic landing Δv (equal to Δv_{bo}), produced a total MLVH's ΔV requirement of 0.88 km/s. Assuming an I_{sp} for LOX/CH_4 of 340 s (see section 3.4.5), the mass ratio (MR) of 1.30 was calculated using the standard rocket equation [1]. Similar analysis was used to find the first Mars landing mass ratio (LMR). During the first landing maneuver, the MLVH has to be slowed down from the velocity of 85 to 0 m/s near the Mars surface (see section 3.7). The ballistic hop range (BR) and the values of ΔV, I_{sp}, LMR, and MR are shown in Table 3.1.

Table 3.1 Mass ratios and Δv requirements.

BR (km)	Δv_{bo}	ΔV	I_{sp} (sec)	LMR	MR
50	0.43	0.88	340	1.03	1.30

Once the dry mass of the MLVH is known, the mass of propellant needed to insert the MLVH into the assumed ballistic trajectory can be calculated. Unfortunately, this calculation is circular because the mass of propellant affects the MLVH's dry mass through the change in the size of tanks and the amount of required seed hydrogen. Also, the propellant production time (PPT) is affected by the above variations. An interactive process had to be employed, and when taking into account the launch vehicle limitations of payload size and mass, given in Section 3.2.2., the optimal value of the PPT and the vehicle's dry mass was found; these are given in Table 3.2. Also, the amount of propellant and the mass of seed hydrogen required for the MLVH to perform the assumed 40 km hop is given in Table 3.2.

Table 3.2 MLVH dry masses and propellant production characteristics.

MLVH Dry Mass (kg)	Propellant Mass (kg)	Seed Hydrogen (kg)	PPT (days)
442	141	16.7	141

3.2.2 Launch Vehicle Considerations
(Matt Hedman)

The payload capabilities of the launch vehicle determine the performance of the MLVH. The launch mass of the MLVH is a function of how quickly the propellant necessary to perform the hop is produced. If a shorter time frame is required, a faster rate of production is needed, therefore, a larger propellant production plant is required. Furthermore, larger propellant tanks are

needed to house more propellant due to the increased mass. A more massive frame is needed to house these items. Other components scale up in size also. An approximate mathematical model was developed to analyze these trends. The resulting graph of vehicle launch mass versus number of days of production time is shown in Fig. 3.2.

Launching the MLVH on the Delta 7925 rocket places two restrictions on the hopper. First of all, the MLVH must have a lower launch mass than the 1000 kg the Delta is capable of transferring to Mars with a C_3 value of 10 km^2/sec^2 [2]. Secondly, the vehicle and aerobrake must fit inside the PAM-D upper stage payload fairing, which has an inner diameter of 2.8 m at the base and a height of 4.2 m.

Rather than the mass restriction, the payload fairing diameter is the limiting factor that determines the size of the MLVH. The symmetric aerobrake is designed with a diameter of 2.7 m, so it will just fit inside the fairing. All of the other items onboard must be configured so that they are not protruding in the wake of the aerobrake during the aerocapture. In order to increase the performance of the MLVH (make a longer hop or have fewer days of propellant production time), the size of the seed hydrogen and propellant tanks must be increased. Due to the limited space that is protected behind the aerobrake, increasing the size of these tanks is not possible beyond a certain point. Therefore, the PAM-D payload fairing diameter dictates the performance of the MLVH.

3.2.3 Component Locations
(Takahisa Kobayashi)

It is desired to place the components of MLVH at appropriate locations to minimize the possibility of different components unfavorably interacting with each other, such as the high temperature propellant plant heating up the refrigerated propellant tanks. However, since the MLVH configuration is designed to fit the vehicle inside the payload fairing of the Delta launch

vehicle, space available for each components is limited. Therefore, components must be allocated properly, utilizing the space efficiently.

The cross-section of the MLVH is octagonal, and therefore it has eight triangular sections when it is viewed from above (see Fig. 3.3). The hydrogen tank (the largest tank) with insulation is located at the center of the MLVH. This is to ensure a well-balanced center of gravity. Two pairs of equally-sized tanks, employed for methane and oxygen storage, are located symmetrically around the hydrogen tank so that the center of gravity can be as close to the vertical axis of the MLVH as possible. In the remaining sections, all of the other components including the propellant plant, radioisotope thermophotovoltaic generator (RTPV), science instruments, avionics and control system, and the communication system are arranged to position the center of gravity as close as possible to the center axis. The parachute, which is jettisoned after its use for initial landing, is located at the top of the MLVH within a canister. When the parachute is deployed, it orients the MLVH toward the Martian surface. The outer surfaces of seven sections are covered by the radiator (see Fig. 3.1). In the section not covered by the radiator, the ground penetrating radar (GPR) is installed so that it can be folded out of the MLVH for the GPR survey.

3.2.4 Center of Mass
(Takahisa Kobayashi)

The location of the center of mass is important for launch stability and attitude control. When the center of mass is located on the centeral axis of the MLVH, the difficulties in controlling the MLVH during the hop are minimized. Also, the Delta launch vehicle requires that the position of the center of mass of the payload must be less than 1 m from the interface of the payload adapter.[2] Thus, the MLVH was designed to locate its center of mass as low as possible. The location of the center of mass varies during the mission because of propellant consumption. The locations of center of mass and the moments of inertia at the time just prior to the ballistic hop is

shown in Table 3.3. These values were found by the finite element program, ANSYS 5.0, which is discussed in section 3.3.3. The three coordinate axes are shown in Fig. 3.4.

Table 3.3. Center of mass and moment of inertia of the MLVH.

Time of Instant	Center of Mass (m)			Moment of Inertia (kg m^2)		
	X	Y	Z	X	Y	Z
Before the Ballistic hop	0.009	0.009	0.195	44	51	238

3.3 STRUCTURAL DESIGN
(Keith Yang)

The structural design of the MLVH is dependent upon the sizes and masses of the components, especially the propellant tanks. Each component was designed and analyzed separately. The following sections discuss in detail the tanks, engines, truss frame, and landing gear.

3.3.1 Tankage Design
(Igor Turek)

Based on the considerations given in section 3.2.1, the propellant and hydrogen tank capacities are 141 kg and 16.7 kg respectively. The tank configuration determines the overall MLVH size, as well as the amount of space available for the other systems and the scientific instrumentation. Several tank shapes and locations were considered; among them were spherical, elliptical, and toroidal. Because spherical tanks have the smallest surface area to volume ratio, these were used for the MLVH propellant and hydrogen storage. The tank configuration and its analysis is described below.

Assuming a 5% ullage factor and a fuel to oxidizer ratio of 0.5 (see section 3.4.5), the volumes needed to store the propellant and seed hydrogen were calculated. The densities, storage pressures, temperatures, and volumes of the propellants and seed hydrogen are listed in Table 3.4.

Table 3.4 Storage characteristics of liquefied gases.

Liquefied Gas	Pressure (atm)	Density (kg/m^3)	Temperature (K)	Volume (m^3)
Methane	1.0	445.0	90	0.10
Oxygen	1.0	1068.0	90	0.09
Hydrogen	25.0	71.9	23	0.23

The limits imposed by the aerobrake and the amount of space available for the MLVH in the Delta's fairing forced our design to use five spherical tanks: one for hydrogen, two for oxygen, and the remaining two for methane. To avoid complexity in the MLVH design, all propellant tanks have the same size; the tank dimensions are given in Table 3.5, and the tanks' relative position is shown in Fig. 3.5.

Since the vehicle is launched from Earth with its propellant tanks nearly empty, and lifts off from Mars with an acceleration of less than one Earth *g*, the wall thicknesses of the methane and oxygen tanks are determined not by launch loads, but by the hoop stress caused by the pressure of the stored propellants.

All tanks are made of Weldalite™ aluminum-lithium 049, which has excellent structural characteristics at cryogenic temperatures [3]; its ultimate strength, yield stress, density, and elastic modulus are given in Table 3.6 in section 3.3.2. Using the standard formula for the pressure–induced maximum hoop stress in the spherical tank[4]:

$$th = \frac{1.5PR}{x\sigma_{ult}} \tag{3.1}$$

where:

t = thickness of tank wall

σ_{ult} = ultimate strength

P = tank pressure

R = tank radius

1.5 = safety factor

x = shape factor ($x = 2$ for spheres)

The required thicknesses of the tank walls were found to be in the order of a fraction of millimeter. Due to the manufacturing and handling concerns, the thicknesses of all propellant tank walls were increased to 1 mm. The calculated and actual thicknesses of the methane and oxygen tanks are given in Table 3.5.

Unlike the propellant tanks analyzed above, the hydrogen tank has to withstand both the storage pressure and the axial and lateral loads due to the launch from Earth and aerobraking at Mars. Both the pressure induced hoop stress analysis and the load analysis were treated separately. The wall thickness needed for the tank to withstand the given pressure was calculated using equation 3.1. This tank wall thickness was then used in the finite element analysis described in section 3.3.3. From the results of the finite element analysis, it has been found that it is the pressure–induced hoop stress that determines the hydrogen tank wall thickness. The calculated and actual thicknesses are given in Table 3.5.

In order to prevent large shifts of the vehicle's center of gravity during flight, each tank is divided into four vertical quadrants by a couple of baffles. The baffles have a thickness of 1 mm and are made of Weldalite™ 049. The total mass of each tank is found by calculating the volume of

each tank external wall and its baffles and multiplying it by the density of Weldalite™ and the factor of 1.05 to account for welds. The tank dimensions and masses are given in Table 3.5.

Table 3.5 Tank characteristics (without insulation)

Tank	Tank radius (m)	Calculated wall thickness (mm)	Designed wall thickness (mm)	Mass (kg)
Methane	0.23	0.025	1	5.8
Oxygen	0.23	0.024	1	5.8
Hydrogen	0.38	0.868	1	7.9

All tanks are fastened to the MLVH main structural rings (see section 3.3.2) by a set of 2 cm diameter composite struts. The hydrogen tank is supported by 8 pairs of struts, as shown in Fig. 3.6, and each methane and oxygen tank is supported by 8 struts. The struts are attached to the tanks and the octagonal rings by means of pivoted joints. Each strut lies in a plane tangential to the tank surface, loading the tank only with in–plane forces. The thickness of each tank, at each strut attachment point, is gradually increased from 1 to 1.4 mm; this enhances the distribution of the load generated by the composite strut. The composite material used for the tank support not only provides the tanks' structural integrity, but also enhances thermal performance by minimizing conductive heat transfer from the tanks to the MLVH structural members.

3.3.2 MLVH Frame Structure
(Matt Hedman, Keith Yang)

The load bearing structure of the MLVH is a frame structure made from aluminum-lithium 2090-T83 tubing. The aluminum-lithium tubes have an outer diameter of 2 cm and a wall thickness of 2 mm. The frame consists of five octagonal rings that are joined by vertical connecting members. The thrust structure is positioned immediately below the main frame

structure and distributes the concentrated loads from the engines. The main frame is illustrated in Fig. 3.7.

Forged nodes form the connections between all of the tubes. These nodes interface with each tube by forming the "male" member of the connection. The tube end fits around the outside of the node to form the "female" member of the connection. The bond between the nodes and tubes is accomplished via electromagnetic forming. Electromagnetic forming is a process that entails coating the touching surfaces of the forged nodes and tubes with a bonding agent that joins the surfaces when an electric current is run through it. After the frame has been assembled, a current is run through the entire structure, and all of the tubes bond to the nodes.

Aluminum-lithium alloys have been used as lightweight, high strength materials for the tubing of frame structures for mountain bikes. So far, the 2090-T83 alloy has not been used for tubing applications. However, because of its higher stiffness and better welding properties compared to other aluminum-lithium alloys, there have been many inquiries into using it for high-strength tubing. Therefore, Alcoa is tentatively planning to start introducing tubing that uses this alloy to the market in the near future [5]. The properties of aluminum lithium 2090, as well as the Weldalite™ used for MLVH tanks, are summarized in Table 3.6.

Table 3.6. Material properties of aluminum lithium 2090 and Weldalite™.

Material Property	Weldalite™*	Al-Li 2090**
Yield stress - σ_y (MPa/ksi)	868/126	545/79
Ultimate stress - σ_{ult} (MPa/ksi)	837/122	600/87
Elastic Modulus - E (GPa/ksi)	79/11.5	78.5/11.4
Elongation (%)	10.5	12
Density - ρ (kg/m^3)	2710	2570

* cryogenic temperatures
** room temperatures

The mass of the structure includes the masses of the aluminum-lithium tubes, forged nodes, tank support struts, and equipment connection clamps. Estimates for the mass of the equipment connection clamps were based on masses given for the Common Lunar Lander. The clamps were estimated to have 15% of the mass of each item they fasten to the structure [6]. Since the propellant plant, power supply, science packages, avionics, reaction control system and communication equipment must all be attached to the main frame, the total mass of the clamps is 37 kg. The tank and engine connections are already accounted for with the tank support struts and thrust structure frame. Table 3.7 gives a breakdown of the total structural mass.

Table 3.7 Structure mass breakdown.

Category	Mass (kg)
Aluminum-Lithium Tubing	17
Forged Nodes	8
Tank Support Struts	10
Equipment Connection Clamps	37
TOTAL	72

3.3.3 Finite Element Structural Analysis
(Igor Turek)

A finite element computer program, ANSYS 5.0, was a primary tool for the MLVH's structural analysis. The main objective of this analysis was to determine the maximum stresses, strains, displacements, and a possible buckling failure of the MLVH's structural parts. By determining the above parameters, the structural elements could be modified to sustain the maximum expected loads and to be as light as possible. This could be accomplished by selecting the geometry and dimensions of structural members, so they experience elastic strains equal to or

less than 67% of ultimate material stresses [7]. In addition, compressive axial forces cannot exceed 67% of the critical buckling force [7].

The structure, and inertial components of the MLVH were represented by an equivalent mathematical model consisting of a discrete number of finite structural elements; number of elements is given in Table 3.9. The MLVH structural parts and their ANSYS matching element types are given in Table 3.8, which also includes information about the number of nodes and degrees of freedom (DOF) per node used for ANSYS elements [8].

Table 3.8 ANSYS finite elements used for MLVH analysis.

MLVH Component	Element Type	Number of Nodes	Number of DOF
Aerobrake	SHELL93	8	6
Main Frame	BEAM24	3	6
Thrust Frame	BEAM24	3	6
Adapter Frame	BEAM24	3	6
Tanks	SHELL93	8	6
Tank Struts	LINK8	2	3
Structural Mass	MASS21	1	3

The MLVH structure was examined via static analysis with respect to the four load–sensitive maneuvers listed in Table 3.9, which also includes inertial and surface/point loads used for the analysis.

Table 3.9 MLVH finite element configurations and applied loads.

Mission Stage	Inertial Load	Point Surface Load	# nodes	# elements
Launch	Axial acceleration Lateral acceleration	All tanks are pressurized	2248	1070
Aerobraking		Aerodynamic pressure acting on the aerobrake's surface, all tanks are pressurized	2240	1062
Parachuting	Mars gravity	Point loads at the parachute attachment points, all tanks are pressurized	1862	784
Ballistic takeoff	Mars gravity	Point loads caused by the thrust of the engines; oxygen and methane tanks are pressurized	1862	776

The ANSYS analysis shows, that the MLVH structural configuration, described in section 3.3.2, experiences internal stresses and strains that guarantee safe functionality of the spacecraft at all stages of its mission. The maximum values of stress and strain for the main MLVH components are listed in Table 3.10. These can be compared to the MLVH structural material characteristics given in Table 3.6 in the previous section. The axial forces never exeed the buckling limits, and the displacements of MLVH's components do not create any conflict with the surrounding objects; the gap between the Delta fairing wall and the aerobrake - the closest of MLVH's parts to the fairing wall - narrows from 5.00 to 0.55 cm - under the maximum lateral loading of 2 Earth *g*.

Table 3.10 Maximum stresses and strains experienced by the MLVH components.

MLVH structural component	Maximum stress (MPa)	Maximum strain (%)
Main Frame	253	7
Thrust Frame	385	4
Tanks	435	8
Composite Struts	286	4

3.3.4 Landing Gear
(Keith Yang)

Once the MLVH deploys the parachute and jettisons the aerobrake, the landing legs are deployed. The main purposes of the landing gear are to provide stability for the MLVH, a safe clearance for the main engines from the rocky Martian surface, and minimize shock due to landing. The entire landing gear is constructed of Al-Li 2090-T83 alloy, the same material as the main structure frame. Each leg is 1.2 m in length at deployed position and provides an engine-to-ground clearance of .8 m. This provides more than adequate clearance for the engines, since the average height of rocks, observed by the Viking missions, is .35 m [9]. With each leg oriented at 45° to the surface, the projected area of the four legs 17 m^2. Also, this configuration allows the MLVH to be tilted at an angle of 60° to the horizontal without toppling.

The landing gear design is a hybrid design adopted from the British Aerospace Vulcan Fighter's main landing gear design and Viking Lander's design[7, 9]. As shown in Fig. 3.8, the gear is first extended into position with a screw actuator system. When the screw actuator extends to its maximum length, a pyrotechnic bolt is activated to release the telescopic strut built within the screw actuator. This is to further unfold the legs to the desired angle. After the leg is fully unfolded to its design angle of 45°, another pyrotechnic bolt is activated to release and extend the

lower part of the leg, as shown in Fig. 3.8. There is a spring-type shock absorption system located at the ankle of each leg. Spring shock absorbers are used instead of pneumatic-types because of the lighter mass and simplicity. Also, steel springs do not pose the problem of freezing up in space as do rubber type shock systems.

To determine the sizing of the gear, a landing force of 10 Martian g's was assumed. For the MLVH with a landing mass of 456 kg, the maximum force the landing gear experiences is 18,300 N. Because it is not for certain that the MLVH will land on all four legs at the same time, each leg most be sized to withstand the maximum impact load of 18,300 N. This force value, with a safety factor of 1.5, was the value used to dimension the legs to withstand yielding from axial and bending compression and buckling.

To determine the critical buckling loads, Eulers equation for beam buckling was used [7].

$$P_{cr} = \frac{\pi^2 EI}{l_e^2} \tag{3.2}$$

where:

P_{cr} = Critical buckling load

E = Modulus of elasticity

I = Moment of inertia of beam column

l_e = Equivalent Length

Using the above equation, the diameter of the bottom portion of the leg was determined. With the given properties of the Al-Li 2090-T83 and assuming the boundary conditions of the lower telescopic leg (one end pinned and one end fixed), the outside diameter of the tube necessary

to resist buckling during landing was calculated to be 3 cm with a wall thickness of 2 mm. To calculate the wall thickness of the upper strut, the following equation was used:

$$\sigma_{ult} = \frac{F}{A} \tag{3.3}$$

where:

σ_{ult} = Ultimate yield stress

1.5 = Factor of safety

F = Force applied to tube

A = Cross-sectional area of tube

With the above equation and σ_{ult} value of 600 MPa for Al-Li 2090-T83, the resulting outer diameter of the tube was 1 cm with a wall thickness of 2 mm. To determine if the leg will withstand the bending stresses upon landing the following equation was used:

$$\sigma_y = \frac{MR}{I} \tag{3.4}$$

where:

σ_y = Bending stress

M = Bending moment

R = Radius of tube

With the legs oriented at 45° with a length of 1.2 m, the minimum outside diamter of the leg was calculated to be 6 cm with a wall thickness of 2 mm. Thus, the minimum sizing for the leg's outside diameter was 6 cm with a wall thickness of 2 mm. Including the screw actuators and the shock absorbers, the mass of each leg was then calculated to be 4 kg each. The total resulting landing gear weight was 16 kg.

3.4 METHANE ROCKET
(Daniel Pasco)

The MLVH uses LCH_4/LOX rockets (Fig. 3.9) for all of its maneuvering upon arrival to Mars. Although no such engines are currently in existence, their theory and design are well understood. In-depth research in light hydrocarbon rocket engines has been conducted since 1965 [10-12]. The performance and behavior of methane engines in particular has been studied extensively by Pratt & Whitney, Aerojet, and Rocketdyne. Fuel-oxidizer combinations such as FLOX/LCH_4 and LOX/LH_2/LCH_4 have been proposed in order to raise the specific impulse of the engines, but are not considered in this paper. Fluorine would have to be imported from Earth, which violates the spirit of the mission, and any hydrogen brought along will be better utilized in the production of methane and oxygen.

The constraints that the MLVH rocket design must satisfy are:

- Oxidizer to fuel mass ratio of 2:1
- Total thrust of 11 kN for ballistic hop
- Ability to restart
- Throttlability
- Engine-out capability

Although a LCH_4/LOX burning variation of the Pratt & Whitney RL-10 engine has been proposed [12], the level of thrust provided by this engine is unsuited to this mission. The ideal oxygen to fuel mass ratio (O/F) is 3.5:1 [12]. Unfortunately, the PPP is only capable of providing oxygen and fuel in a 2.0:1 mass ratio. Thus, the MLVH requires the design of low thrust (625 lbf) engines specifically intended for fuel-rich combustion.

3.4.1 Engine Overview

The MLVH requires 11,000 N of thrust for its initial landing, as well as for its subsequent ballistic jumps. It was decided that this mission would use 4 separate engines, each capable of developing 2750 N of thrust, to meet this requirement. This four-engine configuration allows ease in thrust vectoring and also provides engine-out capability in the event that one of the motors fail. The MLVH rockets are regeneratively cooled and operate on an expander cycle, being based in concept largely upon Pratt and Whitney's RL-10 series of rocket motors. The MLVH rockets will use liquid methane as the regenerative coolant, since it has good heat transfer characteristics and would be less of a detriment to the engine integrity than liquid oxygen.

A major concern that was raised in the design of the engines was the possibility of soot formation during operation due to the fuel-rich equivalence ratio. It turns out that this can be avoided if the fuel mixture is adequately mixed at equivalence ratios within up to 5% of the fuel-rich extinction point [13]. In addition, computer simulations run with the NASA CET-89 combustion code indicate that the performance drop resulting from fuel-rich operation is small, due in part to the lower average molecular weight of the combustion products.

3.4.2 Pre-Existing Technology

Project Genesis utilizes pre-existing technology wherever possible in order to lower development costs and ensure component reliability. This rocket design is based heavily on the Pratt & Whitney RL-10, a regeneratively cooled, expander cycle engine with an excellent performance record.

The turbopumps used by the engine do not exist, but could be designed with little difficulty. A conventional LOX turbopump can be configured for the MLVH engines without difficulty, and a working methane turbopump, although to large for engines this small, was produced by Rockwell International in 1989 [12].

Many conventional rocket designs utilize copper as an inner lining for the rocket thrust chamber due to its high thermal conductivity [14, 15]. Unfortunately, CH_4 has a tendency to erode copper surfaces at high temperatures. A graphite-lined regeneratively cooled chamber using LOX/LCH_4 was constructed and is described as having worked, "very successfully in the test program...".

Another possible design would use a pressure fed, rather than turbo pump driven, engine system. This type of design is not uncommon in engines in the 600 to 1000 lbf thrust range. This configuration would be much simpler to design, but requires an additional supply of helium to be used as a pressurant, as well as heavier fuel and oxygen tanks in order to resist the increased tank pressure. A precombustor stage would also be required, but would be compensated for in terms of additional mass by the absence of the turbopump system.

The last design consideration presented here is the nozzle contour. Three major possibilities were considered in the determining the geometry of the thrust chamber; conical, bell-shaped, and parabolic. The conical nozzle is the simplest to implement, but tends to be the longest of the three options. The bell nozzle offers a shorter thrust chamber at a higher efficiency, being designed specifically with the intent of avoiding the formation of normal shocks in the nozzle. This design is much more complicated than the conical nozzle design, requiring the use of the method of characteristics. The nozzle contour immediately upstream of the throat is a circular arc with a radius of 1.5 times the throat radius (R_t) [15]. The divergent-section nozzle contour is made up of a circular entrance section with a radius of $0.382 \cdot R_t$. This throat configuration is depicted in Fig. 3.10 The resulting engine design has an overall height of 25 cm.

3.4.3 Engine Operation

A schematic of the engine layout appears in Fig. 3.11. During operation, liquid methane and oxygen are directed from the fuel tanks through a pair of shut-off valves and into their

respective turbopumps. The liquid methane is passed through the tubes comprising the trust chamber and operates as a regenerative coolant. This boils the methane, 90% of which is then passed through a low pressure turbine after exiting the cooling jacket. The turbine is used to drive the two turbopumps, which are used to raise the pressures of the incoming fuel and oxidizer streams. The remaining 10% of the methane is injected into the turbine exhaust flow prior to injection into the combustion chamber, igniting the fuel mixture and eliminating the need for a precombustion stage in the engine. The injector system uses shear layer interaction to mix the fuel and oxygen. In light of the RCS failure suffered by Clementine, the MLVH maneuvering system is designed to take advantage of the multiple engine configuration. In the event of RCS failure the thrust is varied by turning individual engines on or off and by throttling all the engines over a relatively narrow range. This activity gives the MLVH redundant control along two spin axes.

A schematic of the pressure-fed version of the MLVH engines appears in Fig. 3.12. High-pressure helium is pumped into an inflatable elastomeric spherical bladder prior to launch, pressurizing the propellant tanks to 1700 psia. A small fraction of the propellant is diverted to an igniter. This propellant is then fed into the combustion chamber, where it ignites the remainder of the fuel/oxider stream. Although this system does not allow for engine throttability, it compensates for it in simplicity.

3.4.4 Fuel-Rich Combustion

The two major concerns associated with fuel-rich combustion are the formation of soot and any compromising effect on engine performance. Research on carbon deposition due to the burning of hydrocarbon fuels has indicated that methane generates about 30% less solid carbon by weight than RP-1 [12]. Additional work has shown that LOX/CH_4 gas generators have no carbon deposition at O/F mass ratios between 0.2 and 0.6. This corresponds to a maximum fuel/oxidizer equivalence ratio of 10. The rockets designed for the MLVH will be operated at an O/F mass ratio of 2:1, corresponding to a fuel/oxidizer equivalence ratio of 2.0. Thus, no sooting will occur.

The NASA CET-89 combustion code [16] was used to simulate oxygen-methane combustion at a pressure of 750 psia under ideal, stoichiometric, and design conditions. The combustion products predicted by these tests appear in Table 3.11 below. As can be seen from the table, virtually no change in the amount of carbon present is in evidence.

Table 3.11 Methane rocket combustion products by mole fraction, for various O/F ratios (P_c=750 psia, T_{oxygen}=$T_{methane}$=120 K)

Component	Ideal: (3.5:1)	Stoichiometric (4:1)	Design (2:1)
H_2O	0.459	0.449	0.295
CO	0.178	0.143	0.297
CO_2	0.121	0.139	0.0357
H_2	0.0827	0.0566	0.366
OH	0.0800	0.0943	0.00121
O_2	0.0348	0.0707	-
H	0.0289	0.0239	0.00550
O	0.0160	0.0228	0.00001
HO_2	0.00016	0.00027	-
H_2O_2	0.00002	0.00003	-
HCO RAD	0.00001	0.00001	0.00001
C	$< 5 \times 10^{-6}$	$< 5 \times 10^{-6}$	$< 5 \times 10^{-6}$

The combustion product distribution of the ideal (3.5:1 O/F ratio) reaction appears in Fig. 3.13. A similar representation of the design reaction appears in Fig. 3.14. These predictions have been qualitatively corroborated by preliminary experimental research performed at the University of Washington. A small methane-oxygen rocket engine was developed and tested at various O/F mass ratios. No noticeable soothing was observed throughout the testing range. Appendix B describes this work.

3.4.5 Engine Design

Expander cycle rockets are impractical at combustion chamber pressures above 1100 psia (7.58 MPa). For this reason the rocket was designed to operate at a chamber pressure of 750 psia (5170 kPa), ensuring a relatively high thrust from a compact engine. The thrust of the rocket can be calculated from [17]:

$$T=C_F P_O A_t \tag{3.5}$$

where:

T = Thrust

C_F = Coefficient of thrust

P_O = Chamber or stagnation pressure

A_t = Nozzle throat area

The coefficient of thrust can be calculated from the following relation [17]:

$$C_F = \sqrt{\left[\frac{2\gamma^2}{\gamma-1}\left(\frac{2}{\gamma+1}\right)\right]^{\frac{\gamma+1}{\gamma-1}}\left[1-\left(\frac{P_e}{P_c}\right)^{\frac{\gamma-1}{\gamma}}\right]}+\frac{P_e-P_a}{P_c}\cdot\frac{A_e}{A_t} \tag{3.6}$$

where:

γ = specific heat ratio, C_p/C_v

P_e = Pressure at nozzle exit

P_a = Ambient pressure

A_e = Nozzle exit area

The exhaust pressure of the rocket is a function of the nozzle area expansion ratio. The conditions of the product gases in the combustion chamber have been calculated using the CET-89 code and are listed in Table 3.12.

A plot of the variation of combustion temperature and the average product molecular mass as a function of appears in Fig. 3.15. The variation of Cp and γ appears in Fig. 3.16.

Table 3.12 Combustion product characteristics as a function of equivalence ratio.

O/F mass ratio	3.5:1	2:1
Chamber pressure (psi, kPa)	750 (5170)	750 (5170)
Chamber temperature (K)	3591	2737
Molecular weight of product gases (kg/kmol)	21.49	15.96
γ, Specific heat ratio of product gases	1.13	1.218
Gas constant (R) of product gases (J/kg-K)	386.7	521.0

The MLVH rocket engines have a design nozzle area expansion ratio of 50:1. This expansion lowers the product gas pressure from 5170 kPa to 3.6 kPa at the nozzle exit. The coefficient of thrust is 2.0, and thus a nozzle throat area of 282 x 10^{-6} m^2, i.e., a throat diameter of 1.90 cm is required for a thrust of 2750 N. The exit area is 14.1 x 10^{-3} m^2 and the exit diameter is 0.134 m.

The exhaust velocity of the combustion products can be determined from the following relation [17]:

$$v_e = \sqrt{\left[\frac{2\gamma}{\gamma-1}\right] RT_o \left[1-\left(\frac{P_a}{P_o}\right)^{\frac{\gamma-1}{\gamma}}\right]} \tag{3.7}$$

where:

v_e = exhaust velocity

T_o = combustion chamber temperature

This can be used in turn to derive the specific impulse, which is equal to the exhaust velocity divided by the Earth's gravitational acceleration. The design yields a specific impulse of 344 sec. For completeness, the variation of I_{sp} with O/F mass ratio appears in Fig. 3.17. As can be seen, the I_{sp}, although reduced, is still high enough to the do the job required for the mission at an O/F ratio of 2.0:1.

3.5 REACTION CONTROL SYSTEM

(Takahisa Kobayashi)

The attitude of the MLVH at any instant during its flight must be controlled by orienting its direction as specified by the avionics computer, and this is done by the reaction control system (RCS). There are a number of techniques available for attitude control, and the one which meets the mission requirements best must be selected. Passive control techniques, such as gravity-gradient control, use the inertial properties of a vehicle in a planet's gravity field to point the vehicle toward the center of a planet. Spin stabilization, another passive control technique, rotates the entire vehicle so that its angular momentum vector remains approximately fixed in inertial space. Three-axis controls are a more common technique, in which the control torques about the three axes are provided by combinations of momentum wheels, reaction wheels, thrusters, or magnetic torquers.

Among these techniques, the three-axis control technique was chosen, because it is the most versatile for frequent reorientation. Also three-axis control, coupled to a star tracker and gyros, is indispensable for a control accuracy of less than 0.001° [1]. Three-axis control is accomplished by an all-thruster system.

3.5.1 Thruster selection

There are many different types and sizes of RCS thrusters availiable off-the-shelf. In order to select the proper thrusters, the following criteria was used:

- Thrusters must provide sufficient thrust to achieve desired angular accerelations
- Thrusters must be simple and reliable
- Thrusters must have low mass and high specific impulse
- Propellant must be storable during the mission

First of all, the thrust levels and thruster locations must be determined so that the torque capability of the RCS is large enough to counterbalance disturbance torques and control the attitude at a sufficient rate during maneuvers. In order to do so, all outside and inside disturbance torques and control torques must be considered. The outside disturbance torques include gravity gradient, solar radiation, magnetic field, and aerodynamic torques, while internal disturbance torques stem from uncertainty in center of gravity, thruster misalignment, and oscillatory behavior of flexible bodies in the vehicle. However, these disturbances are relatively small when compared to control torques needed to orient the vehicle to the correct direction during the sequence of events. Thus the sizing of thrusters was determined on the basis of control torques needed. To provide the capability of controlling the vehicle in any direction, including translational, rotational, and slewing maneuvers, a total of twelve thrusters is located symmetrically on the exterior of the vehicle, as shown in Fig. 3.18. In addition, four RCS engines are located at the top of the MLVH to be used

for the aerocapture maneuver, and they must be capable of reducing the speed of the MLVH by 40 m/sec. The sixteen thrusters are identical to reduce costs, and three types of RCS engine modules are shown in Fig. 3.19.

The steps used to determine the thrust level for attitude control are as follows:. First, it was assumed that 180° of slew maneuver during the ballistic hop would be made in 30 sec, while 5% of that time is needed for acceleration and deceleration. Then, angular rotation would be 6° per sec., and this is less than the saturation point (8° per sec.) at which the gyro is saturated and loses all sense of rate and control [18]. Next, the angular acceleration was approximated by the following equation:

$$\ddot{\theta} = \frac{\dot{\theta}}{t} \tag{3.8}$$

where:

$\dot{\theta}$ = average angular velocity

t = time

Since the angular rate of 6° per sec. is reached within 5% of 30 sec., which is 1.5 sec, the angular acceleration is found to be $4°/s^2$. Finally, the thrust level of the thrusters is calculated from:

$$T = \frac{I\ddot{\theta}}{2L} \tag{3.9}$$

where:

T = Thrust of each thruster

I = Moment of inertia of the MLVH about axis in question

L = Moment arm of the thruster

In order to account the aerodynamic effect during the ballistic hop, the moment of inertia of the MLVH about x or y axis was assumed to be 60 kgm^2 (see Table 3.3 for the actual moments of inertia). Setting the moment arm of the thrusters to be 0.34 m from the center of gravity, the thrust level needed was found to be 62 N. Among many existing thrusters which can provide at least 62 N and satisfy the criteria mentioned previously, the monopropellant hydrazine (N_2H_4) rocket engine was selected. Olin Aerospace Co. in Redmond, WA manufactures a hydrazine thruster, MR120, capable of thrust from 40 to 111 N, which is well suited for this mission. It has the dimensions of 0.15 m in length and 0.041 m in the maximum diameter and requires 45 W_e of pulse power. Its specifications are shown in Table 3.13. When the control system signals for thruster operation, thrusters will fire in short pulses of several milliseconds or in longer duration steady state mode.

Table 3.13 Characteristics of monopropellant hydrazine rocket engine.

Nominal Thrust (N)	Thrust Range (N)	Specific Impulse (sec)	Mass (kg)	Number of Engines	Total Mass (kg)
62	40 - 111	220-230	0.409	16	6.54

3.5.2 Hydrazine requirement

Monopropellant hydrazine is the most widely used type of propellant for spacecraft attitude control because of its excellent handling characteristics. Hydrazine is relatively stable under normal storage conditions.

The amount of hydrazine needed for attitude control depends on the duration of RCS operation and is determined by the following equation:

$$m = \frac{Tt}{I_{sp}g} \tag{3.10}$$

where:

m = mass of hydrazine

T = thrust of each engine

t = total pulse length

Also, the amount of hydrazine needed for aerocapture is found from the equation:

$$\Delta V = I_{sp}g \cdot ln\left(\frac{M_i}{M_i - M_p}\right) \tag{3.11}$$

where:

ΔV = 40 m/s

M_i = mass of the MLVH before the aerocapture

M_p = mass of propellant needed for the aerocapture

Assuming the minimum specific impulse of 220 sec., 1.44 kg of hydrazine is employed for attitude control and 12.08 kg of hydrazine is consumed for the aerocapture, both of them including 5% of ullage and 5% of contingency. With this amount of hydrazine, approximately 50 s of continuous attitude control is available.

Finally, the hydrazine is stored in a titanium tank, reinforced by a diaphragm, onboard the MLVH. The shape of the tank is spherical with dimensions of 0.327 m in diameter and wall thickness of 0.58 mm. The masses of hydrazine and titanium tank are shown in Table 3.14.

Table 3.14. Hydrazine and titanium tank characteristics.

Hydrazine		Titanium Tank	
Mass (kg)	Density (kg/m^3)	Mass (kg)	Storable Volume (m^3)
15	1000	2.72	0.015

3.6 AEROBRAKE DESIGN
(Matt Deger)

Aerobraking is a crucial part of the mission scenario in maximizing the payload delivered to the surface of Mars. Studies have consistently shown that an aerobrake provides enough deceleration in the Martian atmosphere to increase the payload significantly over an all propulsive landing [19]. Raked cone, biconic, and symmetrical cone aerobrake configurations were considered for this mission. In order to reduce aerodynamic heating rates and increase the capture window, it is desirable to have an aerobrake that generates lift [20]. However, higher lift to drag ratios (L/D) mean increased aerobrake mass [21]. It was determined that a symmetrical cone design at angle of attack is best suited to provide the necessary lift required, while still maintaining a low aerobrake weight and effective packaging of the spacecraft in the Delta fairing.

3.6.1 Aerobrake Geometry
(Matt Deger)

The aerobrake geometry chosen is a symmetrical 140° cone as shown in Fig. 3.20. In considering the best possible choice of designs to maximize the payload mass, while still fitting the MLVH and aerobrake into the Delta fairing, the symmetrical cone best suited our mission requirements. A biconic aerobrake was dismissed due to the larger mass fraction this style demands [21]. A raked cone configuration, on the other hand, generally offers lower mass with

reasonable L/D values (0.3 - 0.5), but requires an unfortunate amount of space to effectively package the MLVH into the Delta fairing. In addition, skirt and ballute configurations were dismissed for their deployment complexity and lack of proven reliability.

The diameter of the aerobrake is 2.7 m with a nose radius of 0.5 m and an edge radius of 0.2 m. The edge and nose are rounded to reduce local heating, which is discussed in section 3.6.4. This gives the cone a cross-sectional area of 5.7 m^2 and a surface area of 6.1 m^2. The center of mass of the aerobrake is 0.35 m measured from the nose along the symmetrical axis. The aerobrake provides a coefficient of drag (C_d) of 1.4 and a lift to drag ratio (L/D) of 0.18 at a 20° entry angle of attack. The aerobrake is attached to the bottom of the MLVH as discussed in section 3.6.2. It is necessary to extend the structure of the MLVH downward by 0.2 m so that the aerobrake does not interfere with the engines protruding from the bottom of the MLVH.

3.6.2 Aerobrake Structure
(Matt Deger)

The aerobrake is connected to the MLVH with Al-Li 2090-T83 alloy tubing, the same as used on the MLVH structure. Since the detachment of the aerobrake is critical in the landing procedure, the number of connection points had to be kept low. There are eight connection points to the bottom of the MLVH, four on the outer ring and four on the inner ring, as shown in Fig. 3.21. They are attached at radii of 1.23 m and 0.47 m, respectively. The connection points on the inner and outer rings are staggered to eliminate vibrational instabilities. The structure holds the back plane of the aerobrake 0.1 m below the largest MLVH octagonal structural ring.

The tubes are pinned to the polyimide-graphite (PI-GR) backing by means of an adapter plate as shown in Fig. 3.22. There are two tube members at each connection point pinned at 45° angles to distribute the aerodynamic loads. The thickness of the PI-GR backing is tripled at the connection points to 6 mm to prevent local failure. Figure 3.22 also shows where the pyrotechnic bolts are located for the separation before landing. The connection tubes are joined at this bolt

which is placed below the octagonal MLVH joint. This is done to ensure that the main structure is not compromised when the bolts blow.

3.6.3 Thermal Protection System
(Matt Deger)

The low Mars entry velocity of this mission (5.9 km/s) means that aerodynamic heating is almost entirely in the form of convective heat transfer [22]. Therefore, it is unnecessary to use ablative materials in the design of the thermal protection system (TPS). The TPS uses an emissive surface coating and insulation to reduce heating to acceptable levels. The TPS cross section can be seen in Fig. 3.23.

The TPS consists of a Refractory Cured Glass (RCG) emissive coating which serves to radiate most of the heat flux out into the atmosphere [23]. The insulation used is a Fibrous Refractory Composite Insulation (FRCI-12) which is lightweight and has a low thermal conductivity of 0.1670 W/m·K [24]. A Nomex strain isolation pad is required to relieve the strains encountered by the FRCI - 12 tiles due to the high temperature gradients.

The TPS is supported by a sandwich backing designed to support transverse moments as well as bending moments. The sandwich is made up an Aluminum - 2024 honeycomb core (20 mm thick) and two sheets of PI-GR (2mm thick) to give it bending stiffness [20]. All layers of the TPS and support structure are bonded together with RTV - 560 adhesive. Table 3.15 shows the breakdown of the density, mass, thickness, and allowable heat load of each component.

C-2

Table 3.15 Thermal protection system and supporting structure.

	Density (kg/m^3)	Mass (kg)	Thickness (mm)	Maximum Allowable Temperature (K)
RCG emissive coating (e = 0.85)	1666	4.3	0.25	---
FRCI - 12 composite insulation	192	79.1	40	2701
Nomex SIP strain isolation pad	86.5	2.7	3	717
PI-GR polyimide-graphite face sheets	1550	16.0	1	450
Aluminum-2024 Honeycomb core	56	17.3	30	---
RTV - 560 adhesive	1410	14.5	1	561

3.6.4 Aerodynamic Heating and G-Loading
(Matt Deger)

The heating that the aerobrake receives during capture into the Martian atmosphere is calculated using simplified equations of motions [24]. The MLVH at entry into the Martian atmosphere has a ballistic coefficient ($B = m/C_d \cdot A$) of 78 kg/m^2 calculated from its 625 kg mass, 5.7 m^2 area, and a C_d of 1.4. The nose radius of the aerobrake is 0.5 m and the entry velocity is 5.9 km/s at an altitude of 300 km. The maximum stagnation point heating rate is 27.6 W/cm^2 and occurs at an altitude of 50 km. The average heating occurring at this altitude over the entire

aerobrake is 11 W/cm^2 [25]. This heating rate, along with the maximum allowable temperature limit for the epoxy, sets the required thickness of the insulation discussed in section 3.4.3 [26].

The symmetrical aerobrake is designed to enter the atmosphere at a 20° angle of attack. This creates a 45° wake angle as measured from the bottom plane of the MLVH [27]. The heating produced from the wake is a potential show stopper and is the main driver in the low profile design of the MLVH. This can be seen in Fig. 3.24.

The g-loading due to atmospheric entry is the largest load the aerobrake must undergo and is therefore critical to the design of the structure. The maximum deceleration the aerobrake experiences is 118.5 m/s^2. This corresponds to a deceleration of 12 Earth g. The MLVH experiences a terminal velocity of 366 m/s just before it is jettisoned at an altitude of 7.8 km.

3.7 PARACHUTE
(Francisco Garcia Acosta)

After the aerobrake is jettisoned, a parachute is deployed until terminal propulsion ignition (retrorockets) is started. The purpose of the parachute is, of course, to decelerate the MLVH and to stabilize the MLVH flight by reducing the relative angle between the flight path and the local vertical. The parachute decelerates the MLVH from a velocity of approximately 300 m/s (8 km of altitude) to a velocity of about 73 m/s (1.6 km of altitude). When the deceleration of the parachute is completed, an automatic detachment separates the parachute from the MLVH.

The parachute selected for Project Genesis is the disk-gap-band design as shown in Fig. 3.25 [28, 29]. The design is the same as that successfully used in the Viking missions. However, the material used for the parachute fabric is not nylon but Kevlar-29 (see section 3.7.4). The diameter of the parachute is 12 m, and it is packed in a Teflon deployment bag located in a canister on the top of the MLVH, as shown in Fig. 3.1. The MLVH hangs from the parachute by 50 suspension lines having a total length of 30 m.

3.7.1 Parachute Configuration

Several factors were taken in consideration before selecting the final configuration. General aerodynamic characteristics such as the parachute drag coefficient (C_d), dynamic pressure, atmospheric density, Mach number, as well as the physical properties of the parachute fabric, (average angle of oscillation, material type, strength, porosity, shape and size). Present designs offer a wide variety of configurations but as stated earlier the disk-band-gap design is the only one which is able to withstand the harsh conditions of the Martian environment.

The disk-gap-band design was developed by the NASA-Langley Research Center [30]. The design is intended to operate at a very low dynamic pressure and supersonic speeds. The parachute is designed to have better stability than conventional designs used in high density and low speed situations. As seen in Fig. 3.26, the canopy is constructed as a flat, solid circular disk and a cylindrical band separated vertically by an open space.

A gore (the radial sections into which a parachute is divided) consists of a triangular top and rectangular bottom. The disk, gap, and band areas are 53%, 12%, and 35% of the total area (S_o), respectively. Table 3.16 [30] shows some of the geometric characteristics of the parachute. The value of the nominal diameter (D_n) is computed as the actual three-dimensional canopy constructed diameter length. S_o is the area of the circle whose diameter is D_n. The disk diameter of the parachute (D_d) is the one projected on a planar surface.

3.7.2 Deployment System

When a parachute is performing on Earth, a secondary or drogue parachute is commonly used to extract the deployment bag in which the main parachute is contained. However, the low density of the Martian atmosphere will not provide enough impulse for such an operation. A

reliable means for imparting enough velocity to the parachute bag to ensure its deployment is a mortar.

Table 3.16 Parachute geometric and performance characteristics.

Item	Value	Relative Value
Nominal Diameter (D_n)	17 m	1 D_n
Disk Diameter (D_d)	12 m	0.776 D_n
Total Area (S_o)	230 m^2	(π/4) D_n
Drag Coefficient	0.57	--
Average Angle of Oscillation	$\pm 10^\circ$ to $\pm 15^\circ$	--
Number of Suspension Lines	50	--
Length of Suspension Lines	30 m	1.7 D_n
Total Mass	20 kg	--

The parachute, which is in its deployment bag, is located in a mortar canister located on the top of the MLVH. When the on-board sensors detect the selected altitude, the mortars charge is activated and a sabot ejects the bag out of the canister. A shield protects the fabric from the hot gases generated by the burning charge. The mortar is designed to jettison a mass of 20 kg at a velocity of 30 m/s. Components to be ejected include the parachute assembly, deployment bag, cover, and sabot. The main sequences of the parachute deployment are:

- Explosive nuts are fired
- Cover case is removed
- Mortar fired
- Bag is released
- Suspension lines are stretched
- Canopy initial inflation.

3.7.3 Deployment Bag

A deployment bag provides a controlled, incremental, and orderly deployment of the suspension lines and the canopy as the bag separates from the payload. Teflon cloth of density 7 g/m^2 is used for the deployment bag.

The primary advantages of using a deployment bag are:

- The drag area of the deployed parachute mass is minimized, which reduces the snatch load.
- The canopy is more correctly placed relative to the payload at the start of the opening process, which reduces parachute malfunctions
- Friction damage to the canopy of suspension lines from ribbon or line rubbing is reduced because of the protection afforded by the bag and associated line ties.

3.7.4 Parachute Material

Improvements over the last decade in textile fibers used for parachute fabrics have contributed significantly to the design of lighter and smaller volumes for parachute compartments. One of the great contributions was the development of Kevlar. The use of this material greatly improved greatly the available strength and the useful temperature range of parachute fabric. Table 3.17 illustrates the major differences between several materials used in the construction of parachute fabric [30].

Table 3.17 Comparison of various parachute fabric materials.

	Nylon	Polyester	Nomex	Kevlar 29
Rupture Strength (10^{-6} psi)	90-130	100-140	90	350-400
Rupture Elongation (%)	15-25	12-20	15-20	4
50% Room-Temperature Strength (°F)	350	400	500	550
Initial Tensile Modulus (10^{-6} psi)	0.6	1.8	2.5	10.5
Torsional Shear Modulus (10^{-6} psi)	0.004	0.008	0.17	0.27

After reviewing the data, it is seen that Kevlar is a fiber that exhibits very good strength. Because of its excellent thermal and mechanical properties, Kevlar-29 was selected as the material to construct the parachute fabric for Project Genesis. It has been demonstrated in several design applications and many flight tests that Kevlar-29 can be used successfully for critical applications where parachutes must endure supersonic velocities, and where high temperatures result from aerodynamic heating. In addition, Kevlar-29 can withstand the effects of heat sterilization and densely packed storage until the parachute is deployed in the Martian atmosphere.

3.8 MASS INVENTORY
(Igor Turek, Matt Hedman)

Table 3.18 lists the Earth launch masses of the major components of the MLVH. The mass of the upper stage launch adapter is not included. The total mass of the vehicle is well within the Delta launch vehicle's limitation of maximum payload (1000 kg) to be sent to Mars with a C_3 value of 10 km^2/sec^2. Because the total mass is 610 kg, the C_3 capability is increased to 30 km^2/sec^2 [1], thus opening the possibility of a faster and therefore a higher energy transfer trajectory.

Table 3.18 Launch mass breakdown.

Component	Mass (kg)
Structure	72
Landing Gear	16
Aerobrake	95
Parachute	20
Landing Propellant	20
Oxygen Tank	7
Methane Tank	7
Hydrogen Tank	16
Hydrogen	17
PPP	50
Power Supply	55
Science	8
Engines	25
Avionics + Computers	85
RCS	25
Communications	25
Mass Growth	82
TOTAL	625

3.9 CONCLUSION
(Keith Yang)

For the proposed unmanned mission to Mars, the main objective is to demonstrate *in situ* propellant technology. As a part of this technology demonstration, the MLVH is propelled by four LOX/CH_4 rocket engines. These engines have not yet been developed, but research has been and is presently being conducted. A working prototype could be built in a short time. The MLVH design has the capability of acting as a Mars lander and a Mars surface explorer (hopping vehicle). During the ballistic hops, the MLVH carries with it an array of scientific instruments. These

instruments can collect a significant amount of data in two different regions separated by approximately 30 km.

NOMENCLATURE

A	Area
A_e	Nozzle exit area
A_t	Throat area
B	Ballistic coeficient
BR	Ballistic hop range
c_d	Coefficent of drag
C_F	Coefficient of thrust
$\dot{\theta}$	Angular velocity
$\ddot{\theta}$	Angular acceleration
D	Drag
D_d	Disk diameter
D_n	Nominal diameter
DOF	Degrees of freedom
E	Modulus of elastivity
F	Force
FRCI	Fibrous Refractory Composite Insulation
γ	Specific heat retio
GPR	Ground penetrating radar
I	Moment of inertai
L	Lift
L	Moment arm
L_e	Equivalent length
LMR	Landing mass ratio
LOX	Liquid oxygen
M	Bending moment

m	Mass
M_i	Initial mass
MLVH	Mars Landing Vehicle/Hopper
M_p	Propellant mass
MR	Mass ratio
P	Pressure
P_0	Combustion chamber pressure
P_a	Ambient pressure
P_{cr}	Criticall buckling pressure
P_e	Nozzle exit pressure
PI-GR	Polyimide graphite
PPT	Propellant production time
ρ	Density
R	Gas constant
RCG	Refractory Cured Glass
RCS	Reaction Control System
RTPV	Radioisotope thermophotovoltaic generator
S_0	Total area
σ_{ult}	Ultimate stress
σ_y	Yield stress
T	Thrust
t	Time interval
T_0	Combustion chamber temoerature
th	Thickness of tank wall
TPS	Thermal Protection System
v_e	Exhoust velocity
x	Shape factor

REFERENCES

1. Larson, W.J., and Wertz, J.R., *Space Mission Analysis and Design*, Second Edition, Microcosm, Inc and Kluwer Academic Publishers, 1992, pp345-359, 643-649, 657

2. *Delta II payload Planner's Guide*, McDonnell Douglas, Huntington Beach, CA, 1993

3. Sanders,T.H., and Starke Jnr., E.A., Aluminum-Lithium Alloys, MCE Publications Ltd., Birmingham, UK, vol. III, 1989, pp. 1359.

4. Timoshenko S.and Woinowski-Krieger S., "Theory of Plates and Shells," McGraw-Hill, Inc., New York, NY, 1988, pp. 146.

5. Dixon, J., Alcoa Extrusion and Tube, West Lafayette, IN, Personal communication, May, 1994.

6. "A Common Lunar Lander for the Space Exploration Initiative," NASA Johnson Space Center Report, Presentation to Aaron Cohen, September 19, 1991.

7. Niu, Michael C.Y., "Airframe Structural Design," Conmilit Press LTD., Hong Kong, 1988, pp. 70-71,124-127.

8. ANSYS 5.0, Swanson Analysis Systems, Inc., Houston, PA, 1993.

9. "Viking Lander "As Built" Performance Capabilities," NAS1-9000, Martin Marietta Corporation Denver Division Report, Denver CO 80201June 1976, pp. XII-2,XII-7.

10. Masters, A.I., "Investigation of Light Hydrocarbon Fuels with Flox Mixtures as Liquified Rocket Propellants - Final Report," NASA Report CR-54445, Pratt & Whitney Aircraft Paper FR-11443, Sept. 1, 1965.

11. Martin, J.A., "Hydrocarbon Rocket Engines for Earth-to-Orbit Vehicles," *Journal of Spacecraft and Rockets*, Vol. 20, May-June 1983, pp. 249-256.

12. Champion, R., "LOX/CH4 Test Experience & LOX/CH4 Engine Design for Mars Ascent Stage," Program Development Report, NASA Marshall Space Flight Center, AL, Presented Feb. 25, 1993.

13. Keller, J., personal communication, Department of Aeronautical and Astronautical Engineering, University of Washington, April 1994.

14. Hernacki, T.R., "Design and Fabrication of a Hydrogen/Oxygen Thrust Chamber Assembly," Paper No. AIAA-93-2132, AIAA/SAE/ASME/ASEE 29th Joint Propulsion Conference and Exhibit, Monterey, CA, June 28-30, 1993.

15. Huzel, D.K., and Huang, D.H., "Modern Engineering For Design of Liquid-Propellant Rocket Engines," *Progress in Astronautics and Aeronautics*, Vol. 147, 1992, pp 74-77.

16. Gordon, S. and McBride, B., "Computer Program for Calculation of Complex Chemical Equilibrium Compositions, Rocket Performance, Incident and Reflected Shocks, and Chapman-Jouget Detonations," NASA-Lewis Research Center, 1989.

17. Sutton, G.P., "Rocket Propulsion Elements," 6th Ed. ,John Wiley and Sons, 1992.

18. Carpenter, Anita S., "Control of the Magellan spacecraft during aerobraking," Advances in the Astronautical Science Volume 81 AAS 93-016, American Astronautical Society, 1993, pp 78.

19. Papadopoulos, P., Tauber, M.E.and Chang, I-D., "Heatshield Erosion in a Dusty Martian Atmosphere," *Journal of Spacecraft and Rockets*, Vol. 30, March - April 1993, pp. 140-151.

20. Tauber, M., Chargin, M., Henline, W., Chiu, A., Yang, L., Hamm, K. R., and Miura, H., "Aerobrake Design Studies for Manned Mars Missions," *Journal of Spacecraft and Rockets*, Vol. 30, 1993, pp. 656-664.

21. Tauber, M. E., Palmer, G. E., and Yang, L., "Earth Atmospheric Entry Studies for Manned Mars Missions," *Journal of Thermophysics and Heat Transfer*, Vol. 6, No. 2, April - June 1992, pp. 193-197.

22. Braun, R. D., Powell, R. W., Hartung, L. C., "Effect of Interplanetary Trajectory Options on a Manned Mars Aerobrake Configuration," NASA TP-3019, August 1990.

23. Chiu, S. A., Pitts, W. C., "Reusable Surface Insulations for Reentry Spacecraft," 29th Aerospace Sciences Meeting, AIAA - Paper 91 - 0695, 1991.

24. "Atmospheric Re-entry," NACA TN - 4047.

25. Vinh, Nguyen X., Buesmann, A., and Culp, Robert D., *Hypersonic and Planetary Flight Mechanics*, University of Michigan Press, 1980, p.143.

26. Williams, S.D., Gietzel, M. M., Rochelle, W.C., Curry, D.M., "TPS Design for Aerobraking at Earth and Mars," NASA Technical Memorandum 104739, August 1991, p. 30.

27. Andrews, D. G., Aeroassisted Orbital Transfer Vehicle System Technology Analysis, Boeing D180-27979-1, Vol. 1, pp. 32-34.

28. Viking Lander "As Built" Performance Capabilities. Martin Marietta Corporation, Denver, CO. June, 1976. NAS1-9000

29. Peterson, C.W., and Johnson, D.W., "Advanced Parachute Design", Conference, Parachute Systems Technology: Fundamentals, Concepts, and Applications, June 22-26, 1987.

30. Maydew, R.C., Design and Testing of High-Performance Parachutes. AGARD-AG-319.

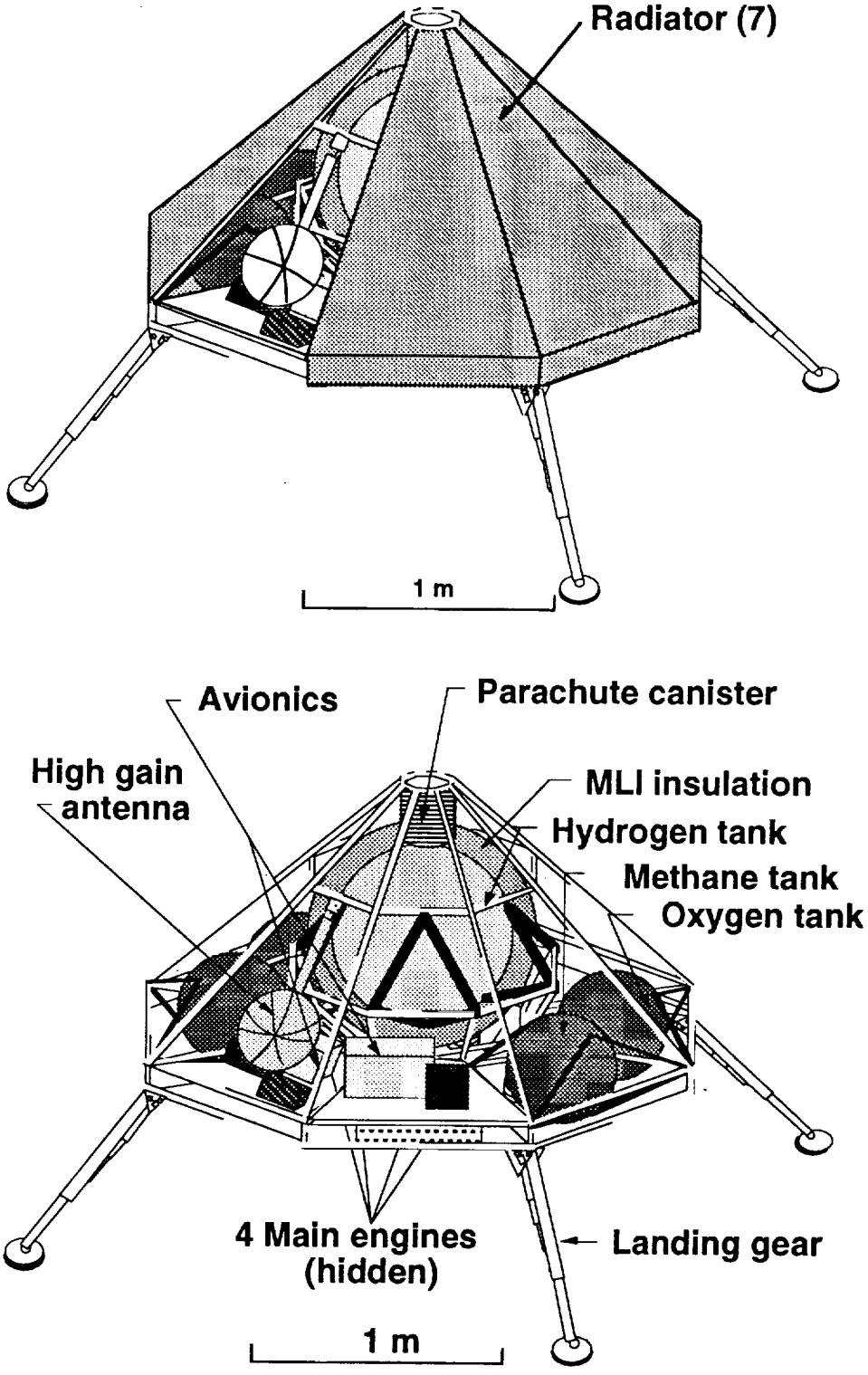

Fig. 3.1 Mars Landing Vehicle and Hopper.

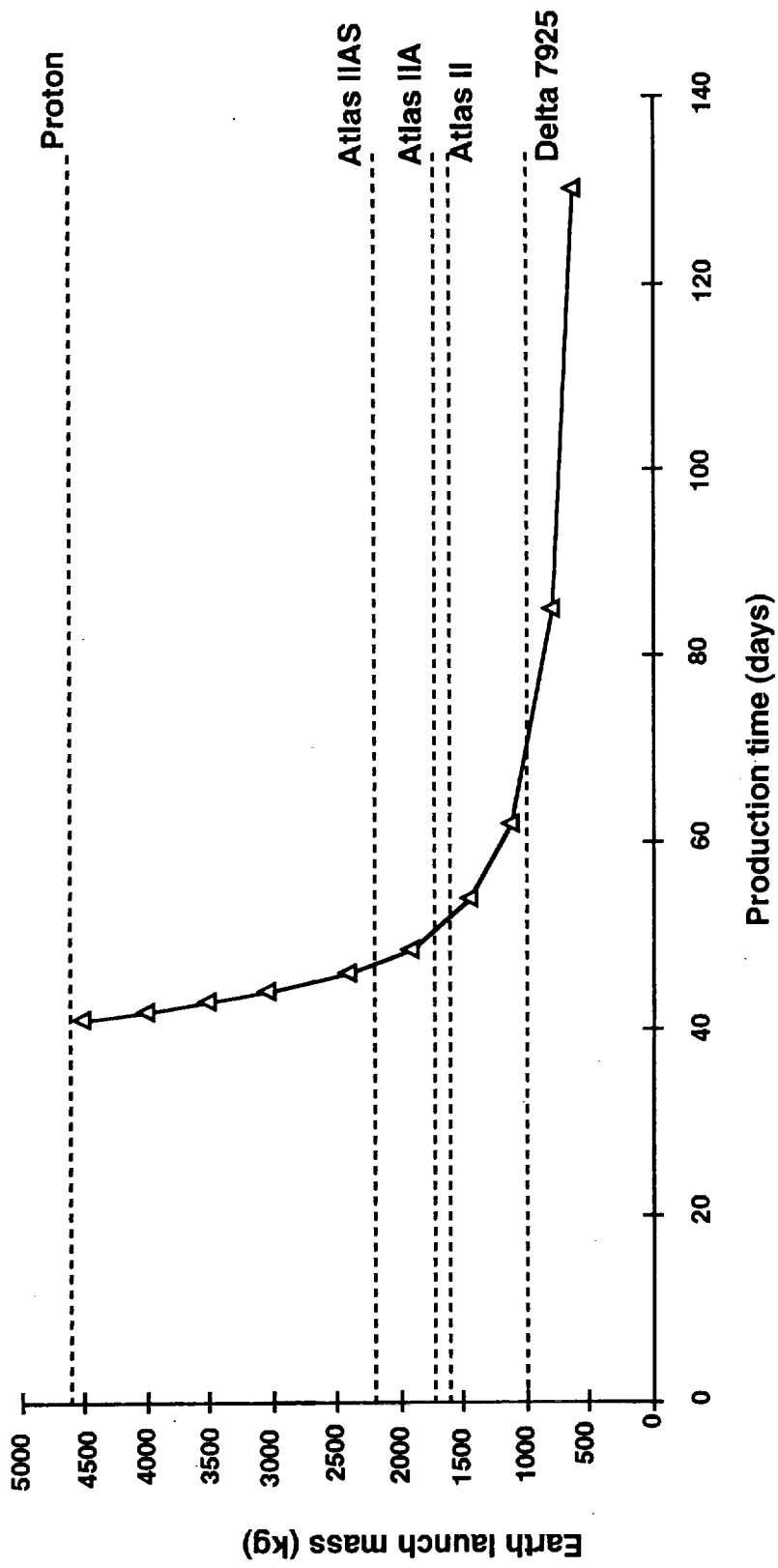

Fig. 3.2. MLVH launch mass vs. propellant production time.

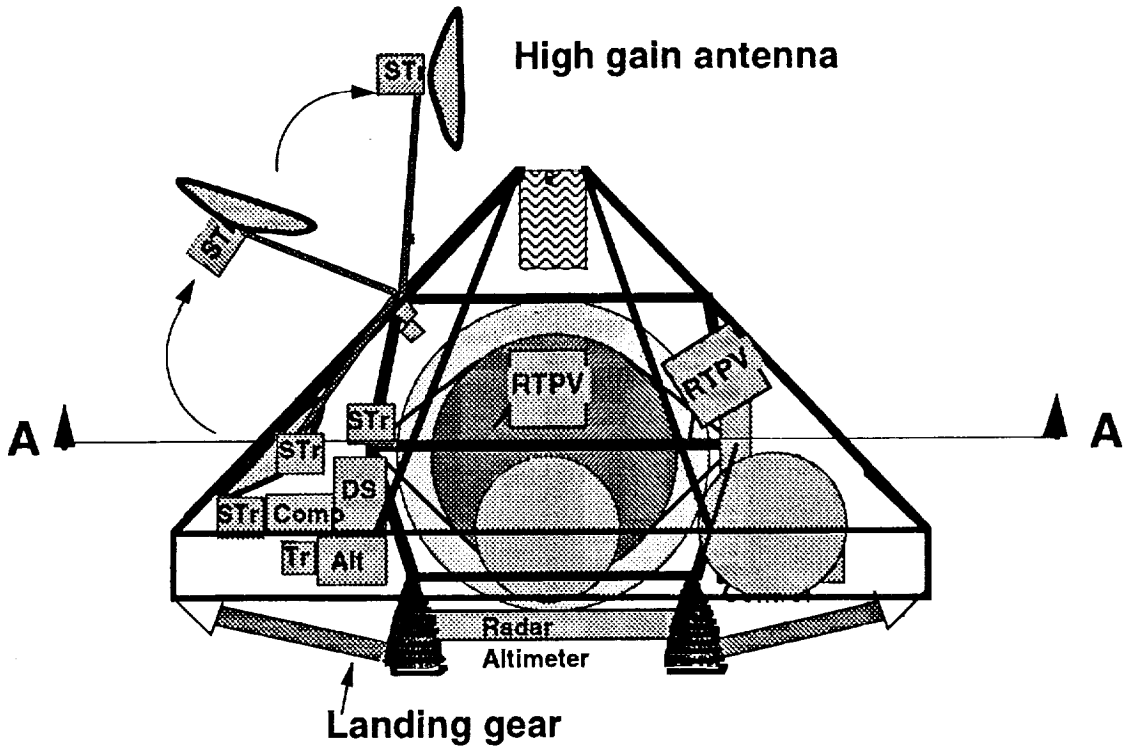

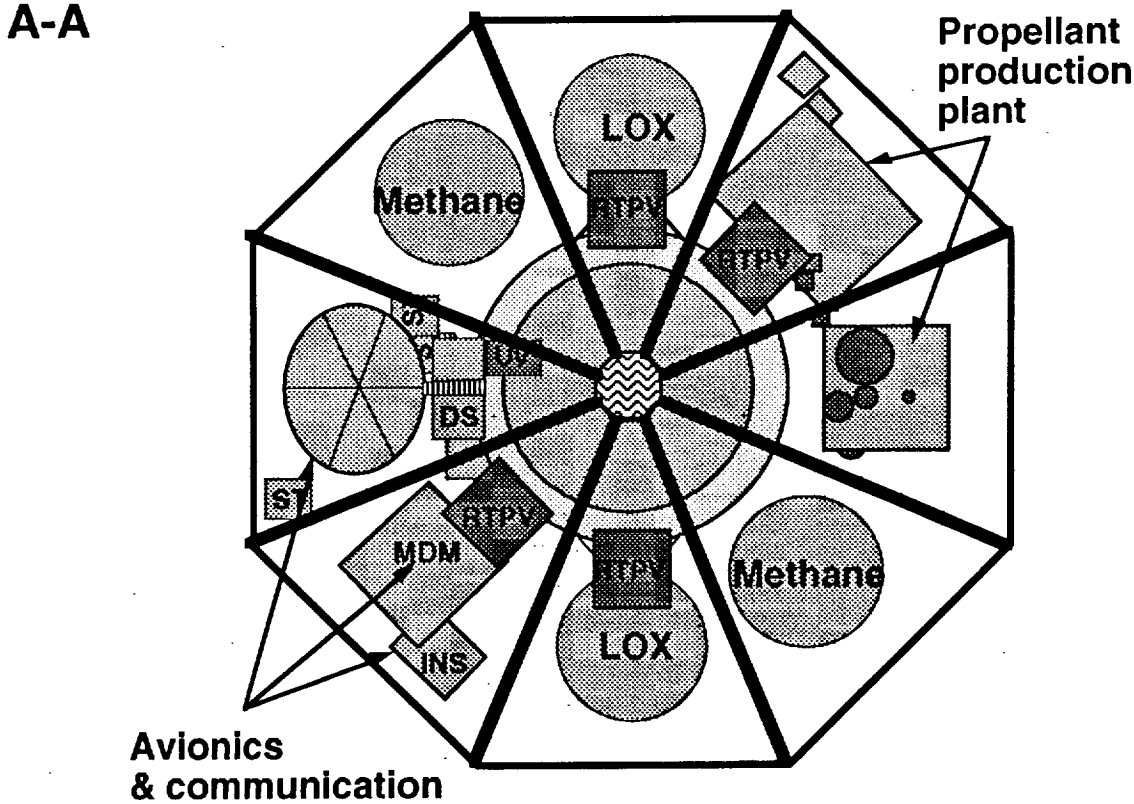

Fig. 3.3 Cross-section of MLVH.

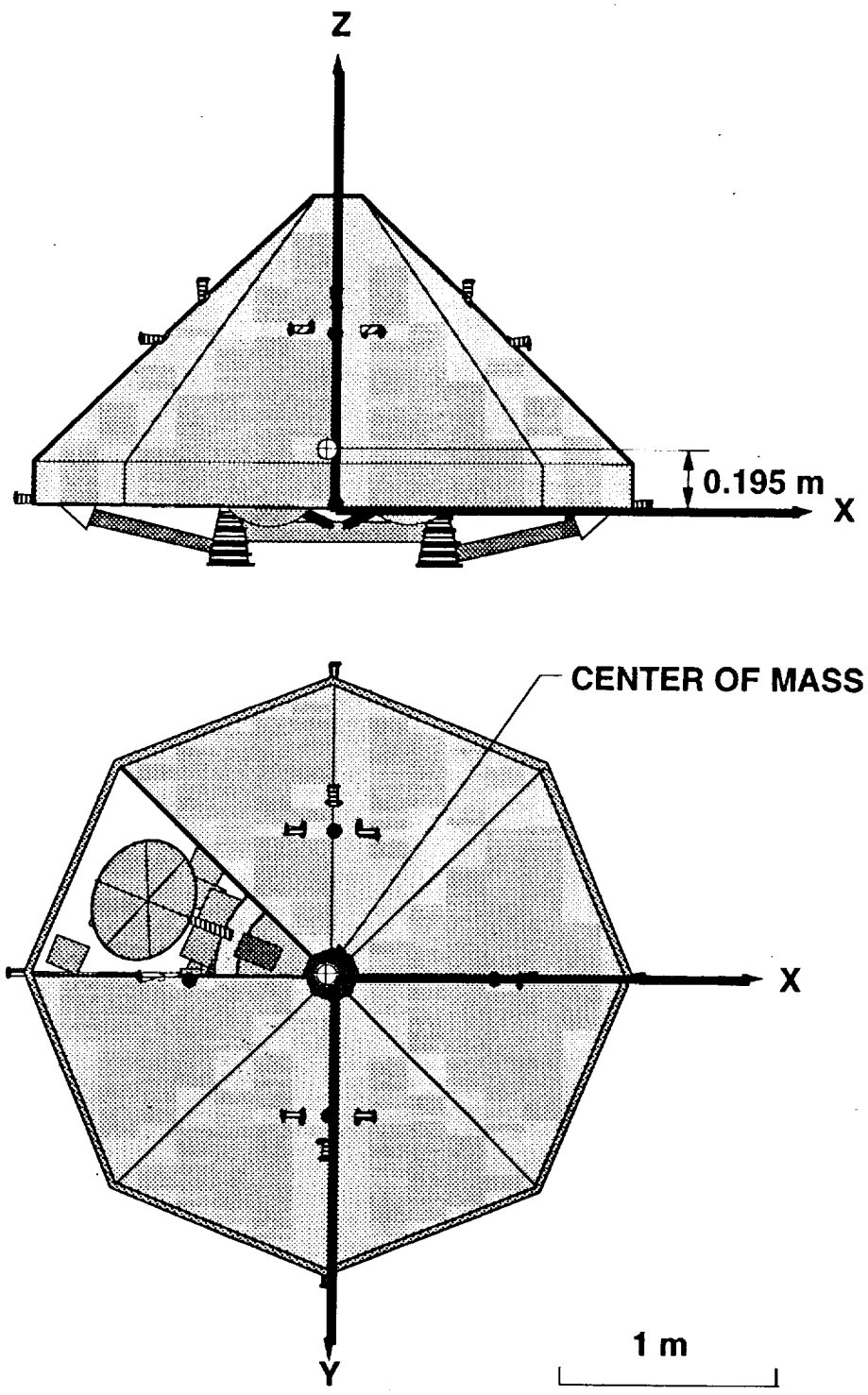

Figure 3.4 Location of center of mass.

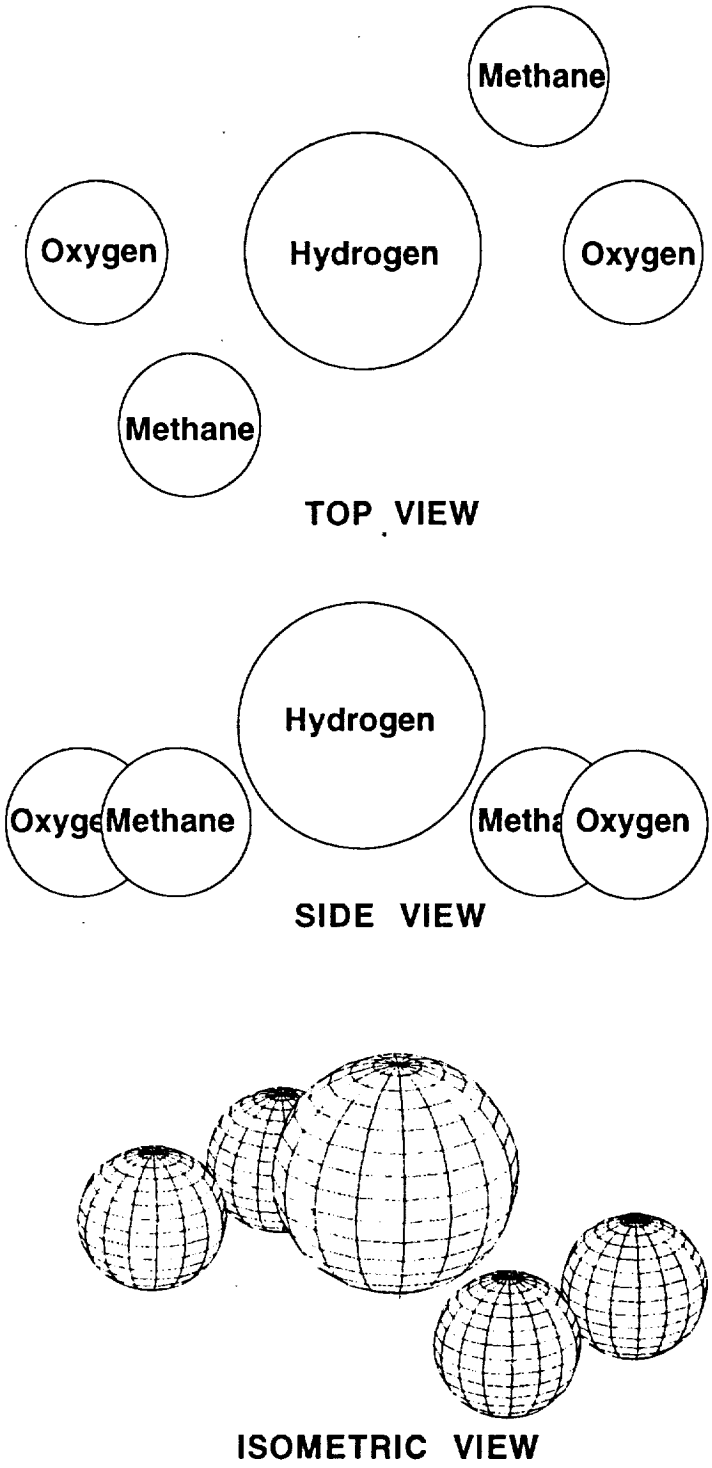

Fig. 3.5 Tank configuration.

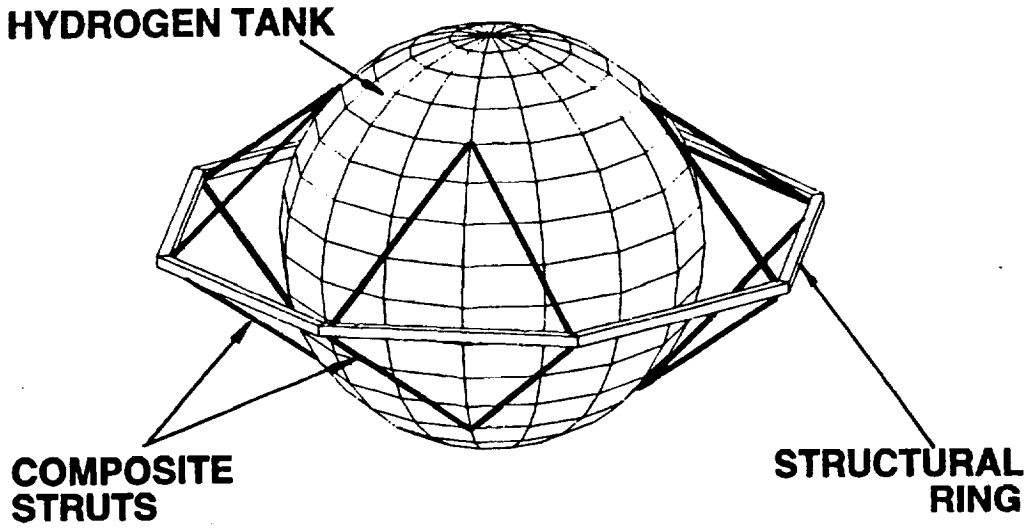

Fig. 3.6 Tank support.

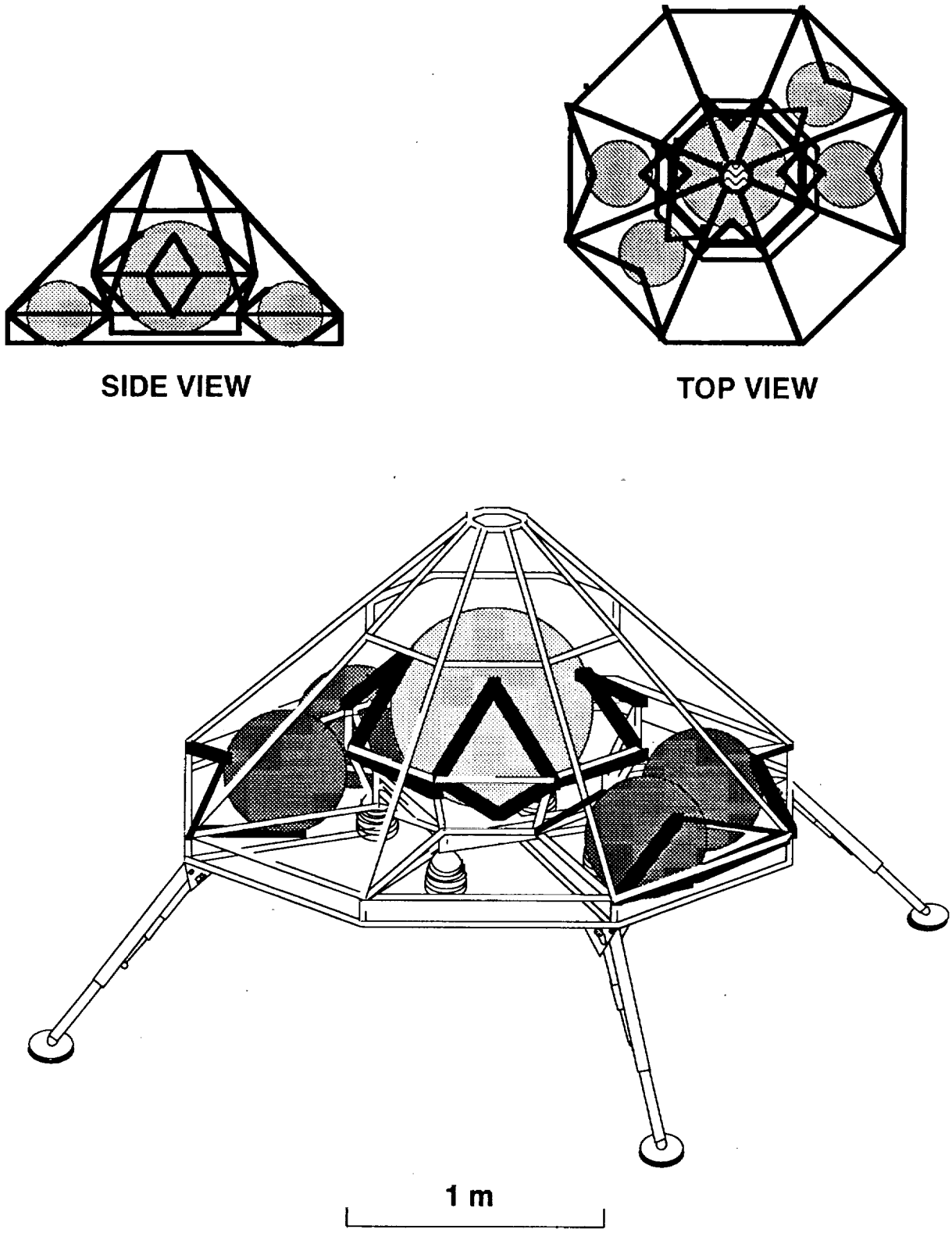

Fig. 3.7 Mars Landing Vehicle and Hopper structure.

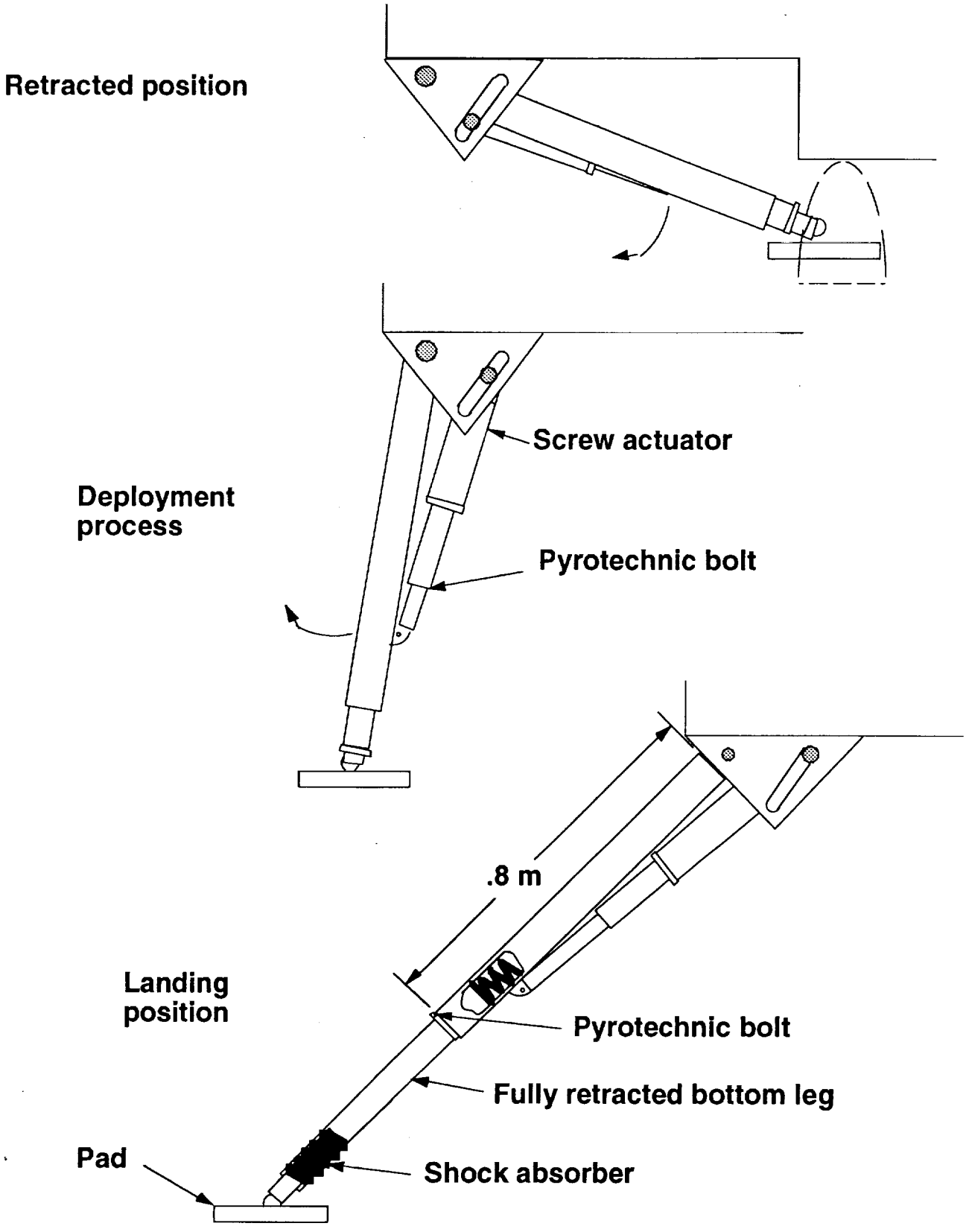

Fig. 3.8 MLVH landing gear.

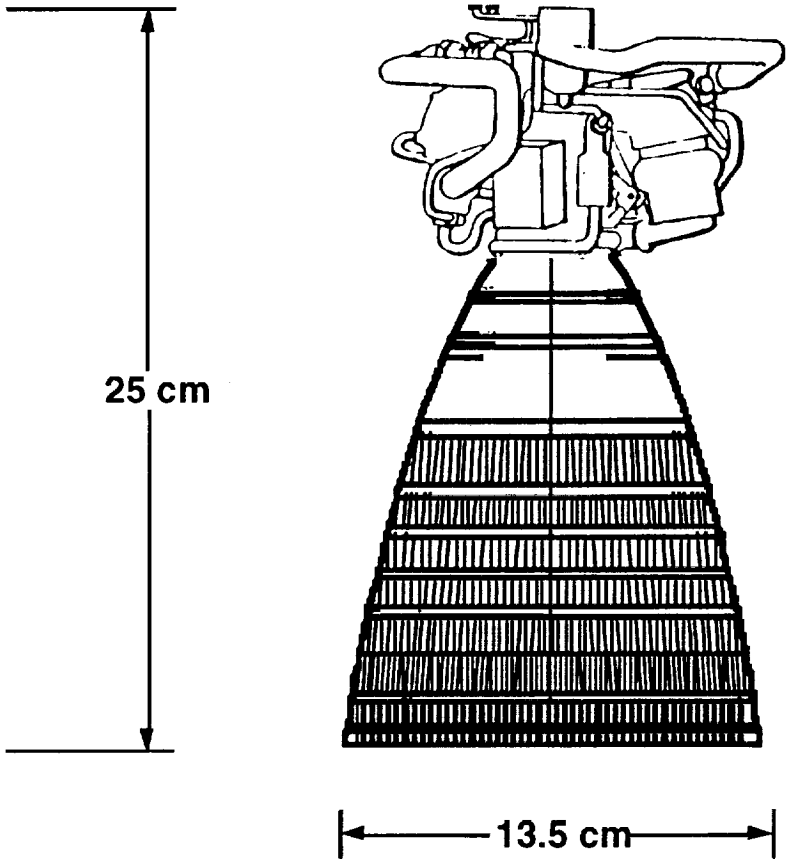

Fig. 3.9 MLVH LOX/CH_4 Landing Engine (625 lbf).

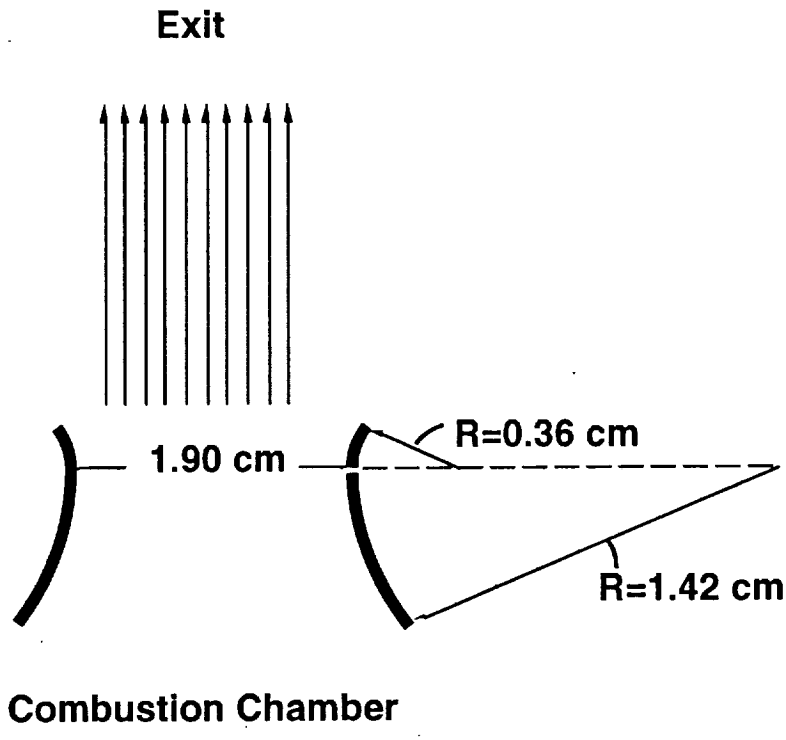

Fig. 3.10 Nozzle throat contour.

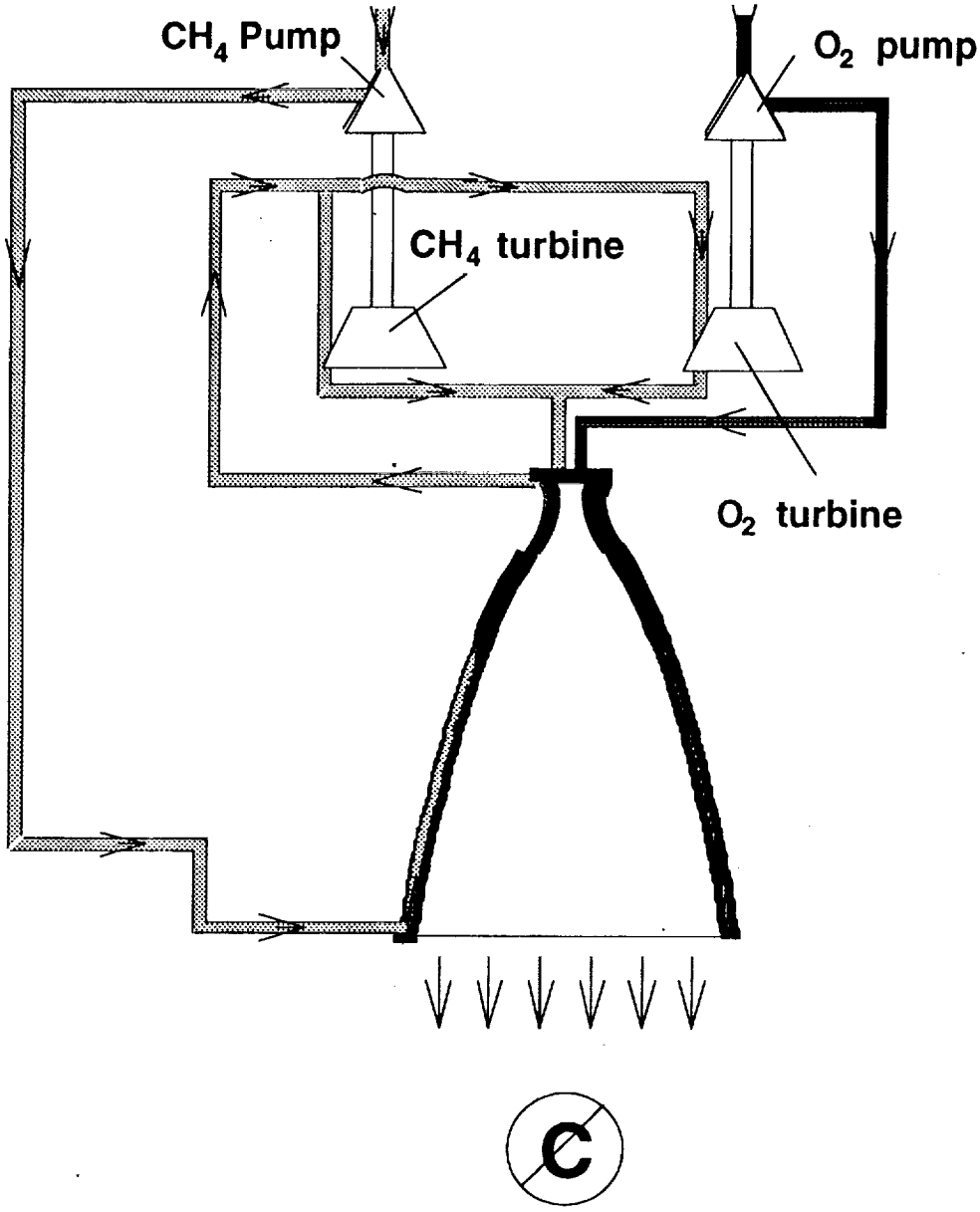

Fig. 3.11 Expander cycle engine schematic.

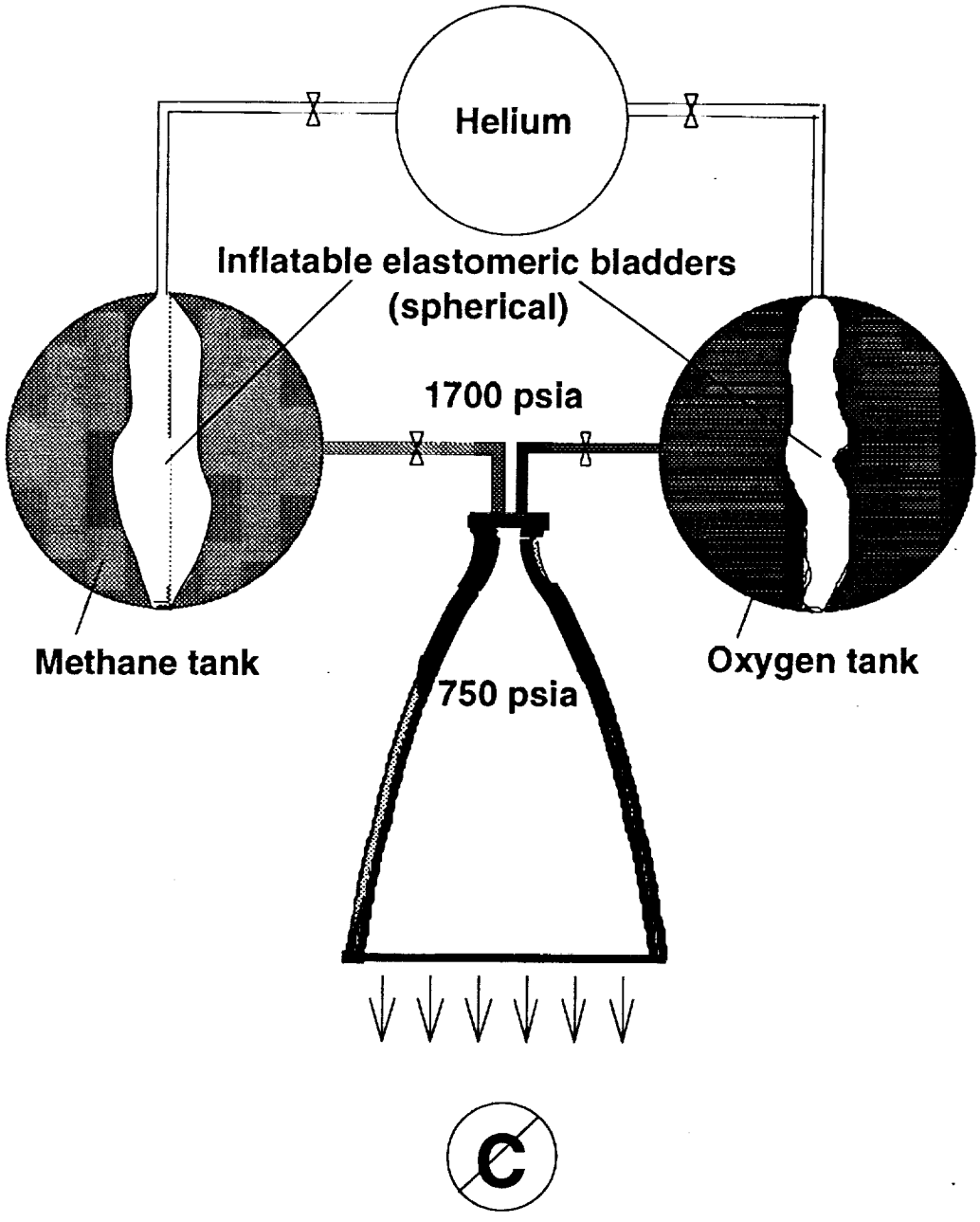

Fig. 3.12 Pressure fed engine schematic.

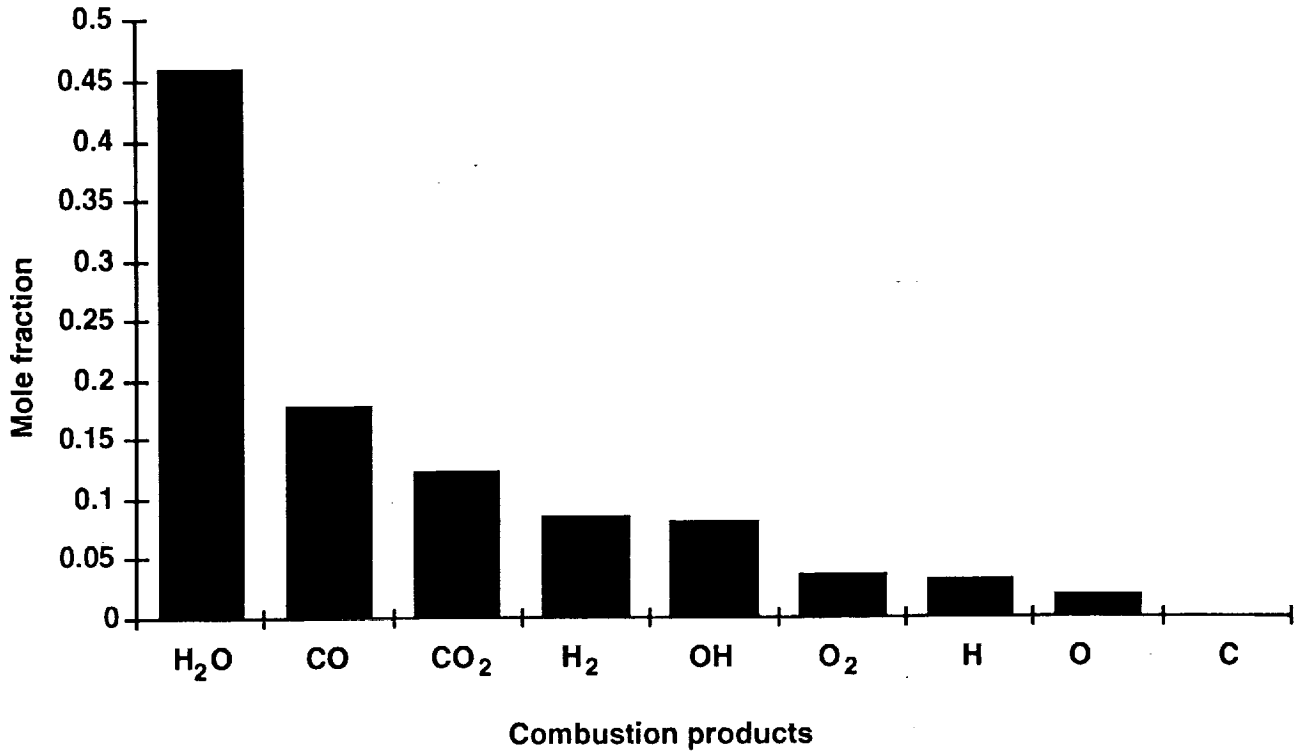

Fig. 3.13 Mole fraction of combustion products at an O/F mass ratio of 3.5:1
P_o=750 psia, $T_{reactants}$=120 K.

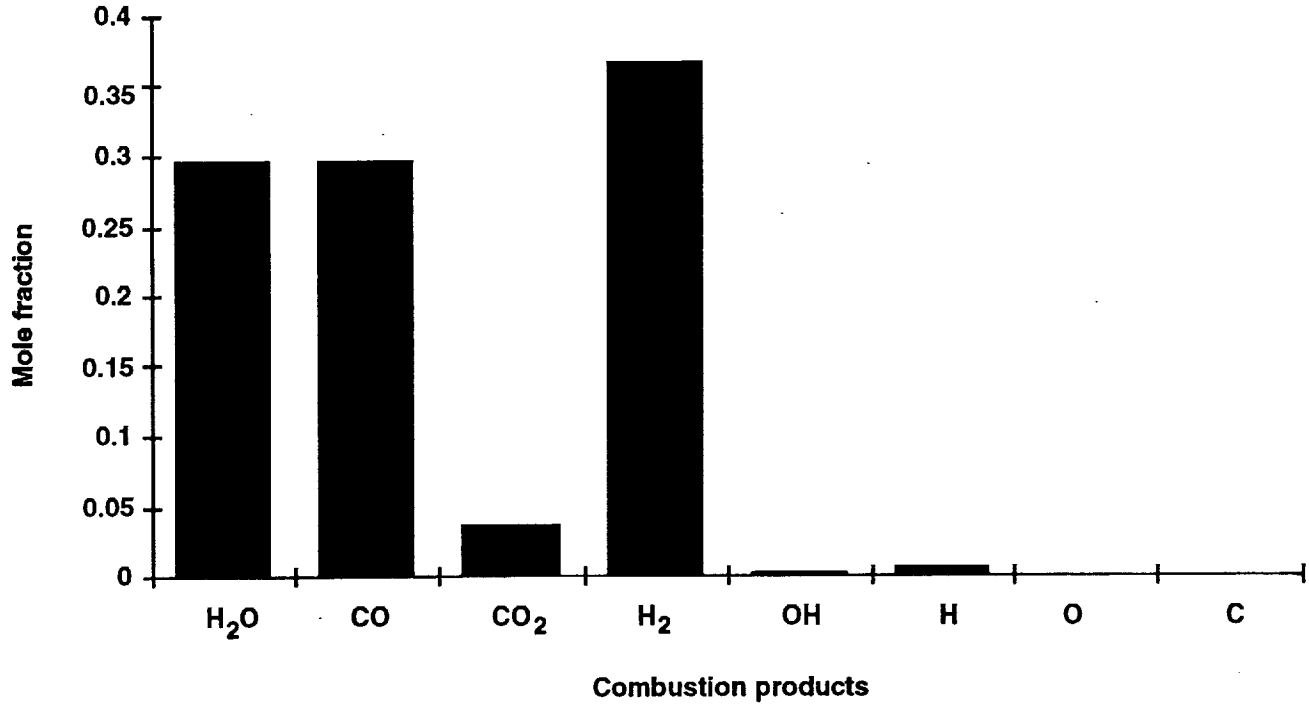

Fig.3.14 Mole fraction of combustion products at an O/F mass ratio of 2:1
P_o=750 psia, $T_{reactants}$=120 K.

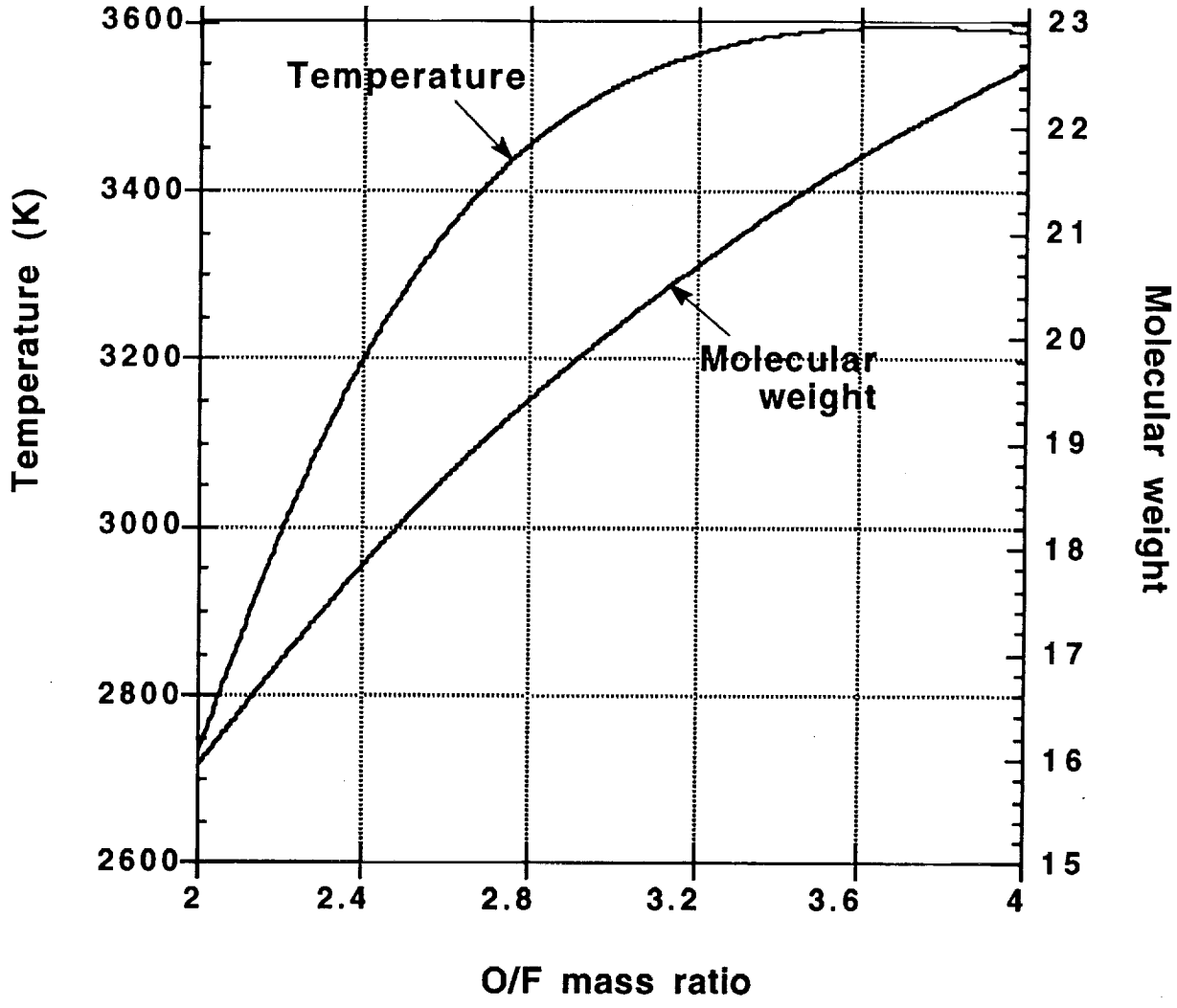

Fig. 3.15 Combustion temperature and product molecular mass vs. O/F mass ratio.
P_o=750 psia, $T_{reactants}$=120 K.

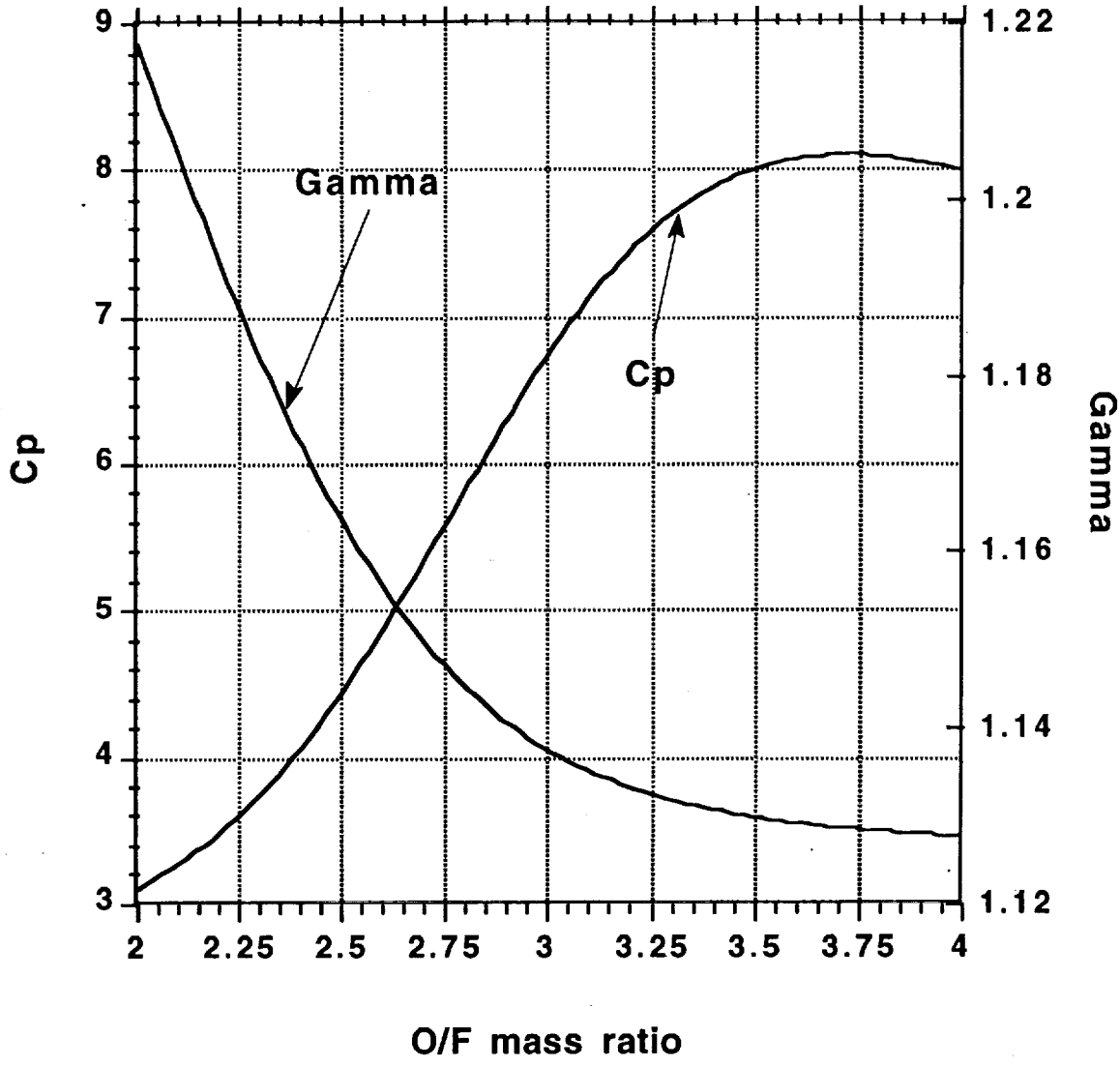

Fig. 3.16 Cp and ratio of specific heats ratio vs. O/F mass ratio.
P_o=750 psia, $T_{reactants}$=120 K.

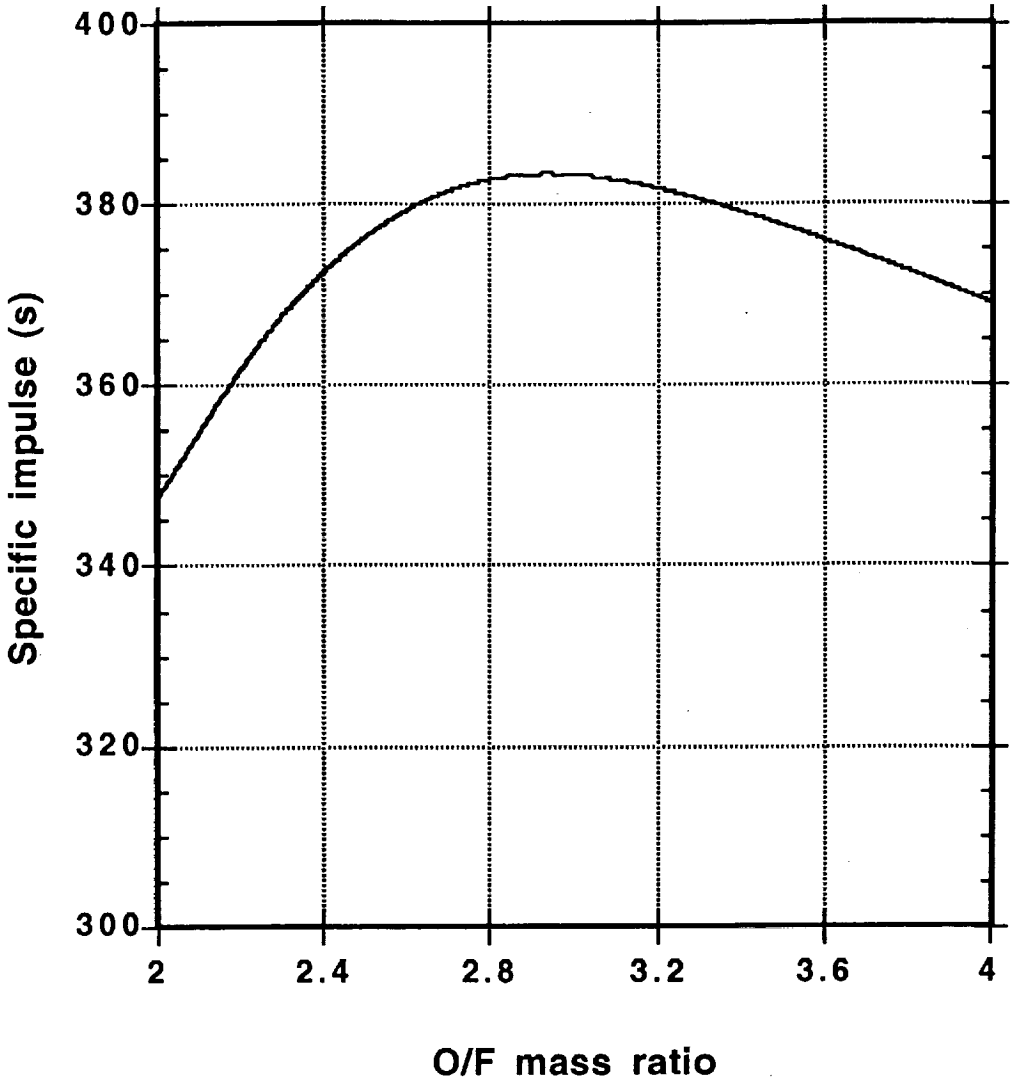

Fig. 3.19 Specific impluse (Isp) vs. O/F mass ratio for a CH_4/O_2 rocket engine. P_o=750 psia, $T_{reactants}$=120 K, A_e/A_t=50.

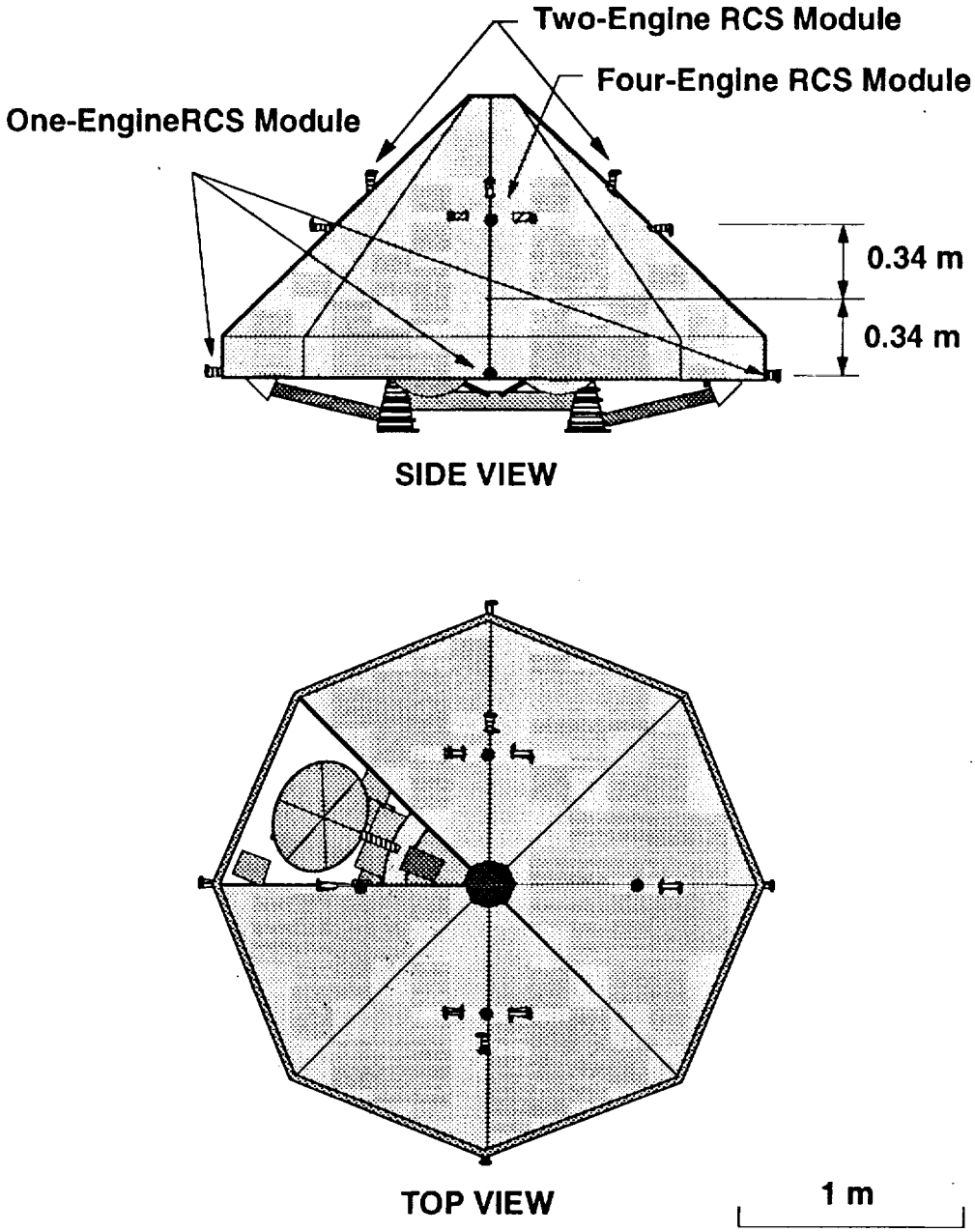

Fig 3.18 Location of reaction control thrusters.

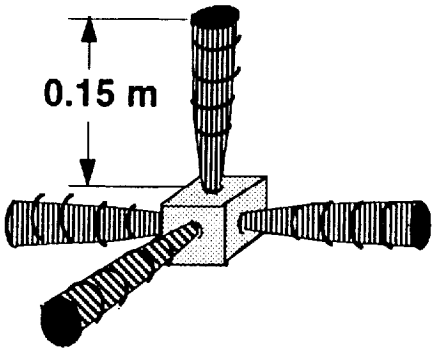

Four-engine RCS module

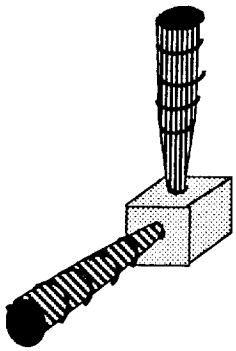

Two-engine RCS module

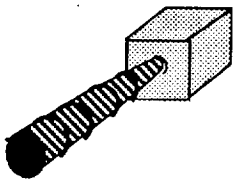

One-engine RCS module

Fig. 3.19 Three types of reaction control system thrusters modules.

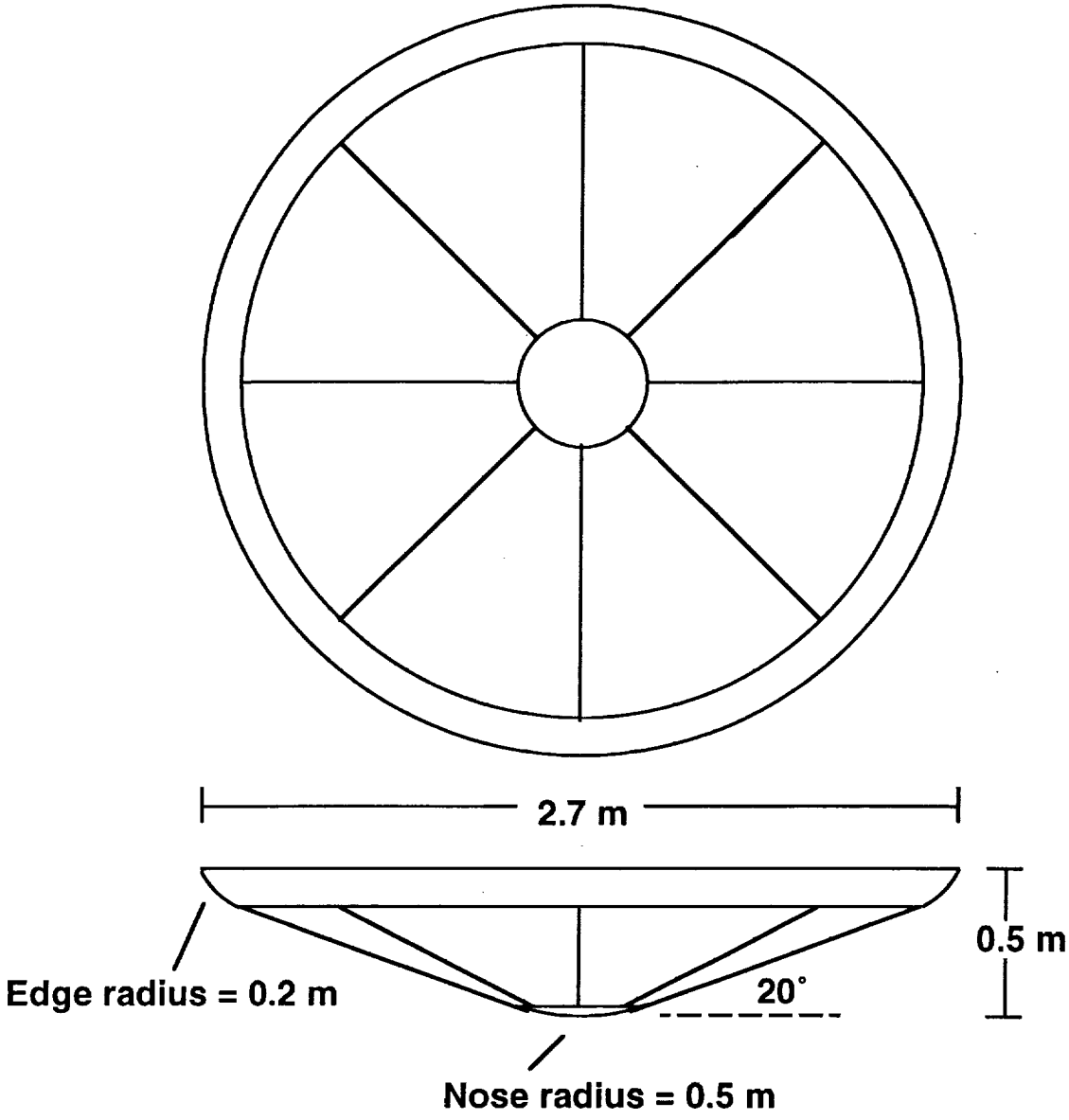

Fig. 3.20 Bottom and side view of aerobrake.

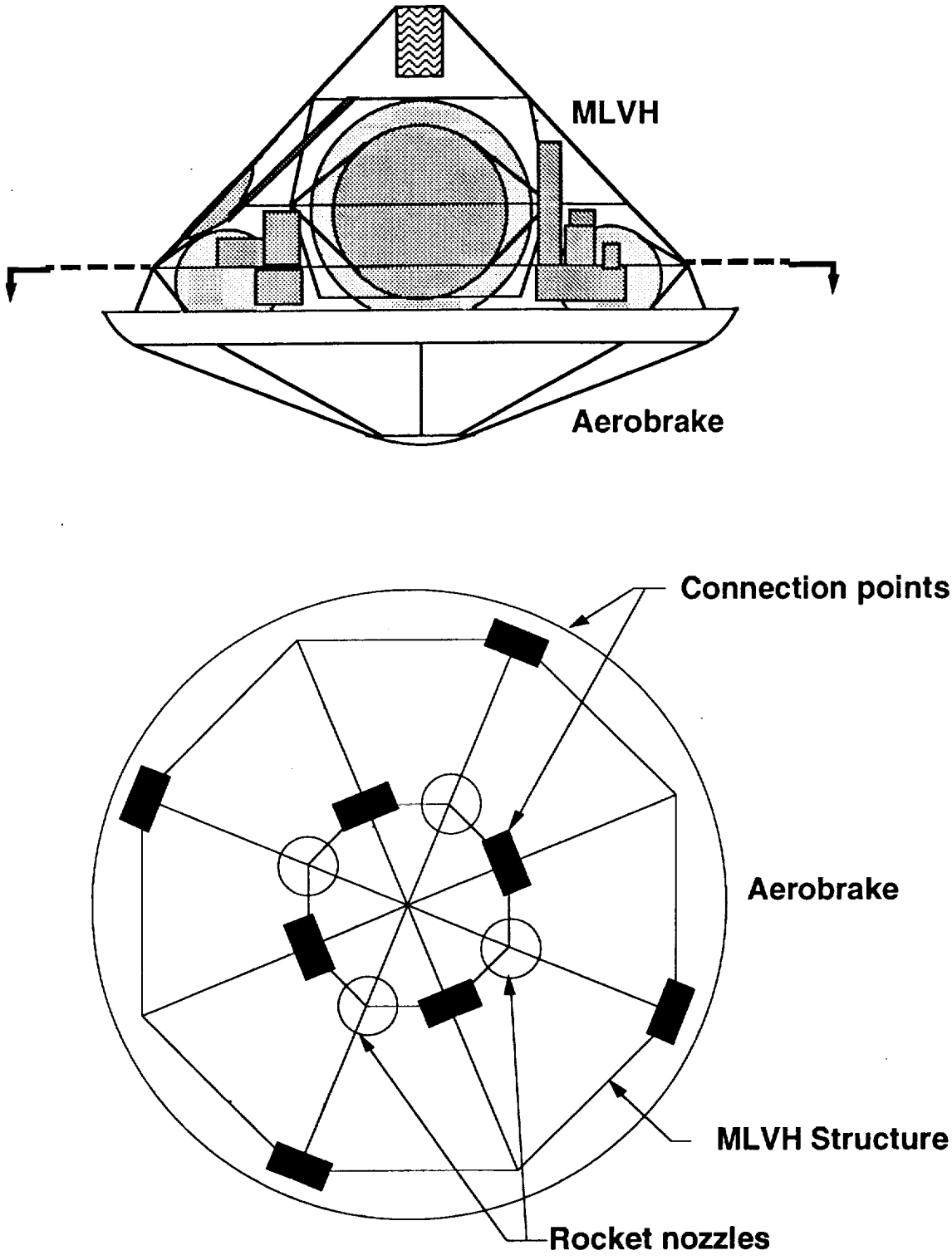

Figure 3.21 Locations of aerobrake connection points.

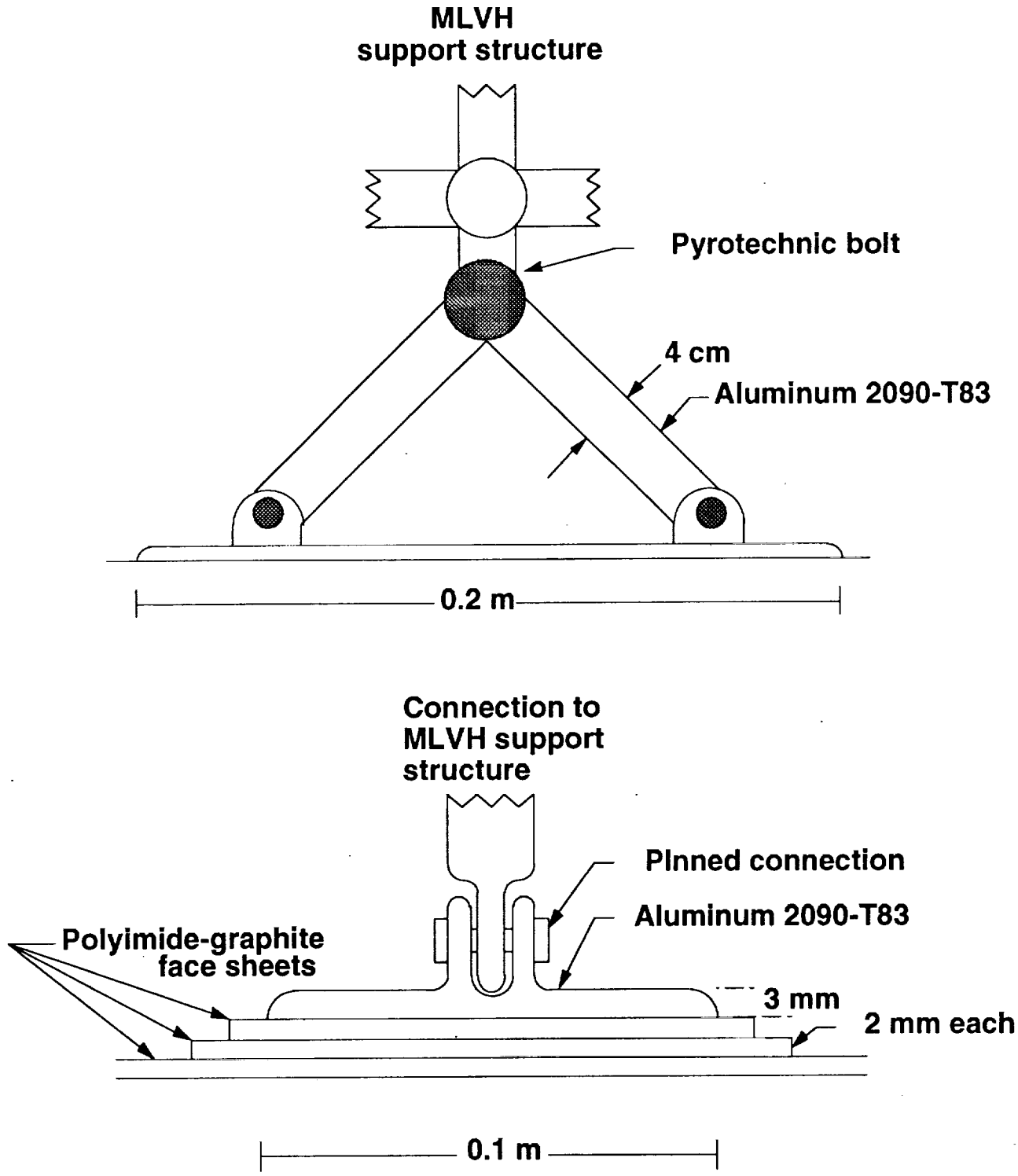

Figure 3.22 Aerobrake support connections.

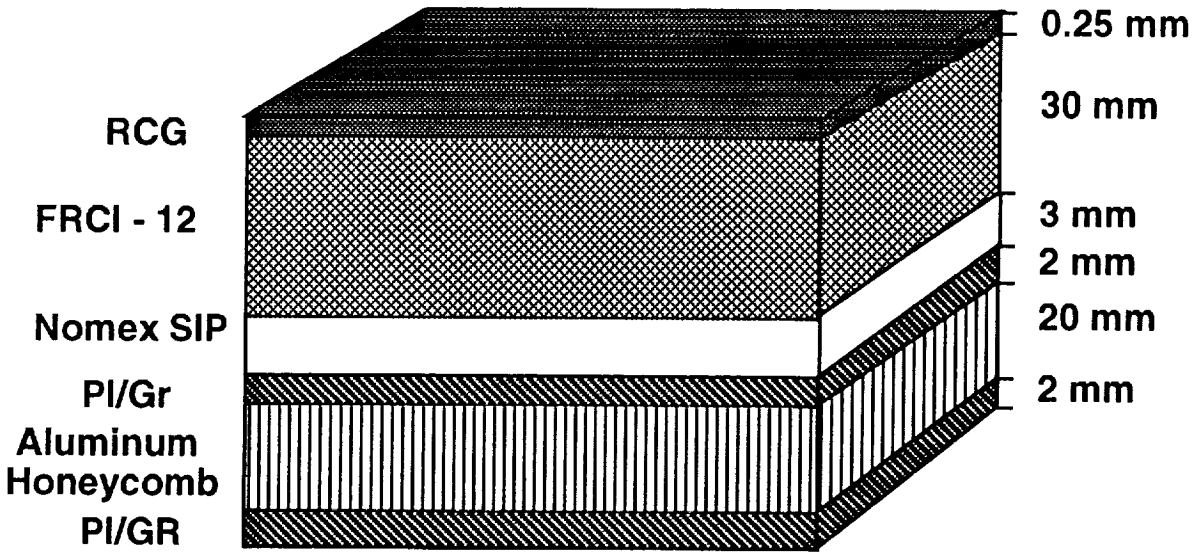

Fig. 3.23 Cross sectional view of the TPS and support structure.

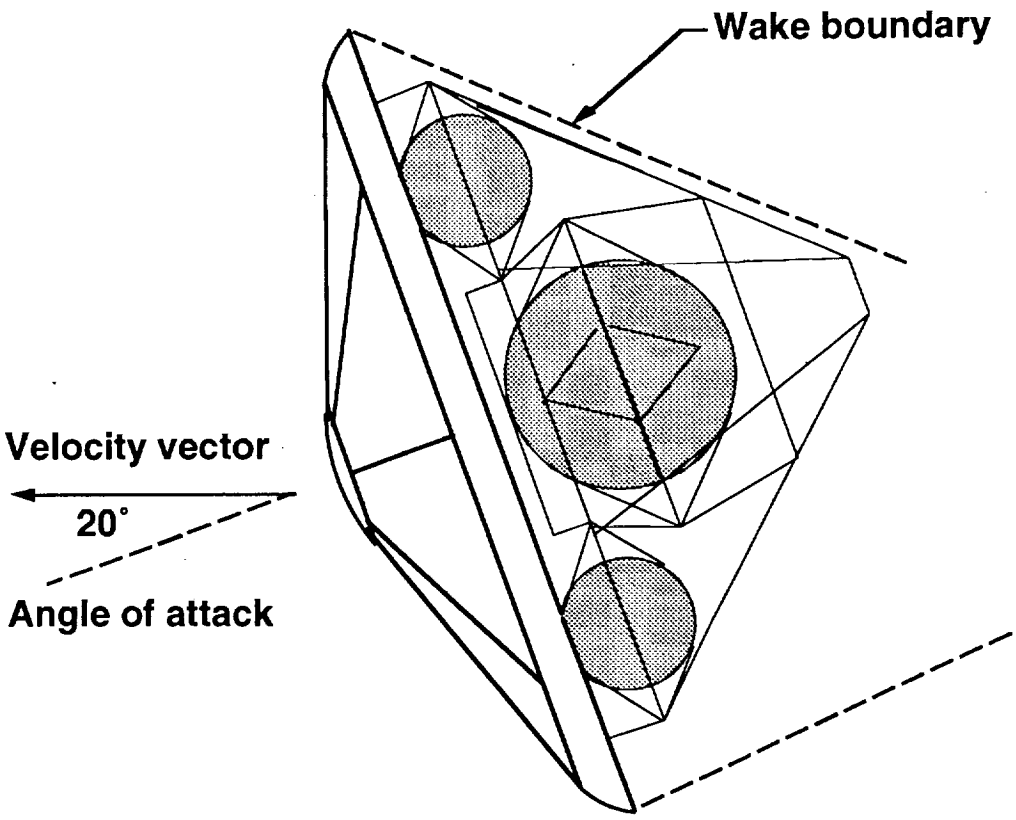

Figure 3.24 Wake boundary at maximum angle of attack.

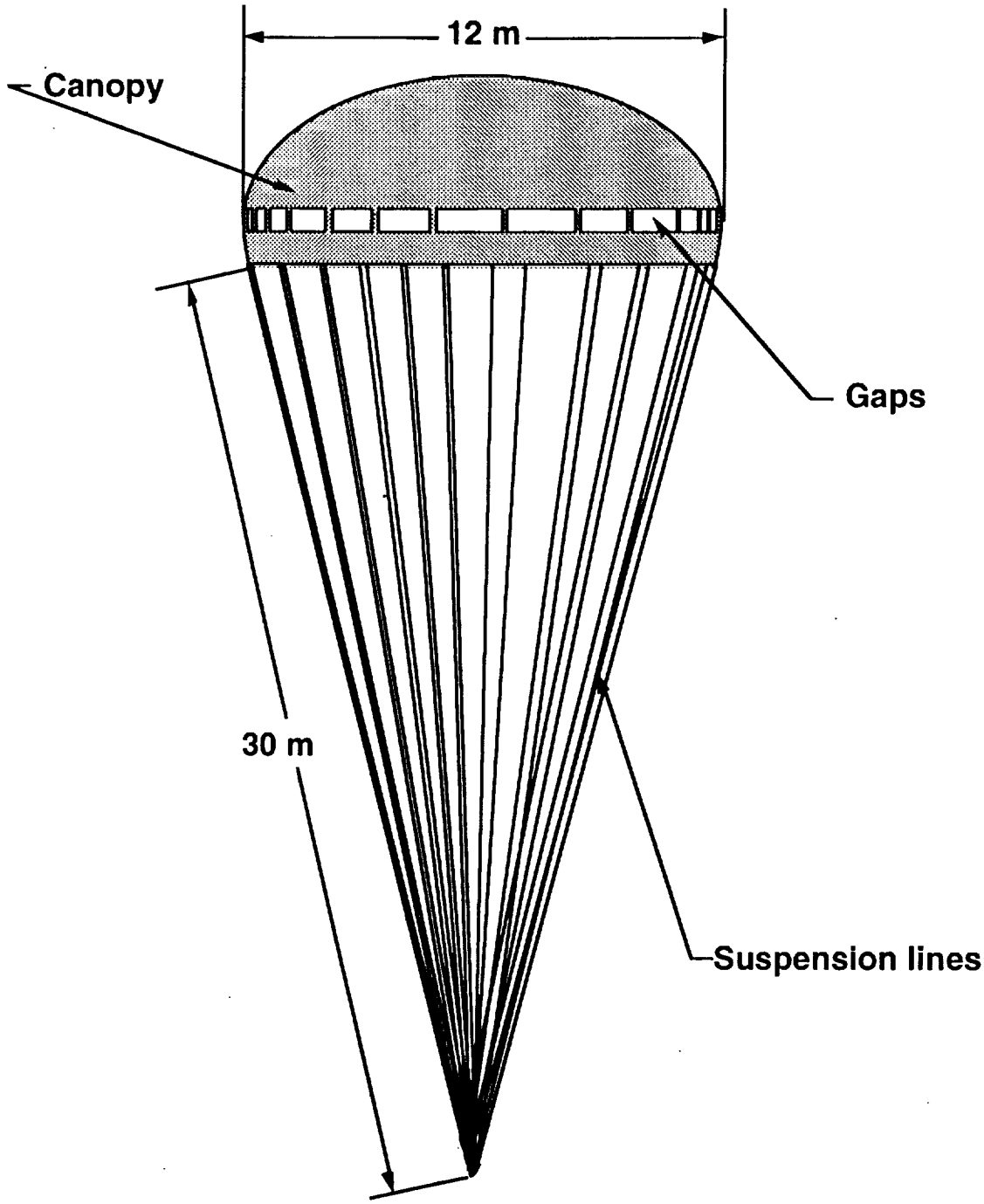

Fig. 3.25 MLVH Parachute.

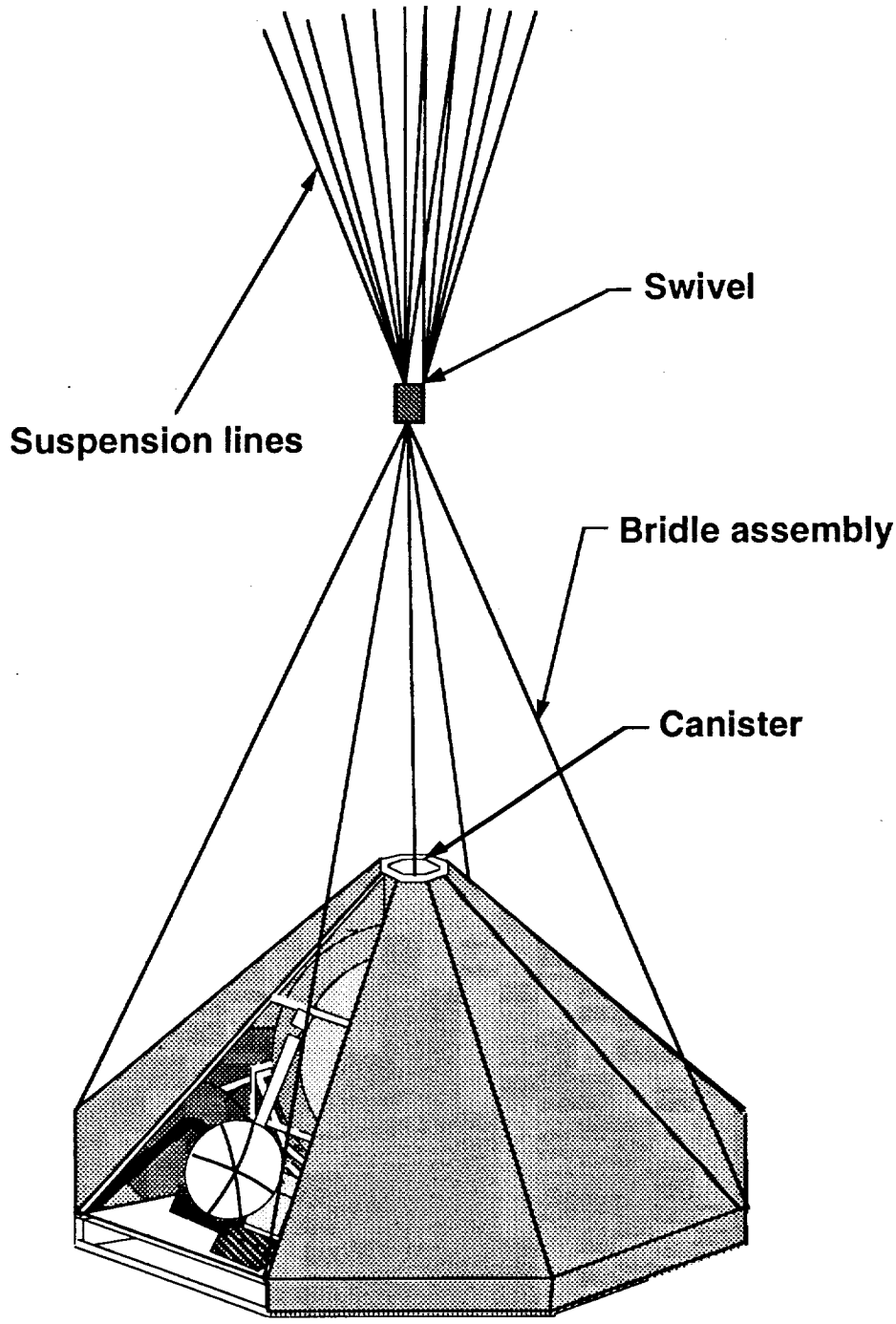

Fig. 3.26 Parachute cables.

4.0 AVIONICS AND COMMUNICATIONS

Jason Andrews

Mark Matheson

Mhorli Marcelo

TABLE OF CONTENTS

4.1 INTRODUCTION
(Mark Matheson)

This chapter describes the major electronics components of the mission. Section 4.2 is an overview of the avionics system, which includes guidance, navigation and control and tracking subsystems. Because these systems require the most computer usage, the avionics system also includes the main computers and data management and storage subsystems. The communications system is discussed in Section 4.3. Section 4.4 gives the mass, power and cost breakdowns of the systems included in this chapter.

4.2 MLVH AVIONICS
(Jason Andrews)

One of the crucial aspects of the proposed mission scenario is the avionics and controls package. The avionics consists of an autonomous system responsible for the safety of the MLVH during entry, landing, and subsequent hops. During the Earth to Mars flight most of the MLVH operations are directed by ground controllers on Earth. Navigational data from star and sun sensors located on the spacecraft transmit back to aid the ground personnel [1].

Once the MLVH reaches Mars, the spacecraft operates on a much faster time scale making human-in-the-loop control impossible. On board systems will guide and control the lander during aerobraking, entry, descent, and, most critically, final touchdown. The mission scenario requires a controlled soft landing in a region of unknown geological topography. Furthermore, a system of this type is not able to rely on a global positioning system (GPS) to determine landing location or flight attitude. The avionics package is responsible for the MLVH during the subsequent 30 km ballistic hop; in which the craft takes-off and reaches altitudes of 12 km before turning around and making a soft landing in a different region of potentially rough terrain.

The design of a fully autonomous system capable of performing the above task may appear daunting. The authors would like to point out that the current testing program outlined by the MacDonald Douglas Company for the DC-X proves such a scenario is possible [2]. The DC-X

will re-enter and perform an upper atmospheric turn maneuver before landing softly at a designated point. The current test program outlined by MacDonald Douglas requires the DC-X to autonomously take-off and climb to 20,000 ft before turning around and landing. This technology demonstration is vital to the success of this, as well as future, planetary exploration missions. The DC-X avionics package consists of a radar altimeter, inertial GPS, and gyroscopes. The MLVH uses a similar package but does not have the advantage of a global positioning system.

The proposed avionics package combines features of the DC-X and the Clementine spacecraft, as well as concepts for the Common Lunar Lander. The spacecraft avionics and control system can be divided into three different subsections: Guidance, Navigation and Control; Data Management System (DMS); and Communications and Tracking. The instrumentation incorporated into the MLVH for navigation guidance and control, is also used as scientific instruments to minimize the cost of development and to decrease the total mass of the spacecraft.

4.2.1 Guidance, Navigation and Control

The bulk of the avionics package relies on an Inertial Measurement Unit (IMU) consisting of ring laser gyroscopes and accelerometers to control spacecraft orientation and accelerations. The MLVH uses the same Honeywell H-764 Laser Inertial Navigation System flown on a number of military and civilian aircraft [3]. The Honeywell H-764 uses three ring-laser gyroscopes and three accelerometers giving the lander a velocity accurate to 1 m/s and an attitude accuracy of 0.2°. The Inertial Navigation System weighs 7.3 kg and requires 40 W. It is capable of processing inputs from all of the guidance instrumentation, specifically the altimeter and radar velocimeter, to provide a quick response output.

Star trackers are required for deep space navigation and spacecraft orientation. The instruments themselves consist of small cameras that are always pointed towards a specified point, usually a star, thus giving the spacecraft attitude in relation to a reference frame. Three star trackers were chosen for the MLVH. The first consists of the on-board camera used to photograph Mars both from orbit and the surface. This camera is a copy of the Ultra-Violet/Visual Camera

used for the Clementine mission that flew in early 1994. The camera itself weighs only 400 g, requires 4.5 W of power, and has a narrow 4.2° x 5.6° field of view. The second and third cameras are extremely small and taken from the Clementine as well, weighing only 290 g each and requiring 4.5 W of power with a larger 29° x 43° field of view.

A flight computer, developed by Honeywell for military space operations [4], serves as the main processor responsible for control of the MLVH during atmospheric entry and subsequent ballistic hops. The specific computer chosen is the RH-32 32 bit processor and is included as part of the Guidance, Navigation, and Control subsystem. Inputs from the star trackers, inertial navigation unit, and landing radar system are all fed directly into the flight computer, which makes decisions and relays commands to the reaction control system and main engines.

4.2.2 Data Management System (DMS)

The data management system consists of a Multiplexer/DeMultiplexer (MDM) developed by Honeywell to be used aboard Space Station Freedom [5]. The system is in charge of overseeing all mission components, serving as the CPU for the MLVH. The unit became available in 1992 as space qualified hardware and can be integrated through the use of workstations to do all of the programming, debugging and hardware integration. An overall system schematic incorporating all of the MLVH subsystems is shown in Fig. 4.1.

Data storage for all of the spacecraft subsystems is carried out by an Amptek FDR-8200 10 Gbyte spaceflight data recorder [6]. The system was originally designed to operate within the Space Shuttle Payload Bay. The 10 Gbyte recorder is required to store the large amount of data obtained from the UV/Vis camera, the GPR while the spacecraft is in orbit, and the other instruments.

4.2.3 Instrumentation and Tracking

The MLVH incorporates the same basic landing control and guidance techniques used by the Surveyor, Apollo, and Viking programs during descent. Specifically, the system includes an altimeter to determine range to the surface and a velocity sensing radar to determine velocity along three axes.

A vendor survey conducted by the Boeing Company in October of 1991 [7] assessed the availability of off-the-shelf hardware capable of the above tasks. The Boeing study was done in conjunction with the development of the Common Lunar Lander to autonomously ferry payloads to and from the surface of the Moon. They found that some existing altimeters may be close to the design requirement but that no suitable radar was known to exist [8]. The vendor survey revealed that the cost to develop such systems in a three year time frame was on the order of $4 million, with hardware costing $1.5 million a copy for both the radar and altimeter.

Our proposed system is the result of a vendor survey response by Teledyne Ryan Co. The landing radar and altimeter have a range of 16 km. The landing radar system uses four individual beams to provide redundancy. The pulse altimeter requires a single cone-shaped antenna pointed toward the ground. The instrumentation requires a surface area of 76.5 x 76.2 cm and has range and velocity accuracy of 5% of the actual range and 30 cm/sec, respectively.

4.3 MLVH COMMUNICATIONS LINK WITH THE EARTH
(Mhorli Marcelo, Mark Matheson)

This section discusses the communication link between the MLVH and the Earth. It is divided into three sections. The first, 4.3.1, describes the system requirements and architecture. Section 4.3.2 gives details on the specific transmission technique chosen. The system hardware is presented in Section 4.3.3.

4.3.1 Communications Architecture

The MLVH will communicate directly to NASA's Deep Space Network (DSN) on Earth. Currently DSN is capable of uplink in S band and downlink in S and K bands. Due to budget restrictions, it does not appear that transmission capability in the Ku band will be available before the 2001 mission date [9].

Transmission times vary during various phases of the mission. During interplanetary transit, the antenna is always Earth-pointing, allowing communication to occur at any time. While performing the in-orbit mapping phase of the mission, the antenna is also used by the Ground Penetrating Radar (GPR), and must be pointed toward the surface. During this time, communication and GPR measurements alternate. Communication is also intermittent after the MLVH has arrived at the surface. Communication can only occur when the Earth appears above the horizon of the MLVH. The actual time available for transmission depends on the season and daily variations in the optical depth of the Martian atmosphere. One-way transmission delay times vary between 3 and 20 minutes, depending on the relative position of the two planets [11].

4.3.2 Communications Technique

There are several different types of data that will be transmitted. Uplinked data includes tracking, telemetry and command (TT&C), navigation data, and additional command functions. Downlinked information includes the science data stream and the engineering data stream (e.g. health of the vehicle, propellant tank conditions, etc.) [16]. The data rates are listed in table 4.1

All data are recorded in digital format, eliminating the need for analog to digital conversion. Once the data are collected they are compressed and stored in the DMS (see Section 4.2.2). When a communication channel is open (limited by antenna line-of site and DSN availability) the information is multiplexed into a single data stream and transmitted directly to the Earth.

Table 4.1 Data rate requirements [6].

Instrument	Data rate
APX	64 Kbits per analysis
MRS	64 Kbits per analysis
Atmospheric	1 Mbit per Martian day
GPR	4 Mbits per image
Cameras	3.9 Mbits per image
Engineering	1200 bits per second

4.3.3 Communications Hardware

The hardware components are all solid state which allows for low power consumption, low mass, high dependability and no moving mechanical parts. The Viking mission for example, used a 1970's technology magnetic tape drive data storage system that has moving mechanical parts. Although it performed remarkably well, it was unnecessarily massive. Weight savings, longer service, and higher storage capacity (2×10^9 bits of data) can be realized by solid state data storage memory. The transponder (consisting of receiver and transmitter), filters, and the antenna tracking motor circuits are also solid state as well [13].

The MLVH has two sets of transponders (2 pairs of receivers and transmitters) for redundancy. The MLVH antenna is a directional, parabolic dish, transceiving type antenna. The material chosen is honey-combed composite for less mass and more weather resistance. There is the option of designing it to be foldable for storage ease, but this necessitates the material to be wire-mesh(which is denser than composite) and adds control complexity. All antenna components are mounted directly on the drive motor, making the system compact and rugged [14]. Finally, the high-gain antenna is mounted on a retractable boom. During the flight to Mars and on the Martian surface the boom is extended to act as an observation platform for scientific instruments and also allows the antenna to orient itself in relation to the MLVH and Earth.

4.4 COMPONENT MASS, POWER, AND COST BREAKDOWN
(Jason Andrews, Mhorli Marcelo, Mark Matheson)

The basic hardware components for the avionics and communication packages and the breakdown of their masses and power requirements are listed in Table 4.2 below [10].

Table 4.2 Hardware component masses and power requirements.

Component	Quantity	Mass (kg)	Size (cm)	Peak Input Power (W)
Guidance & Navigation				
Laser Inertial Navigation Sys.	1	7.3	46x19.3x20	40
Flight Computer	1	9.0	20.3x26.2x7.0	25.3
UV-Vis	1	0.41	10.5x12x16	4.5
Star trackers	2	0.58	12x12x14	9.0
Data Management Sys.				
Multiplexer/DeMultiplexer	1	20	37x23x34	144
Data Storage (FDR-8200)	1	8.2	30.5x23x15	18
Instrumentation/ Tracking				
Landing Radar	1	22.1	76.2x76.2x8.26	68
Altimeter	1	5.1	23.4x14.7x20.1	28.5
Altimeter Antenna	1	0.7	15.25 dia.x15.5	0
Mounting Brackets/Wiring		12.9		
Communications				
Transponders	2	9	10 x 10 x 20	32
Antenna	1	1	50 dia.x 10	N/A
Filters, switches, etc.	N/A	2	N/A	N/A
Cables	N/A	2	N/A	N/A
TOTAL		100.6		370

4.5 CONCLUSION
(Mark Matheson)

In order to reach Mars, Project Genesis uses its star trackers and communications system to ensure proper pointing. During descent the MLVH is controlled by the guidance, navigation and

control subsystem. This system is again used during the ballistic hop. During the entire mission data are recorded and compressed; information is transmitted from Earth to the MLVH and back. All data and instructions are handled by the data management system. All of these functions are handled by the Avionics and Communications System, as described in this chapter.

NOMENCLATURE

ACTS	Advanced Communications Technology Satellite
APX	Alpha Proton X-Ray Spectrometer
CPU	Central Processing Unit
DMS	Data Management System
DSN	Deep Space Network
GPR	Ground Penetrating Radar
GPS	Global Positioning System
IMU	Inertial Measurement Unit
MDM	Multiplexer/DeMultiplexer
MLVH	Mars landing vehicle and hopper
MRS	Magnetic Resonance Spectrometer
TT&C	Tracking, telemetry and control
UV/Vis	Ultra-Violet/Visible Camera

REFERENCES

1. "A Common Lunar Lander for the Space Exploration Initiative," NASA Johnson Space Center Report, Presentation to Aaron Cohen, September 19, 1991.

2. Clapp, Col. M., USAF, Personal communication, March 4, 1994.

3. "H-423 Laser Inertial Navigation System," Honeywell Military Avionics Publications, August 1990.

4. "Honeywell Space Computer," Honeywell Space Systems Group, Clearwater, FL., August 1993.

5. Kit Kitto, Honeywell Space Systems Group, Clearwater, FL., Personal communications, May 1994.

6. AMPTEK FDR-8200 advertisement, "Space News," January 3-9, 1994, p. 17.

7. "A Common Lunar Lander for the Space Exploration Initiative," NASA Johnson Space Center Report, Presentation to Aaron Cohen, September 19, 1991.

8. "A Common Lunar Lander for the Space Exploration Initiative," NASA Johnson Space Center Report, Presentation to Aaron Cohen, September 19, 1991.

9. Bertotti, B., "An Introduction to the Cassini-Huygens Mission," *Il Nuovo Cimento*, Vol.15 C, November-December 1992, pp. 1129-1132.

10. Hall, J. R. and Rolf, H. C., "Telecommunications and Navigation Systems Design for Manned Mars Exploration Missions," *SPIE*, vol.1059, 1989, pp. 60-72.

11. Bruckner, Professor Adam, Department of Aerospace Engineering, University of Washington, Personal communication, April, 1994.

12. Sahr, Professor John, Department of Electrical Engineering, University of Washington, Personal communication, May -June, 1994.

13. Rao, Ron, The Boeing Company, Personal communication, March, 1994.

14. Ramos, Ruben, NASA Ames Research Center, Personal communication, April-June, 1994.

15. Tommi, Dan, Motorola, Personal communication, June, 1994.

16. Larson, W., Wertz, J., "Space Mission Analysis and Design," Microcosm, Inc. and Kluwer Academic Publishers, Torrance, CA, 1992.

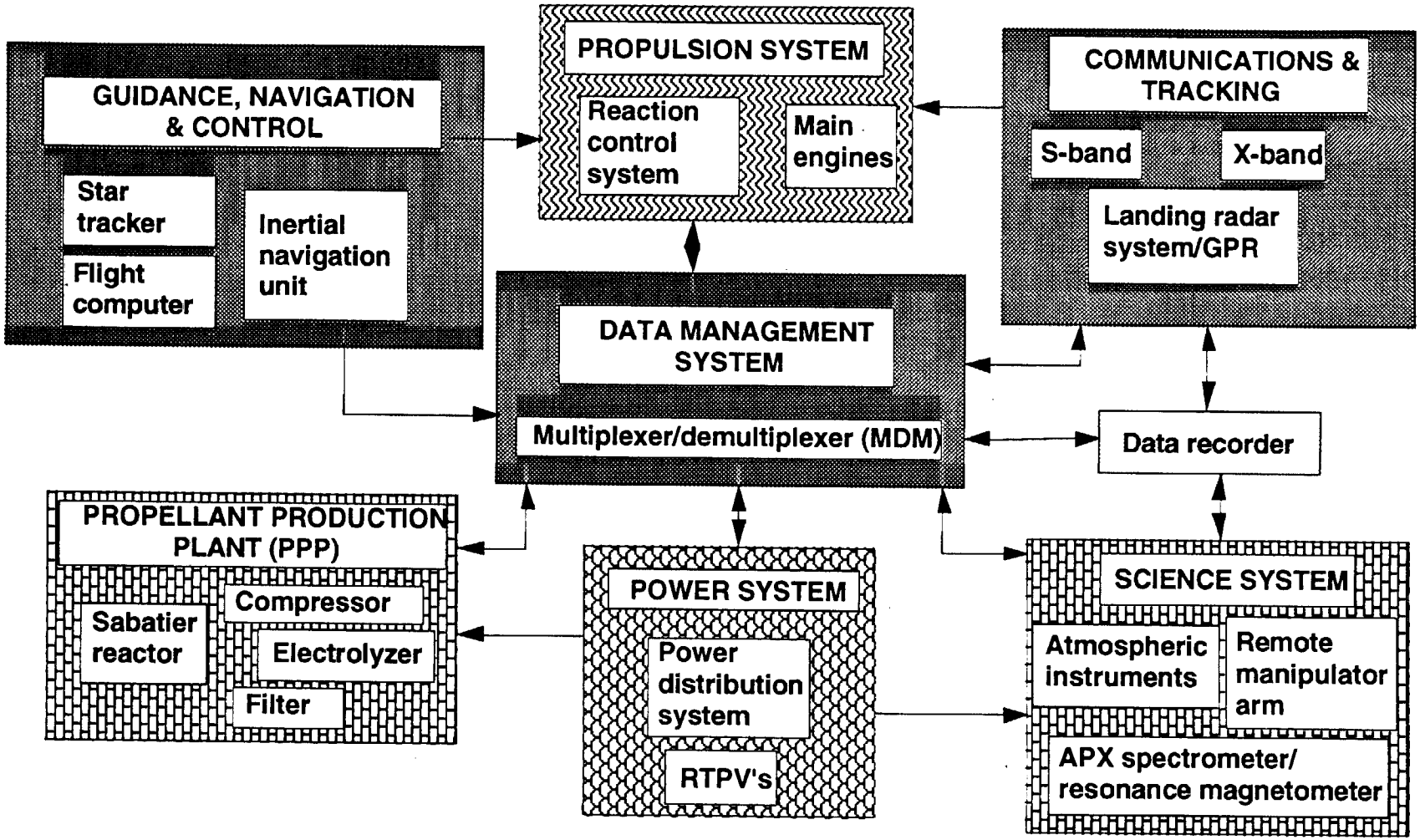

Fig. 4.1 MLVH system schematic.

5.0 MARS SCIENCE

Jason Andrews

Francisco J. Garcia Acosta

Jared Kipp

TABLE OF CONTENTS

5.1 INTRODUCTION
(Acosta)

An important step to an eventual human presence on Mars is a precursor mission to explore and characterize the local Martian environments. Following the initial exploration of Mars by the Mariner spacecraft, the Soviet Mars-series, and the Viking landers, it is still necessary to expand our knowledge of Mars in all areas of scientific interest. In order to achieve this understanding it is useful to explore the diverse Martian environments by utilizing *in situ* resources. Project Genesis is capable of achieving this goal, providing unique science data not possible from any other proposed mission, thus expanding our knowledge of Mars.

In situ measurements from two locations initiate a new phase in the exploration of Mars, collecting information which cannot be obtained from an orbiter or a conventional lander. Mars is a terrestrial planet with a rich and varied geologic history that includes extensive volcanism and tectonism, an atmosphere with substantial interaction with surface materials, volatile-rich polar caps and extensive evidence for the former existence of liquid water on and below the surface. As a result, Mars remains a major scientific objective for exploration and study.

Specific scientific objectives for Project Genesis are as follows:

- Establish the chemical and mineralogical character of surface materials.
- Determine some of the aspects related to the atmosphere environment.
- Determine the abundance and distribution of possible locations of water or ice.

Each of these objectives is discussed in the following sections.

5.2 SCIENTIFIC GOALS
(Jared Kipp)

The goals for this mission complement other suggestions for the continued exploration of Mars, such as the scientific objectives stated by the U.S. National Academy of Sciences Committee on Planetary Exploration (COMPLEX) [1,2]. After the Viking landings in 1976, the U.S. National Academy of Sciences' COMPLEX made the following recommendations on the primary objectives for the continued exploration of Mars by unmanned missions:

- The intensive study of local areas;
- To explore the structure and general circulation of the Martian atmosphere;
- To explore the structure and dynamics of Mars' interior;
- To establish the nature of the Martian magnetic field and the character of the upper atmosphere and its interaction with the solar wind;
- And to establish the global chemical and physical characteristics of the Martian surface.

Considerable information about Mars is still needed. In the present mission, surface and atmospheric composition is investigated. Soil and rock samples are examined in order to determine the state of water, if any, in the material. Also, they are examined to identify any active oxygen species present, as well as other radical species and oxidation states of paramagnetic ions and color centers in icy samples. The possibility of ice on Mars opens up a number of important opportunities for future missions, such as *in situ* H_2/O_2 propellant production, and life support. Therefore, water ice deposits are sought. Finally, since the Viking experiments for the existence of life were inconclusive, this mission will conduct experiments to try to further clarify the possibility of life on Mars by characterizing the electronic state and molecular structure of the oxidant in the Martial soil.

5.3 REQUIREMENTS
(Jared Kipp)

The scientific instruments chosen to accomplish the stated goals had to meet certain requirements. Because this project is primarily a technology demonstrator, limiting the mass of the payload is of great importance. Therefore, instruments of small mass (<5 kg) were chosen for the surface experiments. Also, instruments with little power consumption (<10 W_e) were sought. The cost for the scientific package was also of concern, therefore, "off-the-shelf" instruments were chosen to avoid developmental expenses. Lastly, simplicity of the instruments was considered.

All of the surface instruments for this project meet the stated requirements, with the exception of the Magnetic Resonance Spectrometer (15 W_e). This instrument has the potential to consume less than 10 W, and is currently under development at the Jet Propulsion Laboratory [3]. Although this instrument is currently not "off-the-shelf", it will be by the proposed mission launch date, and it is relatively inexpensive (less than one million dollars) and simple to use.

5.4 REMOTE MANIPULATOR ARM
(Jared Kipp)

The Remote Manipulator Arm (RMA) is located on the Mars Landing Vehicle/Hopper (MLVH) near the bottom of the structure, as shown in Fig. 5.1. The sampling arm has a length of 1.5 m, mass of 2 kg, and can lift up to 2 kg on Mars. The structural material used for the arm is graphite-ether-ketone: a graphite thermoplastic which has a higher stiffness to weight ratio (12.6×10^7 m^2/s^2) than aluminum (2.7×10^7 m^2/s^2). The sampling arm consists of two 0.6 m beams connected to each other, with a third 0.3 m beam connected at the end. On the end of this shorter beam a small sample collector is attached.

The beams are all joined by hinges, which allows the RMA to be folded in when not in use. To operate these hinges, a cable drive, which has superior characteristics compared to a direct

drive, was selected The cable drive has a motor located at the base, and controls the beams by pulling on the cables, which extends and retracts the arm. The direct drive uses a motor at each joint, increasing the structural mass of the arm. This method also requires electric wiring inside the beams and through the joints, which also adds to the total mass. Because the cable drive does not require any of these, the beam achieves a lower moment of inertia and lighter mass.

5.5 SCIENTIFIC INSTRUMENTS
(Jared Kipp, Jason Andrews)

The scientific instruments installed on the MLVH accomplish the stated goals of this mission. In order to allow for unexpected problems or malfunctions, it is desirable to have two sets of instruments on the MLVH, but mass and power considerations make this impossible. The scientific goals for this mission require sample acquisition, which is accomplished through the use of the RMA on the lander, and the use of an Ultraviolet Visual (UV-Vis) camera, which provides stereo and three-color images of the surrounding terrain.

5.5.1 Surface Study
(Jared Kipp)

Surface study for this mission will consist of the investigation of top soil, underground soil, rocks, lava, surface composition, water deposits, and oxygen species. The instruments used for surface study includes: a Magnetic Resonance Spectrometer (MRS), Alpha-Proton-X-ray Spectrometer (APX), Ground Penetrating Radar (GPR), RMA, Decent Imager, and a UV-Vis Camera.

Magnetic Resonance Spectrometer (MRS)

The MRS [3] has a combined capability of Electron Paramagnetic Resonance (EPR) and Nuclear Magnetic Resonance (NMR). In one miniature instrument, the MRS incorporates these

two powerful spectroscopic disciplines with the capability and versatility to perform *in situ* planetary sample analyses. This instrument is currently under development at the Jet Propulsion Laboratory with the hopes of obtaining much needed Martian surface chemical information.

The MRS collects samples by means of the RMA. Of concern is surface contamination from retro rocket fire upon landing, but because there is little oxygen in the exhaust, and because the RMA has the capability to dig, surface contamination is not a problem. The RMA will scoop samples and place them into silica tubes. Although surface contamination caused by the landing engines is not considered a problem, Project Genesis requires the MRS to perform one analysis soon after landing, and one analysis right before the ballistic hop inorder to provide for more accurate results. This requirment provides for a margin of error due to small traces of oxygen in the engine exhaust.

One advantage of using the MRS is that the samples require little preparation with no disruption of surface structures. MRS instruments study atoms or molecules with unpaired electrons (EPR) or nuclear spins (NMR) in an applied magnetic field by irradiation with microwave or radio frequency to induce transitions between electronic or nuclear spin states. When the magnetic field is scanned to the point that the energy difference between the spin states of the sample matches the microwave or radio frequency quantum, an atom or molecule with unpaired spin shows a characteristic magnetic resonance spectrum, and from the measurement of magnetic field strength and microwave or radio frequency at resonance, one can characterize the chemical structure of the sample [3]. The following can be studied through the use of the MRS:

- Nature of oxidants in Martian soil
- Detection of physically or chemically bound water in the soil, minerals, and rocks
- Oxidation states of paramagnetic ions
- Color centers in icy samples
- Detection of possible organics from subsoil

As can be seen, Magnetic Resonance Spectroscopy is a powerful technique for understanding the chemical aspects of the Martian soil.

Alpha-Proton-X-ray Spectrometer

The APX [4] determines the elemental composition of soil or rock by stimulating the target surface with alpha particles emitted from a Curium source contained in the sensor head and by recording the alpha, proton, and X-ray spectra emitted from the sample. A measurement is made by mechanically bringing the sensor head to each sample and placing it in contact with the rock or soil sample. This is accomplished with the RMA. The APX is also proposed for the MESUR/Surveyor mission, but for Project Genesis, it has the luxury of measuring samples from separate locations that are at a great distance form one another.

The MESUR mission requires the APX to achieve measurements and return data during the first 30 Sols after landing, assuming four measurements over this period. Project Genesis also requires the APX to achieve measurements during the first 30 Sols after the initial landing, as well as after the ballisitic hop landing. Individual measurements require a 10-hour integration period with the sensor head touching the sample and not moving. The MLVH deploys the sensor head with the RMA and will keep it stationary for the 10 hour integration period. At this time, the Descent Imaging camera can locate the next suitable site for measurement.

Table 5.1 Surface study instruments [1].

Instrument	Volume (cm^3)	Mass (kg)	Power (W)
MRS	300	3.0	15.0
APX	650	0.7	0.3
UV-Vis (ea)	2016	0.41	4.5
Descent Imager	1980	0.29	4.5
RMA	2025	2.0	10.0
TOTAL	6971	6.40	34.3

Ultraviolet-Visible Camera

This instrument is the same as used in the Clementine mission, but with Project Genesis, it has the same advantages as stated for the APX. The UV-Vis Camera, once deployed, is located above the MLVH on the backside of the high-gain antenna to provide unobstructed images of the Martian surface. The camera was placed on the high-gain antenna boom so that it could be raised above the MLVH and have a two-axis 360° field of view. Furthermore, by placing the camera above the MLVH the visual distortion due to rising convective heat currents from the radiators can be minimized. This instrument is also discussed in Section 4 as part of the MLVH avionics package. Table 5.1 shows the volume, mass, and power characteristics for each of the instruments.

Descent Imaging Camera

The Descent Imaging Camera is actually a 3-color startracking camera developed for the Clementine mission by the Department of Defense. The Descent Imager is located on the underside of the MLVH and is allowed to gimbal such that it can track objects through a protective plexiglass bubble. This allows the camera to point directly down to record aerial images after the aerobrake is released during descent and the ballistic hop. Furthermore, the camera can re-orient itself to aid in the control and operation of the RMA.

5.5.4 Atmospheric Science

(Francisco Garcia-Acosta, Jason Andrews)

Recent trends in planetary instrumentation for atmospheric science include the development of compact, low-mass, low-power instruments that enable optimum measurements from the Martian environment [5]. Project Genesis shares this philosophy, including a variety of sensors that will provide current weather information and will be used to study Mars atmospheric dynamics and to describe the seasonal variations. The module used on the MLVH incorporates state-of-the-

art electronics and silicon micromachined structures, along with more conventional measurement technologies to reduce size, cost, and power consumption. Requirements for meteorological measurements on Mars include devices for measuring pressure, temperature, wind-speed and direction, and humidity. The sensors placed on board the MLVH are based on technologies that are durable, and inherently accurate. Descriptions of the module and its instrumentation is given below:

Mars Environment Monitor (MEM)

The instrumentation for monitoring the Martian environment consists of a very compact, lightweight module: the Mars Environment Monitor (MEM). The measurements taken from the MEM are completely immune to the atmospheric dust and ice particle loads and their sensitivity exceeds the requirements for Mars and upper atmosphere applications. The mass of the MEM is 1 kg, and the power requirement is approximately 5 W. The MEM has a 0.1 m cubic shape and is mounted atop the high-gain antenna. By placing this instrument on top of the high gain antenna it will be shielded from the radiative heat given off by the radiators and is located in an ideal, unobstructed position to gather atmospheric data. Furthermore, by retracting the antenna boom the relative distance above the ground can be altered between 0.3 meters and 1.5 meters which is ideal for determining atmospheric surface effects.

Pressure sensor. The meteorological station has an atmospheric sensor which is mounted inside the module to be shielded from wind. The pressure sensor measures absolute pressure using a thermal conductance technique. The sensor consists of a vibrating quartz membrane whose oscillating frequency is a function of the mechanical stress imposed by the ambient pressure. Temperature dependence, although small, must be taken into account in

interpreting the data. The response time of the sensor to changes in pressure is less than two seconds. These devices employ silicon micromachined structural elements[6].

Temperature Sensors. Temperature is measured by two sensors made of thin metal, film-resistance thermometers, whose accuracy is better than 1 K. The Finnish company Vaisala is currently developing these devices[7].

Wind Speed and Direction Sensors. Measuring both wind speed and direction is achieved by an ion gauge. The carbon dioxide is ionized by using a reference source, and the point with the greatest current gives an indication of the wind speed and direction. A hot wire-anemometer (as used on the Viking Mission) was ruled out because of its high power requirements.

Humidity Sensors. The weather station also includes a hygrometer, recently designed and developed by JPL. This sensor is designed to study the water vapor distribution in the Mars atmosphere, and it is designed to operate based on accurate dewpoint principles. This device combines a millimeter scale surface acoustic wave oscillator element with a compact temperature control element. This compact structure, packaged on a conventional power transistor header, has a volume of approximately 1 cm^3. Precision testing of this instrument demonstrates 0.1 K dewpoint accuracy[8].

5.6 GROUND PENETRATING RADAR
(Jason Andrews)

To supplement the capabilities of the MLVH, a Ground Penetrating Radar (GPR) is used from orbit during the first weeks of the mission. The GPR is capable of probing beneath the Martian surface with VHF, UHF, and microwave radio waves. The waves reflect off subterranean

features and the return signal is sent back to Earth and analyzed. By analyzing the radar return, scientist can locate ground water and ice deposits as well as accumulate a wealth of geological data. Currently, research regarding a small space-based GPR is nearly non-existent. The design used for this mission mimics larger arrays carried aboard the Apollo 17 Moon mission and the Space Shuttle [9]. Several existing systems are combined to create a small power-conscious GPR, capable of meeting the following mission requirements:

- Search and location of water or water ice.
- Subsurface geological mapping.
- Generation of surface profile, surface mapping, and imaging.
- Measurement of galactic noise in the Martian environment.

The primary mission goal of the GPR is to search for and locate water or ice trapped near or beneath the surface. This mission aspect is considered a top science priority because of the implications for future Martian exploration. The secondary effect of using a GPR is that subsurface discontinuities and formations are detected and mapped and a surface profile will be created from the radar return signal. Examples of the useful information obtained from the surface profile and sounding include the location of dips of fault scarps, detection of subsurface river beds covered by layers of Martian dust, disposition of lava flows, slope information, and three-dimensional crater and volcanic shape formulation. The GPR itself is a powerful tool but when combined with other aspects of the mission it greatly augments the overall scientific capabilities of the mission. For example, comparisons between video images and subsurface and surface profiles yields important information regarding the geological history of different regions. The use of the GPR to locate and identify important geological regions of interest is a invaluable asset. Such capabilities ensure that the scientific yield from the mission is maximized.

5.6.1 GPR Design

The GPR operates at wavelengths of 30 cm and 2.0 m. These longer waves are capable of penetrating the top few layers of the Martian surface before they are reflected by the more solid layers beneath the surface. The reasons for using a broadband, relatively low-frequency system for ground penetration and imaging stems from the increase in dielectric losses with frequency exhibited by terrestrial materials, and the requirement for resolution at long range. Furthermore, a spaceborne radar in a polar orbit has the advantage of covering the entire Martian surface with a constant power density, guaranteeing consistent results. The use of a polar orbit eliminates the need for a side looking radar transmitter and receiver. By pointing the transmitter and receiver directly down, the radar effectiveness is increased and the control of the satellite is simplified.

The major problem hindering the effectiveness of a spaceborne radar system is the strong return from the Martian surface against which the weak subsurface returns must be observed. The surface return, undesirable for subsurface probing, is precisely the desired signal required to meet the third mission objective of surface profiling and imaging. Data for sounding, profiling, and imaging are different for all three objectives but must be gathered simultaneously. As a result, the raw data are digitized, stored by the onboard data recorder, and later beamed to Earth for analysis.

The amount of energy reflected by the surface is determined by the characteristic roughness. Roth and Elachi [10] found that scattering losses are not significant for subsurface penetration when individual grain sizes are smaller than one-tenth wavelength. Scattering losses become appreciable for particle sizes larger than one-fifth wavelength. For our operating regime, the higher frequency 1 GHz waves (wavelength=30 cm) provides high resolution subsurface imaging up to 2 m in depth. Wavelengths in this range have been operated by both the Space Shuttle SIR-A [11] and SIR-B [12] missions with favorable results in extremely arid climates. The 150 MHz waves (wavelength 2.0 m) are capable of probing 150 meters beneath the surface. The

longer wavelengths provide greater depth of penetration but lack the high resolution attained by operating at higher frequencies.

The surface return is composed of two components, a specular or smooth surface component and a diffuse or rough surface component. The specular surface component is described below by the Rayleigh criterion and makes up the surface profiling component of the radar return. A simplified electromagnetic specular model is illustrated in Fig. 5.2.

When a radar beam passes from the low-loss atmospheric medium into the surface, the radar signal experiences a wavelength shortening as the microwave energy is passed from the air into the denser regolith. The equation governing the relationship between wavelength and incidence angle to micro-scale (surface) roughness is defined by the Rayleigh criterion [12], which considers the surface to be smooth if:

$$h < \frac{\lambda}{8 \cos\theta} \tag{5.1}$$

where:

h = average vertical height of the micro-relief

λ = operating radar wavelength

θ = incidence angle of the radar beam

From this it is easy to see that the optimal radar incidence angle is 0°, or directly overhead. The fact that the satellite is in a polar orbit is an added benefit because it optimizes the radar effectiveness. By solving this equation for h, the theoretical breakpoint or boundary between radar-smooth and radar rough surfaces is defined for a given wavelength and incidence angle. The maximum breakpoint boundary for a radar-smooth surface is 0.25 meters for 150 MHz waves [11]. This frequency is capable of peering beneath the surface in the rock strewn regions of Mars where boulders of up to 0.25 meters in diameter will have little effect.

5.6.2 Antenna System

To reduce size and power requirements, as well as increase resolution, the antenna chosen for the mission is a 0.50 m diameter high-gain dish antenna. The Apollo 17 lunar sounder mission used a seven-element Yagi VHF antenna operating in the 150 to 166 MHz band [13]. Our design requires an antenna in the 150 MHz to 1 GHz band. To miniminze the number of antennas required for the communications, GPR, and avionics subsystems, the different antennas are combined into a universal design. Using a 0.50 m parabilic antenna, the gain for the 1 GHz waves is 104.7 and for the 150 MHz waves it is 2.4.

5.6.3 Radar Subsystem

The transmitter is comprised of a sequencer, a code generator, and an FM phase modulator. Before the wave is fed to the antenna, the signal passes through a power amplifier where it is boosted to 90 W. The receiver is made of a broadband direct amplifier, a two-channel synchronous demodulator, several analog to digital converters, and a storage unit. The raw data are stored on an FDR-8200 10 Gb data recorder outlined in Section 4.1. A schematic of the radar subsystems and their layout can be found at the end of this chapter as Fig. 5.3.

The GPR system has a mass of 25 kg and a total power requirement of 90 W. Because the entire Martian surface is viewed during a single day by the satellite's polar orbit, the radar can shift between the three operating frequencies to save power and data storage space. The GPR itself is versatile and robust enough to meet all of the mission requirements. The two different operating frequencies provide a range of penetration depths. In the high frequency mode (1 GHz) the radar produces a high resolution image of the top few meters of the Martian surface. In the 150 MHz mode the radar is capable of detecting subsurface features that may be instrumental in determining

the geological history of the Mars. Finally, the GPR system is used by the MLVH during final descent and the ballistic hop as a radar altimeter and velocimeter.

5.7 LANDING SITES
(Jared Kipp)

It is not critical that a landing site be chosen at this time. In fact, important information about Mars will be gathered by missions that will precede this one, and that information will have significant impact on the choice of a landing site. Project Genesis is designed to land on a rocky surface. A landing site must conform to the following criteria: it must be smooth enough for the MLVH to land safely, and it needs to be in close proximity to one or more scientifically interesting surface features which are within the ballistic hop range of 30 km. These features may be geological formations (e.g. lava flows, ancient crated terrain, or ancient water erosion valleys), be candidates for subsurface water, or be candidates for biological organisms. If the GPR detects subsurface water and/or ice, it is desirable to land in the vicinity of its location, if it is possible. The most likely landing sites are in the vicinity of Vallis Marineris and Olympus Mons.

5.8 CONCLUSION
(Acosta)

A prominent feature of the future exploration of Mars is the detailed study of the planet's atmosphere and surface. Moreover, it would be inconceivable to send humans without data sent from precursor missions. The more detailed and substantiated the science models are, the more clearly future missions will be defined. Mars will be studied from a low orbit, during the entry maneuvers, and from the surface. Instrumentation on board of the MLVH will search for deposits of ice or permafrost, and a single jump of the MLVH will analyze a cross section of the Martian atmosphere. At the surface level, long-term meteorological measurements will collect data from the atmosphere while analyses of the Martian soil are performed. Mars has had a long and a complex

history with almost as wide a range of processes as on Earth. Elucidation of this history requires a comprehensive program of *in situ* analysis of samples which will provide a better understanding of the atmosphere and interior, as well as the possibility of indigenous life. The potential scientific benefits of Project Genesis will change our perspective about Mars and will provide some of the precursor information necessary for human exploration of the Red Planet.

NOMENCLATURE

APX	Alpha Proton X-Ray Spectrometer
COMPLEX	U.S. National Academy of Sciences Committee on Planetary Exploration
EPR	Electron Paramagnetic Resonance
GPR	Ground Penetrating Radar
MEM	Mars Environment Monitor
MLVH	Mars Landing Vehicle and Hopper
MRS	Magnetic Resonance Spectrometer
NMR	Nuclear Magnetic Resonance
RMA	Remote Manipulator Arm
UV-Vis	Ultraviolet/Visible

REFERENCES

1. *COMPLEX, Strategy for Exploration of the Inner Planets*: 1977-1987, National Academy of Sciences, Washington, DC., 1978

2. "Project Hyreus: Mars Sample Return Mission Utilizing In Situ Propellant Production", Final Report, AA420/421 Space Systems Design, NASA/USRA Advanced Design Program, Department of Aeronautics and Astromautics, University of Washington, July 1993.

3. "Development of a Miniature Magnetic Resonance Spectrometer for the In-Situ Sample Analyses for Mars ad Other Planetary Exploratrion", NASA Research Announcement NRA 93-OSS-04, Jet Propulsion Laboratory, 1993.

4. Request for Proposal for MESUR, Exhibit I to Contract NO., NASA, March 10, 1993

5. Jos-hi, P.B. "Lightweight Modular Instrumentation for Planetary Applications," *Workshop in Advanced Technologies for Planetary Instruments,* Lunar and Planetary Institute, LPI Februay 1993, Part I.

6. Muhleman, D.O. "Temperature/Pressure and water vapor sounding with microwave spectroscopy," *Workshop in Advanced Technologies for Planetary Instruments,* Lunar and Planetary Institute, LPI July 1992.

7. Mars Environmental Survey (MESUR). *Science Objectives & Mission Description.* NASA, Ames Research Center, July 19, 1991.

8. Kaiser, W. J., "Micro Weather Station for Earth and Mars" *Workshop in Advanced Technologies for Planetary Instruments,* Lunar and Planetary Institute, LPI Februay 1993, Part II.

9. Porcello, L.J., Jordan, R.L., Zelenka, J.S., Adams, S.H., Phillips, R.J., Brown Jr.,W.E., and Jackson, P.L., "The Apollo Lunar Sounder Radar System," *Proceedings of the IEEE*, Vol. 62, No. 6, 1974, pp. 769-783.

10. Roth, L.E. and Elachi, C., "Coherent Electromagnetic Losses by Scatering from Volume Inhomogeneities," *IEEE Transactions Antennas Propagation*, vol. AP-23, pp. 674-675, 1975.

11. Berlin, G.L., Tarabzouni, M.A., Al-Naser, A.H., Sheikho, K.M., and Larson, R. W., "SIR-B Subsurface Imaging of a Sand-Buried Landscape: Al Labbah Plateau, Saudi Arabia," *IEEE Transactions on Geoscience and Remote Sensing*, Vol. GE-24, No. 4, July 1986, pp. 595-601.

12. Farr, T.G., Elachi, C., Hartl, P., Chowdhury, K., "Microwave Penetration and Attenuation in Desert Soil: A Field Experiment with the Shuttle Imaging Radar," *IEEE Transactions on Geoscience and Remote Sensing*, Vol. GE-24, No. 4, 1986, pp. 590-593.

13. Nicollin, F., Barbin, Y., Kofman, W., Mathieu, D., Hamran, S., Bauer, P., Achache, J., and Blamont, J., "An HF Bi-Phase Shift Keying Radar: Application to Ice Sounding in Western Alps and Sptisbergen Glaciers," *IEEE Transactions on Geoscience and Remote Sensing*, Vol. 30, No. 5, pp. 1025-1032.

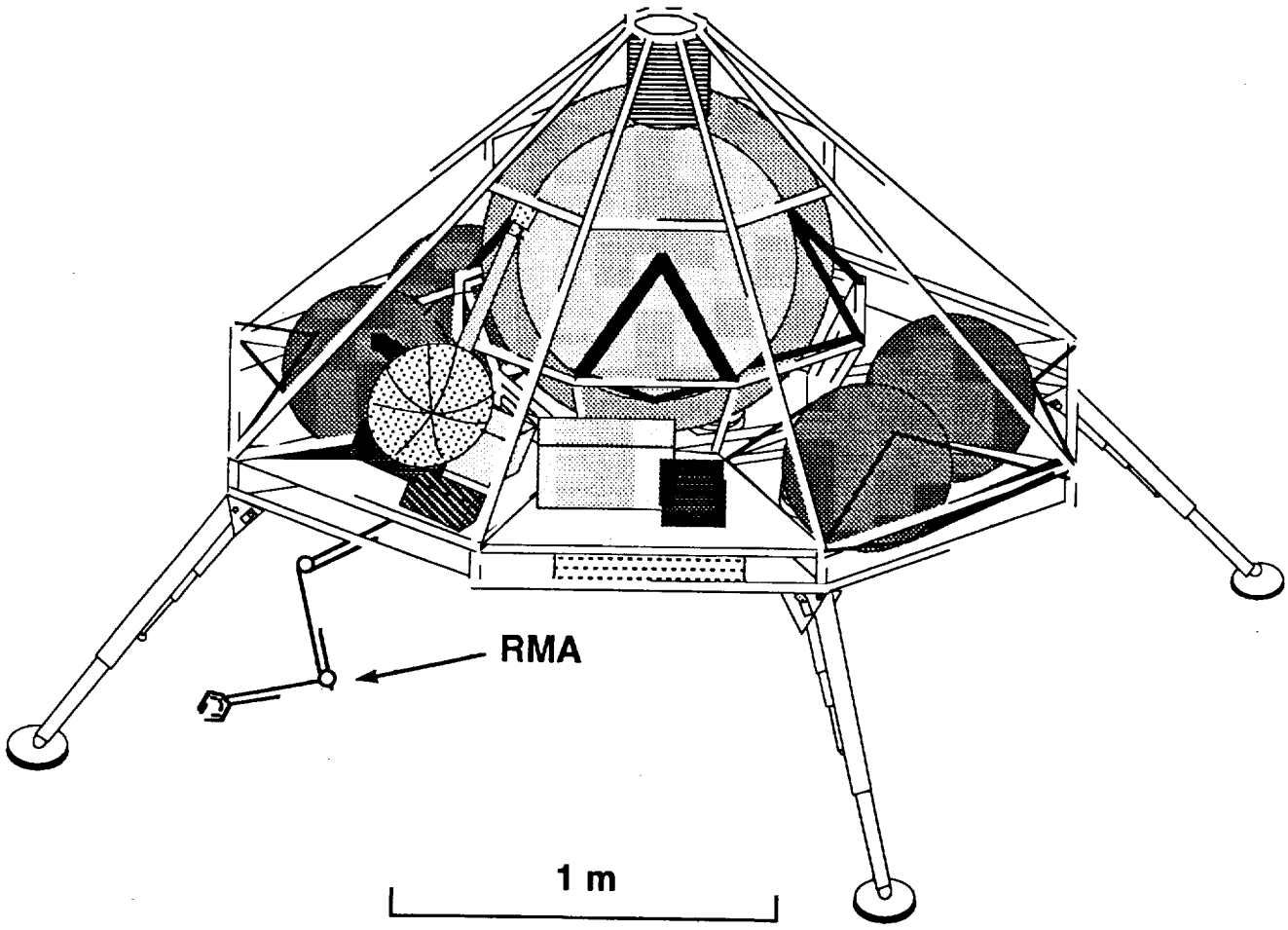

Fig. 5.1 MLVH showing RMA.

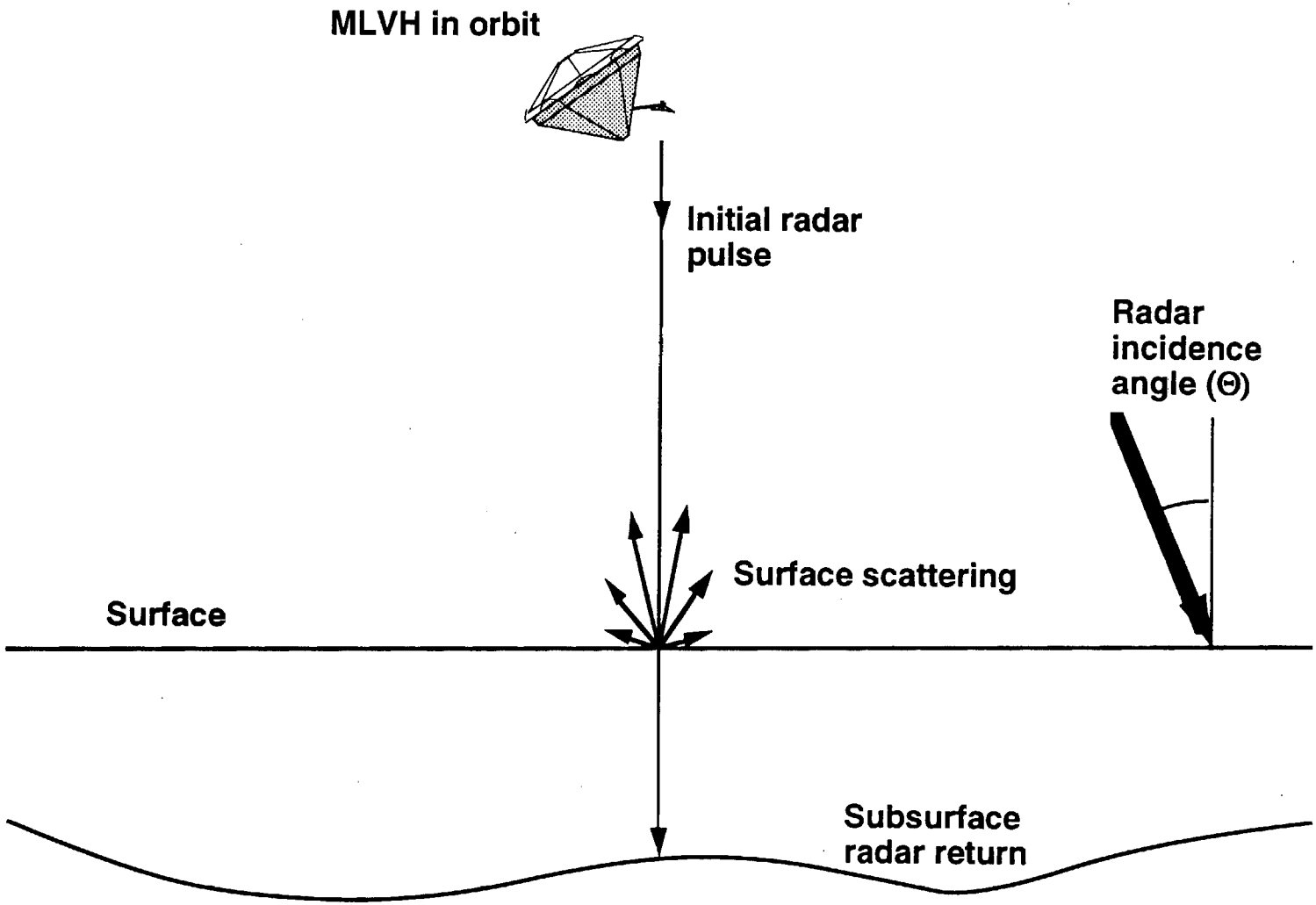

Fig. 5.2 Schematic of GPR operation.

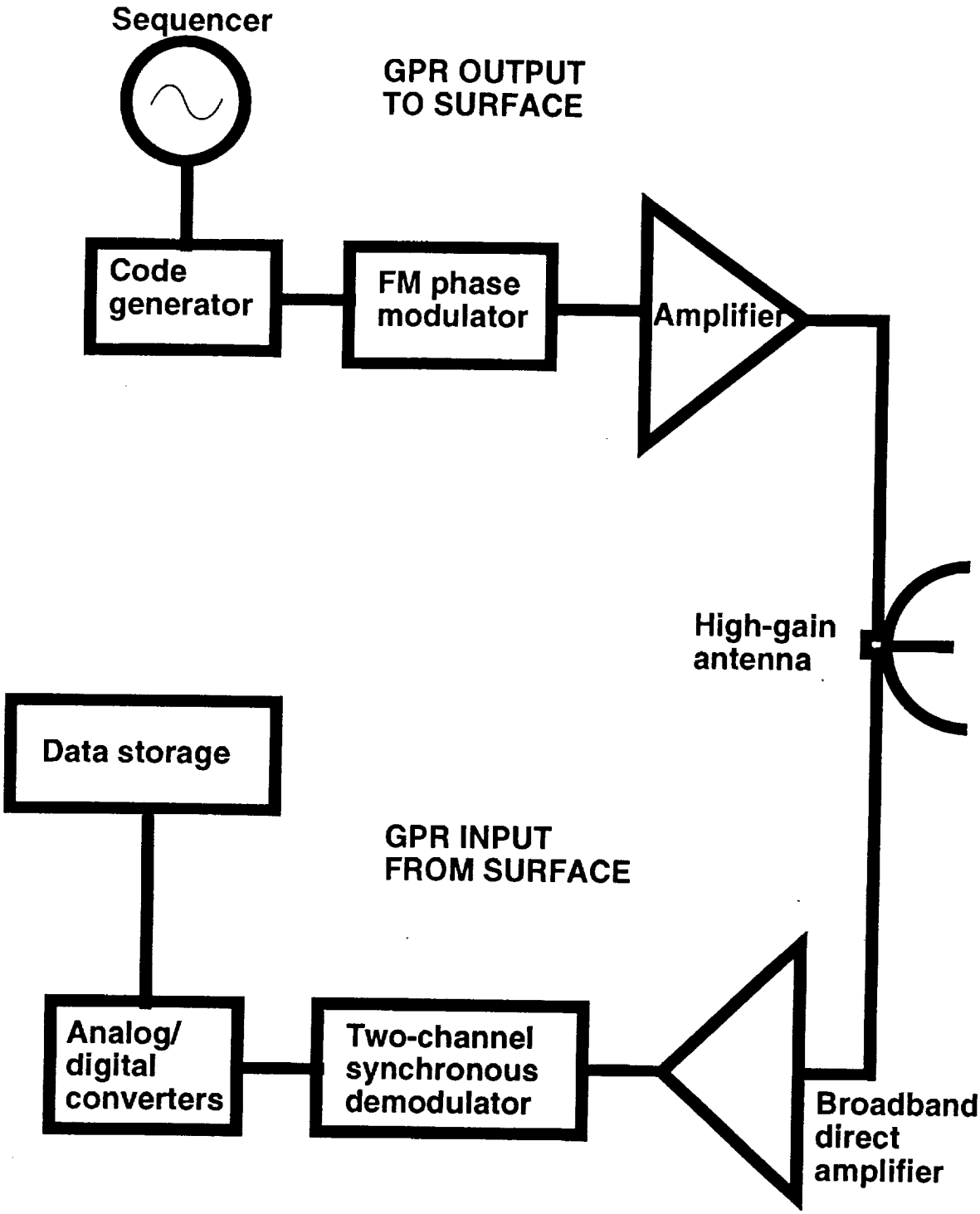

Fig. 5.3 Schematic of GPR subsystems and operation.

6.0 LAUNCH VEHICLE AND ASTRODYNAMICS

Matt Hedman

Chris Willman

TABLE OF CONTENTS

6.1 INTRODUCTION
(Chris Willman)

Mobility is one of the prime drivers behind societies. Roads made it easier to trade in the Roman Empire. The British built and exploited the Suez Canal to improve access to resources in India, and the United States built the Panama Canal to link the East and West Coasts for trade and defense. Henry Ford mass produced the automobile, giving individuals access to quick, cheap, and flexible transportation. Similarly, the exploration of other planets is driven by our ability to move around; to accelerate and decelerate; and to safely and reliably deliver a payload. This section discusses the methods of transportation employed by Project Genesis, both from Earth to Mars and across the surface of Mars. There are five major phases of transportation: launch from Earth, astrodynamics to Mars, capture at Mars, descent to the surface, and surface mobility.

For Project Genesis, some less conventional methods were chosen for parts of the transportation strategy. The mission is designed to launch on a Delta 7925. The launch mass is small enough to allow for larger C_3 values which have shorter transit times. Mars capture is achieved using an aeroassist through the atmosphere to substantially reduce the amount of fuel necessary to achieve orbit. A combination of aerobrake, parachute, and thrusters is used to obtain a soft landing on the surface. The MLVH can move to a new location on the surface via a ballistic hop, using fuel created from seed hydrogen from Earth and carbon monoxide from the Martian atmosphere. These innovations allow Project Genesis to do more things for much less money.

6.2 LAUNCH VEHICLE
(Matt Hedman)

There are several criteria that the launch system has to satisfy. First, the system has to have the ability to send the mass of the MLVH to Mars. Second, the payload fairing has to be large enough to accommodate the volume of the MLVH with an aerobrake. Third, the launch system

has to have a high launch success rate. Lastly, the vehicle has to be the most economical launch system that satisfies the above three requirements.

Five different launch systems were considered for sending the Mars Landing Vehicle and Hopper (MLVH) to Mars. The systems analyzed were the Russian Proton, American Atlas II, Atlas IIA, Atlas IIAS, and the Delta 7925 (See Fig 6.1). Of the systems considered, the Russian Proton has the largest payload capacity and lowest price. However, politics may not allow a Proton to be used. Therefore, the four remaining systems had to be evaluated for payload, price, and reliability. The Atlas models have a higher performance capability than the Delta 7925. However, the Delta is cheaper and has a higher launch success rate than any of the Atlas models. Therefore, the Delta 7925 was chosen because it represents the best compromise between the three categories. In the event that a Proton is available, the Proton could easily accommodate our vehicle and may be able to allow MLVH mass increases that can add to the benefits of the mission. Each of these vehicles is described in further detail below.

6.2.1 Proton
(Matt Hedman)

The Proton is the most attractive choice of the launch systems considered. Not only does it have the ability to send a greater mass to Mars than the Delta or Atlas vehicles, but it is also cheaper than the American systems. The Proton has the ability to send 4600 kg to Mars with a C_3 value of 10 km^2/sec^2. The upper stage payload fairing has a diameter of 3.8 m at the base and a height of 8 m [1]. The launch cost is estimated to be between $35 and $70 million in 1990 [1]. Due to the current economic condition of Russia, the future launch price may be even lower than $35 million. The four other launch systems cannot match the Proton in any of these categories.

The larger payload capacity of the Proton enables the MLVH to be redesigned to carry a larger and faster propellant production plant (PPP). A more massive structure is needed to house

the larger PPP. Therefore, the propellant tanks must be bigger to hold the extra propellant to make the required hop. Many other components scale up in size. A rough model was developed to analyze these trends. The following assumptions were made.

- The mass of the PPP scales linearly with the mass of propellant it produces per day. The scale factor assumed was 50 kg of plant per kg of propellant produced per day.
- The RTPV power source produces 18 Watts per kilogram of power source.
- The frame structure constitutes 15% of the launch mass of the MLVH.
- The masses of the main engines scale linearly with the MLVH takeoff thrust to weight ratio.
- The mass of the parachutes constitutes 3% of the MLVH landing mass.
- The mass of the aerobrake makes up 15% of the landing mass.
- 15% mass growth of the launch mass is allowed.
- Assumed masses:
  - science equipment = 8 kg
  - avionics = 90 kg
  - reaction control system = 25 kg
  - communications equipment = 25 kg
- Main engine Isp = 348 sec.
- Drag and gravity losses during burning time are not accounted for when calculating the hop distance.

The model shows that for a fixed hop distance, the MLVH launch mass is a function of how many days of propellant production time are needed to make the hop. The resulting plot of these two quantities for a 35 km hop is shown in Fig. 6.2. For the Proton launch capability of 4600 kg, the number of production days required for a 35 km hop would be only 43 days. This

time is shorter than the 72 days of production time needed for a 1000 kg MLVH required for a Delta 7925. Another option is to produce propellant for longer than the 43 days required for a 35 km hop and make a longer jump.

Unfortunately, politics plays a role in our ability to acquire a Proton rocket. Because the Proton is made by Russia, the United States may not want to launch a US mission in a Russian rocket and/or launch the mission from Russia. If a Proton is available, it is the obvious choice to launch our mission. However, because of the Proton's uncertain availability, the four remaining systems had to be evaluated for their payload capacity, reliability, and cost.

6.2.2 Atlas II
(Matt Hedman)

The Atlas II is manufactured by General Dynamics in San Diego, CA, and allows a payload of 1600 kg to be transferred to Mars [2]. A Centaur upper stage attaches to the Atlas to provide the third stage of the launch system. The Centaur payload fairing has a diameter of 3.65 m at the base and is 9.49 m in height [3]. The average launch success rate of all of the Atlas models from 1980 to 1990 was 91% [1]. The price of the vehicle is estimated between $70 million and $80 million [1].

The same rough model that is discussed in the Proton section was used to determine how many production days must be spent between hops if the MLVH is redesigned with a larger launch mass. As Fig 6.2 shows, the production time for a 35 km hop with a 1600 kg launch mass is 53 days. When compared with the 72 days of production time required when using a Delta 7925, there is a significant improvement. However, the smaller cost and better reliability of the Delta 7925 makes it preferable over the Atlas II.

6.2.3 Atlas IIA
(Matt Hedman)

The Atlas IIA has a slightly larger payload capacity than the Atlas II (1725 kg to Mars compared to 1600 kg for the Atlas II [2]). However, the IIA model also costs approximately $10 million more than the Atlas II [1]. According to Fig 6.2, an MLVH designed with a launch mass of 1725 kg would take 51 days to produce enough propellant for a 35 km hop. The slightly faster production time does not justify the added cost of the Atlas IIA over the smaller Atlas II or Delta 7925.

6.2.4 Atlas IIAS
(Matt Hedman)

The Atlas IIAS is the largest American launch system that was considered. With the capability of sending 2200 kg to Mars [2], the IIAS model is easily able to launch the current design of the MLVH. However, the IIAS model costs approximately $40 million more than the Atlas II and $70 million more than the Delta 7925 [1]. Using the MLVH launch mass model made for Fig 6.2, an MLVH with a launch mass of 2200 kg would take 47 days to manufacture the propellant necessary to make a 35 km hop. Compared to the production time of 53 days for the Atlas II, the quicker production time does not justify spending $40 million more on the IIAS model.

6.2.5 Delta 7925
(Matt Hedman)

The MLVH is designed to be launched on the Delta 7925. It is the cheapest, smallest, and most reliable American rocket that was analyzed. Since 1980, the Delta has had a launch success rate of 98% [1,4]. The last failed launch of a Delta vehicle was in 1986. The price of the 7925 model is approximately $50 million. Although it has a lower payload performance than any of the

other systems considered, its low cost and extremely high launch success rate caused the Delta 7925 to be chosen as the launch system for Project Genesis.

The PAM-D is the upper stage of the system. There are several payload fairing sizes that can be used with the PAM-D. Using the 8 ft (2.4 m) diameter fairing, 1100 kg can be transferred to Mars with a C_3 value of 10 km^2/sec^2 [4]. With the 9.5 ft (2.9 m) fairing, 1050 kg can be sent to Mars. The 10 ft (3.0 m) fairing allows 1000 kg to be transferred to Mars.

The size of the aerobrake of the MLVH requires the 10 ft (3.0 m) fairing. The 1000 kg performance capability already includes the mass of the upper stage adapter which is approximately 35 kg. The adapter is the 37-12 model which is 37 in. (0.95 m) in diameter and 12 in. (0.308 m) in height. The inside of the payload fairing is 2.8 m wide at the base and 4.2 m in height.

Table 6.1. Launch sequence of the Delta 7925.

Event	Time (sec)
Main engine ignition	0
Main Engine Cutoff	265
Stage I separates	273
Stage II ignition	278
Second stage burnout	951
Fire spin rockets	1001
Separation from stage II	1004
Stage III ignition	1041
Stage III burnout	1128
MLVH separation from stage III	1240

The total burn time of the entire system takes approximately 20 minutes before the MLVH separates from the upper stage. Table 6.1 lists the sequence of major events of the Delta 7925 after takeoff [1].

6.3 ASTRODYNAMICS
(Chris Willman)

One of the major trade-offs in choosing a flight path to Mars is the conflict between the cost of higher energy and the cost of longer time in transit. Higher energy would result in the aerobrake having to do more work and dissipate more heat in order to capture at Mars, and less mass able to be sent to Mars. Longer time would result in more seed hydrogen boiling off, wasting both space and mass, or would require more insulation, again using space and mass, or more refrigeration, using space, mass and power resources.

Taking all of these factors into account, it was decided that the best option was to avoid the complications of radiative heat transfer during the aerocapture. Fig. 6.3 depicts the range of C_3 values and hyperbolioc velocities for various launch dates. A low C_3 available for a launch date of 4/01/2001 is 10 km^2/s^2. This corresponds to an arrival date of 9/23/2001, for a trip duration of 141 days. The MLVH arrives at Mars with a hyperbolic velocity of 4.0 km/s, and thus a velocity of 6.28 km/s at an altitude of 300 km. (The actual trajectory will likely use a slightly smaller approach velocity, but corresponding numbers are not available at this time.)

6.4 AEROCAPTURE AND ENTRY
(Chris Willman)

It is a well-established fact that a successful aeroassisted capture at Mars can have an effective I_{sp} well above any conventional propulsion system. The risk lies in the lack of precise daily knowledge of the Martian atmosphere. If the atmosphere is somewhat more dense or less

dense than expected when the MLVH arrives, it could receive a ΔV different enough to cause it to become trapped in the atmosphere, or to continue on its hyperbolic trajectory and exit Mars orbit entirely. A good aeroassist strategy needs to be as robust as possible, in order to deal with problems such as density fluctuations and path perturbations as they happen.

After the lander is captured into an orbit, a short burn by the control thrusters raises the perigee of the orbit slightly to insure that the lander does not immediately pass again through the atmosphere. Once in a stable orbit, the lander performs a variety of scientific and communication functions. When the lander is finally ready to descend to the surface, a short burn lowers the perigee of the orbit into the atmosphere. Aerodynamic drag slows the lander sufficiently to drop it completely out of orbit.

The descent phase is divided into three major stages. The first is the aerobrake phase, during which the lander remains in its initial configuration. At a sufficiently low altitude, the lander begins the second phase by releasing its aerobrake, and deploying a parachute clear of the wake of the aerobrake. The final phase consists of a thrust-controlled descent, and the shedding of the parachute.

Each of these phases has a specific purpose. During the aerobrake phase the largest part of the enrgy is dissipated. The parachute further slows the vehicle to a sufficiently slow speed that the thruster burn is as small as possible. This reduces landing propellant requirements, which reduces Earth launch mass.

All decelerations are heavily dependent on the ballistic coefficient, ß, which compares the effect of drag to the effects of inertia and gravity. That coefficient is given by the following equation:

$$\beta = \frac{C_d A}{M} \tag{6.1}$$

where β = ballistic coefficient,

C_d = drag coefficient,

A = cross-sectional area,

and M = mass.

Higher coefficients give higher decelerations, and have lower terminal velocities. This justifies the use of a parachute, since a parachute has a much larger area, while not significantly increasing the mass. We are attempting a soft landing, and the terminal velocity for such would require a prohibitively large parachute area. Thus, a final thrust-controlled landing is required.

6.4.1 Aerocapture
(Chris Willman)

Based on the selection of the Mars transfer orbit, the MLVH will be approaching Mars with a velocity of 5.9 km/s. In order to be captured into any orbit, a minimum ΔV of 800 m/s would be necessary, requiring a mass ratio of 1.27 given a specific impulse of 348 s. Thus 131 kg of the 625 kg Earth launch mass would have to be propellant, leaving only 494 kg for payload. It is clear from these data that aeroassisted capture is essential.

The theory is quite simple. The MLVH, with an aerobrake shell mounted, passes near enough to Mars to penetrate the atmosphere. The angle of entry determines the depth of the penetration, which in turn determines the total drag and the total decrease in velocity, as well as the attitude of the resulting orbit.

The actual practice is more difficult. Because of the dependence on the path angle, the guidance onboard the craft must be sufficiently accurate to determine the craft's motion relative to the planet to a high degree of accuracy. Because of the dependence on drag, which is proportional

to the density of the atmosphere, the MLVH must be able to handle or react to variations in density as they are encountered. Thus, a robust control system is necessary for real-time contingencies.

The use of lift makes an aerobrake attempt much more controllable and robust. Our MLVH will be capable of using its control thrusters to obtain an angle of attack of 20°, providing a lift coefficient of up to 0.18. To design the mission to rely on this amount of lift would reduce the capability to compensate for a denser atmosphere than was expected. So the aerocapture data listed here assumes that no lift is used. Any perturbations can be corrected using the potential lift.

The MLVH will arrive at an altitude of 300 km with a velocity of 5.9 km/s. Allowable angles at that altitude and speed zero lift are from 16.8° to 17.2° below horizontal. At a medial entry angle of 16.9°, the craft would gently slow through the atmosphere, finally exiting at a velocity of 4.5 km/s and an angle of 13.8° above horizontal. This represents a ΔV of 1.4 km/s, while keeping the deceleration near one Earth-g. Fig. shows the path and dynamic pressures during the aerocapture. The resulting orbit has an apoaereon of 20,500 km, with an orbital period of 13.4 hours. Unfortunately the eccentricity of 0.75 makes GPR coverage of the surface more irregular, but it helps to reduce the ΔV for orbit adjustments, as covered in the next section.

6.4.2 Orbit
(Chris Willman)

When the MLVH finishes its aerocapture pass and leaves the atmosphere, it is destined to reenter the atmosphere after one orbit, as noted above. Since it is desirable to keep the MLVH in orbit for several weeks in order to perform a GPR survey, the control rockets fire a short burn at the apoareon of the orbit to raise the periareon to 300 km. The ΔV required for this depends on the altitude at apoareon. Higher apoareons have lower ΔVs. At 20,500 km, the ΔV is 20 m/s for orbit and another 20 m/s for deorbit, for a total of 40 m/s [5].

Once in this stable orbit, the MLVH can perform its experiments using the GPR. Any points of interest can be catalogued as potential landing sites. Although the MLVH will only spend approximately a month in this orbit, it could remain there without significant orbital decay for hundreds of years. (Of course all of the hydrogen would have boiled off by then, but the GPR could still be collecting data.)

To begin its descent toward the surface, the MLVH performs a second burn at the apogee which lowers the perigee back into the atmosphere. The entry angle can be controlled by the exact value of the ΔV, but even slightly smaller angles require significantly larger ΔVs. Fig. 6.5 depicts the orbit scenario. (The drawing is not to scale, because the real altitudes during the aeroassist and Mars Entry are much smaller than the radius of Mars, and would not be distinguishable from the surface itself.)

6.4.3 Mars Entry
(Chris Willman)

The Mars final entry consists of three phases. The first phase is aerobraking deceleration from an orbital speed of 4.5 km/s at 300 km to 366 m/s at 7.8 km altitude. During this phase most of the energy of the craft is dissipated. The second phase is parachute deceleration, from the previous velocity to the terminal velocity of the parachute configuration which is about 70 m/s at an altitude of 5 km. The use of a parachute reduces the ΔV required in the third phase, which is the thrust-controlled descent to landing.

Following the aerobraking maneuver, at an altitude of about 7.8 km, the aerobrake separates from the MLVH and a parachute is deployed. To affect a soft landing, the parachute is released, and the thrusters are fired. The ΔV required for this is ideally 66.3 m/s, using only 10 kg of fuel. That leaves 10 kg of fuel for boulder evasion. Fig. 6.6 shows the path and dynamic pressures for the Mars entry.

When the aerobrake is released, it will have a larger terminal velocity than the MLVH-with-parachute configuration, so they separate and move apart. Then when the parachute is released, it has a much smaller terminal velocity than the MLVH, and the parachute will be much more subject to winds, so it will separate from the MLVH both vertically and horizontally.

6.4.4 Assumptions and Equations
(Chris Willman)

The equations governing dynamics are quite non-linear, and the MLVH will experience regimes of high and low drag, high and low path angle, and distances from local to global scale. These extremes make it difficult to linerize equations about a given point, so it is necessary to simulate the path of the MLVH. Although a simulation could be arbitrarily precise based on the input, some assumptions are still made to simplify the calculations. They include:

- Atmosphere has constant thermal properties: $\gamma = 1.4$, R=189 J/kg·K, T=215 K.
- Atmosphere density is exponential:

$$\rho = \rho_0 exp\left(\frac{-h}{H_0}\right) \tag{6.2}$$

where ρ = Atmospheric density

ρ_0 = Atmospheric density at zero altitude

h = Altitude

and H_0 = Atmospheric scale height.

- Ignore atmospheric drag above 300 km
- Drag coefficient, C_d, is constant over range of Reynold's numbers.
- Path angle = Thrust angle.
- Main engines are throttlable without affecting performance.

Although the hop is local compared to the global scale of the aerocapture and Mars entry phases, global coordinates are used in all regimes in order to facilitate a single simulation program. The equations of motion in that coordinate system are as follows:

$$\frac{dr}{dt} = v \ sin \ \gamma \tag{6.3}$$

$$\frac{d\theta}{dt} = \frac{v}{r} \ cos \ \gamma \tag{6.4}$$

$$\frac{dv}{dt} = -g \ sin \ \gamma + \frac{T - D}{m} \tag{6.5}$$

$$\frac{d\gamma}{dt} = \frac{\left[\left(\frac{v^2}{r} - g\right) cos \ \gamma + \frac{L}{m}\right]}{v} \tag{6.6}$$

where the lift and drag forces are given by the following relations:

$$L = C_l \ A \ q \tag{6.7}$$

$$D = C_d \ A \ q \tag{6.8}$$

$$q = \frac{1}{2} \rho \ v^2 \tag{6.9}$$

where r = Radius from Mars center

v = Velocity

t = Time

g = Variable Mars gravity

γ = Angle of velocity above horizontal

θ = Angle around Mars from reference Meridian

L = Lift

A = Area

and D = Drag

These equations can be entered into a mathematical analysis program such as MATLAB, and a simulation can be run to numerically integrate the above equations with sufficiently small time steps to obtain results accurate to within 1%.

6.5 BALLISTIC HOP

(Chris Willman)

Hopping from point to point on the surface of Mars has two distinct advantages over standard rover exploration. First, various obstacles such as ravines or boulders are easily avoided. Second, a hop take-off can easily be extended to become an Earth return take-off, given a large enough propellant capacity. The MLVH does not have sufficient propellant to return to Earth, but the mission will demonstrate the technology that makes it possible in the future.

The MLVH has a dry mass of 450 kg, and has 131 kg of fuel. This results in a mass ratio of 1.29, giving a total ΔV of 866 m/s. This ΔV gives a theoretical range of 50 km. Unfortunately there is an atmosphere to deal with, as well as gravity losses and a safety margin to make sure there is extra propellant in case of unexpected surface features at the landing site or variations in the density of the atmosphere. Thus the analysis that follows is for a 32 km hop, with 10% left over for safety. The trajectory of the hop is shown in Fig. 6.7. Even though the atmosphere of Mars is very tenuous, there is a noticeable effect of drag during the second half of the flight, seen in the asymmetry of the flight path.

The hop is divided into three phases. The first is the gravity turn thrust ascent, during which the main engines give the MLVH the required ΔV, and the path angle is regulated by the control thrusters if necessary. The second phase is the ballistic flight, during which the main engines are off, but the control thrusters must turn the MLVH around in preparation for landing. The third phase is the thrust descent, during which the main engines burn to slow the vehicle and

then soft-land on the surface, again with control thrusters working as necessary to correct the heading.

6.5.1 Thrust Ascent
(Chris Willman)

Two types of losses affect the performance of a hop during this phase. They are gravity losses and drag losses. Gravity losses come from longer times of thrust, while drag losses come from higher velocities in higher densities. These two conditions conflict directly, and there is an optimum compromise solution. Although that optimum is undetermined, Project Genesis errs on the side of higher thrust to weight capacity. Also, it is a distinct advantage for the mission to have the ability to lose one or two of the four main engines while still having the ability to take off and land, thus completing its mission as a technology demonstrator.

The optimum trajectory with an impulsive ΔV and no drag is to take off at a 45° from the horizon. In reality this is not advisable because the burn time is finite, so the flight angle is decreased by the force of gravity. Another problem is that the main engines are at 90° to the surface at take off, so the flight path must initially also be at 90°. Thus, gravity turning is used, launching at near 90°, and ending at near 45°. This gravity turn is path dependent, so it must either be actively controlled in real-time or it must be carefully calculated and catalogued beforehand.

For our hop, the time of thrust during take-off is about 26 seconds, so the gravity loss is ~70 m/s, which is more than 8.4% of the total hop ΔV.

6.5.2 Ballistic Flight
(Chris Willman)

For longer flights, one could assume that the upper portion of the flight takes place in a negligible drag environment. But our hop is short enough that the dynamic pressure at the peak

altitude is still 156 N/m^2, compared to the maximum of 798 N/m^2. For a complete history of the dynamic pressure, see Fig. 6.7. Drag in this region can significantly reduce the range of the hop. Of course, the range is not so important as the demonstration of the technology, but keeping the range as close to the theoretical value as possible would require occasional burns of either the main engines or the control thrusters.

During the approximately 2.5 minutes of ballistic flight, the control thruster must turn the MLVH around in order to switch from ascent thrusting to descent thrusting. Depending on the flight characteristics of the MLVH at angle of attack, the MLVH may equilibrate automatically to face in the direction of the flight path. This could vary the required turning angle from as little as 90° or 100° to as much as 180°. Thus, a minimum turning rate of 1.2°/s is required. Gyroscopes cannot handle more than 8°/sec, so a maximum of 5°/s average is used during rotation, with the acceleration/deceleration portions of the turn included. The total time for the turn is no more than 36 s out of the 148 s of ballistic flight.

6.5.3 Thrust Descent
(Chris Willman)

Thrust descent is similar in theory to the thrust ascent, except for two major differences. First, drag helps decrease the velocity during descent, where it fought the increase of velocity during ascent. Second, the boundary conditions of final velocity and altitude equaling zero are based on path dependent properties, and must be either controlled in real time using throttling or pulsing of the main engines, or must be predicted accurately in advance.

To illustrate the difference between ascent and descent thrusting, it is useful to compare the ΔVs. When the ascent ΔV is 644 m/s, the descent ΔV is 222 m/s. This is almost a three-to-one ratio, demonstrating that the contribution due to drag is significant.

6.6 CONCLUSION

(Matt Hedman, Chris Willman)

After analyzing all 5 launch systems, the Proton is the obvious choice for Project Genesis because of its low cost and high performance capability. However, politics probably will not allow Project Genesis to use a Proton. The higher cost of the Atlas IIA and Atlas IIAS rockets over the Atlas II do not justify their increased performance capabilities. Therefore, a choice between the Atlas II and the Delta 7925 is required. The Atlas II has a higher performance capability than the Delta 7925. However, the Delta is cheaper and has a higher launch success rate than the Atlas II. These two advantages of the Delta 7925 outweighed its lower payload capacity. Therefore, the MLVH is designed to be launched onboard the three stage Delta 7925 with the 10 ft. (3.0 m) payload fairing.

From Earth launch to Mars capture, to attitude control, to ballistic hopping, all of the mission ΔVs are well achievable. Using an aerocapture which takes an equivalent booster ΔV of 1390 m/s, the the total Mars capture ΔV is reduced from 1430 m/s to 40 m/s. The MLVH is capable of making a soft landing on Mars with a ΔV of only 55 m/s. *In situ* propellants are used to perform a ballistic hop of 32 km, which is more than 10 times the distance to the local horizon. When considering this mission, it should be kept in mind that the range of the hop is not as important as the fact that a hop is occurring. Many of the potential problems, such as hydrogen boil-off which limits the amount of propellant available, or engine failure which limits the thrust to weight ratio and increases gravity losses, merely decrease the range of a hop which would already be the longest hop ever made on Mars.

NOMENCLATURE

A_X	Cross-sectional area
β	Ballistic coefficient
C_d	Drag coefficient
C_l	Lift coefficient
ΔV	Change in velocity
D	Drag
γ	Angle of velocity above horizontal
g	Variable Mars gravity
h	Altitude
H_0	Atmospheric scale height
L	Lift
M	Mass
MLVH	Mars landing vehicle and hopper
PPP	Propellant production plant
θ	Angle around Mars from reference Meridian
q	Dynamic pressure
ρ	Atmospheric density
ρ_0	Atmospheric density at zero altitude
r	Radius from Mars center
RTPV	Radioisotope thermophotovoltaic power source
t	Time
v	Velocity

REFERENCES

1. Isakowitz, S.J., *International Reference Guide to Space Launch Systems*, American Institute of Aeronautics and Astronautics, Washington, DC, 1991.

2. General Dynamics. Atlas Mission Planner's Guide. San Diego, CA, 1993.

3. McDonnell Douglas. Delta II Payload Planner's Guide. Huntington Beach, CA, 1993.

4. Marin, Dan, McDonnell Douglas, Personal Communication, May 1994.

5. Bate, Roger R., Mueller, Donald D., White, Jerry E., *Fundamentals of Astrodynamics*, Dover Publications, Inc., New York, NY, 1971.

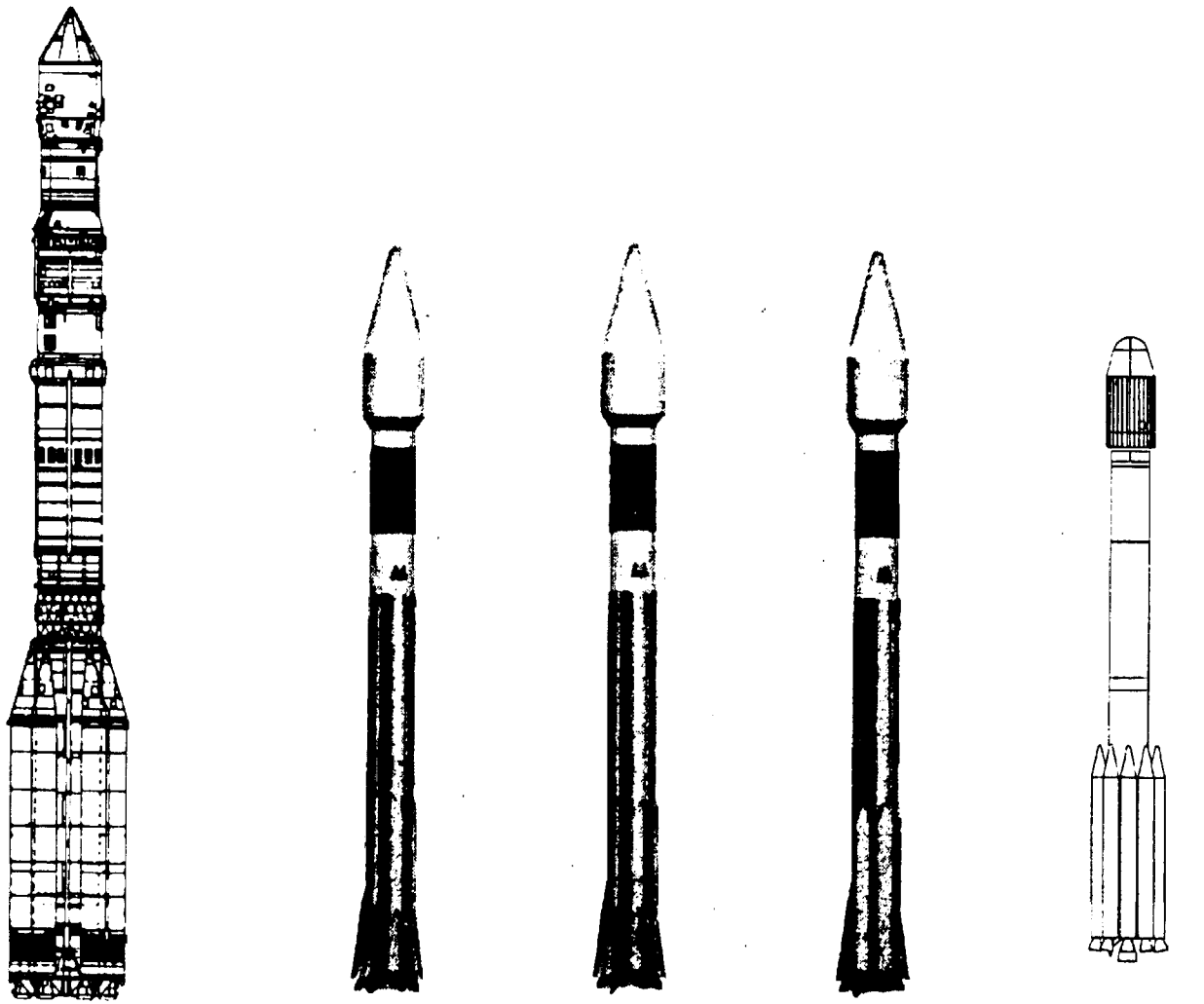

Fig. 6.1 Launch systems considered for Project Genesis.

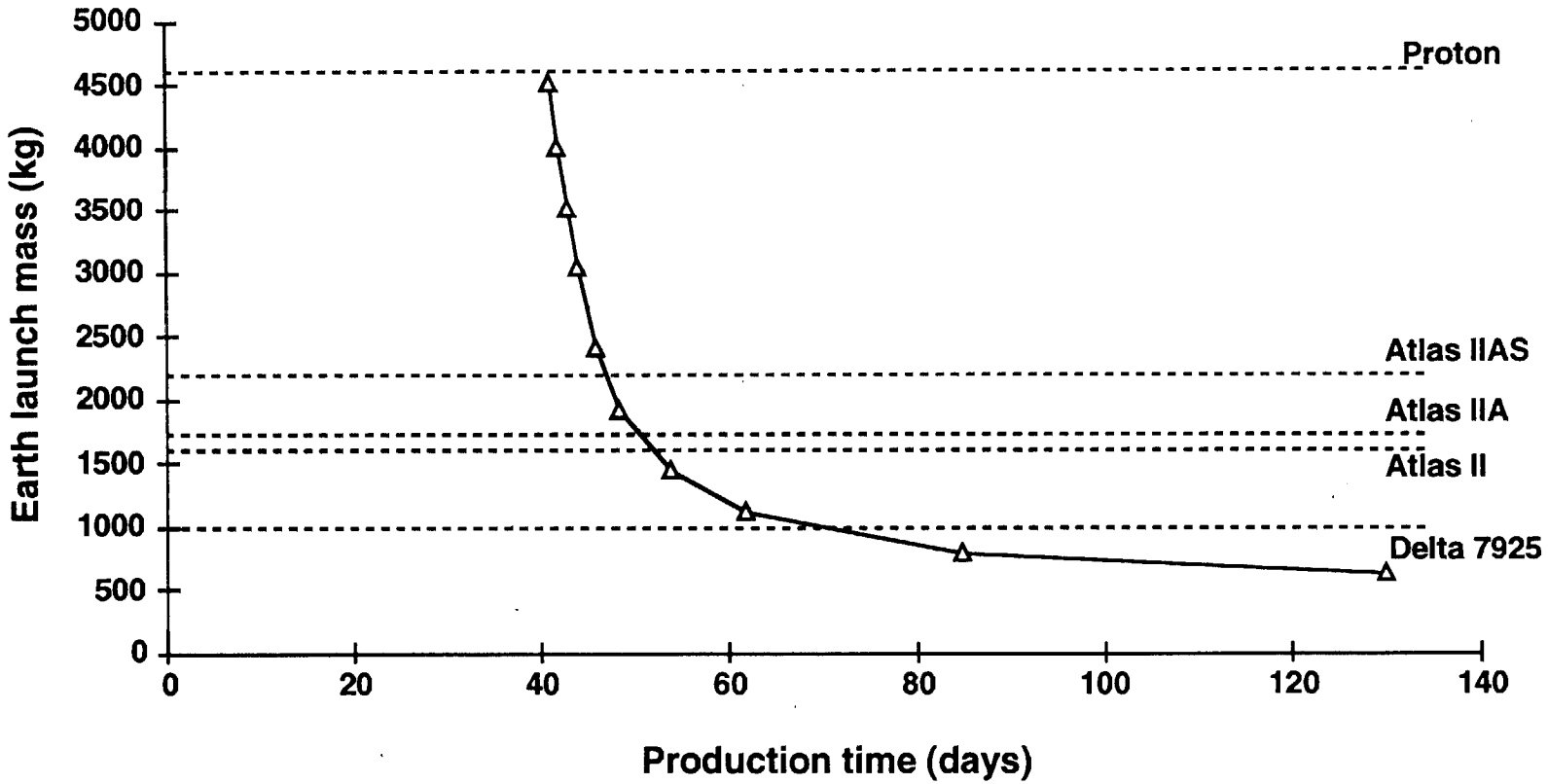

Fig. 6.2. MLVH launch mass vs. propellant production time.

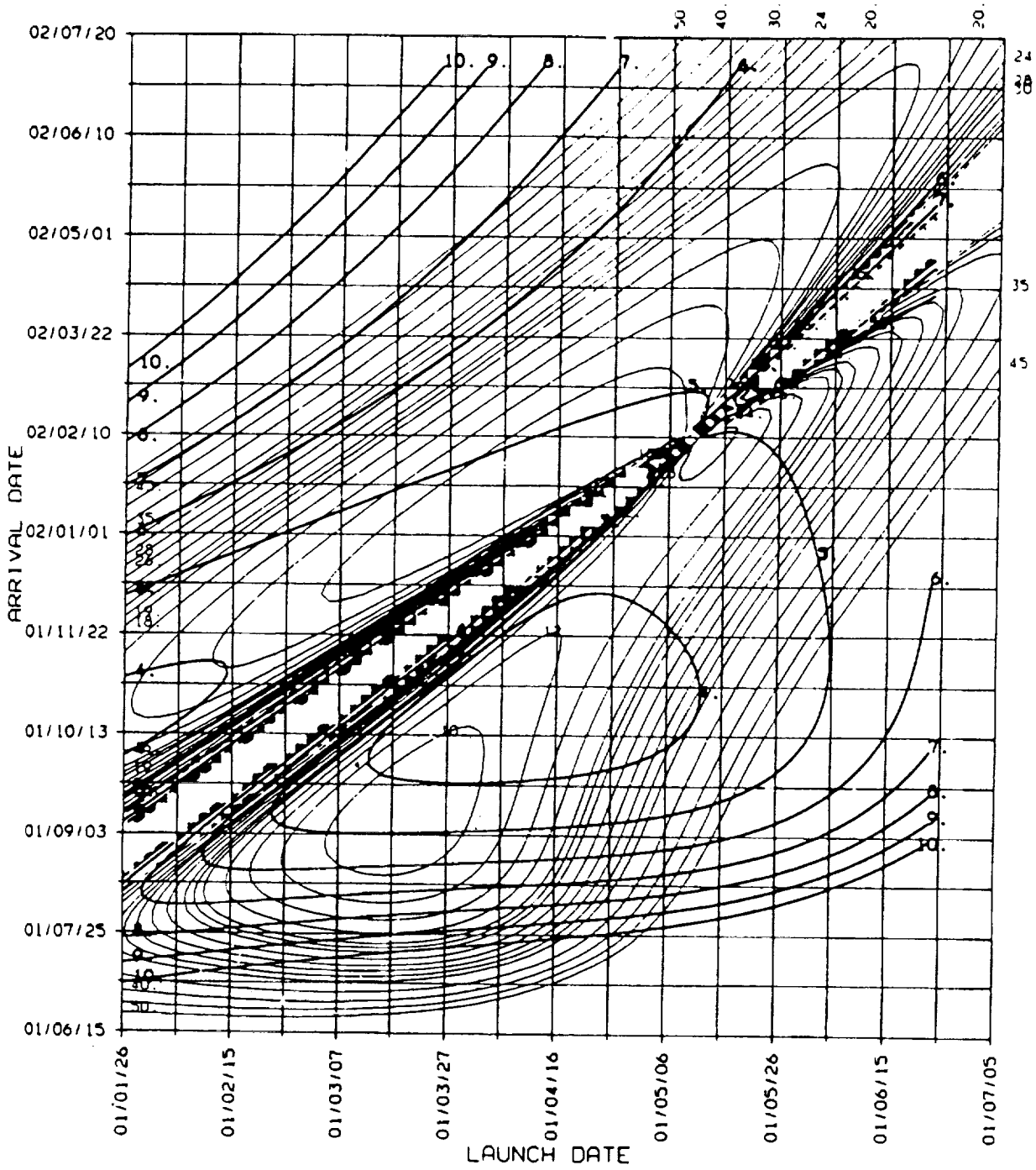

Fig. 6.3 Arrival velocity and C_3 for Mars transfer.

C-3

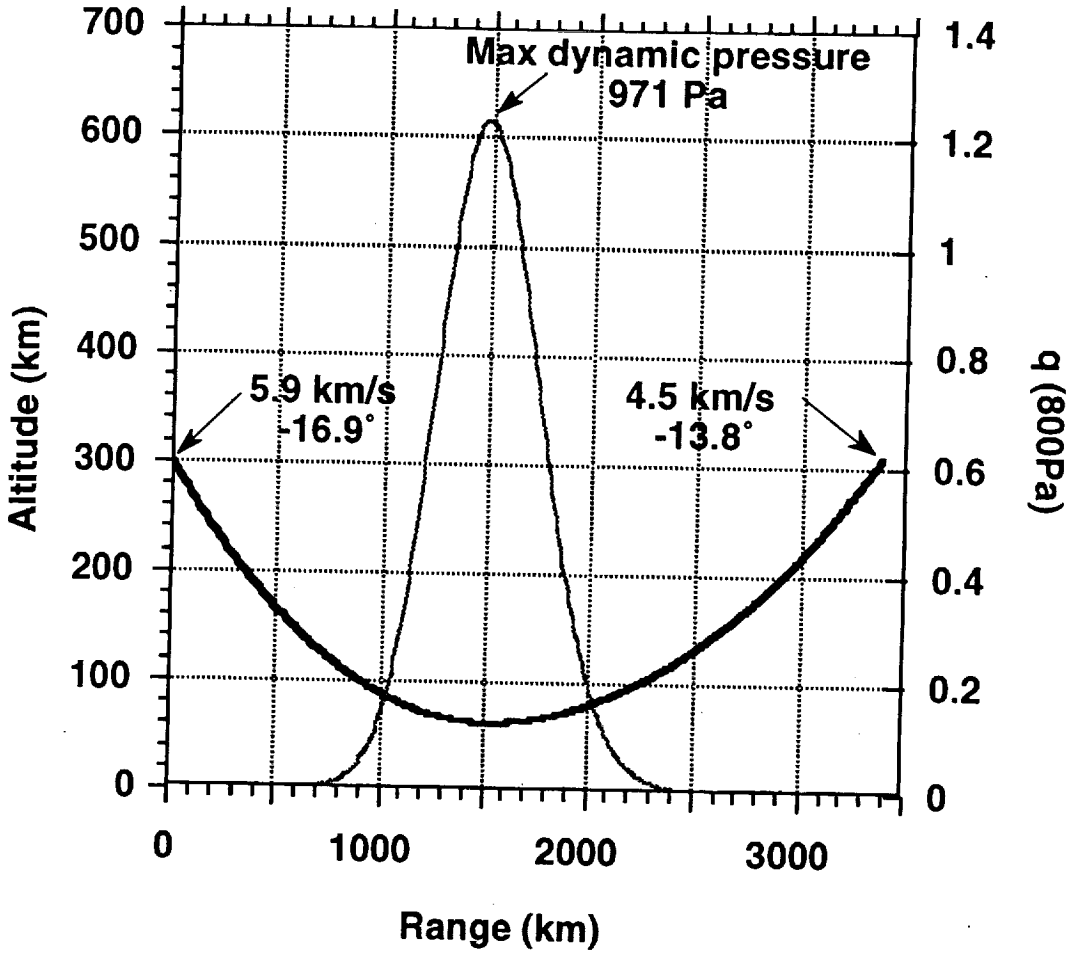

Fig. 6.4 Aerocapture.

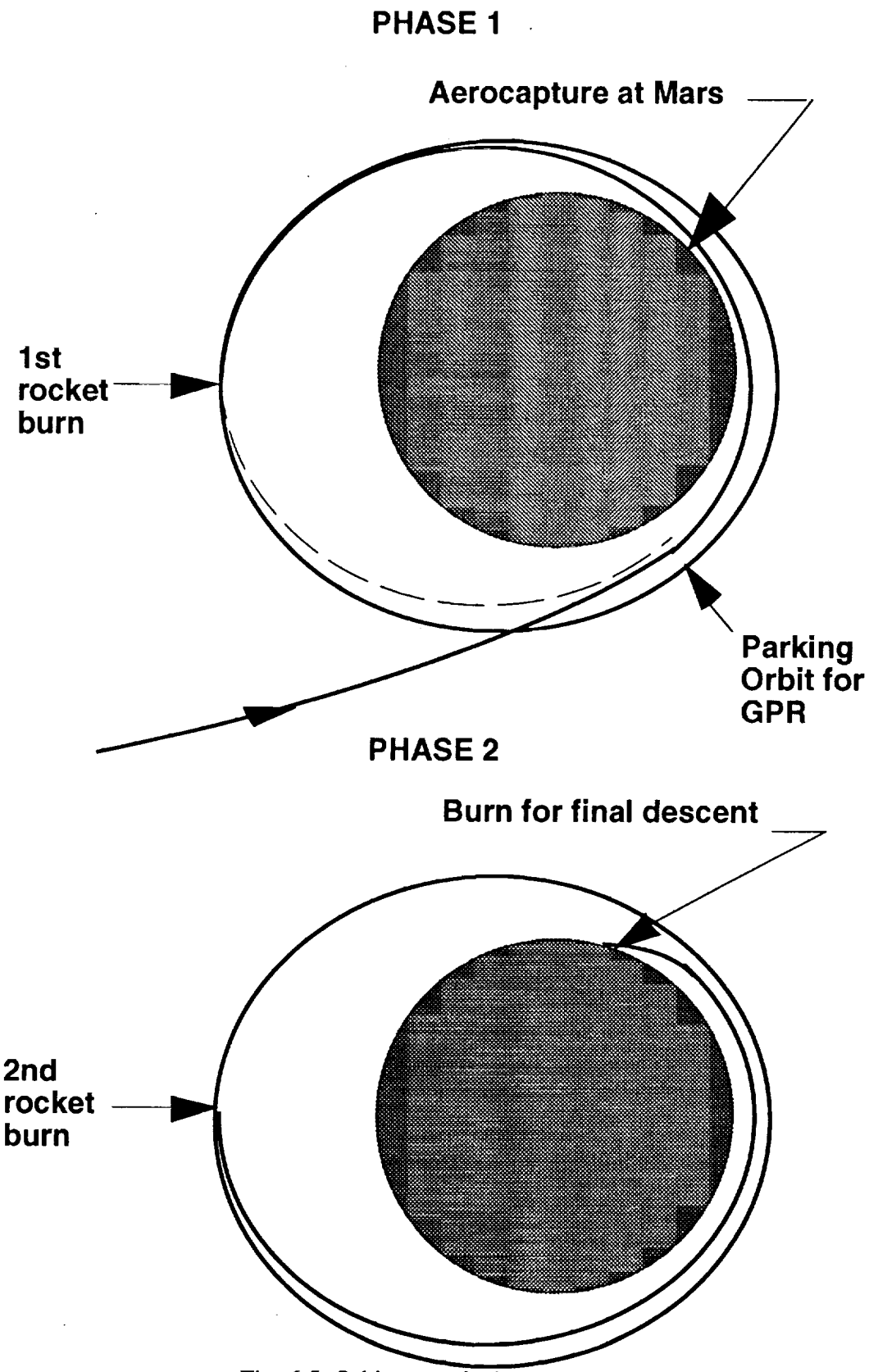

Fig. 6.5 Orbit scenario (not to scale)

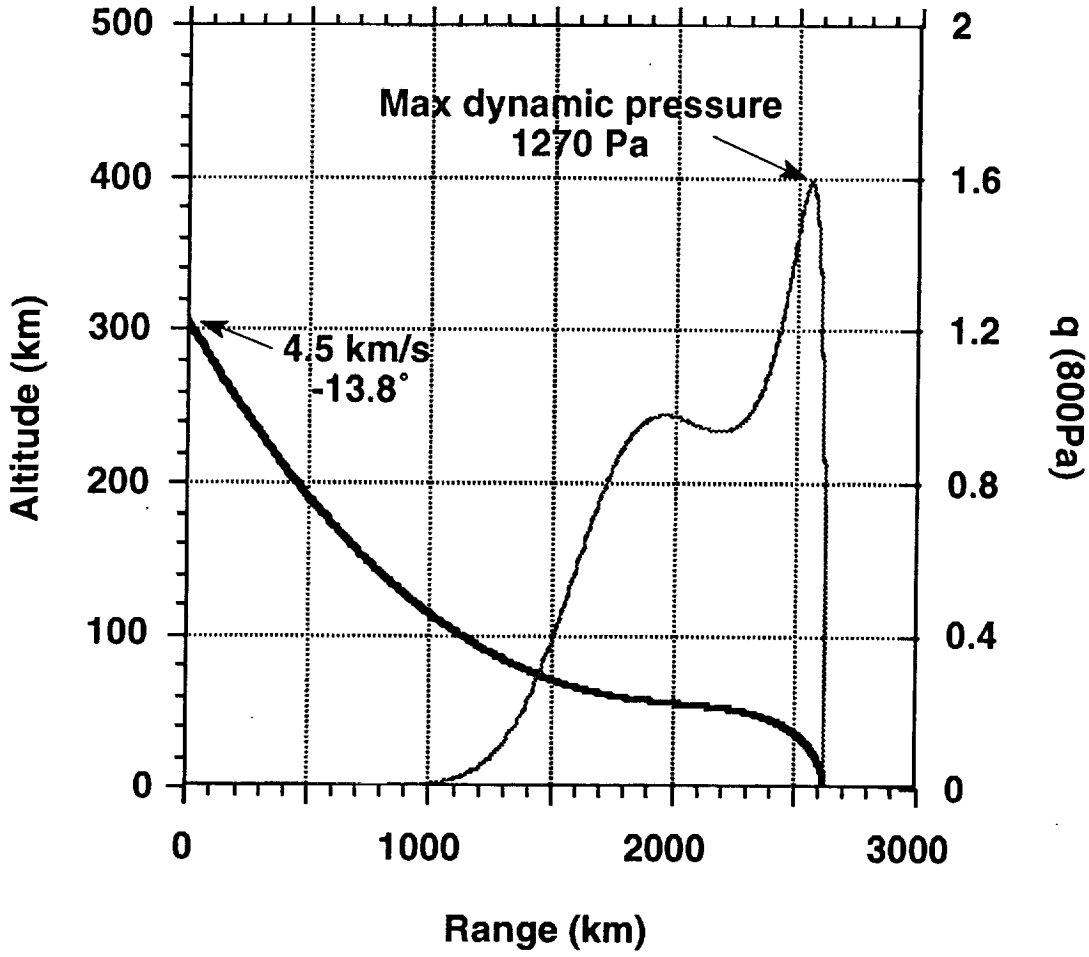

Fig. 6.6 Mars Entry.

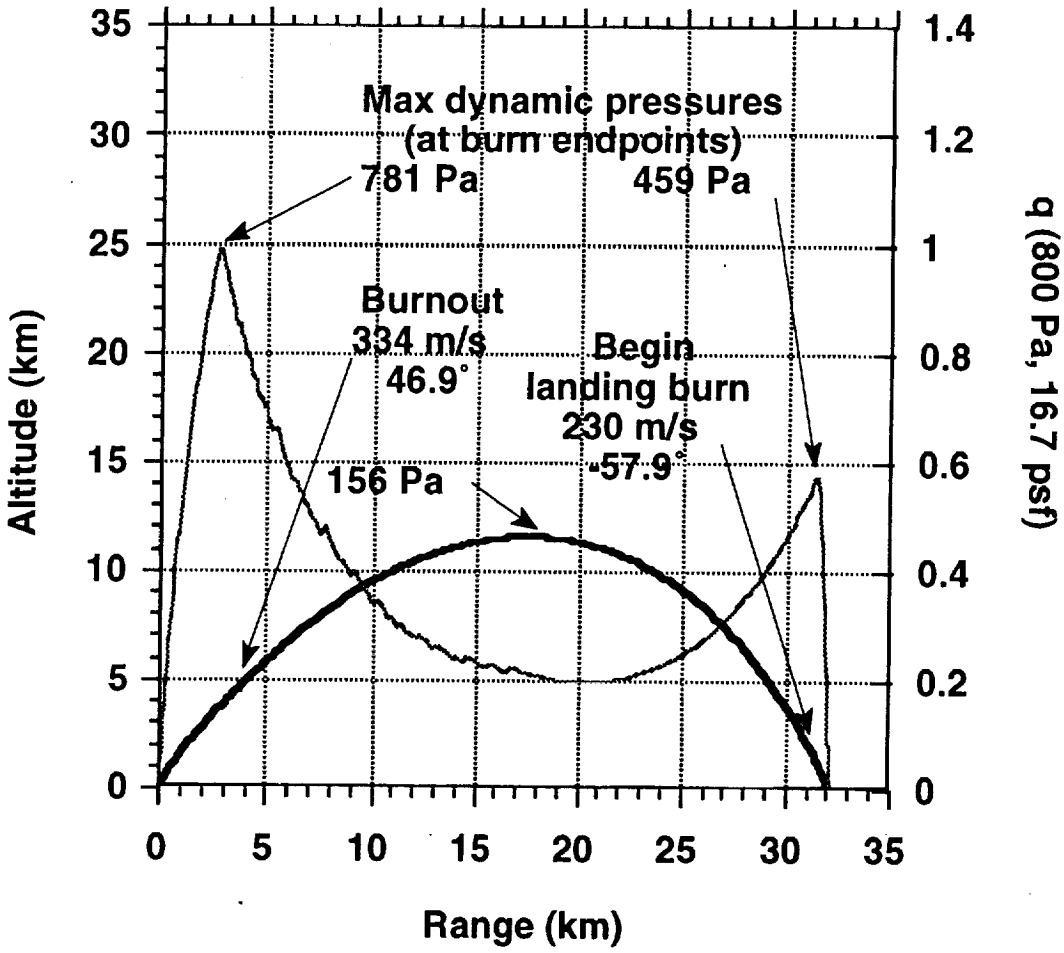

Fig. 6.7 Ballistic hop.

7.0 MISSION COST ANALYSIS

Jason Andrews

Matt Hedman

TABLE OF CONTENTS

7.1 INTRODUCTION
(Matt Hedman)

One of the goals of Project Genesis is to provide an ISRU demonstrator mission that has a total cost similar to or lower than that of a Discovery Class mission. This goal is accomplished by using off-the-shelf technology whenever possible and eliminating any unnecessary, costly items. The cost analysis of Project Genesis is performed by obtaining price estimates of all hardware items of the mission. This list includes the launch vehicle, aerobrake, and all other hardware components of the Mars Landing Vehicle and Hopper (MLVH). The cost of the hardware is further subdivided into the cost of research and development (R&D) and procurement cost for each item. This chapter is ordered to show how the individual item costs are determined.

7.2 LAUNCH SYSTEM
(Matt Hedman)

Five different launch systems are considered to launch Project Genesis as described in Chapter 6. The systems considered are the Proton, Atlas II, Atlas IIA, Atlas IIAS, and Delta 7925. Although payload capacity and launch reliability are also determining factors, price is a major consideration due to the low budget goals of Project Genesis. Table 7.1 lists the prices of the five launch systems that were considered [1,2].

Table 7.1. Launch system prices.

Launch Vehicle	Price (Millions of 1994 Dollars)
Proton	35
Atlas II	80
Atlas IIA	90
Atlas IIAS	120
Delta 7925	50

Although the Proton has the lowest estimated cost , politics probably will not allow a Proton to be used. Therefore, the MLVH is not designed to require a Proton. Of the remaining vehicles, the Delta 7925 has the lowest cost. Its low price played a large role in it being selected as the launch vehicle for Project Genesis. The Delta 7925 is a product currently manufactured by the McDonnell Douglas company in Huntington Beach, CA. There are no R&D costs. Its procurement cost is $50 million [1,2].

7.3 HARDWARE
(Matt Hedman)

The cost analysis of all mission hardware items is analyzed in the following sections. This list includes all MLVH components, the aerobrake, and the parachute.

7.3.1 Propellant Production Plant
(Matt Hedman)

The Propellant Production Plant (PPP) is comprised of several components. The filters, compressor, Sabatier reactor, condenser, liquefaction system, and refrigeration system combine to form the PPP. The R&D and procurement costs of each component are listed in Table 7.2 [3,4,5].

Most of the system technology has already been developed which makes the total price lower than if every component needed further R&D. The filters, Sabatier reactor, condenser, electrolyzer, and refrigerator are all off-the-shelf technology. However, there are significant R&D costs for the compressor and liquefaction systems. Although the components of the liquefaction system are off-the-shelf technology, there will be development costs associated with putting the system together as well as optimizing its performance. Both R&D and procurement costs combine to make the total price of the PPP $9.5 million.

Table 7.2 PPP Costs (Millions of Dollars).

Components	Research and Development Costs	Procurement Cost
Filters	0	0.002
Compressor	5	1
Sabatier Reactor	0	0.015
Condenser	0	0.001
Electrolyzer	0	0.015
Liquefaction System	2.5	0.5
Refrigerator	0	0.5
TOTALS*	7.5	2.0

*Totals are to the nearest $0.5 million.

7.3.2 Engines

(Jason Andrews)

A methane/liquid oxygen engine that meets the performance requirements for the MLVH is not commercially available yet. To gauge the cost of development of this engine, the estimates given by Diane Linne at NASA Lewis Research Center for developing a similar 1000 lb. thrust carbon monoxide *ISRU* engine are used. Further estimates were supplied by Pratt & Witney aircraft. The research and development cost decreases greatly if the rocket engine's thrust is less than 1000 lb. This is mainly due to the size of the personnel and facilities required to test and flight qualify the engine. Aan intermediate estimate of $15 million was chosen for the R&D necessary to develop such an engine [6]. However, due to the potential future applications of a flight qualified Mars *ISRU* methane/oxygen engine, it is possible that the development cost of $15 million may be split between NASA and the engine manufacturers. Another $1 million will be required to purchase the engines [6].

7.3.3 Power

(Jason Andrews, Matt Hedman)

The radioisotope thermophotovoltaic (RTPV) power source used onboard the MLVH is currently being developed at the Boeing Power Systems Division in Seattle, WA. The total R&D costs required to finish the development of a space qualified RTPV is expected to be approximately $35 million [7]. The RTPV was under development for the planned Pluto Fast Flyby mission.

The purchase cost of the RTPV is broken down as follows. Each fuel brick that produces 51.5 W_e will cost approximately $1 million [7]. To meet the requirement of 464 W_e needed for the MLVH, nine bricks are needed. The procurement cost of the total RTPV package includes 80% of the total cost allocated for the fuel bricks and 20% of the total cost for miscellaneous materials such as radiators. Therefore, nine fuel bricks will cost $9 million, and another $2.3 million will be spent on miscellaneous materials giving a total procurement cost of $11.3 million. With the R&D cost of $35 million, the total cost of the power system will be approximately $46.3 million.

7.3.4 Structure

(Matt Hedman)

The 90 kg structure of the MLVH includes the aluminum-lithium 2090 tubing, forged nodes, tank support struts, and equipment connection clamps. The cost of the tubing, forged nodes, and tank supports is $85 per kilogram [8]. However, to account for the specialized equipment connection clamps, the average cost of the total structure is increased to $400 per kilogram. Since the mass of the structure is 90 kg, the cost of the manufactured materials are approximately $36,000.

Extra cost is associated with the frame assembly and equipment attachment. The tubes are connected with forged nodes and attached by electromagnetic forming. Even though the connection process is quite simple to do, the frame assembly cost is not trivial because skilled labor is always expensive. Furthermore, equipment attachment is more complicated than the

electromagnetic forming of the frame. $450,000 is estimated for the cost of labor for assembly and attachment. Therefore, the total cost of the structure including materials and labor is approximately $486,000.

7.3.5 Tanks
(Matt Hedman)

The four propellant tanks and seed hydrogen tank are designed to be made out of Weldalite 049. The procurement cost for each tank is approximately $3000 [9]. Therefore, the total procurement cost of the five tanks is $15,000. However, the largest cost of the tanks lies in R&D. Each tank costs approximately $50,000 to qualify [9]. Total R&D for the tanks is $250,000, making the total cost of the tanks $265,000.

7.3.6 Aerobrake
(Matt Hedman)

The aerobrake used for Project Genesis is a symmetric, nonlifting type similar to those used by the Viking missions. The simplicity of the symmetric aerobrake allows it to be cheaper than a model that needs more R&D, such as a raked sphere-cone. It is estimated that $7.5 million for further R&D of the symmetric aerobrake will be required, along with a procurement cost of approximately $3 million [10]. The total cost of the aerobrake is thus $10.5 million.

7.3.7 Parachute
(Matt Hedman)

The parachute is more expensive than a conventional Earth parachute because it is designed to withstand supersonic speeds and the extraterrestrial environment. The price includes the cost of fabric, suspension lines, pyrotechnic bolts, etc. The total procurement cost of the parachute is $500,000 [11]. No R&D costs are required.

7.3.8 Communications
(Jason Andrews)

The communications equipment uses off-the-shelf technology. Motorola can supply the communications transponder, filters, and cable at a total purchase price of $1 million [12]. The communications antenna is incorporated into the science package such that it is a dual mode system, employed by both the GPR and the communications package. The antenna itself costs $25,000 for development and construction [13]. An additional $5,000 is required for the mounting structure and drive motors.

7.3.9 Avionics
(Jason Andrews)

The avionics and computer package required for Project Genesis is an off-the-shelf system. The computers, inertial navigation system, and Multiplexer/DeMultiplexer (MDM) is made by Honeywell and capable of being integrated using a workstation computer. The general system mimics the MacDonell Douglas DC-X. Conversations with Mitchel Clapp of the Air Force indicated that the system integration cost would be $200,000. The landing radar and Ground Penetrating Radar (GPR) does not currently exist and must be developed. The cost of developing such a system was obtained from a Boeing Company proposal for the Common Lunar Lander [14]. In their report, Boeing chose Lawrence Livermore Labs to do the research and development for $5 million with an additional $1.5 million to purchase the flight hardware. The total price of each component of the avionics system is listed in Table 7.3.

7.3.10 Reaction Control System
(Matt Hedman)

The MLVH has an off-the-shelf reaction control system (RCS) that uses monopropellant hydrazine. The system is made by Olin Aerospace in Richmond, WA. Since no R&D costs are required, the system is cheaper than designing a new system that would use methane and oxygen

as propellants. Table 7.4 lists the individual procurement costs of each component of the RCS [15].

Table 7.3. Avionics procurement costs.

Component	Manufacturer	Procurement Cost (Millions of $)
Laser Inertial Navigation System	Honeywell	0.275
UV-Vis Camera and Startrackers	Department of Defense	1.0
Multiplexer/DeMultiplexer	Honeywell	0.45
Data Storage (FDR-8200)	Amptek	0.1
Instrumentation/Tracking	Livermore Labs	6.5
Mounting Brackets/Wiring/Integration	N/A	0.4
TOTAL		8.7

Table 7.4. Component procurement costs of the RCS.

Component	Procurement Cost (Millions of Dollars)
16 Thrusters	0.64
Hydrazine tank	0.13
Tubing, valves, etc.	0.25
TOTAL*	1.0

*Total is rounded to the nearest $0.1 million.

7.3.11 Science Equipment
(Matt Hedman)

The science equipment costs a total of $7.5 million. The R&D and procurement costs of the scientific packages are listed in Table 7.5 [16, 17,18].

Table 7.5. Science costs

Component	R&D Cost (Millions of Dollars)	Procurement cost (Millions of Dollars)
Magnetic Resonance Spectrometer	0.5	0.5
Alpha Proton X-ray Spectrometer	0	3.5
Remote Manipulator Arm	1.2	0.4
Atmospheric Science Package	0	1.36
TOTAL	1.7	5.8

7.4 TOTAL MISSION COST
(Matt Hedman)

A summary of the costs for the individual MLVH systems is listed below in Table 7.6. In order to compare the cost of Project Genesis to the cost of a Discovery Class mission, the launch system cost is not included in this table. A total system integration and cost growth factor of 20% was included [19]. This figure takes into account the total cost of system integration and testing as well as any unforseen mission costs.

The R&D and procurement costs of the mission without the launch system are $95 million. Since the maximum cost of a Discovery class mission is $150 million, Project Genesis is well within these restrictions. The cost of the Delta 7925 launch system is $50 million, making the total mission cost with launch system $145 million.

Table 7.6 Mission costs (Millions of Dollars).

Subsystem	R&D*	Procurement cost*
PPP	8.0	2.0
Power	35	12
Engines	15	1.0
Structure	0	0.5
Tanks	0	0.3
Aerobrake	7.5	3
Parachute	0	0.5
Communications	0	1.0
Avionics	0	10
Reaction Control System	0	1.2
Science	2	6
System Integration/Growth (20%)	N/A	10.0
TOTALS**	67.5	47.5

*Rounded to the nearest $0.1 million.
**Totals rounded to the nearest $0.5 million.

7.5 CONCLUSION
(Matt Hedman)

One of the primary goals of Project Genesis is to provide a mission that has a total mission cost similar to a Discovery Class mission. A Discovery Class mission must be under $150 million (not including the launch vehicle) and must focus on science. The total mission cost of Project Genesis without the launch vehicle cost is $95 million which is well under the limit for a Discovery Class mission. Project Genesis differs from a Discovery Class mission in that it focuses on technology demonstration rather than science, although it does carry a surface and atmospheric

science package. However, the possible future scientific benefits are staggering. Since Project Genesis is a precursor to more cost-effective manned and unmanned Mars missions using ISRU, the future scientific achievements made possible by ISRU technology easily justifies the cost of this mission.

NOMENCLATURE

GPR	Ground penetrating radar
ISRU	*In situ* resource utilization
MDM	Multiplexer/DeMultiplexer
MLVH	Mars landing vehicle and hopper
NASA	National Aeronautics and Space Administration
PPP	Propellant production plant
R&D	Research and development
RCS	Reaction control system
RTPV	Radioisotope thermophotovoltaic power source
UV-Vis	Ultraviolet visual camera

REFERENCES

1. Isakowitz, S.J., *International Reference Guide to Space Launch Systems*, American Institute of Aeronautics and Astronautics, Washington, DC, 1991.

2. Marin, D., McDonnell Douglas Company, Huntington Beach, CA, Personal communication, May 1994.

3. Johnson, D., Jet Propulsion Laboratory, Pasadena, CA, Personal communication, May 1994.

4. Thomas, P., Philips Laboratory, Edwards Air Force Base, CA, Personal communication, May 1994.

5. Washburn, M., Calhoun and De Jong Inc., Seattle, WA, Personal communication, May 1994.

6. Linne, D., NASA Lewis Reasearch Center, Cleveland, OH, Personal communication, March 1994.

7. Horne, E., Boeing Power Systems Division, Seattle, WA, Personal communication, May 1994.

8. Dixon, J., Alcoa Extrusion and Tube Company, West Lafayette, IN, Personal communication, May 1994.

9. Braun, C., Structural Composites Industries, Pomona, CA, Personal communication, March 1994.

10. Tauber, M., NASA Ames Reasearch Center, Personal communication, May 1994.

11. Aerotex Products (HLC), Bala Cynwyd, PA, Perosnal communication, May 1994.

12. Tommi, D., Motorola Government and Systems Technology Group, Scottsdale, AZ, Personal communication, June 1994.

13. Brand Griffinn, Boeing Aerospace, Huntsville AL, Personal communication,.June 1994.

14. "A Common Lunar Lander for the Space Exploration Initiative," NASA Johnson Space Center Report, Presentation to Aaron Cohen, September 19, 1991.

15. Huxtable, D., Olin Aerospace Company, Redmond, WA, Personal communication, May 1994.

16. Kaiser, W., Jet Propulsion Laboratory, Pasadena, CA, Personal communication, May 1994.

17. Economov, T., University of Chicago, Laboratory for Astrophysics in Space Research, Chicago, IL, Personal communication, May 1994.

18. Kim, S., Jet Propulsion Laboratory, Pasadena, CA, Personal communication, May 1994.

19. Dana Andrews, Boeing Aerospace Company, Kent, WA, Personal communication, June 1994.

8.0 CONCLUSIONS

Daniel Pasco

8.0 CONCLUSIONS
(Dan Pasco)

The human race is destined to expand beyond the boundaries of this world. As our forebears expanded and pioneered, so shall we; by living off what our environment provides. *In situ* resource utilization offers a cheap, reliable source of power and fuel that is indispensable in planetary exploration in the years to come. This technology is not simply a possible choice for space missions to come - it is a *necessary* one.

Project Minerva, presented by the 1992 University of Washington NASA/USRA design team, is a fully developed, manned ISRU mission to Mars. The proposal called for a series of manned expedition to Mars. The propellant for the Earth return voyages would be produced from carbon dioxide in the Martian atmosphere and a small supply of liquid hydrogen brought to Mars from Earth.

Project Hyreus, which was developed the following year at the University of Washington, represented a Minerva precursor. The Hyreus mission included a Mars-orbiting satellite and a large rover. As a sample return mission, Hyreus delivers approximately 27 kg of Martian material to Earth, representing a two order of magnitude increase over many other sample return missions currently being evaluated. Such an increase is possible due to ISRU.

Project Genesis, as implied by its name, represents the beginning of this series of Mars missions. It is a necessary first step, the physical proof that propellants can be produced on another planet using the resources provided by that environment. Such a proof is necessary in order to show that missions such as Hyreus, Minerva, and others can and will succeed.

Genesis utilizes the resources of Mars with maximum efficiency for the technology available at this time. Although this mission has been presented with methane and oxygen as the desired propellant combination, it has been developed with the understanding that the best

possible propellant production scheme would be used. Other architectures, including (but not limited to) the usage of carbon monoxide were carefully considered before moving on to the mission presented here. The findings of this study indicate that although carbon monoxide production may perhaps be the choice of the future, the level of technology required for such a mission is beyond the capabilities of industry at present.

The problems associated with using methane and oxygen, namely the need for an oxygen supply greater that provided by the Sabatier-electrolyzer plant, have been dealt with by examining the possibilities inherent in fuel-rich combustion. This research has provided a useful and rational alternative that eliminates the immediate need for improved technology by utilizing the propellants in the oxygen-to-fuel mass ratio provided by the propellant production plant.

Genesis literally offers a new look at Mars, with its imaging equipment and a ground penetrating radar. It also offers a new look at the fundamental elements of our space missions, and provides the demonstration of technology we need to continue out into the solar system.

APPENDIX A:

PROPELLANT PRODUCTION PLANT ALTERNATIVE: CARBON MONOXIDE

Scott Anderson

Jason Andrews

TABLE OF CONTENTS

A.1 INTRODUCTION
(Jason Andrews, Scott Anderson)

An alternative to using methane and oxygen as a source of rocket propellant on Mars is the use of carbon monoxide and oxygen. Carbon monoxide and oxygen are readily available from the Martian atmosphere through either thermal dissociation of, or chemical extraction from, the indigenous carbon dioxide. The advantages of carbon monoxide over methane stem from the fact that seed hydrogen, crucial for the methane scenario, plays either a superficial role or is not at all required in the production of carbon monoxide. By using carbon monoxide, the propellant production plant could theoretically operate indefinitely, continuously drawing upon the Martian atmosphere as a source of carbon dioxide.

This section focuses on the operating principles and problems of the various methods of carbon monoxide production. The specific propellant production components (e.g., water electrolyzers, compressors, refrigeration) and the respective operating principles are not discussed. The analysis focuses on two different techniques: the Reverse Water Gas Shift reaction and the Zirconia Electrolyzer.

A.2 REVERSE WATER GAS SHIFT REACTOR (RWGS)
(Jason Andrews, Scott Anderson)

A Reverse water gas shift reactor combines carbon dioxide and hydrogen to form carbon monoxide and water:

$$CO_2 + H_2 \rightarrow CO + H_2O \qquad \Delta H = 35.6 \text{ J/kg}$$

A schematic of a carbon monoxide plant using at reverse water gas shift reactor is presented in Fig. A.1. One problem with this reaction is that it is endothermic, meaning that energy is required to drive the reaction to the right and form carbon monoxide and water. The second

major problem is that the reaction is not complete. In other words, all of the carbon dioxide and hydrogen do not react. Significant residual amounts of each gas are present in the exhaust gases containing the products and they have to be separated later, using complicated techniques.

There are currently no Reverse Water Gas Shift reactors available on the market. There are a few small prototype reactors being developed around the country and funded through research or university funds. These reactors are test models only and exist strictly in the scientific realm. The reactors currently under study operate with a small equilibrium reaction coordinate. The equilibrium reaction coordinate, also known as the degree of reaction, determines what percentage of the reactants react to form products. Previously designed RWGS reactors have equilibrium reaction coordinates of 0.1, indicating that only 10% of the reactants are actually combining to form products. For our design requirement, an equilibrium reaction coordinate of 0.1 creates problems when considering that the few products that do form have to be separated from the leftover reactants. Many of these separation processes are very difficult to control and the added complexity of such a system makes all of the current prototype designs undesirable.

The key to operating a RWGS reactor is to control ε_e, the equilibrium reaction coordinate. The reaction coordinate, also known as the degree of reaction, characterizes the extent or degree to which a reaction has taken place. By definition, ε_e is zero for the initial state of the system prior to reaction [1]. A value for ε_e of 0.5 means that 50% of the reactants have reacted to form product. Therefore, values of ε_e approaching 1.0 are ideal. To optimize the reaction coordinate, ways of controlling the reaction through the use of pressure and temperature are examined.

For pressure to drive a reaction, the number of moles produced by a reaction must be different from the number of moles which reacted. For the reverse water gas shift reaction, the number of moles that react equals the number of moles of product. Thus, for this reaction, pressure has no effect on the equilibrium of the reaction.

Temperature controls the reaction because the RWGS is endothermic, i.e., it requires heat to run it in the desired direction. By increasing the temperature, the reaction is driven to the right. The effect of temperature on the equilibrium constant is determined by the sign of ΔH, where ΔH is the heat of reaction. When the heat of reaction is positive, the reaction is endothermic and an increase in temperature results in an increase in the equilibrium constant.

The equilibrium constant, K, is directly related to the operational temperature by the following equation:

$$lnK = \frac{-J}{RT} + \Delta A lnT + \frac{\Delta B}{2}T + \frac{\Delta C}{6}T^2 + \frac{\Delta D}{2T^2} + I \qquad \text{(A.1)}$$

where:

J and I = integration constants

R = the universal gas constant

T = the temperature of the reaction

Δ = value for CO plus value for H_2O minus the values for CO_2 and H_2

The remaining values depend on the heat capacity relations for each product and reactant. Each variation of Δ can be characterized by the relationship given below:

$$\Delta = CO + H_2O - CO_2 - H_2 \qquad \text{(A.2)}$$

From the heat capacity data, the values of A, B, C, and D can be determined for each constituent gas, and thus each value of Δ. The integration constants are solved for by knowing the heat of formation and Gibbs energy of formation for each of the gases at a certain temperature. The relation looks like the following equation after inserting all of these values back into Eq. A.1:

$$lnK = \frac{-5872.17}{T} - 1.86lnT + 2.7x10^{-4}T + \frac{58200}{T^2} + 21.465 \qquad \text{(A.3)}$$

Table A.1 below lists the equilibrium constant as a function of the operating temperature of the reactor. A graphical representation of these results can be found in Fig. A.2.

For a reaction that begins with no product present, the equilibrium reaction coordinate is related to the equilibrium constant by the following equation:

$$\varepsilon_e = \frac{\sqrt{K}}{1+\sqrt{K}} \tag{A.4}$$

where: ε_e = equilibrium reaction coordinate

K = equilibrium constant

Table A.1 Equilibrium constant and equilibrium reaction coordinate as a function of operating temperature.

Operating Temperature (K)	Equilibrium Constant, K	Equilibrium Reaction Coordinate, ε_e
200	0.0000	0.00
300	0.0003	0.02
400	0.0205	0.13
500	0.2298	0.32
600	1.109	0.51
700	3.316	0.65
800	7.377	0.73
900	13.50	0.79
1000	21.59	0.82
1100	31.37	0.85
1200	42.45	0.87
1300	54.43	0.88
1400	66.95	0.89

The equilibrium constant is in turn directly related to the operating temperature as discussed above. Table A.1 and Fig. A.3 depict the relationship between the equilibrium reaction coordinate and the operating temperature.

From Fig. A.2, it is evident that the performance of a RWGS reactor improves dramatically as the temperature increases to 600 K. Above 600 K, the yield increases further but

at a slower rate and the design tradeoffs become issues over materials and power requirements versus product output.

For the reactor, a design operating temperature of 900 K is chosen. Working with this as a design requirement the equilibrium reaction coordinate is 0.79, which means that nearly 80% of the reactants combine to form products. The operating temperature of 900 K is chosen because of concerns regarding the separation of residual hydrogen from the unreacted and reacted gases. There has been a good deal of research done on the separation of carbon monoxide from carbon dioxide. The process, although difficult, is a workable method of separating the carbon monoxide from the product and reactant gas mixture and is discussed later. It was also determined that the condensation of water out of the exhaust gases is not a difficult task. However, because the RWGS is critically dependent on complete recycling of the seed hydrogen, a high equilibrium reaction coordinate is chosen to ensure that as much H_2 reacts as possible. To further improve the amount of reacting hydrogen, the amount of carbon monoxide in the reactor is increased by a factor of four. The chemical equation now reads as follows:

$$4CO_2 + H_2 \leftrightarrow 3CO_2 + CO + H_2O$$

At 900 K this reaction has an equilibrium reaction coordinate of 0.9722 meaning that all but 2.88% of the hydrogen reacts. At this point we have to note that the analysis assumes ideal conditions and does not take into effect mixing conditions.

To further increase the operating efficiency of the RWGS, the reaction can be performed in the presence of a catalyst. The catalyst used for the RWGS is the same as those used in industry for high temperature water gas shift reactors [2]. Two types of catalysts, used as part of an ammonia production plant, are iron-oxide and a chromia-promoted iron oxide [3]. Other catalysts that have shown promise are copper-zinc and cobalt-molybdenum [4]. However, there are problems associated with the use of a catalyst. Carbon deposition is the most likely cause of catalyst deactivation. To avoid this problem, the RWGS should be operated with high H_2/CO or

H_2O/CO ratio and at high operational temperatures. Performance analysis has not been conducted to determine the effect of a catalyst on the RWGS reaction.

A reactor temperature of 900 K requires a large amount of energy to maintain the equilibrium reaction temperature in the Mars environment. To provide this energy, primary heat from the radioisotope heaters is recycled using heat pipes filled with liquid sodium. Sodium was chosen over other liquid metals because of its higher heat capacity to density ratio [2]. Carbon fiber tubing passes through the inner shell of the radioisotope heaters where the liquid sodium is superheated by the 1200 K environment inside the radioisotope heaters. The carbon tubing transfers the superheated sodium to titanium tubing as it exits the radioisotope heaters and then wraps around the inner core of the chemical reactor. The heat is transferred to the reactor core through conduction. To further increase heat transfer, the carbon dioxide is allowed to pass over the titanium tubing before it enters the reactor chamber. To determine the amount of heat required, a heat transfer analysis was performed for the RWGS reactor.

The endothermic heat of reaction was calculated to be 775 kJ/kg at 900 K. The mass flow of the products is 0.1042 g/sec. Using this value, the total heat required for thermal equilibrium is calculated as 80.7 W_{th}. The reactor itself is insulated with MLI such that the radiation loss to the Martian atmosphere is 120 W_{th}, for a total steady state reactor energy requirement of 200 W_{th} supplied by RTPV heat.

A.3 ZIRCONIA ELECTROLYZER

(Scott Anderson, Jason Andrews)

An alternative to the reverse water gas shift reaction for producing carbon monoxide and oxygen from carbon dioxide taken from the Martian atmosphere is the zirconia electrolyzer. A significant amount of research has been conducted on the possibility of using zirconia electrolyzers as a means of in situ propellant production[3,4]. In a zirconia electrolyzer, carbon

dioxide is electrolytically dissociated at high temperatures into carbon monoxide and oxygen by the following reaction:

$$2CO_2 \rightarrow CO + O_2$$

A schematic of a zirconia electrolyzer cell is presented in Fig. A.4. The oxygen is separated from the carbon monoxide and carbon dioxide by a zirconia (ZrO_2) membrane, which selectively transports oxygen when a voltage is applied across it. The solid zirconia electrolyte has the ability to conduct electricity by ionic rather than electronic conduction. In this process molecular oxygen at the cathode is reduced to atomic oxygen ions which migrate to the anode, where the ions surrender electrons and reform molecular oxygen. The oxygen separated by the zirconia electrolyzer is essentially pure and can be liquefied and stored. Due to inefficiencies, the exhaust flow from the zirconia electrolyzer contains both carbon monoxide and carbon dioxide. The carbon monoxide can be separated from the carbon dioxide through the use of catalyst beds as described in Section A.6.

The carbon dioxide must enter the zirconia electrolyzer at very high temperatures, in the range of 1070 to 1270 K. The operation must occur at these temperatures so that the carbon dioxide will dissociate. The carbon dioxide can be raised to these high temperatures with electrical heating of the flow. This procedure requires a fairly sizable power requirement. For the process to work well, the zirconia membrane has to operate at high voltage. The surface area of the membrane is prohibitively large unless high current densities are used. The need for high voltages and large current densities translates to large power requirements. Thus, to operate a zirconia electrolyzer, a lot of power is required to limit membrane size and ensure adequate oxygen separation. However, if the power supplied to the zirconia electrolyzer is great enough, the increased oxygen output could create a high enough pressure in the system to eliminate the need for the oxygen compressor currently required for oxygen storage.

A serious problem with zirconia electrolyzers is the possibility of failure. The stresses of Earth launch, Mars aerobraking, and landing on Mars could very well create cracks in the ceramic components or seals, causing leaks that would lead to oxygen contamination and potential mission failure. The electrolyzer seals and electrodes must be able to hold up reliably at high temperatures over prolonged usage. This has been a problem in past experimental efforts[4]. The system could also fail electrically due to a short across a membrane. If the individual membranes are in series, a short in one would cause the whole system to shut down. To design around this problem, each membrane could be individually electrically controlled. However, this would add considerable complexity to the computer control system and would require more power. Furthermore, if a shut-down occurs during regular operation, the system must be restarted and problems occur if the components do not stay matched to their pre-shut down configuration.

A.4 GLOW DISCHARGE
(Jason Andrews)

The glow discharge propellant production plant is a variation of the zirconia electrolyzer[4]. Glow discharge relies on the electrolytic dissociation of carbon dioxide into oxygen and carbon monoxide as in the zirconia electrolyzer. A glow discharge is used to cause this dissociation. It occurs just before the electrode membrane. A fundamental difference between the two systems is the use of silver electrode membranes instead of platinum. Silver electrode membranes operate at lower temperatures and are more permeable to oxygen ions, making the glow discharge more efficient than the electrolyzer[4].

Using the glow discharge method of oxygen separation, the operating temperature is lowered from 1000 K to 500–800 K. Experiments have shown that when silver membranes are used for the electrode interface anodes for both glow discharge and oxygen separation, oxygen yields are comparable to the permeation rates of pure oxygen[4]. As a result, the use of silver

membranes enhances the output capabilities of the zirconia electrolyzer but does not address or solve the inherent problems associated with its fragility. The use of glow discharge increases the operating efficiency of the zirconia electrolyzer from 15% to 75%[5].

A.5 ZIRCONIA ELECTROLYZER PLANT DESIGN
(Jason Andrews)

To optimize the output of the zirconia electrolyzer, silver membranes are used to augment the throughput capabilities of the zirconia membrane. Using the glow discharge technique the operating temperature of the electrolyzer is 550 K and plant efficiency is increased to 75%. The zirconia/glow discharge propellant unit requires 176 W_e per kilogram of O_2 produced per day, in addition to the necessary heating. A schematic of the zirconia electrolyzer plant design can be seen in Fig. A.5.

The actual propellant plant compresses Martian atmospheric carbon dioxide to four times ambient pressure before passing it through a series of heat pipes inside the RTPV. The heat pipes are responsible for heating the carbon dioxide from 335 K up to 600 K before it passes into the zirconia/glow discharge propellant production unit. The dissociated pure oxygen is liquefied and cooled using the same techniques discussed in Chapter 2 of this report.

A.6 CARBON MONOXIDE SEPARATION
(Jason Andrews)

Both reactor designs require a separate stage that separates the carbon monoxide from the carbon dioxide in the exhaust. The exhaust gas consisting of mixed carbon monoxide and carbon dioxide is passed directly into a series of catalyst beds. The design was taken from Project Hyreus [6] and uses two catalysts beds. A schematic of the separation beds can be found in Fig. A.7. One unit operates at 700 K and rejects heat while breaking the CO into C and CO_2.

The other bed requires heat input nearly equal to the heat output of the first unit. The second unit gasifies the deposited C which combines with CO_2 to form nearly pure CO.[7] The CO is then liquefied and stored using the process described in Chapter 2 of this report. When a large amount of carbon has accumulated on one catalyst bed, the flow is reversed and the roles of the two beds reverse.

A.7 CONCLUSIONS

(Jason Andrews, Scott Anderson)

The Martian environment is very harsh. With the fragility of the zirconia electrolyzer, the possibility of failure is very high. For this reason, the zirconia electrolyzer is not our primary choice for the production of carbon monoxide and oxygen on Mars. However, the depth of current research being performed on the RWGS makes it an unlikely candidate as well. Our analysis indicates that both processes are theoretically capable of producing the needed propellant. However, much further research into the actual developmental status of each technique is necessary before a practical unit can be developed.

NOMENCLATURE

ε_e	Equilibrium reaction coordinate
ΔH	Heat of reaction
I	Integration constant
J	Integration constant
K	Equilibrium constant
R	Universal gas constant
RTPV	Radioisotope thermophotovoltaic generator
RWGS	Reverse water gas shift
T	Temperature of reaction

REFERENCES

1. Smith, J.M., and Van Ness, H.C., "Chemical-Reaction Equilibria," *Introduction to Chemical Engineering Thermodynamics*, 4th ed., McGraw Hill, 1987, pp. 100-150, 496-527.

2. P. Nolan, University of Arizona, Tucson, AZ, Private communication, February 1994.

3. Incropera, F.P., and DeWitt, D.P., "Radiation Intensity, Appendix," *Fundamentals of Heat and Mass Transfer*, 3rd ed., John Wiley and Sons, 1981, pp. 702-735, A1, B1.

4. Ash, R.L., Dongchuan, W., and Outlaw, R.A., "Extraction of Oxygen from the Mars Atmosphere Using Glow-Discharge and Permeation Techniques," Paper No. AIAA 93-2243, AIAA/SAE/ASME/ASEE 29th Joint Propulsion Conference and Exhibit, Monterey, CA, June 28-30, 1993.

5. Linne, D., NASA Lewis Research Center, Cleveland, OH, Private communication, February 1994.

6. "Project Hyreus: Mars Sample Return Mission Utilizing In Situ Propellant Production," AA420/421 Space Systems Design, NASA/USRA Advanced Design Program, Department of Aeronautics and Astronautics, University of Washington, Seattle, WA, June 1993.

7. Bruckner, A.P., Nill, L., Schubert, H., Thill, B., and Warwick, R., "Mars Rover Sample Return Mission Utilizing In Situ Production of the Return Propellants," Paper No. AIAA 93-2242, AIAA/SAE/ASME/ASEE 29th Joint Propulsion Conference and Exhibit, Monterey, CA, June 28-30, 1993.

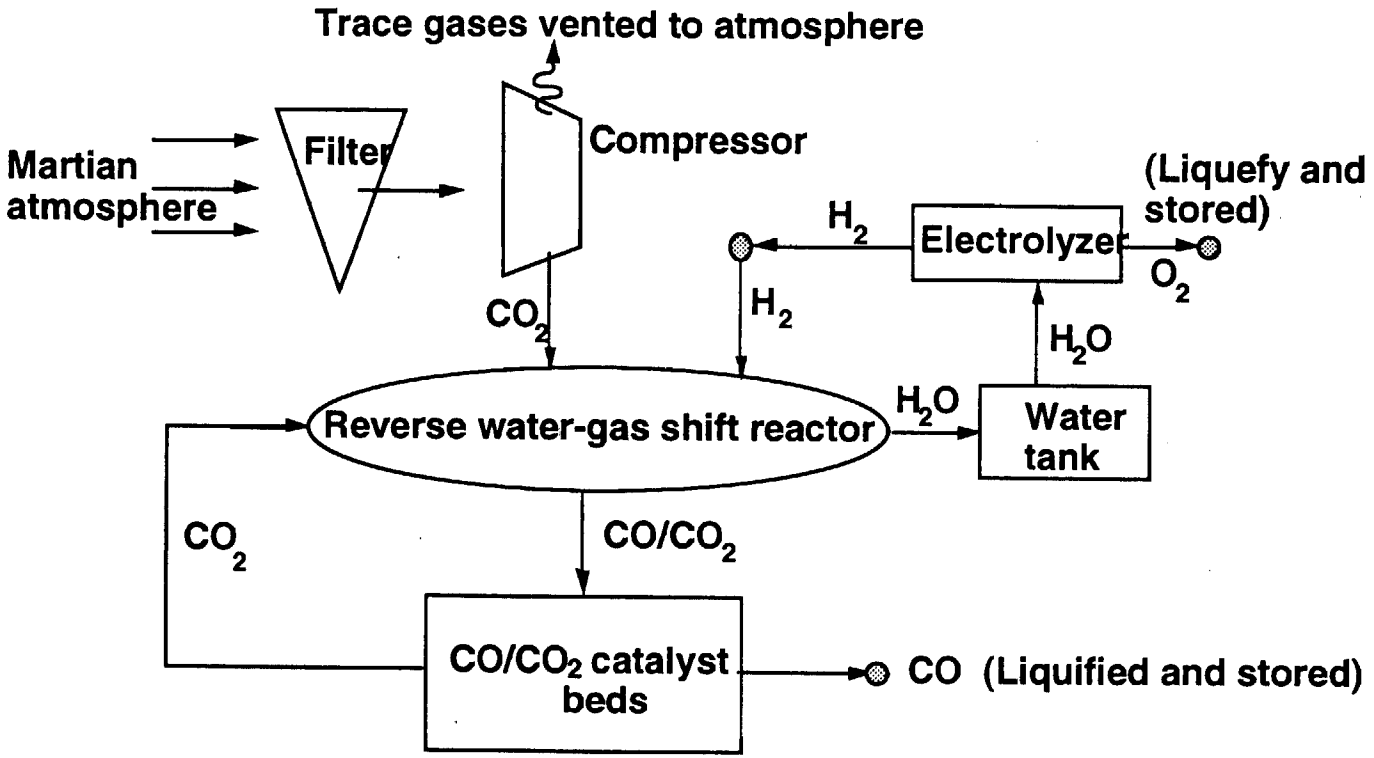

Fig. A.1 Carbon monoxide propellant plant flow diagram.

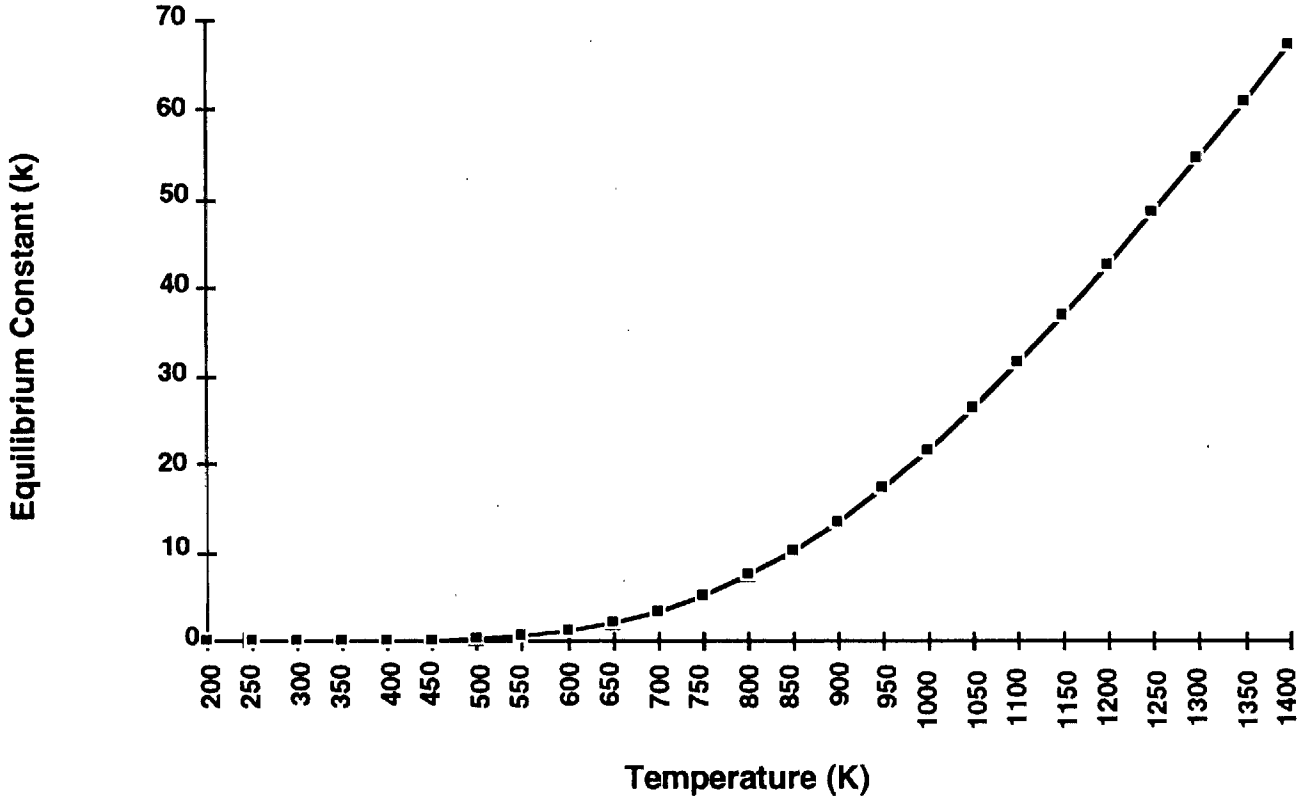

Fig. A.2 Equilibrium constant as a function of temperature, for reverse water gas shift reaction.

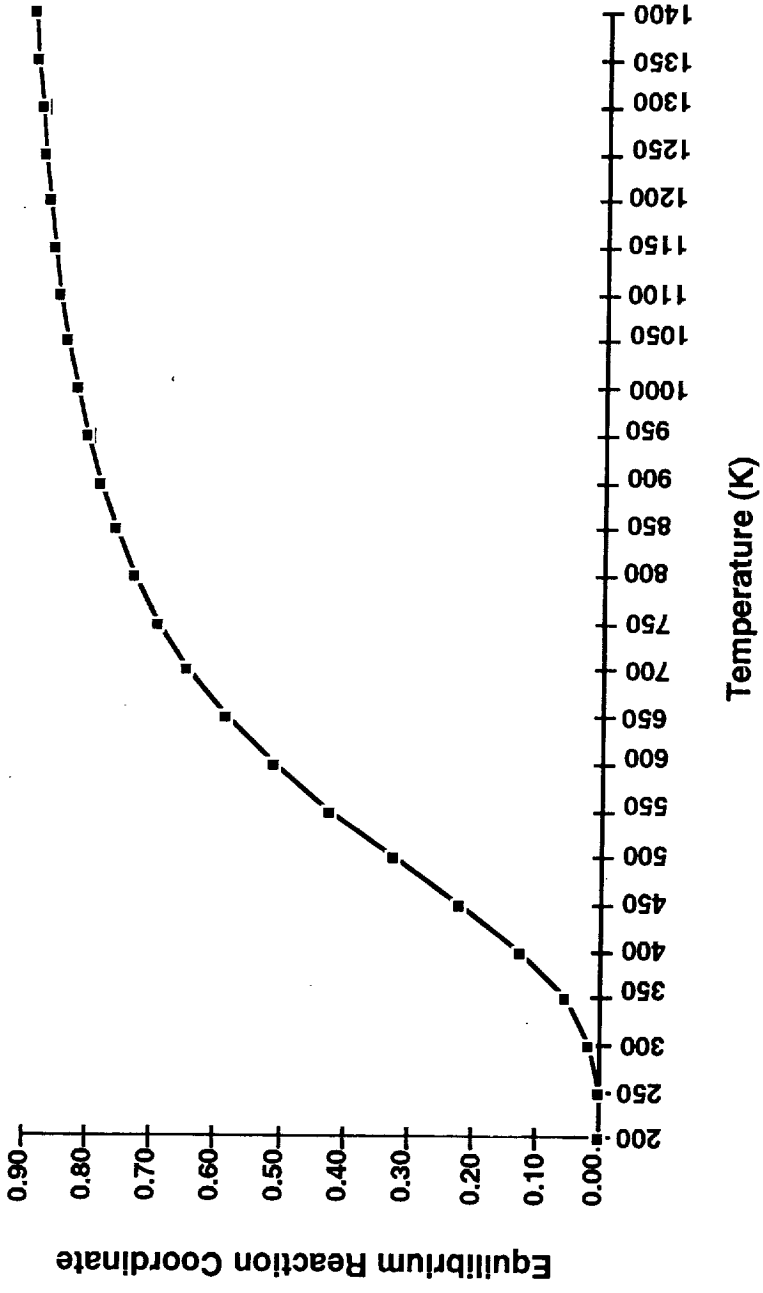

Fig. A3 Equilibrium reaction coordinate as a function of temperature, for reverse water gas shift reaction.

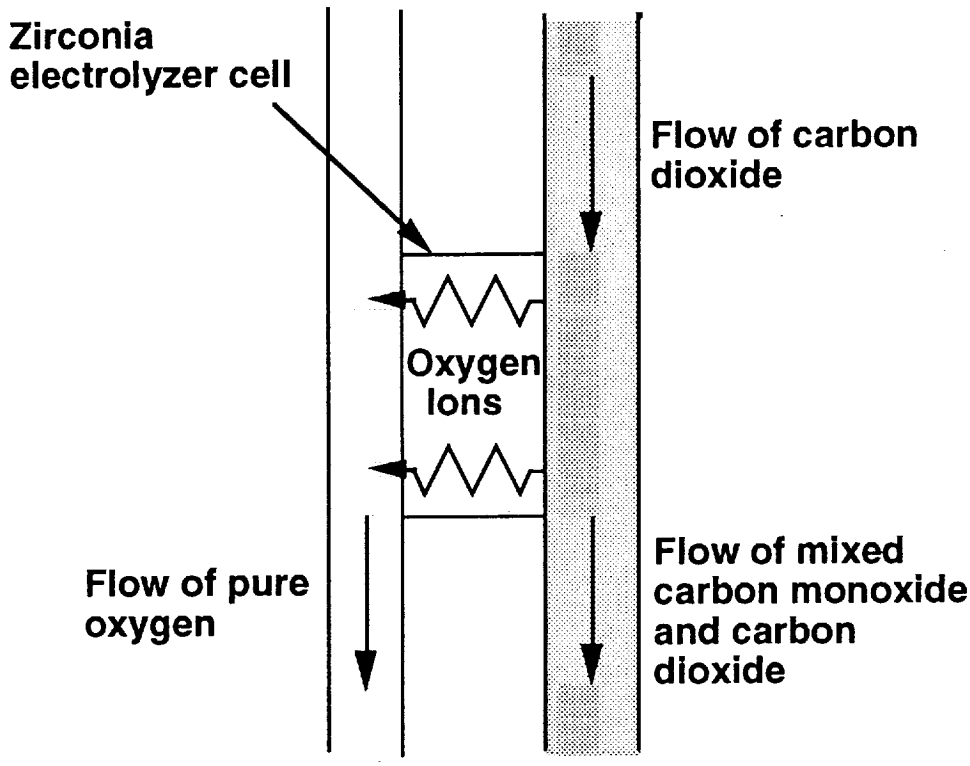

Fig. A.4 Working diagram of oxygen dissociation for a single zirconia electrolyzer cell.

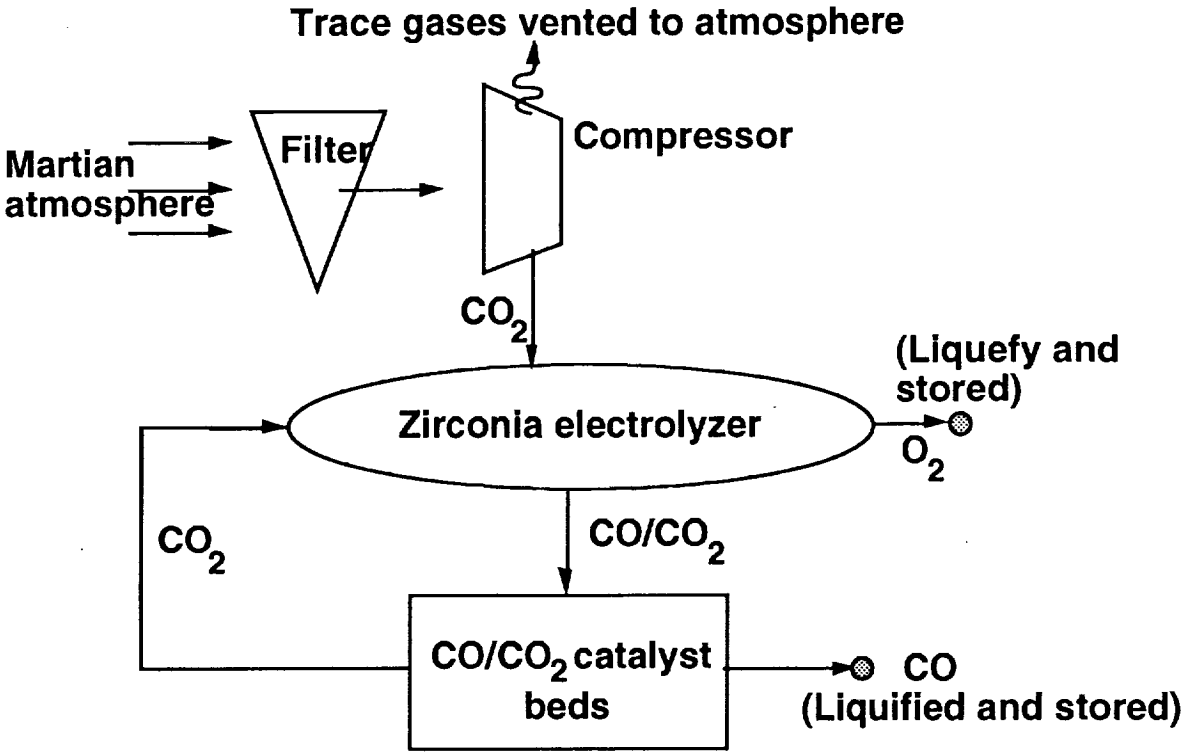

Fig. A.5 Zirconia electrolyzer propellant plant flow diagram.

APPENDIX B:

METHANE ROCKET EXPERIMENTS

Daniel Pasco

TABLE OF CONTENTS

B.1 INTRODUCTION

One of the differences between Project Genesis and other proposed ISRU missions is that the methane-oxygen rocket motors used by the MLVH operate at an oxygen-to-fuel mass ratio of 2:1, i.e., fuel rich. A large number of questions were raised by the decision to go to this mass ratio, particularly in terms of sooting and realized thrust. Fortuitously, a small rocket motor had been developed previously by two University of Washington seniors [1]. Although designed to operate using methane and air, the engine was easily modified to use methane and oxygen instead. This appendix presents an overview of the rocket design and the results of the experimentations with fuel-rich combustion.

B.2 ROCKET CONFIGURATION

Figure B.1 shows a schematic of the rocket motor as modified by the author, including the combustion chamber, injector head, and exhaust nozzle assembly. These components are described below.

Combustion Chamber

The combustion chamber, shown in Fig. B.2, is a 10 in. (25.4 cm) long section of Type 306 stainless steel tube. It has an inner diameter of 1.5 in. (3.81 cm) and an outer diameter of 2.5 in (6.35 cm). Each end of the chamber has a flange with six evenly spaced 0.375 in. (9.53 mm) diameter holes. The holes are designed to accommodate the bolts used to attach the injector and nozzle sections of the rocket. A pressure tap is located 1.5 in. (3.81 cm) from the nozzle end of the chamber. A .55 in. (14 mm) hole, threaded for a standard automobile spark plug, is located 3.0 in. (7.62 cm) from the injector end. The combustion chamber was originally intended to operate at pressures up to 250 psig (1.72 MPa). Its robust design results in a very

large safety factor even at high temperatures. For the present work the operating pressure was kept below 200 psig (1.38 MPa).

Gas Handling System

The gas injection and mass-flow regulating system for the experiments is shown in Fig. B.3. Oxygen and methane are pressure fed from standard commercial gas bottles located behind a protective wall. The mass flow of each constituent gas into the mixing chamber is regulated by the feed pressure and a choked metering orifice. Once the sizes of the metering orifices are fixed, the mass flow into the rocket is governed by the upstream pressure in the feed lines. By adjusting the pressure regulators, the relative mass flows of methane and oxygen can be adjusted and controlled as desired. The oxygen and methane pass through 15 ft (460 cm) of 0.375 in. (9.53 mm) copper tubing to the rocket motor. Pressure gauges and one-way check valves placed upstream of the sonic metering orifices respectively monitor the inlet pressure and prevent blow back during possible ignition pressure transients.

It was known from previous experience that significant pressure fluctuations, i.e., chugging, can occur during ignition. If these pressure fluctuations are great enough, they can unchoke the metering orifices and alter the fuel-air ratio in the combustion chamber. To circumvent this problem the pressure upstream of the sonic orifices was set at 250 psig (1.72 MPa), resulting in a 3.33:1 operational pressure ratio across the orifices. A minimum pressure ratio of slightly under 2:1 is required to assure sonic flow in the orifices [2].

Exhaust Nozzle

The exhaust nozzle, shown in Fig. B.4, is machined from graphite and is designed to be easily removable from the stainless steel nozzle block of the rocket. Graphite was chosen because of its ability to withstand the high heat flux at the throat. The nozzle insert is held in place

primarily by the internal pressure of the combustion chamber and is sealed with Permatex Hi-Temp RTV™ engine manifold sealant. The insert has a throat diameter of 0.125 in (3.175 mm) and an exit diameter of 0.144 in. (3.66 mm). These dimensions result in an area expansion ratio of 1.32, which fully expands the products to ambient atmospheric pressure [2].

Gas Injector and Mixer

The gas injectors were designed to regulate the mass flow of the rocket motor and work in conjunction with the nozzle to maintain a constant combustion chamber pressure during operation. Methane is injected tangentially to an axial oxygen stream, creating a cyclonic fuel-oxidizer mixture [3], as depicted in Fig. B.5. The dimensions of the injector head and mixing chamber are shown in Fig. B.6.

In order to determine the correct diameters for the metering orifices it was necessary to determine the total mass flow rate, $\dot{m}$, through the rocket motor, which can be calculated using the following equation [2]:

$$\dot{m} = A_t P_o \gamma \left[\frac{\left[\frac{2}{\gamma+1} \right]^{\frac{\gamma+1}{2(\gamma-1)}}}{\sqrt{(\gamma R T_o)}} \right] \tag{B.1}$$

where: A_t = Sonic throat area

P_0 = Stagnation or chamber pressure

γ = Specific heat ratio

R = Universal gas constant

and T_0 = Stagnation or chamber temperature

The mass flow through the rocket is governed by the chamber conditions and the throat of the exhaust nozzle, which has a diameter of 0.125 in. (3.175 mm). The temperature, molecular mass,

and specific heat ratio of the combustion products were calculated using CET-89, a combustion analysis program written at the NASA Lewis Research Center [4]. The simulation was run at an assumed combustion chamber pressure of 75 psia (517 kPa) and a wide range of fuel-oxygen equivalence ratios, Φ. These are defined by the following equation:

$$\Phi = \frac{\frac{\dot{m}_{methane}}{\dot{m}_{oxygen}}}{\left(\frac{\dot{m}_{methane}}{\dot{m}_{oxygen}}\right)_{Stoichiometric}} \tag{B.2}$$

Table B.1 shows selected results of the calculations for equivalence ratios of 1.0 and 2.0. A nominal equivalence ratio of 2.0, corresponding to the operating conditions of the Project Genesis MLVH rocket engines, was selected as the design point. With this mixture ratio and a combustion pressure of 75 psia (517 kPa) the theoretical combustion temperature is 4359 °F (2677 K), and the corresponding mass flow through the nozzle is 2.25 g/s. The required mass flow of methane is 0.75 g/s and the mass flow of oxygen is 1.5 g/s.

Table B.1 Operating characteristics of the rocket motor.

	Equivalence ratio of 1.0	Equivalence ratio of 2.0
γ	1.19	1.2
Chamber temperature	3265	2677
Molecular weight of products	21.924	15.879
Gas constant of products	379	524

The injection system is equipped with removable inlet metering orifices. In the current design each of the orifices is drilled through a 0.375 in. (9.53 mm) diameter, 0.25 in. (6.35 mm) thick brass disc which is inserted into the female NPT pipe thread connection in the mixing chamber, as shown in Fig. B.7. Each disc is held in place by the male connector of the one-way check valve and an O-ring seal.

Ignition System

The gas ignition system, shown in Fig. B.8, uses a standard automotive spark plug with flush electrodes to ignite the gas mixture. The spark plug is powered by a 6 V battery connected to a Tesla coil, which boosts the output voltage to ~10,000 VAC. The coil is connected to the spark plug and rocket chamber via an RG-8U high-voltage coaxial cable. The ignition system is activated by a switch placed between the battery and Tesla coil. Pressing the switch completes the circuit and triggers a continuous spark at the spark plug. Once ignition occurs, the spark plug is turned off.

B.3 RESULTS

The test engine combustion chamber is equiped with a pressure tap and gauge to measure the average operating pressure inside the chamber. The combustion chamber pressure, used in tandem with calculated thermodynamic properties, can be used to calculate the operating characteristics of the engine. The temperature of the combustion products has not yet been determined by direct measurements. For future tests a thermocouple probe capable of withstanding combustion chamber temperatures up to 3000 K will be used. A thrust measuring system is currently under construction. Until such a time as it is completed, a good estimate of the thrust can be made from the known and derived chamber conditions, and the nozzle throat diameter and expansion ratio.

The thrust is determined from the following relation:

$$T = C_F P_{\circ} A_t \tag{B.3}$$

where: T = Engine thrust

and C_F = Thrust coefficient

Where C_F, the thrust coefficient, is obtained from [2]:

$$C_F = \left[\frac{2\gamma^2}{\gamma - 1} \left(\frac{2}{\gamma + 1} \right)^{\frac{(\gamma+1)}{(\gamma-1)}} \left[1 - \left(\frac{P_e}{P_O} \right)^{\frac{(\gamma-1)}{\gamma}} \right] \right]^{\frac{1}{2}} + \frac{P_e - P_a}{P_O} \cdot \frac{A_2}{A_t} \qquad \text{(B.4)}$$

where: P_e = Nozzle exit pressure

P_a = Ambient pressure

and A_2 = Nozzle exit area

Values of C_F and the resulting thrust are shown in Table B.2 for measured values of P_C.

Table B.2 Thrust values as a function of chamber pressure.

P_C (psia)	Stoichiometric C_F	Stoichiometric Thrust (lbf)	Fuel Rich (O/F=2) C_F	Fuel Rich (O/F=2) Thrust (lbf)
60	1.03	0.76	1.03	0.75
70	1.08	0.93	1.08	0.92
80	1.11	1.09	1.11	1.09
90	1.14	1.26	1.14	1.25
100	1.16	1.42	1.16	1.42
110	1.18	1.59	1.18	1.58
120	1.19	1.75	1.19	1.75
130	1.20	1.92	1.20	1.92
140	1.22	2.09	1.22	2.08
150	1.22	2.25	1.22	2.25
160	1.23	2.42	1.23	2.41
170	1.24	2.58	1.24	2.58
180	1.25	2.75	1.25	2.74
190	1.25	2.92	1.25	2.91

The exhaust velocity, v_e, can be calculated from [2]:

$$v_e = \sqrt{\left[\frac{2\gamma}{\gamma - 1} \right] RT_o \left[1 - \left(\frac{P_a}{P_o} \right)^{\frac{\gamma-1}{\gamma}} \right]} \qquad \text{(B.5)}$$

The exhaust velocity can then be used to calculate the specific impulse of the rocket, defined as the exhaust velocity divided by one earth gravity. The calculated specific impulses for the rocket at a O/F mass ratio of 4:1 appear in Table B.3.

Table B.3. Variation of Isp with chamber pressure at an O/F ratio of 1.0.

Chamber pressure (psia)	Exhaust velocity (m/s):	I_{sp} (sec)
60	1912	195.1
70	1914	195.3
80	1917	195.6
90	1920	195.9
100	1923	196.2
110	1925	196.4
120	1927	196.6
130	1929	196.8
140	1931	197.0
150	1933	197.2
160	1934	197.4
170	1936	197.5
180	1937	197.7
190	1938	197.8

NOMENCLATURE

Φ	Equivalence ratio
ρ	Mass density
γ	Specific heat ratio
A_e	Nozzle exit area
A_t	Sonic throat area
C_f	Thrust coefficient
ISRU	*In Situ* Resource Utilization
M	Molecular weight
$\dot{m}$	Mass flow rate
MLVH	Mars Landing Vehicle/Hopper
P_e	Nozzle exit pressure
P_a	Ambient pressure
P_0	Stagnation or chamber pressure
R	Universal gas constant
T	Temperature
T	Thrust
T_0	Stagnation or chamber temperature

REFERENCES

1. Andrews, J.E., and Pasco, D.L.., "Development and Operation of a Methane-Air Rocket Motor," AIAA Region VI Student Conference, San Jose, CA, March 31 - April 2, 1994

2. Sutton, G.P., *Rocket Propulsion Elements*, 6th ed., John Wiley & Sons, New York, 1992, pp. 54-82.

3. Albright, L. F. and Alexander, L. G., "Stable Cyclonic Flames of Natural Gas and Air," *Jet Propulsion*, Vol. 26, 1956, pp. 867-873.

4. NASA-Lewis "Thermodynamic Equilibrium Code," Copy right 1990 Ergo Computing, Inc.

5. Champion, R., "LOX/CH4 Test Experience & LOX/CH4 Engine Design for Mars Ascent Stage," Program Development Report, NASA Marshall Space Flight Center, AL, Presented Feb. 25, 1993.

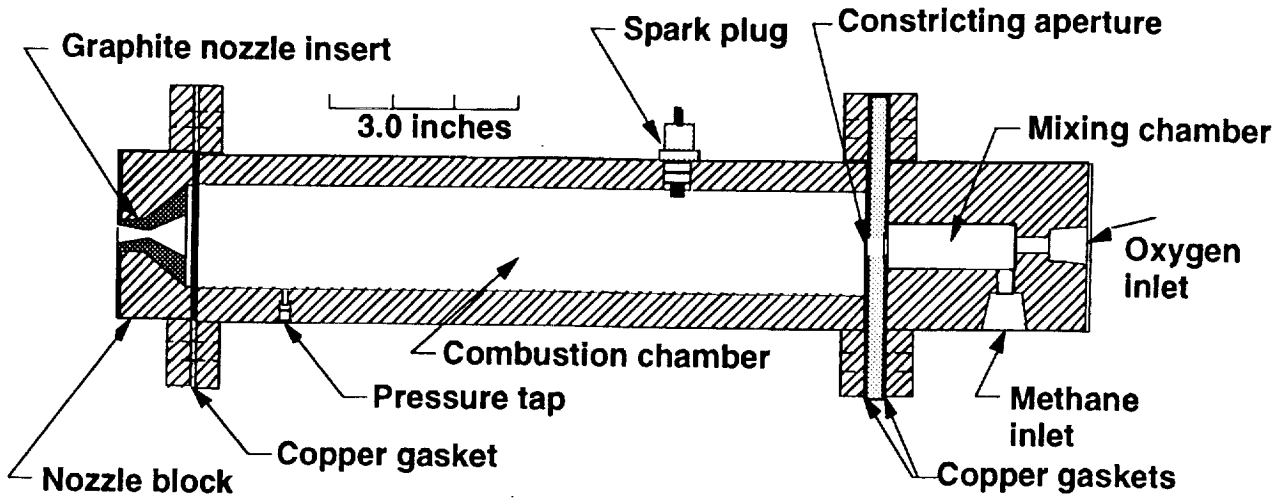

Fig. B.1 Rocket motor configuration with ignition system.

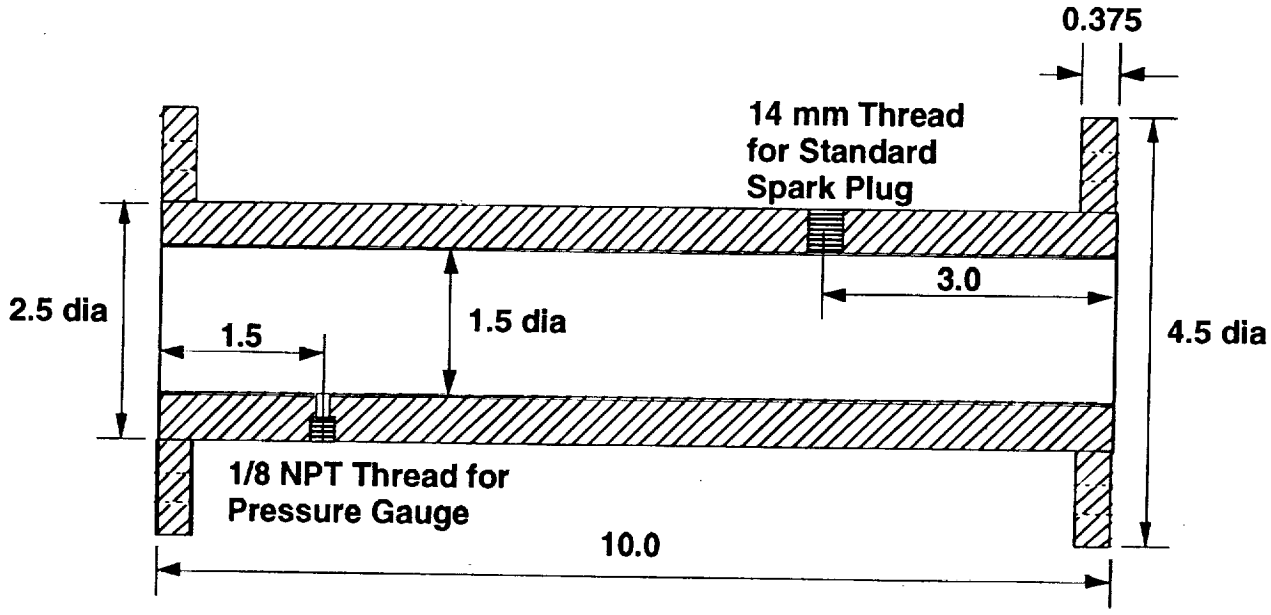

Fig. B.2 Combustion chamber configuration. (All dimensions in inches).

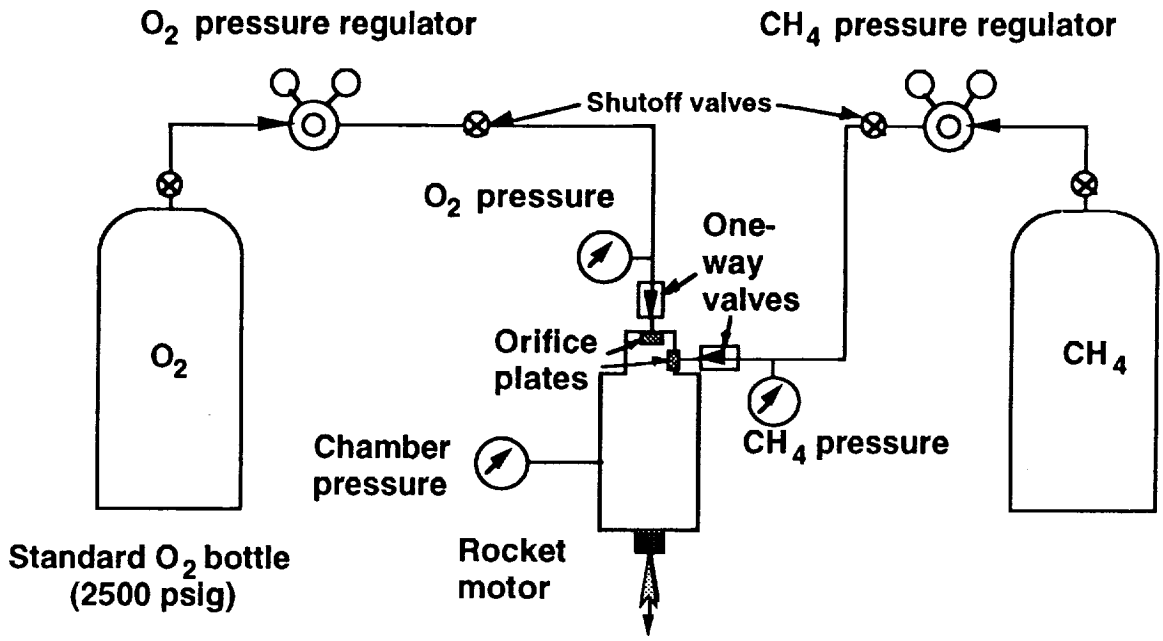

Fig. B.3 Gas handling system.

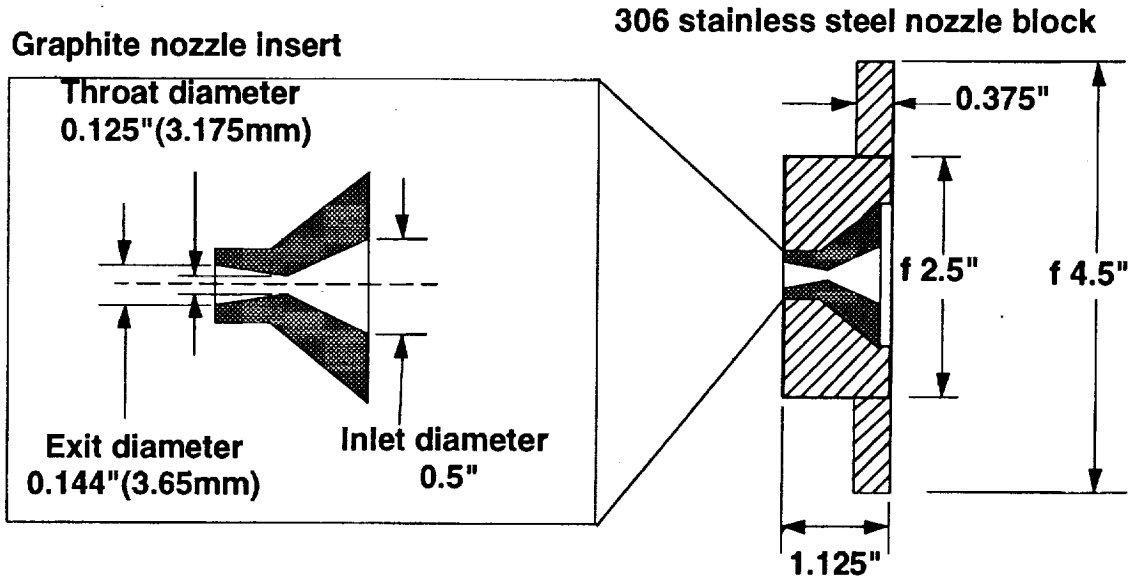

Fig. B.4 Exhaust nozzle section.

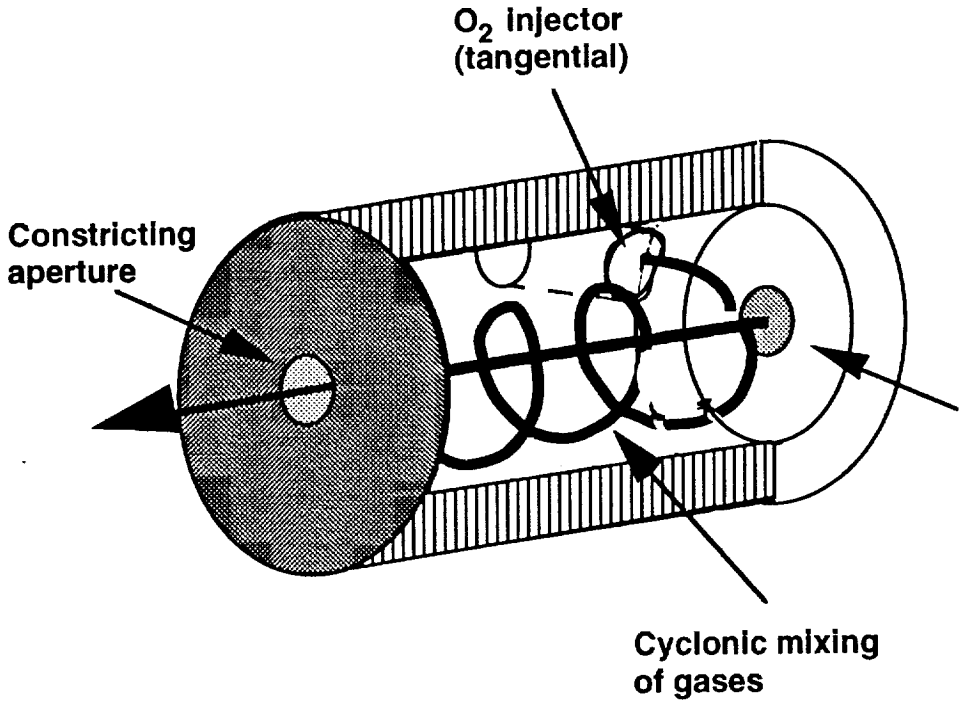

Fig. B.5 Cyclonic injection system.

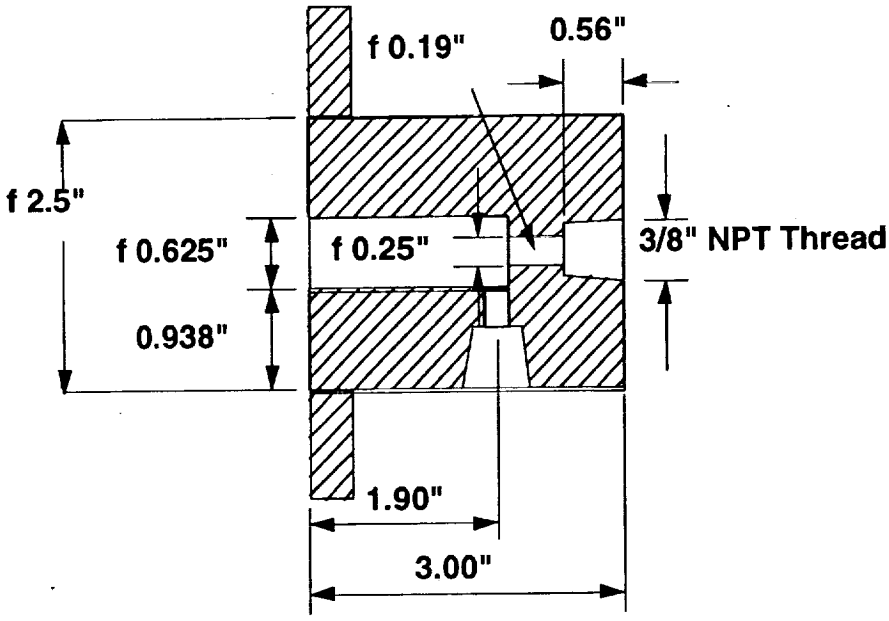

Fig. B.6 Mixing chamber dimensions.

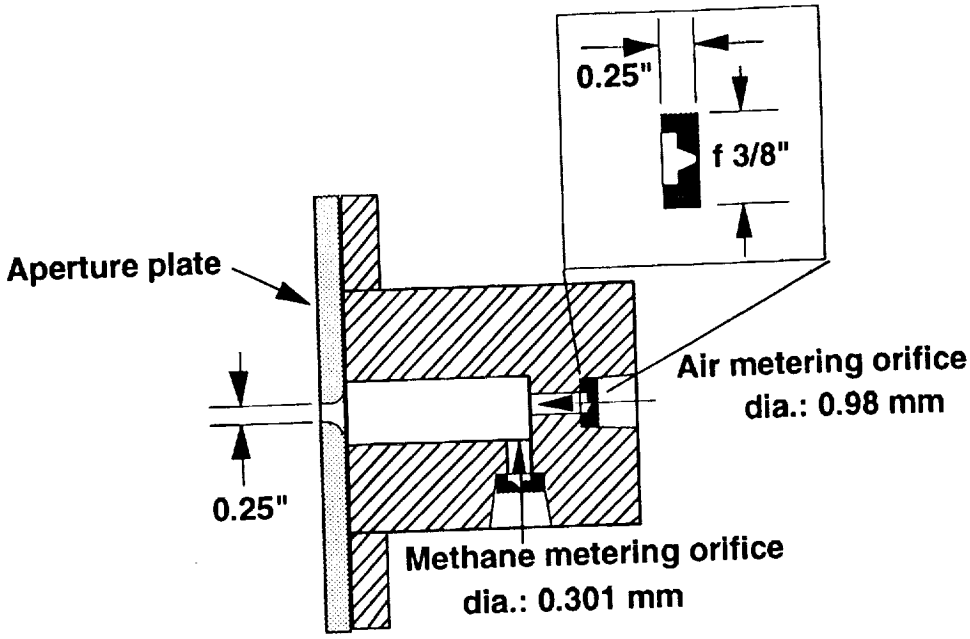

Fig B.7 Injection system configuration with sonic orifice inserts.

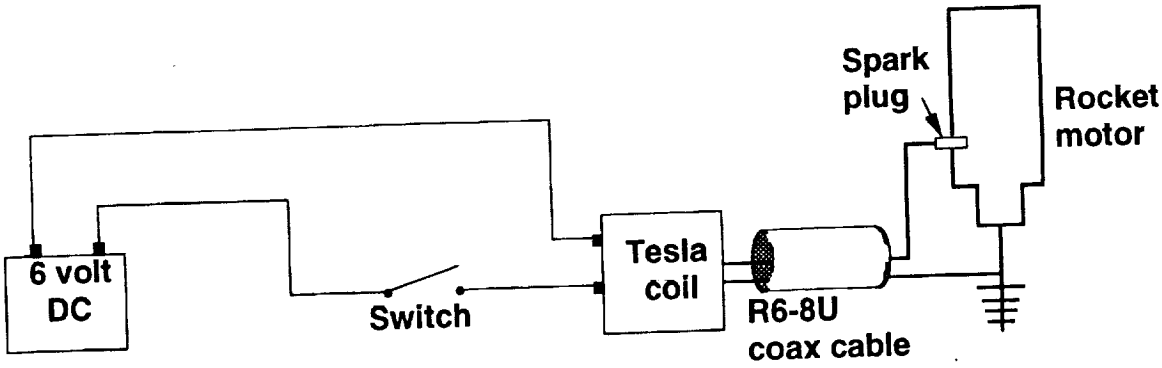

Fig. B.8 Rocket ignition system.